A CONTROL-VOLUME FINITE-ELEMENT METHOD FOR THREE-DIMENSIONAL PARABOLIC FLOW AND HEAT TRANSFER IN DUCTS, WITH APPLICATION TO LAMINAR THERMAL-HYDRAULICS IN ROD-BUNDLE GEOMETRIES

by

Trung-Tri PHAM

A Thesis Submitted to the Faculty of Graduate Studies and Research in Partial Fulfillment of the Requirements for the Degree of Master of Engineering

Department of Mechanical Engineering
McGill University
Montreal, Canada

CONTROL-VOLUME FINITE-ELEMENT METHOD FOR 3-D PARABOLIC FLOWS

ABSTRACT

The formulation of a general control-volume finite-element method for the prediction of laminar three-dimensional parabolic duct flow and heat transfer is presented. Consideration is given to straight ducts of arbitrary but constant cross-sections.

In the proposed method, the calculation domain is first discretized into twelve-node prism macroelements. Then each macroelement is divided into four six-node prism subelements. Prism control volumes of polygonal cross-sections are then associated with the nodes of these elements. All dependent variables, except pressure, are stored at the nodes of the subelements, and they are interpolated in the cross-sectional plane by upwind-type functions. The pressure is stored at the vertices of the macroelements and it is interpolated linearly in the cross-section of these elements. In the axial direction, the downstream values of all dependent variables are assumed to prevail over the elements. The discretized equations are derived by applying integral conservation equations to the prism control volumes, and they are solved using an iterative scheme akin to SIMPLER. The proposed method employs a marching integration procedure and an automatic step size algorithm which allow computational efficiency. The validity and capabilities of the proposed method are established by applying it to

developing flow and heat transfer in a square cross-section duct and comparing its results with published results. Satisfactory agreement is found.

The proposed method has been applied to longitudinal flow and heat transfer over an infinite triangular rod-bundle array for several pitch-to-diameter ratios. Both fully-developed and developing regions have been investigated. Local and overall results are presented in appropriately non-dimensionalized forms.

SOMMAIRE

Une méthode générale d'éléments finis basée sur le principle de volume de contrôle est présentée pour résoudre les problèmes des écoulements paraboliques, laminaires, tridimensionels. La méthode est applicable à des conduits droits aux coupes transversales de forme arbitraire mais constante.

Dans la méthode ici-proposée, le domaine de calcul est d'abord divisé en des macro-éléments de douze noeuds. Puis, chaque macro-élément est divisé en quatre sous-éléments de six noeuds. On associe ensuite des volumes de contrôle à chacun des noeuds de ces éléments. Les variables dépendentes autre que la pression sont mises en mémoire aux noeuds des sous-éléments, et elles sont interpolées dans le plan transversal par des fonctions de type "upwind". La pression est mise en mémoire aux extrémités des macro-éléments et on l'interpole linéairement dans le plan transversal de ces éléments. Dans la direction axiale, on assume que les valeurs en amont de toutes les variables dépendentes prévalent dans les éléments. On dérive les équations de discrétization en appliquant les équations intégrales de conservation aux volumes de contrôle, et on les résoud en utilisant une méthode itérative similaire à SIMPLER. La méthode proposée emploie une procédure d'intégration pas-par-pas et un algorithme automatique d'adjustement de

pas axial, permettant l'efficacité de calcul. On établit la validité et les capacités de la méthode proposée en appliquant celle-ci au problème des écoulements et échanges de chaleur dans un conduit carré. La comparison entre les résultats présents et publiés est satisfaisante.

La méthode proposée est aussi appliquée au problème des écoulements et échanges de chaleur au long d'un faisceau triangulaire infini de cylindres. On étudie le régime des écoulements établis ainsi qu'en dévelopement. Les résultats locaux et globaux sont présentés dans des formes non-dimensionelles appropriées.

ACKNOWLEDGEMENTS

I am deeply indebted to my thesis supervisor, Prof. B.R. Baliga, for the invaluable guidance, advice and encouragement he offered throughout the course of this work. His warm friendship and continued support provided me tremendous motivation, and they made the successful completion of this thesis both possible and enjoyable.

I would also like to express my gratitude to the Natural Sciences and Engineering Research Council of Canada who funded this work through a postgraduate fellowship and a research grant. The concluding phase of this work was also partially supported by Atomic Energy of Canada Limited, whose financial help is gratefully acknowledged.

And I wish to give thanks of a very special kind to Ms. Assunta Cerrone-Mancini and Dinah Ross who both did a splendid job of typing a difficult manuscript. Last, but not least, I wish to extend my gratitude to my parents whose love and support contributed so much to the production of this thesis.

TABLE OF CONTENTS

LIST OF FIGURES

LIST OF TABLES

NOMENCLATURE

a,b,c	Coefficients in the interpolation function for pressure, Eqn. (3.13)
A	Cross-section area; also aspect ratio, Eqn. (5.2)
A,B,C	Coefficients in the interpolation function for ϕ, Eqn. (3.11)
a_i, a_{nb}, a_i^U, b_i	Coefficients in the discretization equation for ϕ, Eqn. (3.32)
$a_i^u, a_{nb}^u, a_i^{u,U}, b_i^u$	Coefficients in the discretization equation for u, Eqn. (3.40)
$a_i^v, a_{nb}^v, a_i^{v,U}, b_i^v$	Coefficients in the discretization equation for v, Eqn. (3.41)
$a_i^w, a_{nb}^w, a_i^{w,U}, b_i^w$	Coefficients in the discretization equation for w, Eqn. (3.42)
a_i^p, a_{nb}^p, b_i^p	Coefficients in the discretization equation for pressure, Eqn. (3.61)
AC,AE,ANE,AN,AW, ASW,AS,ACON	Coefficients in the discretization equation for ϕ, Eqn. (4.14)
APC,APE,APNE,APN, APNW,APW,APSW, APS,APSE,APENE, APNNE,APWSW, APSSW,APCON	Coefficients in the discretization equation for pressure, Eqn. (4.19)
A_{165}	Area of element 165
c_p	Specific heat at constant pressure
CONT1,CONT5,CONT6	Contributions of subelement 165 to the ϕ discretization equation of nodes 1, 5 and 6, respectively
d	Diameter of the cylinders in the rod-bundle problem
D_H	Hydraulic diameter, Eqn. (2.19)
D_i^u, D_i^v	Coefficients in Eqns. (3.37) and (3.38)

ds	Differential element of the control volume surface ∂V
E,N,W,S,C	East, North, West, South, Centre nodes used in the geographic labelling scheme
f	Friction factor, Eqn. (2.30)
$\bar{h}$	Average heat transfer coefficient
(H)	Prescribed uniform wall heat flux boundary condition
$\vec{i}, \vec{j}$	Unit vectors in the x and y directions, respectively
I,J	Node addressing scheme for the vertices of the subelements
IP,JP	Node addressing scheme for the vertices of the macroelement
$\vec{J}$	Combined convection-diffusion flux vector, Eqn. (3.2)
J_X, J_Y	Component of $\vec{J}$ in the X and Y directions, respectively
k	Fluid thermal conductivity
$\vec{k}, \vec{\ell}$	Unit vectors in the X and Y directions, respectively
L	Length of one side of the duct in the square duct problem
Ll,Ml	Maximum velocity node numbers
LPl,MPl	Maximum pressure node numbers
$\dot{m}$	Mass flow rate
n	Normal direction
$\vec{n}$	Unit outward normal to ds
Nu	Nusselt number, Eqn. (5.7)
Nu_z, (T), Nu_z, (H)	Local peripherally-averaged Nusselt numbers at axial location z for the (T) and (H) boundary conditions, respectively

$Nu_{m,(T)}$, $Nu_{m,(H)}$	Flow length averaged Nusselt numbers at axial location z for the (T) and (H) boundary conditions, respectively
$Nu_{(T)}$, $Nu_{(H)}$	Fully-developed peripherally-averaged Nusselt numbers for the (T) and (H) boundary conditions, respectively
p	Cross-sectional pressure, Eqn. (2.5)
$\bar{p}$	Cross-sectional averaged pressure, Eqn. (2.6)
P	Pressure
$p^*, \bar{p}^*$	Non-dimensional pressures, Eqn. (2.18)
p'	Pressure correction
P	Perimeter of the duct
Pr	Prandtl number, $(= \mu c_p/k)$
Pe_Δ	Subelement Peclet number, Eqn. (3.10)
PCONT1, PCONT2, PCONT3	Contribution of macroelement 123 to the integral mass conservation equations for nodes 1, 2 and 3, respectively
POWER	Coefficient used to determine the distribution of grid lines
q_z	Peripherally-averaged wall heat flux at axial location z
q_m	Flow length averaged wall heat flux at axial location z
q_w	Constant uniform wall heat flux
Ra	Rayleigh number, Eqn. (5.2)
Re	Reynolds number
S	Source term
S_C, S_P	Coefficients in the linearized source term, Eqn. (3.6)
T	Fluid temperature
T_b	Bulk fluid temperature

t^*	Non-dimensional temperature, Eqn. (2.6)
T^*	Non-dimensional temperature, Eqn. (2.37)
(T)	Prescribed constant uniform wall temperature boundary condition
$\bar{T}_w$	Peripherally averaged wall temperature
u,v,w	Velocity components in the x, y and z directions, respectively
u^*,v^*,w^*	Non-dimensional velocity components, Eqn. (2.17)
$\hat{u},\hat{v},\hat{w}$	Pseudovelocity components, Eqns. (3.43) to (3.45)
u',v',w'	Velocity corrections
u^*,v^*	Non-dimensional velocity components, Eqn. (5.2)
U,V	Velocity components in the X and Y directions, respectively
$\vec{v}$	Velocity vector
v_i	Subelement control volume surrounding node i
V_i	Macroelement control volume surrounding node i
$V,\partial V$	Control volume, and control volume surface
$\bar{w}$	Mean axial velocity component
w_{max}	Maximum axial velocity component over the cross-section
W	Non-dimensional axial velocity component, Eqn. (2.27)
$\bar{W}$	Mean non-dimensional axial velocity component, Eqn. (2.32)
x,y,z	Global Cartesian coordinates
x^*,y^*,z^*	Non-dimensional coordinates, Eqn. (2.16)
X,Y,Z	Cross-sectional flow-oriented Cartesian coordinates for a subelement

z^*	$z/D_H Re$)
z'	$z/(D_H RePr)$

Greek Symbols

α	Under-relaxation parameter
Γ	Diffusion coefficient
Δz	Axial step size
θ	Non-dimensional temperature, Eqn. (2.49)
θ	Non-dimensional temperature, Eqn. (5.2)
θ	Angle in the rod-bundle geometry, Fig. 6.2(b)
Θ	Non-dimensional temperature, Eqn. (2.55)
λ	Eigenvalue, Eqn. (2.54)
λ_j^u, λ_j^v	Coefficients of pressure in discretized momentum equations, Eqns. (3.40) and (3.41)
μ	Fluid dynamic viscosity
ν	Fluid kinematic viscosity
ξ	Exponential function, Eqn. (3.11)
ξ, η	Non-dimensional x and y coordinates, Eqn. (5.2)
ρ	Fluid density
ρ_o	Fluid density at $T=T_c$
ϕ	General scalar dependent variable
χ	Non-dimensional temperature, Eqn. (2.69)
ψ	Non-dimensional stream function, Eqn. (5.9)
Ω	Non-dimensional vorticity, Eqn. (5.11)

Subscripts

a,b,c,o,r,s,t	Values at particular locations in a typical subelement, Fig. 3.6
av	Element-averaged value
f.d.	Fully-developed value
i	Value at the inlet (z=0)
i	Value at node i
nb	Neighbour-node values
o	Value at subelement centroids
O	Value at macroelement centroids
w	Wall value
1,2,3,4,5,6	Values at the nodes of a typical macroelement and its subelement, Fig. 3.4
o1,o2,o3	Values at the outer vertices of associated macroelements, Fig. 3.8

Superscripts

D	Downstream value
U	Upstream value
$a, b, c, u_i, d_i,$ A, B, C, U_i, D_i	Pertaining to these respective control volume surfaces, Fig. 3.4
u,v,w,p	Pertaining to the u-, v-, w- and p-equations, respectively
*	Non-dimensional value; also, guessed value, or value from previous iteration
#	Calculated value

CHAPTER I

INTRODUCTION

1.1 AIMS OF THE THESIS

The main objective of this thesis is the formulation, computer implementation and testing of a general numerical method for the prediction of fluid flow and heat transfer phenomena in duct-like geometries. Such phenomena are encountered in an endless variety of engineering equipment. For example, fluid transport systems, heat exchangers, turbomachines, nuclear reactors and aircraft propulsion systems present challenging duct flow and heat transfer problems. Quantitatively accurate solutions to these problems would be extremely useful in the design, optimal use and control of such devices. The numerical method presented in this thesis represents an effort to enable such solutions.

A majority of practically important duct flow and heat transfer problems involve domains with boundaries that do not lie along commonly-used coordinate axes. Therefore, numerical methods for the solution of such problems should be able to handle irregularly-shaped domains. In addition, these methods must be designed to work with uniform and non-uniform distributions of grid points inside the calculation domain;

this capability is necessary for the efficient solution of problems in which the dependent variables vary steeply in certain regions of the domain, near solid boundaries for instance, and relatively mildly elsewhere. These features are given primary importance in this thesis.

In general, duct flows could be subsonic, transonic or supersonic. Only subsonic flows are considered in this thesis; transonic and supersonic flows are not within its scope. Subsonic flows could be laminar or turbulent, and single-phase or two-phase problems may be encountered. In addition, such flows could involve compressible fluids. In this thesis, however, only laminar, incompressible fluid flows will be studied. This limitation of the scope of this work was needed so that attention could be concentrated on the formulation and development of the proposed numerical method. The testing and performance evaluation of general numerical methods for fluid flow and heat transfer are best done by applying them to problems with well-established mathematical models. It is to be noted in this connection, that the proposed method is based on the control-volume finite-element formulation recently proposed by Baliga and Patankar [1,2]. These formulations are akin to control-volume finite-difference procedures which are widely used for the solution of fluid flows in regular-shaped domains, but with all of the other aforementioned complexities [3,4]. Thus it may be deduced that the method presented in this thesis has the potential to solve at least currently available mathematical models of turbulent and two-phase

flows. The actual application of the method to such flows is not included in the scope of this thesis: rather, the analysis of such flows is suggested as a possible extension of this work.

Steady subsonic flows in ducts can be categorized as elliptic, parabolic or partially-parabolic [4,5]. In elliptic flows, the conditions at any point in the flow can influence conditions at any other point. The mechanisms that cause this interaction are convection, diffusion and pressure transmission [5]. Parabolic duct flows have the following characteristics: there exists a predominant flow along the duct, and no flow reversal is encountered in that direction; diffusional transport in the direction of the main flow is negligible compared to the corresponding convective transport and the cross-stream diffusional transport; and the downstream pressure field has relatively very little influence on the upstream flow conditions [3,6]. When these conditions are satisfied, the main flow direction can be regarded as a one-way coordinate [3,4]; the upstream conditions can influence the downstream conditions, but not vice-versa. The term partially-parabolic is used to describe a class of flows that is intermediate to the parabolic and elliptic categories. They have a predominant flow direction along which there is no flow reversal, and diffusional transport in that direction is negligible; in this regard, they are similar to parabolic flows. On the other hand, the pressure transmission in partially-parabolic flows is similar to that in elliptic flows, and it

is the dominant transmitter of influences in the upstream direction [5].

Flow and heat transfer in straight unobstructed portions of duct-like geometries can be regarded as parabolic [3,4,6]. In curved ducts and in the vicinity of obstructions or contractions, there could be significant turning of the local flow with respect to the mean flow direction. Such flows could fall into the partially-parabolic category. If the curvature of duct is considerable, or if the size of obstruction is large compared to the duct cross-section, local flow reversal or recirculating flow regions may be encountered. In these regions, the flow and heat transfer is fully-elliptic. In this thesis, only parabolic flow and heat transfer in straight unobstructed duct-like geometries are considered.

The computer implementation and testing of the proposed method form an important part of the work reported in this thesis. The implementation activity involves three main groups of tasks: (i) generation and storage of domain discretization information; (ii) generation and storage of the coefficients in the discretization equations; and (iii) solution of the discretization equations. For the discretization of cross-sectional planes in duct-like geometries, a semi-automatic domain discretization scheme is formulated according to the following guidelines: (a) there should be no requirement for any special geometrical input devices such as computer graphics digitizers, light pens and microcomputers; (b) the scheme should be able to generate all necessary topological information

for the assembly and solutions of the discretization equations, without requiring excessive computer core storage and costly input/output operations; and (c) it should facilitate the use of iterative methods for the solution of the discretization equations. In the axial direction, the dependent variables vary rather severely close to the entrance of the duct and relatively mildly as the fully-developed region is approached, and the exact nature of this variation is not known a priori. Therefore, an efficient numerical method for parabolic duct flows should be capable of automatically adjusting the axial step size according to the relative magnitudes of gradients encountered in the variation of the dependent variables. Such an automatic step size selector is formulated and incorporated in the domain discretization scheme.

The application of the proposed method to laminar flow and heat transfer in rod-bundles is another important part of this thesis. Though this problem is commonly encountered in nuclear reactor cores, steam generators and heat exchangers, to the best knowledge of the author, no in-depth experimental or numerical investigation of it is reported in the published literature. In this work, flow and heat transfer in an infinite rod-bundle array are investigated with geometric parameters relevant to the design of nuclear reactor cores. Three categories of problems are considered in this context: (i) fully-developed flow and heat transfer; (ii) fully-developed flow and developing heat transfer; and (iii) simultaneously developing flow and heat transfer. Local and

overall results are presented in suitably non-dimensionalized forms.

1.2 SYNOPSIS OF AVAILABLE METHODS FOR THREE-DIMENSIONAL PARABOLIC FLOW AND HEAT TRANSFER

Numerous papers in the published literature deal with analytical, semi-analytical and numerical methods for three-dimensional flow and heat transfer in ducts. In this section, a few key papers directly relevant to the present work are reviewed. A more extensive survey of this subject is available in [7].

The equations governing parabolic flow in ducts are intrinsically non-linear and coupled to each other. Consequently, unless drastic simplifications are introduced, analytical and semi-analytical solutions to these equations are extremely difficult, if not impossible, to obtain. A commonly-invoked simplification in studies of this nature consists of linearizing the inertia terms in the momentum equations and neglecting the cross-stream pressure gradients [8,9]. The major shortcoming of such methods is that they are limited to problems in which the cross-stream velocity components are either zero or negligible. Furthermore, even in the absence of cross-stream velocities, analytical and semi-analytical methods usually fail when non-linearities introduced by non-constant fluid properties are encountered.

Numerical methods, on the other hand, enjoy a great deal of versatility and are better suited for the solution of

practical problems [4]. As a result, they have received considerable attention in the last two decades [7]. It is usual to group currently available numerical methods for three-dimensional duct flows and heat transfer into two main categories: finite-difference and finite-element methods. This categorization is adopted in the following discussion.

FINITE-DIFFERENCE METHODS

Early works in this area concentrated on solving the three-dimensional boundary layers equations. The pressure gradient in one cross-stream direction and the diffusional flux in the other are neglected. In this way, only two momentum equations need to be solved, the third velocity component being extracted from continuity requirements. Methods employing procedures of this kind include those reported in [10,11]. In general, these methods have a limited range of applicability. Furthermore, they cannot easily be adapted to internal flow problems, and they may give rise to considerable errors in problems exhibiting boundary discontinuities and fail completely in others [12].

In the last decade, the pioneering works of Curr et al. [13,14] and Patankar and Spalding [6] have led the way to the development of more general methods which take full account of the fluid stresses, diffusional fluxes and pressure variation in the cross-stream plane. Curr et al. [13,14] analyzed three-dimensional parabolic flows using two different finite-difference schemes: a vorticity-velocity formulation is used

in one, and the other employs velocity components and pressure as the dependent variables. Both these schemes use non-iterative "marching" integration in the direction of the main flow. In the method based on the vorticity-velocity formulation, Curr et al. used a point-by-point Gauss-Seidel scheme to solve the discretized momentum and continuity equations. In the pressure-velocity formulation, they used a point-by-point iterative solution method based on a SImultaneous-Variable-Adjustment scheme (SIVA). Using these methods, they obtained accurate solutions of the entrance flow in a square cross-section duct with stationary boundaries and also with one wall moving.

The method proposed by Patankar and Spalding [6] is probably the most widely-referenced of the currently-available finite-difference methods for three-dimensional duct flows. It is based on a pressure-velocity formulation, and it uses a non-iterative marching integration technique to advance the solution in the downstream direction. The non-iterative nature of this scheme is achieved by using the upstream values of the dependent variables at each axial step to calculate the coefficients in the discretization equations. At each axial station, the pressure-velocity coupling is handled by a Semi-Implicit-Method-for-Pressure-Linked-Equations (SIMPLE). In SIMPLE, a tentative velocity field is obtained by solving the discretized momentum equations with a guessed pressure field. Then the pressure and velocity fields are corrected so as to satisfy the overall and local mass conservation requirements.

Experience with the aforementioned methods has shown that the Patankar-Spalding procedure [6] is superior to those advanced by Curr et al. [13,14]. Furthermore, the SIMPLE procedure advanced in [6] has also been successfully used to handle the pressure-velocity coupling in complex two- and three-dimensional elliptic flow problems [3,4]. In subsequent papers, Carlson and Hornbeck [15] and Briley [16] have proposed methods which are variations of the Patankar-Spalding method. Briley [16] used his method to solve duct flow problems with significant cross-stream velocities.

In general, the finite-difference methods proposed in [6,13-16] have been quite successful in the prediction of three-dimensional parabolic duct flows. Nevertheless, they suffer from a few shortcomings: (i) they are limited to ducts of regular-shaped and constant cross-sections; (ii) the non-iterative marching integration schemes used in these methods necessitate the use of relatively small axial step sizes; and (iii) in complex fluid flow problems involving a large number of dependent variables, the overall solution scheme, due to its non-iterative nature, tends to be sensitive to the sequence in which the dependent variables are solved.

Flow and heat transfer in irregular-shaped ducts can be solved by finite-difference methods which employ coordinate transformation techniques. For example, in the works of Roberts and Forester [17], flows in irregular-shaped ducts are handled by a curvilinear boundary-fitted computational mesh; Ghia and Sathyanarayana [18] used a non-orthogonal surface-

oriented coordinate system and a calculation procedure akin to that of Briley [16] to analyze flow development in variable cross-sectional area ducts. In these methods, the conservation equations must be transformed from the physical domain into the computational domain before their finite-difference analogues can be formed. This usually complicates the governing equations and makes a physical interpretation of the overall formulation quite difficult. Moreover, these methods are not well-suited for problems involving multiply-connected domain shapes. Such problems are best handled by finite-element methods.

FINITE-ELEMENT METHODS

The ability to handle complex irregular-shaped domains represents one of the most important advantages of finite-element methods over finite-difference methods. Indeed, it is mainly for this reason that, over the last decade, there has been a considerable amount of research on the formulation and computer implementation of finite-element methods for practical fluid flow and heat transfer problems [19]. In recent years, the solution of such problems by the finite-element method is becoming widespread and gaining in popularity [19,20].

Most currently-available finite-element methods for three-dimensional parabolic flow and heat transfer are based on the Galerkin formulation. One of the earliest attempts to develop such methods is that of Baker [21] who proposed a finite-element scheme for three-dimensional reacting and compressible

boundary-layer flows. In this scheme, all governing equations are solved simultaneously; this practice could require disproportionally large computer core storage and time, especially in complex problems involving several coupled governing equations [4]. Furthermore, it cannot be adapted to confined flow problems.

Several finite-element solution techniques based on linearized analyses have been proposed for three-dimensional parabolic flow and heat transfer in straight ducts of arbitrary shape. One such procedure is described by Davids et al. [22]. In a series of papers by Del Giudice et al. [23-26], a linearized formulation akin to the semi-analytical procedure of Sparrow et al. [9] is merged with a simple finite-element algorithm for Poisson-type equations. They have applied these procedures to hydrodynamically fully-developed and thermally developing problems and, also, to flow and heat transfer in a number of different duct geometries. It is to be noted, however, that the limitations associated with linearized formulations afflict these methods and restrict their application to problems with negligible cross-stream velocities.

The restricted range of applicability of linearized procedures has led Del Giudice et al. to consider a more general approach that deals directly with the full three-dimensional parabolized Navier-Stokes equations [27]. In this approach, a non-iterative sequential solution of the finite-element analogues of the governing equations is obtained by a procedure akin to that used by Briley [16]. Thus the limitations associated with a non-iterative marching integration in the

main flow direction afflict this method. In addition, it cannot compute the pressure in the cross-section. It also seems to experience difficulties in starting the solution.

Practical fluid flow and heat transfer problems could involve a wide range of Reynolds and Peclet numbers. Special upwind-type numerical schemes are required to solve such problems efficiently [4]. None of the currently-available finite-element methods for three-dimensional duct flow and heat transfer employ such upwind schemes. Thus, when significant cross-stream velocities are encountered, these methods could experience stability problems unless excessively fine grids are used.

Comments

From the above discussion, it is seen that a considerable amount of research has been devoted to the development of numerical methods for three-dimensional parabolic flow and heat transfer in ducts. However, there is a need for new and better methods. The method proposed in this thesis represents an effort to fulfill this need.

1.3 OVERVIEW OF THE PROPOSED METHOD

In this section, the main features of the proposed method are described in general terms so as to give the reader a synopsis of the overall formulation. Full details are presented in subsequent chapters.

The method proposed in this thesis may be viewed as an extension of the control-volume finite-element method formulated by Baliga and Patankar for two-dimensional elliptic situations [1,2]. It is composed of four main building blocks: (i) domain discretization scheme; (ii) selection of suitable interpolation functions for the dependent variables; (iii) derivation of the discretization equations; and (iv) solution of the discretization equations.

In the domain discretization scheme, the duct is first divided into a series of slabs, each slab being made up of two adjacent cross-sectional planes. In each of these cross-sectional planes, the calculation domain is divided into six-node triangular macroelements. Following this, each macroelement is further divided into four three-node subelements. All dependent variables, except pressure, are stored at all six nodes of the macroelements. Prism-shaped control-volumes of polygonal cross-section are then associated with each node. The procedure used to construct these control volumes will be discussed in a later chapter. It suffices here to say that the resulting control-volumes do not overlap, and collectively they fill up the calculation domain completely. This discretization scheme is due to Baliga and Patankar [1,2].

In the cross-sectional planes, all dependent variables, except pressure, are interpolated in each subelement by functions which are exponential in the direction of an element-averaged cross-stream velocity vector and linear in the direction normal to it. The pressure is linearly interpolated

in each macroelement. These interpolation functions are taken from the works of Baliga and Patankar [1,2]. They allow the proposed method to solve fluid flow and heat transfer problems over the whole range of Peclet numbers without incurring the false diffusion difficulties that commonly afflict upwind finite-difference methods. In the axial direction, downstream values are assumed to prevail over the control-volume for all variables. This is the so-called fully-implicit formulation in the numerical solution of parabolic problems [4]. It is used to avoid stability problems associated with the axial step size [4].

Discretization equations are algebraic approximations of the governing equations. In the control-volume approach, an integral formulation is arrived at directly by applying the conservation principles for the dependent variables to the control-volumes associated with the nodes. Following this, the integrals and derivatives of the dependent variables which appear in the integral formulation are approximated by algebraic expressions using the interpolation functions discussed in the last paragraph. The control-volume approach results in a method which has the so-called conservative property [4], and it facilitates the physical interpretation of the overall formulation.

The resulting discretization equations are solved by a marching integration technique which advances the solution step-by-step from the upstream initial conditions to the downstream outflow boundary. At each axial station, a sequential

iterative procedure similar to SIMPLER [4] is employed to handle the pressure-velocity coupling and the non-linearity of the discretization equations. An automatic axial step size adjustment procedure is incorporated into the marching scheme; thus, relatively small axial steps are taken in regions where the dependent variables vary steeply, and in regions where they vary mildly, larger axial steps are used.

1.4 SURVEY OF THE THESIS

This thesis consists of seven chapters which are organized as follows. In Chapter II, the equations governing laminar, three-dimensional parabolic flow and heat transfer in ducts are presented. These equations are described for both the developing as well as the fully-developed regions. Chapter III concentrates on the detailed formulation of the proposed numerical method, and Chapter IV outlines its computer implementation. Chapter V is devoted to the application of the proposed method to a few illustrative two- and three-dimensional test problems used to establish the validity and capabilities of the proposed method. In Chapter VI, longitudinal flow and heat transfer over an infinite triangular array of circular cylinders are studied: the developing and fully-developed regions are investigated, and appropriately non-dimensionalized results are presented for several

cylinder spacing ratios.

Finally, in Chapter VII, the main contributions of this thesis are reviewed and some suggestions concerning possible improvements and extensions of this work are presented.

CHAPTER II

MATHEMATICAL MODELS OF LAMINAR FLUID FLOW AND HEAT TRANSFER IN DUCTS

In this chapter, the differential equations which govern the duct flow and heat transfer problems considered in this thesis are presented. Detailed derivations of these equations are not within the scope of this chapter; they are available in standard text books on fluid flow and heat transfer [28,29]. Instead, commonly used forms of the governing equations are presented and their salient features are discussed.

In the following sections of this chapter, a concise description of the problems of interest in this thesis is given first. Then the equations which govern the fluid flow problems are presented and discussed. Following that, mathematical descriptions of the heat transfer problems are presented. Finally, it is shown that all these governing equations have a common form, and a general representation of these equations is presented.

2.1 PROBLEM STATEMENT

The problems of interest in this thesis involve parabolic, laminar flow and heat transfer in straight uniform ducts. The cross-sections of these ducts could be regular- or irregular-shaped and singly- or multiply-connected; four

examples are given in Fig. 2-1.

In all problems considered in this thesis, the fluid is assumed to be incompressible. In addition, though the proposed numerical method can handle non-constant fluid properties with relative ease, these properties are assumed to be constant. This is done mainly to generalize the results presented in this thesis. In spirit, this approach is similar to that used in the presentation of experimental results: actual experiments are done using fluids with variable properties, but the final results, usually in the form of empirical correlations, are based on bulk-mean or some other appropriately averaged property values.

In the heat transfer considerations, two boundary conditions are investigated; in one, the walls of the duct are maintained at a constant temperature; in the other, a uniform heat flux is prescribed over the walls of the duct. These two thermal boundary conditions represent extreme or bounding cases of the conditions encountered in practice [28,30].

The work in this thesis is mainly concerned with developing flow and heat transfer in ducts. Nevertheless, as will be discussed in later chapters, an independent investigation of fully-developed conditions is often useful in the formulation of efficient numerical procedures for the prediction of flow and heat transfer in the developing region. In this chapter, the equations governing both the developing and fully-developed regimes are presented.

2.2 FLUID FLOW ANALYSIS

In this section, the equations governing the fluid flow problem are presented. The Cartesian coordinate system (x,y,z) is used in the presentation of these equations. The z-axis coincides with the direction of the mean flow in the duct, and x and y denote the cross-sectional coordinates; typical calculation domains and their associated coordinate systems are shown in Fig. 2-1. The fluid velocity components in the x, y and z directions are denoted by u, v and w, respectively. In this thesis, w is called the main flow velocity, and u and v are referred to as secondary or cross-sectional velocities.

In the following discussion, the equations governing developing flow conditions are discussed first. Then the mathematical description of fully-developed flows is presented.

2.2.1 Developing Flow Regime

The equations governing the fluid flow problem are obtained by an appropriate combination of the laws of conservation of mass and momentum and the equations relating viscous stresses to the rate of strain of the fluid [28]. Application of these laws to the problems of interest results in the following set of partial differential equations:

Continuity

$$\left[\frac{\partial}{\partial x}(\rho u)+\frac{\partial}{\partial y}(\rho v)+\frac{\partial}{\partial z}(\rho w)\right] = 0 \qquad (2\text{-}1)$$

x-momentum

$$\left[\frac{\partial}{\partial x}(\rho uu)+\frac{\partial}{\partial y}(\rho vu)+\frac{\partial}{\partial z}(\rho wu)\right] = -\frac{\partial P}{\partial x}+\left[\frac{\partial}{\partial x}(\mu\frac{\partial u}{\partial x})+\frac{\partial}{\partial y}(\mu\frac{\partial u}{\partial y})+\frac{\partial}{\partial z}(\mu\frac{\partial u}{\partial z})\right] \qquad (2\text{-}2)$$

y-momentum

$$\left[\frac{\partial}{\partial x}(\rho uv)+\frac{\partial}{\partial y}(\rho vv)+\frac{\partial}{\partial z}(\rho wv)\right] = -\frac{\partial P}{\partial y}+\left[\frac{\partial}{\partial x}(\mu\frac{\partial v}{\partial x})+\frac{\partial}{\partial y}(\mu\frac{\partial v}{\partial y})+\frac{\partial}{\partial z}(\mu\frac{\partial v}{\partial z})\right] \qquad (2\text{-}3)$$

z-momentum

$$\left[\frac{\partial}{\partial x}(\rho uw)+\frac{\partial}{\partial y}(\rho vw)+\frac{\partial}{\partial z}(\rho ww)\right] = -\frac{\partial P}{\partial z}+\left[\frac{\partial}{\partial x}(\mu\frac{\partial w}{\partial x})+\frac{\partial}{\partial y}(\mu\frac{\partial w}{\partial y})+\frac{\partial}{\partial z}(\mu\frac{\partial w}{\partial z})\right] \qquad (2\text{-}4)$$

In the above equations, ρ and μ denote the fluid density and dynamic viscosity, respectively, and P is the pressure.

It is to be noted that, though the proposed numerical method can handle volumetric source terms in the x, y and z momentum equations, these terms are assumed to be negligible. In Eqns. (2-2)-(2-4), the terms enclosed in square brackets on the left-hand sides of these equations represent the rate of convection transport of momentum per unit volume, whereas the bracketed expressions on the right-hand sides of these equations denote the corresponding transport of momentum by "diffusion" or viscous action.

The foregoing set of equations constitutes an elliptic system which can be used for the description of most steady, laminar fluid flows [4]. In the parabolic fluid flow problems under consideration, however, it is reasonable to neglect the viscous stresses in the z-direction [6]. Thus the terms $(\mu \frac{\partial u}{\partial z})$, $(\mu \frac{\partial v}{\partial z})$ and $(\mu \frac{\partial w}{\partial z})$ can be dropped from Eqns. (2-2)-(2-4). Furthermore, the pressure gradient $(-\frac{\partial P}{\partial z})$ that drives the main flow may be decoupled from its lateral counterparts $(-\frac{\partial P}{\partial x})$ and $(-\frac{\partial P}{\partial y})$ [6]. This is done by decomposing the pressure P as follows:

$$P(x,y,z) = \bar{p}(z) + p(x,y,z), \tag{2-5}$$

where $\bar{p}$ is a cross-sectional average pressure defined as

$$\bar{p}(z) = \frac{1}{A} \int_A P(x,y,z)\,dxdy, \tag{2-6}$$

and p can be interpreted as a perturbation pressure. Assuming that $(\frac{\partial p}{\partial z}) << (\frac{d\bar{p}}{dz})$, it follows that

$$\left.\begin{aligned} \frac{\partial P}{\partial z} &\simeq \frac{d\bar{p}}{dz} \\ \frac{\partial P}{\partial y} &= \frac{\partial p}{\partial y} \\ \frac{\partial P}{\partial x} &= \frac{\partial p}{\partial x} \end{aligned}\right\} \quad (2\text{-}7)$$

The approximation (2-7) is, in general, reasonable for most straight unobstructed duct flows with no strong cross-stream velocities [6]. The above method of uncoupling the axial and transverse pressure gradients is due to Patankar and Spalding [6]; it is essential in keeping downstream influences from propagating upstream by way of the pressure transmission mechanism [5].

With the above-mentioned approximations, the equations governing fluid flow reduce to the following set of partial differential equations:

Continuity

$$\left[\frac{\partial}{\partial x}(\rho u) + \frac{\partial}{\partial y}(\rho v) + \frac{\partial}{\partial z}(\rho w)\right] = 0 \quad (2\text{-}8)$$

x-momentum

$$\left[\frac{\partial}{\partial x}(\rho uu) + \frac{\partial}{\partial y}(\rho vu) + \frac{\partial}{\partial z}(\rho wu)\right] = -\frac{\partial p}{\partial x} + \frac{\partial}{\partial x}(\mu\frac{\partial u}{\partial x}) + \frac{\partial}{\partial y}(\mu\frac{\partial u}{\partial y}) \quad (2\text{-}9)$$

y-momentum

$$\frac{\partial}{\partial x}(\rho uv)+\frac{\partial}{\partial y}(\rho vv)+\frac{\partial}{\partial z}(\rho wv) = -\frac{\partial p}{\partial y}+\frac{\partial}{\partial x}(\mu\frac{\partial v}{\partial x})+\frac{\partial}{\partial y}(\mu\frac{\partial v}{\partial y}) \qquad (2\text{-}10)$$

z-momentum

$$\frac{\partial}{\partial x}(\rho uw)+\frac{\partial}{\partial y}(\rho vw)+\frac{\partial}{\partial z}(\rho ww) = -\frac{d\bar{p}}{dz}+\frac{\partial}{\partial x}(\mu\frac{\partial w}{\partial x})+\frac{\partial}{\partial y}(\mu\frac{\partial w}{\partial y}) \qquad (2\text{-}11)$$

In addition, there is a constraint on the total mass flow rate through the duct. For steady flow in a duct with impermeable walls, this leads to the following equation:

$$\dot{m} = \int_{\substack{\text{Cross-sectional}\\ \text{Area}}} \rho w dA = \text{constant} \qquad (2\text{-}12)$$

The set of equations (2-8)-(2-12) form a parabolic system which can be solved by stepwise integration in the z-direction. The unknowns in these equations are u, v, w, p and $(-\frac{d\bar{p}}{dz})$ [†], and thus the total number of unknowns matches the number of equations. To specify the problem completely, however, two types of auxiliary equations are required: initial and boundary conditions. They are described below.

[†] $(-\frac{d\bar{p}}{dz})$ shall be treated as unknown here, rather than $\bar{p}$ itself, mainly for calculation convenience; $\bar{p}$ can be obtained from $(-\frac{d\bar{p}}{dz})$ by a straightforward integration.

Initial and Boundary Conditions

The proposed numerical method can handle any commonly encountered flow conditions at the duct entrance (z=0). In the testing and application of the method, however, uniform flow at constant pressure is assumed at the inlet. Mathematically, this can be expressed as follows:

$$\left.\begin{aligned} w(x,y,0) &= \bar{w} \ , \\ u(x,y,0) &= v(x,y,0) = 0 \ , \\ p(x,y,0) &= 0 \ , \ \bar{p}(0) = p_i \ , \end{aligned}\right\} \quad (2\text{-}13)$$

where p_i is a constant and $\bar{w}$ is the mean axial velocity defined by

$$\bar{w} = \dot{m}/\rho A. \quad (2\text{-}14)$$

For steady incompressible fluid flow in constant area ducts with impermeable walls, $\bar{w}$ is a constant.

The no-slip and impermeability conditions imply that

$$u = v = w = 0, \text{ on the duct walls.} \quad (2\text{-}15)$$

Nondimensionalization

The following nondimensional variables are used in the analysis of fluid flow problems:

$$x^* = \frac{x}{D_H}, \qquad y^* = \frac{Y}{D_H}, \qquad z^* = \frac{z}{D_H\,Re}, \tag{2-16}$$

$$u^* = \frac{u}{(\nu/D_H)}, \quad v^* = \frac{v}{(\nu/D_H)}, \quad w^* = \frac{w}{\bar{w}}, \tag{2-17}$$

$$p^* = \frac{p}{\rho(\frac{\nu}{D_H})^2}, \qquad \bar{p}^* = \frac{\bar{p}-p_i}{\rho\bar{w}^2} \tag{2-18}$$

where D_H is the hydraulic diameter defined as

$$D_H = \frac{4(\text{Cross-sectional area for flow})}{(\text{Wetted perimeter})} = \frac{4A}{P}, \tag{2-19}$$

ν is the kinematic viscosity ($= \mu/\rho$) and Re denotes the Reynolds number:

$$Re = \frac{\rho\bar{w}D_H}{\mu}.$$

Upon substitution of these nondimensional variables into Eqns. (2-8)-(2-11), the governing equations become:

Continuity

$$\left[\frac{\partial u^*}{\partial x^*} + \frac{\partial v^*}{\partial y^*} + \frac{\partial w^*}{\partial z^*}\right] = 0 \tag{2-20}$$

x-momentum

$$\left[\frac{\partial}{\partial x^*}(u^*u^*) + \frac{\partial}{\partial y^*}(v^*u^*) + \frac{\partial}{\partial z^*}(w^*u^*)\right] = -\frac{\partial p^*}{\partial x^*} + \left[\frac{\partial^2 u^*}{\partial x^{*2}} + \frac{\partial^2 u^*}{\partial y^{*2}}\right] \tag{2-21}$$

y-momentum

$$\left[\frac{\partial}{\partial x^*}(u^*v^*) + \frac{\partial}{\partial y^*}(v^*v^*) + \frac{\partial}{\partial z^*}(w^*v^*)\right] = -\frac{\partial p^*}{\partial y^*} + \left[\frac{\partial^2 v^*}{\partial x^{*2}} + \frac{\partial^2 v^*}{\partial y^{*2}}\right] \quad (2\text{-}22)$$

z-momentum

$$\left[\frac{\partial}{\partial x^*}(u^*w^*) + \frac{\partial}{\partial y^*}(v^*w^*) + \frac{\partial}{\partial z^*}(w^*w^*)\right] = -\frac{d\bar{p}^*}{dz^*} + \left[\frac{\partial^2 w^*}{\partial x^{*2}} + \frac{\partial^2 w^*}{\partial y^{*2}}\right] \quad (2\text{-}23)$$

In terms of the nondimensional variables defined in Eqn. (2-17), the initial conditions given by Eqn. (2-13) can be written as follows:

$$w^*(x^*,y^*,0) = 1,$$
$$u^*(x^*,y^*,0) = v^*(x^*,y^*,0) = 0, \quad (2\text{-}24)$$
and $$p^* = \bar{p}^* = 0.$$

Similarly, the boundary conditions are

$$u^* = v^* = w^* = 0, \text{ on the duct walls.} \quad (2\text{-}25)$$

It is to be noted that, with this nondimensionalization, the Reynolds number does not appear explicitly in Eqns. (2-20)-(2-25). Thus the only parameter in the flow problems considered in this thesis is the duct geometry.

2.2.2 Specialization to the Fully-Developed Regime

In a region sufficiently downstream from the entrance of the duct, the fluid velocity distribution ceases to change with the axial distance. This velocity profile is called the fully-developed velocity profile. Fully-developed flows are usually grouped into two categories: "simple" and "complex" fully-developed flows. In the former, no cross-stream velocities exist: $u=v=0$, and $w=w(x,y)$. Laminar fully-developed flows in straight uniform ducts fall into this category. In complex fully-developed flows, cross-stream velocities are present but are invariant with z: $u=u(x,y)$, $v=v(x,y)$ and $w=w(x,y)$. Examples of such flows include fully-developed flows in curved ducts and fully-developed flows affected by buoyancy forces. In this thesis, attention is focused exclusively on "simple" fully-developed flows.

For simple fully-developed flows, the continuity equation and the x- and y-momentum equations, Eqns. (2-8)-(2-10), are satisfied identically; and the z-momentum equation, Eqn. (2-11), now becomes

$$\mu\left[\frac{\partial^2 w}{\partial x^2} + \frac{\partial^2 w}{\partial y^2}\right] = \frac{d\bar{p}}{dz} \qquad (2\text{-}26)$$

where $(\frac{d\bar{p}}{dz})$ is a constant. The mean pressure $\bar{p}$ is now the same as P since the pressure is constant over the cross-section in the absence of any secondary flow. Eqn. (2-26) is a statement of the exact balance between viscous forces

(left-hand side) and pressure forces (right-hand side); it has the form of a standard Poisson equation.

A convenient dimensionless form of Eqn. (2-26) can be obtained by defining a new nondimensional axial velocity W as follows:

$$W \triangleq \frac{w}{\left(\frac{D_H^2}{\mu}\right)\left(-\frac{d\bar{p}}{dz}\right)} \tag{2-27}$$

In terms of this nondimensional velocity and the nondimensional coordinates introduced in Eqn. (2-16), Eqn. (2-26) can be written in the following compact form:

$$\frac{\partial^2 W}{\partial x^{*2}} + \frac{\partial^2 W}{\partial y^{*2}} + 1 = 0. \tag{2-28}$$

On the duct walls, the no-slip condition implies

$$W\Big|_{\text{duct walls}} = 0. \tag{2-29}$$

It is customary to present simple fully-developed duct flow results in terms of the product of a friction factor and the Reynolds number [7]. In such flows, this product is only a function of the duct geometry. The friction factor is defined by

$$f \triangleq \frac{(-\frac{d\bar{p}}{dz}) D_H}{\frac{1}{2} \rho \bar{w}^2} . \qquad (2\text{-}30)$$

The friction factor - Reynolds number product can then be obtained from

$$f \cdot Re = \frac{2}{\bar{W}} , \qquad (2\text{-}31)$$

where $\bar{W}$ is the average nondimensional velocity:

$$\bar{W} = \frac{\bar{w}}{[\frac{D_H}{\mu}]^2 (-\frac{d\bar{p}}{dz})} \qquad (2\text{-}32)$$

2.3 HEAT TRANSFER ANALYSIS: PRESCRIBED CONSTANT DUCT WALL TEMPERATURE (T)

In this section, the equations which govern laminar convection heat transfer in a duct with its walls maintained at a constant temperature T_w are presented. These equations can be derived by an appropriate combination of the law of conservation of energy and Fourier's law of heat conduction [28]. It is to be noted that this thermal boundary condition of constant duct wall temperature is denoted by the symbol (T) throughout this thesis. As was done in the description of the fluid flow problem, attention is focused on both the developing and the fully-developed regions.

2.3.1 Thermally Developing Regime

For steady duct flow and heat transfer problems being considered in this thesis, the energy equation may be written as follows [28]:

$$\left[\frac{\partial}{\partial x}(\rho u\, c_p\, T)+ \frac{\partial}{\partial y}(\rho v\, c_p\, T)+ \frac{\partial}{\partial z}(\rho w\, c_p\, T)\right] =$$

$$\left[\frac{\partial}{\partial x}\left(k\, \frac{\partial T}{\partial x}\right) + \frac{\partial}{\partial y}\left(k\, \frac{\partial T}{\partial y}\right)+ \frac{\partial}{\partial z}\left(k\, \frac{\partial T}{\partial z}\right)\right] \qquad (2\text{-}33)$$

where c_p and k are the specific heat at constant pressure and thermal conductivity of the fluid, respectively, and T denotes the fluid temperature. In Eqn. (2-33), the assumption has been made that no internal heat source or sink exists in the duct. The left-hand side of this equation represents the rate of transport of specific enthalpy per unit volume by convection and the bracketed term on the right-hand side denotes the rate of transport of energy per unit volume by conduction.

In the parabolic problems of interest in this thesis, the streamwise heat conduction term $\frac{\partial}{\partial z}\left(k\, \frac{\partial T}{\partial z}\right)$ is negligibly small in comparison to the convection term $\frac{\partial(\rho w\, c_p\, T)}{\partial z}$. Neglecting this term therefore, Eqn. (2-33) reduces to the following form:

$$\left[\frac{\partial}{\partial x}(\rho u\, c_p\, T) + \frac{\partial}{\partial y}(\rho v\, c_p\, T) + \frac{\partial}{\partial z}(\rho w\, c_p\, T) \right] =$$

$$\left[\frac{\partial}{\partial x}\left(k \frac{\partial T}{\partial x}\right) + \frac{\partial}{\partial y}\left(k \frac{\partial T}{\partial y}\right) \right] \qquad (2\text{-}34)$$

For a complete specification of the problem, thermal initial and boundary conditions are required.

Initial and Boundary Conditions

The proposed numerical method can handle any commonly-encountered distribution of temperature at the inlet of the duct ($z = 0$). In the testing and application of this method, however, a uniform temperature distribution is assumed at the duct inlet:

$$T(x,y,0) = T_i = \text{constant}. \qquad (2\text{-}35)$$

The duct walls are maintained at a constant temperature, T_w; thus

$$T = T_w = \text{constant, on the duct walls}. \qquad (2\text{-}36)$$

Nondimensionalization

Using the nondimensionalization already introduced in Eqns. (2-16) and (2-17), and defining a dimensionless temperature for the (T) boundary condition as

$$T^* \triangleq \frac{T - T_i}{T_w - T_i} \tag{2-37}$$

the parabolized energy equation (2-34) can be written as follows:

$$\left[\frac{\partial}{\partial x^*}(u^*T^*) + \frac{\partial}{\partial y^*}(v^*T^*) + \frac{\partial}{\partial z^*}(w^*T^*)\right] = \frac{1}{Pr}\left[\frac{\partial^2 T^*}{\partial x^{*2}} + \frac{\partial^2 T^*}{\partial y^{*2}}\right] \tag{2-38}$$

where Pr is the Prandtl number:

$$Pr = \frac{\mu c_p}{k} .$$

Similarly, the initial and boundary conditions can be expressed in nondimensional form as

$$T^*(x^*,y^*,0) = 0 , \tag{2-39}$$

$$T^* = 1 , \text{ on the duct walls.} \tag{2-40}$$

An examination of Eqn. (2-38) shows that the duct geometry and the Prandtl number of the fluid are the only parameters in this heat transfer problem.

The peripherally-averaged local Nusselt number is defined as

$$Nu_{z,(T)} = \frac{q_z D_H}{(T_w - T_b)k} \tag{2-41}$$

where q_z is the peripherally-averaged wall heat flux at axial location z; it can be obtained from an energy balance over a portion of the duct of length dz:

$$q_z = \left(\frac{dT_b}{dz}\right)\left(\frac{\rho A \bar{w} c_p}{P}\right) \tag{2-42}$$

where A represents the cross-sectional area for flow, P is the heated perimeter of the duct, and T_b is the bulk temperature defined by

$$T_b = \frac{\int_A \rho w c_p T \, dA}{\int_A \rho w c_p \, dA} . \tag{2-43}$$

Eqn. (2-42) can be substituted into Eqn. (2-41) to get:

$$Nu_{z,(T)} = \left(\frac{D_H}{4}\right)\left(\frac{Re\ Pr}{(T_w - T_b)}\right)\left(\frac{dT_b}{dz}\right) \tag{2-44}$$

and in terms of the dimensionless quantities introduced earlier,

$$Nu_{z,(T)} = \frac{1}{4} \frac{Pr}{(1-T_b^*)} \frac{dT_b^*}{dz^*} . \tag{2-45}$$

Often, in heat exchanger analysis, a flow length average Nusselt number is more useful than the peripherally-averaged local Nusselt number. The former is defined as

$$Nu_{m,\textcircled{T}} \triangleq \frac{1}{z}\int_0^z Nu_{z,\textcircled{T}}\,dz \ . \tag{2-46}$$

It can be shown that, for the $\textcircled{T}$ boundary condition,

$$Nu_{m,\textcircled{T}} = \frac{q_m D_H}{k(\Delta T)_{LMTD}} \tag{2-47}$$

where $(\Delta T)_{LMTD}$ is the log-mean temperature difference

$$(\Delta T)_{LMTD} = \frac{(T_w-T_i) - (T_w-T_b(z))}{\ell n\left(\frac{T_w-T_i}{T_w-T_b(z)}\right)} \tag{2-48}$$

and q_m is the mean duct wall heat flux from 0 to z.

2.3.2 Specialization to the Thermally Fully-Developed Regime

In this problem, the fluid temperature T starts from the specified initial conditions at the inlet and eventually reaches the wall temperature T_w. The duct region in which $T \simeq T_w$ is uninteresting, since the temperature is constant everywhere and no heat transfer occurs. However, much before

this uninteresting region is reached, a dimensionless temperature θ defined as

$$\theta \triangleq \frac{T_w - T}{T_w - T_b} \tag{2-49}$$

becomes invariant with z. The portion of the duct where this happens is referred to as the thermally fully-developed region [7].

The energy equation under fully-developed flow conditions can be written as

$$\left[\frac{\partial}{\partial z}(\rho w\ c_p\ T)\right] = \left[\frac{\partial}{\partial x}\left(k\ \frac{\partial T}{\partial x}\right) + \frac{\partial}{\partial y}\left(k\ \frac{\partial T}{\partial y}\right)\right]. \tag{2-50}$$

In terms of θ, x* and y*, this equation becomes

$$\rho w\ c_p\ \theta\ \frac{dT_b}{dz} = -\ k\ \frac{(T_w - T_b)}{D_H^2}\left[\frac{\partial^2 \theta}{\partial x^{*2}} + \frac{\partial^2 \theta}{\partial y^{*2}}\right]. \tag{2-51}$$

An overall energy balance over a slice of the duct of thickness dz gives

$$\frac{dT_b}{dz} = \frac{q_z\ P}{\dot{m}\ c_p} \tag{2-52}$$

Using Eqn. (2-52), the energy equation can be rewritten in the following form:

$$\frac{\partial^2 \theta}{\partial x^{*2}} + \frac{\partial^2 \theta}{\partial y^{*2}} + \frac{W}{\bar{W}}\lambda\ \theta = 0 \tag{2-53}$$

where

$$\lambda = 4 \left(\frac{D_H}{k}\right) \frac{q_z}{T_w - T_b} \qquad (2\text{-}54)$$

In the thermally fully-developed region, $\theta = \theta(x^*,y^*)$ and it can be shown [7] that λ is a constant.

At this stage, it is convenient to introduce a scaled temperature $\Theta \triangleq \theta/\lambda$ [31]. Since λ is a constant, the energy equation in terms of Θ has the same form as Eqn. (2-53):

$$\frac{\partial^2 \Theta}{\partial x^{*2}} + \frac{\partial^2 \Theta}{\partial y^{*2}} + \frac{W}{\bar{W}} \lambda \Theta = 0 \qquad (2\text{-}55)$$

The boundary condition for Θ is

$$\Theta = 0 \text{ , on the duct walls.} \qquad (2\text{-}56)$$

Subject to this boundary condition, Eqn. (2-55) poses an eigenvalue problem, with λ as the unknown eigenvalue. The value of λ must be such that the solution Θ is compatible with the definition of bulk temperature. This compatibility criterion leads to the following relation for λ:

$$\lambda = \frac{1}{\int_A \frac{W}{\bar{W}} \Theta \, dA} \qquad (2\text{-}57)$$

The above treatment of the energy equation in the thermally fully-developed regime is due to Sparrow et al. [31]. It is to be noted that the Prandtl number Pr does not appear in Eqns. (2-55)-(2-57). Therefore, it is not a parameter in the fully-developed regime.

The overall Nusselt number in the thermally fully-developed region is defined by

$$Nu_{(T)} \triangleq \frac{\bar{h} D_H}{k} = \frac{\lambda}{4} \qquad (2-58)$$

where $\bar{h}$ is the average heat transfer coefficient.

2.4 HEAT TRANSFER ANALYSIS: PRESCRIBED UNIFORM WALL HEAT FLUX (H)

In this section, consideration is given to the situation where a constant rate of heat transfer per unit area is imposed on the duct walls. This thermal boundary condition is denoted by (H) in this thesis. As before, the analyses of thermally developing and fully-developed regimes are presented in sequence in this section.

2.4.1 Thermally Developing Regime

Since only the thermal boundary condition is different from that in the previous section, the same governing equation, Eqn. (2-34), applies:

$$\left[\frac{\partial}{\partial x}(\rho u\, c_p\, T) + \frac{\partial}{\partial y}(\rho v\, c_p\, T) + \frac{\partial}{\partial z}(\rho w\, c_p\, T)\right] =$$

$$\left[\frac{\partial}{\partial x}\left(k\,\frac{\partial T}{\partial x}\right) + \frac{\partial}{\partial y}\left(k\,\frac{\partial T}{\partial y}\right)\right] \qquad (2\text{-}34)$$

It is again emphasized that any of the commonly-encountered initial conditions can be handled by the proposed numerical method. In the testing and application of this method, however, the following initial condition is used:

$$T(x,y,0) = T_i = \text{constant.} \qquad (2\text{-}59)$$

The thermal boundary condition in this problem is

$$k\left.\frac{\partial T}{\partial n}\right|_{\text{wall}} = q_w = \text{constant,} \qquad (2\text{-}60)$$

where n denotes the outward normal to the duct walls and q_w is the prescribed wall heat flux.

By defining a dimensionless temperature t* as

$$t^* \triangleq \frac{T - T_i}{(q_w\, D_H / k)} \qquad (2\text{-}61)$$

and making use of the nondimensional variables introduced in Eqns. (2-16) and (2-17), the following convenient dimensionless form of the energy equation can be arrived at:

$$\left[\frac{\partial}{\partial x^*}(u^*t^*)+\frac{\partial}{\partial y^*}(v^*t^*)+\frac{\partial}{\partial z^*}(w^*t^*)\right]=\frac{1}{Pr}\left[\frac{\partial^2 t^*}{\partial x^{*2}}+\frac{\partial^2 t^*}{\partial y^{*2}}\right] \qquad (2\text{-}62)$$

Examination of Eqn. (2-62) shows that it has the same form as Eqn. (2-38) for the (T) boundary condition. Again, the Prandtl number and the geometry of the duct are the only parameters in this problem.

In terms of the dimensionless temperature t*, the initial and boundary conditions may be rewritten as

$$t^*(x^*,y^*,0) = 0 \qquad (2\text{-}63)$$

and

$$\left.\frac{\partial t^*}{\partial n^*}\right|_{\text{wall}} = 1 \qquad (2\text{-}64)$$

where n* is the normalized outward normal (= n/D_H).

The local peripherally-averaged Nusselt number is defined as follows:

$$Nu_{z,\,(H)} \triangleq \frac{q_w D_H}{(\overline{T}_w - T_b)k} \qquad (2\text{-}65)$$

where $\overline{T}_w$ is a peripheral mean wall temperature. This Nusselt number definition is consistent with that suggested by Shah and London [7].

Eqn. (2-65) can be rewritten in terms of the non-dimensional variables defined earlier as

$$Nu_{z,\,(H)} = \frac{1}{(\bar{t}^*_w - t^*_b)} \tag{2-66}$$

A flow length average Nusselt number can be arrived at, as before, by integration of the local peripherally-averaged Nusselt number:

$$Nu_{m,\,(H)} = \frac{1}{z}\int_0^z Nu_{z,\,(H)}\, dz \tag{2-67}$$

2.4.2 Specialization to the Thermally Fully-Developed Regime

The applicable governing equation here is the same as that for the (T) boundary condition:

$$\frac{\partial}{\partial z}(\rho w\, c_p\, T) = \frac{\partial}{\partial x}(k\,\frac{\partial T}{\partial x}) + \frac{\partial}{\partial y}(k\,\frac{\partial T}{\partial y}) \ . \tag{2-50}$$

In the thermally developed region in this problem,

$$\frac{\partial T}{\partial z} = \frac{dT_b}{dz} = \frac{q_w\, P}{\dot{m}\, c_p} = \text{constant.} \tag{2-68}$$

Let

$$\chi \triangleq \frac{T - T_b}{(q_w\, D_H/k)} \tag{2-69}$$

Using Eqn. (2-68), it can be shown that this nondimensional temperature is invariant with z in the thermally fully-developed region. Using χ and Eqn. (2-68), Eqn. (2-50) can be nondimensionalized as follows:

$$\frac{\partial^2 \chi}{\partial x^{*2}} + \frac{\partial^2 \chi}{\partial y^{*2}} - 4\left(\frac{W}{\overline{W}}\right) = 0 , \qquad (2\text{-}70)$$

where $(W/\overline{W})$ is obtained from the solution of the fully-developed fluid flow analysis. On the walls of the duct,

$$\frac{\partial \chi}{\partial n^*} = 1 \qquad (2\text{-}71)$$

Eqn. (2-71) is a Neumann-type boundary condition; it determines the shape of the χ distribution, but it does not fix the level of χ uniquely. However, from the definition of χ in Eqn. (2-69), it follows that:

$$\chi_b = 0 . \qquad (2\text{-}72)$$

This condition can be used to establish a unique solution for χ.

A peripherally-averaged Nusselt number has already been defined in Eqn. (2-65) for the thermally developing region. In the fully-developed region, this reduces to the following form:

$$Nu_{(H)} = \frac{q_w D_H}{(\bar{T}_w - T_b)k} = \frac{1}{\bar{\chi}_w}, \qquad (2\text{-}73)$$

where $\bar{\chi}_w$ is the average of χ over the periphery.

2.5 GENERAL FORM OF THE GOVERNING EQUATIONS

All governing equations presented in the previous sections of this chapter can be cast into the following general form:

$$\left[\frac{\partial}{\partial x}(\rho u\phi) + \frac{\partial}{\partial y}(\rho v\phi) + \frac{\partial}{\partial z}(\rho w\phi)\right] = \left[\frac{\partial}{\partial x}\left(\Gamma \frac{\partial \phi}{\partial x}\right) + \frac{\partial}{\partial y}\left(\Gamma \frac{\partial \phi}{\partial y}\right)\right] + S \qquad (2\text{-}74)$$

where ϕ is a general scalar dependent variable, Γ is the corresponding diffusion coefficient and S is interpreted as a volumetric generation or "source" term of ϕ. The left-hand side of Eqn. (2-74) represents the rate of convection transport of ϕ per unit volume and the expression enclosed in square brackets on the right-hand side represents the rate of transport of ϕ per unit volume by diffusion.

Table 2-1 shows how the various governing equations presented in the previous sections of this chapter can be obtained from Eqn. (2-74) by assigning particular meanings to ϕ, Γ and S. It is to be noted that the velocity components u, v, w and the coordinates x,y,z in Eqn. (2-74) are

dimensional or nondimensional depending on whether ϕ is dimensional or nondimensional.

The recognition that all relevant governing equations possess a general common form offers significant advantages in the formulation and computer implementation of a general numerical solution procedure [4].

2.6 CONCLUDING REMARKS

In this thesis, three classes of duct flow and heat transfer problems are considered. In one, it is assumed that hydrodynamically and thermally fully-developed conditions prevail; this situation occurs in regions sufficiently downstream from the duct entrance. In the second class of problems, the velocity profile is considered to be fully-developed while the temperature field develops. The last class of problems deals with the situation in which both velocity and temperature fields develop simultaneously.

In all the above problems, since the fluid properties are assumed to be constant, the solution of the flow field can be obtained without a knowledge of the temperature distribution. Once the solution of the flow field has been obtained, it is used as an input in the energy equation: at this stage, the energy equation is a linear convection-diffusion equation [4] which can be solved to obtain the temperature field.

The developing duct flow and heat transfer problems considered in this thesis are parabolic in nature: the

conditions at a point in the flow can influence conditions at downstream points but not vice-versa. Thus a marching integration procedure can be used to solve these problems: starting with a specified set of initial conditions at the inlet of the duct, a step-by-step procedure can be used to advance the solution downstream. This feature of the problems of interest offers considerable advantages in the formulation and computer implementation of the proposed numerical method.

CHAPTER III

FORMULATION OF THE NUMERICAL METHOD

The formulation of a control-volume finite-element method for the solution of three-dimensional parabolic flow and heat transfer in ducts is presented in this chapter. In the construction of this method, some key ideas of two existing methods are used: a control-volume finite-element method proposed by Baliga and Patankar [1,2] for two-dimensional elliptic situations; and a finite-difference method developed by Patankar and Spalding [6] for three-dimensional parabolic flows.

Standard finite-element methods have the following characteristic features: (1) the calculation domain is divided or discretized into non-overlapping subdomains or elements of simple geometric shapes; (2) the dependent variables are interpolated in each element by suitably-chosen shape or interpolation functions; (3) discretization equations are obtained by using a variational method or the Galerkin method of weighted residuals; and (4) an element-by-element assembly is used to compile the global discretization equations. The proposed numerical method has all of these characteristics but differs from a standard finite-element formulation in that a control volume approach rather than the Galerkin technique is used to obtain the discretization equations. Therefore, it was decided that the method could be considered as a

finite-element method, with the term 'control-volume' used as a qualifier.

Details of the various building blocks of the proposed method are given in the following sections.

3.1 DOMAIN DISCRETIZATION

The calculation domains in the problems of interest in this thesis are straight uniform ducts of regular- or irregular-shaped cross-sections; an example is given in Fig.3-1(a). In the proposed domain discretization scheme, the duct is first sectioned into a series of slabs perpendicular to the z-axis, as shown in Fig. 3-1(b). Each slab can be viewed as being made up of two adjacent parallel cross-sectional planes. Different slabs need not have the same thickness; indeed, in the numerical prediction of developing flows and heat transfer, the ability to work with a nonuniform distribution of axial step size Δz, which is the slab thickness in this case, is crucial to the formulation of computationally-efficient methods.

Following the division of the calculation domain into slabs, the cross-section of each of the slabs is further discretized using a four-stage procedure illustrated in Figs. 3-2(a) to 3-2(d): first, it is divided into six-node triangular macroelements; then each six-node element is divided into four three-node triangular subelements by joining the midpoints of its sides; following that, all nodes of the three-node triangular elements are associated with control

volumes of polygonal cross-section; finally, the vertices of the six-node triangular elements are associated with a separate set of control volumes of polygonal cross-section. This cross-sectional discretization is swept through each slab in the axial direction to generate the three-dimensional grid. This procedure divides each slab into prism-shaped elements of triangular cross-section and prism-shaped control volumes of polygonal cross-section. In the proposed method, all slabs are discretized in the same manner.

A typical prism macroelement and its four subelements are shown in Fig. 3-3(a). In each cross-section, all dependent variables other than the pressure are stored at all six nodes of each macroelement; the pressure is stored only at the vertices of the macroelements. Thus the pressure field is discretized by a coarser grid than that used to discretize other dependent variables. This unequal-order pressure-velocity discretization scheme is one way of avoiding physically unrealistic checkerboard-type pressure fields that commonly afflict equal-order finite-element methods [32,33].

The polygonal cross-sections of the prism-shaped control-volumes are generated by joining the centroids of the triangular elements to the midpoints of the corresponding sides: application of this procedure to triangular subelements generates the cross-sections of subelement control volumes shown in Fig. 3-2(c); the cross-sections of the macroelement control volumes shown in Fig. 3-2(d) are obtained by applying this procedure to the six-node triangular macroelements.

Typical prism-shaped subelement and macroelement control volumes and the associated nomenclature are illustrated in Figs. 3-3(b) and 3-3(c), respectively. It is to be noted that this method of generating control volumes can be used with any triangulation of the duct cross-sectional planes, including those involving obtuse triangles. Furthermore, the subelement control volumes do not overlap, their boundaries do not involve interelement surfaces, and collectively, they fill the calculation domain completely. The macroelement control volumes also possess these desirable features.

In the proposed method, triangular elements are preferred to quadrilateral elements in the discretization of cross-sectional planes for the following reasons: general quadrilateral elements necessitate the use of isoparametric transformations [34], but the triangular elements used here are free from this complication; for the same number of nodes, triangles provide greater flexibility than quadrilaterals in the distribution of the nodes inside the calculation domain; and highly irregular-shaped cross-sections can be more easily divided into triangles than into quadrilaterals. If the duct cross-section is bounded by curved lines, it is approximated by piecewise-straight lines, and the resulting polygonal region is assumed to be the calculation domain; a triangulation using macroelements and subelements is then possible.

The local node numbering and labelling schemes shown in Fig. 3-3 are used in presenting the formulation of the proposed numerical method. In each cross-sectional plane, the

vertices of a typical six-node macroelement are numbered 1, 2 and 3, and the mid-side nodes are numbered 4, 5 and 6, as shown in Fig. 3-3(a). The centroid of the macroelement 123 is denoted by O and that of the subelement 165 is called o. The same node numbers and labels are used in the upstream and downstream planes of the typical prism-shaped macroelement shown in Fig. 3-3(a); this is done mainly to avoid the use of too many subscripts and superscripts in subsequent discussions. The values of a dependent variable ϕ at upstream and downstream nodes are denoted by ϕ^U and ϕ^D, respectively; if a dependent variable is not superscripted, it is to be understood that it pertains to downstream nodes.

Fig. 3-4(a) shows the different subelement control volume faces associated with the typical subelement 165. Macroelement control volume faces associated with the typical macroelement 123 are illustrated in Fig. 3-4(b). The notation presented in these figures is used in all discussions presented in the remainder of this thesis.

3.2 CONTROL-VOLUME CONSERVATION EQUATIONS

The differential equations which govern the duct flow and heat transfer problems being considered in this thesis were presented in Chapter II. In addition, it was shown that all these equations can be considered as particular forms of the following general differential equation:

$$\left[\frac{\partial}{\partial x}(\rho u\phi)+\frac{\partial}{\partial y}(\rho v\phi)+\frac{\partial}{\partial z}(\rho w\phi)\right] = \left[\frac{\partial}{\partial x}(\Gamma\frac{\partial\phi}{\partial x})+\frac{\partial}{\partial y}(\Gamma\frac{\partial\phi}{\partial y})\right] + S \qquad (2\text{-}74)$$

In vector notation, this equation may be rewritten as follows:

$$\text{div}(\vec{J}) = S \qquad (3\text{-}1)$$

where $\vec{J}$ is the combined convection and diffusion flux of ϕ:

$$\vec{J} = [\rho u\phi - \Gamma\frac{\partial\phi}{\partial x}]\,\vec{i} + [\rho v\phi - \Gamma\frac{\partial\phi}{\partial y}]\,\vec{j} + [\rho w\phi]\,\vec{k}\,. \qquad (3\text{-}2)$$

In Eqn. (3-2), $\vec{i}$, $\vec{j}$ and $\vec{k}$ are unit vectors in the x, y and z directions, respectively. It is to be noted that the component of $\vec{J}$ in the z-direction represents only the convection of ϕ in that direction; in parabolic duct flow and heat transfer, the diffusion transport of ϕ in the z-direction is negligible compared to the corresponding convection transport.

An integral conservation equation corresponding to Eqn. (3-1) can be obtained by integrating it over a control volume V and using the Gauss divergence theorem:

$$\int_{\partial V}\vec{J}\cdot\vec{n}\,ds - \int_{V}S\,dV = 0 \qquad (3\text{-}3)$$

where ∂V is the boundary surface of the control volume and $\vec{n}$ is the unit <u>outward</u> normal to the infinitesimal surface area ds.

Consider the typical subelement 165 shown in Figs. 3-3(b) and 3-4(a). When applied to the subelement control volume associated with node 1, the integral conservation equation for ϕ can be written as follows:

$$\left[\int_{u_1} \vec{J}\cdot\vec{n}\,ds + \int_{d_1} \vec{J}\cdot\vec{n}\,ds + \int_{a} \vec{J}\cdot\vec{n}\,ds + \int_{c} \vec{J}\cdot\vec{n}\,ds - \int_{v_1} S\,dV\right]$$

$$+ \left[\begin{array}{l}\text{similar contributions from other}\\ \text{subelements associated with node 1}\end{array}\right]$$

$$+ [\text{boundary contributions, if applicable}] = 0 \qquad (3\text{-}4)$$

The form of Eqn. (3-4) emphasizes that it can be assembled by using an element-by-element procedure.

In the proposed method, the momentum conservation equations are also imposed on subelement control volumes. Thus, the integral momentum equations in the x, y and z directions can be obtained from Eqns. (3-2) and (3-4), with the appropriate interpretations of ϕ, Γ and S given in Table 2-1.

In the incompressible duct flow problems being considered in this thesis, there are no explicit equations which govern the cross-sectional pressure p and the axial gradient of the cross-sectional average pressure $(d\bar{p}/dz)$. They are both indirectly specified: substitution of correct values of p and $(d\bar{p}/dz)$ into the momentum equations yields a

velocity distribution that also satisfies the local continuity equation, Eqn. (2-8), and the overall continuity equation, Eqn. (2-12). In the proposed method, the mass conservation equation, corresponding to the integral form of Eqn. (2-8), is imposed on the macroelement control volumes shown in Fig. 3-2(d) and Fig. 3-3(c). With reference to the macroelement control volume surrounding node 1 in Fig. 3-4(b), this equation can be written as follows:

$$\left[\int_{U_1} \rho \vec{v} \cdot \vec{n} \, ds + \int_{D_1} \rho \vec{v} \cdot \vec{n} \, ds + \int_{A} \rho \vec{v} \cdot \vec{n} \, ds + \int_{C} \rho \vec{v} \cdot \vec{n} \, ds \right]$$

$$+ \left[\begin{array}{l} \text{similar contributions from other} \\ \text{macroelements associated with node 1} \end{array} \right]$$

$$+ [\text{boundary contributions, if applicable}] = 0 \, . \qquad (3\text{-}5)$$

Eqn. (3-5) can be assembled by using a macroelement-by-macroelement procedure.

3.3 INTERPOLATION FUNCTIONS

The derivation of algebraic approximations to the control-volume conservation equations discussed in the last section requires the specification of element interpolation functions for all dependent variables, the corresponding diffusion coefficients and source terms, and the mass density. These interpolation functions approximate the variation of

the variables of interest: (a) along the duct axis, and (b) in the duct cross-section. The following discussion is categorized accordingly.

3.3.1 . z-Direction Interpolation Functions

In the z-direction, within each element, the downstream values of all dependent variables (ϕ,u,v,w,p and $d\bar{p}/dz$) and properties (ρ, Γ and S) are assumed to prevail over the axial step size Δz. A graphical representation of the corresponding interpolation function for the scalar dependent variable ϕ is shown by the solid line in Fig. 3-5.

This interpolation practice is equivalent to the so-called fully-implicit formulation used in the numerical solution of parabolic problems [4]. The other well-known formulations for parabolic problems are the so-called Crank-Nicolson and explicit methods [4]. Of the three interpolation functions shown in Fig. 3-5, the one corresponding to the fully-implicit formulation does not necessarily lead to the most accurate method for all values of Δz and flow conditions. However, the other two interpolation practices require stability-related limitations on the axial step size Δz, which could get unusually restrictive under certain flow conditions; but the fully-implicit formulation imposes no such limitations [4]. It is for this reason that the fully-implicit formulation is adopted in the proposed method.

3.3.2 Cross-Sectional Interpolation Functions

Interpolation function for ρ, Γ and S

In the duct cross-section, the values of ρ and Γ at the centroids of the triangular subelements are stored, and they are assumed to prevail over the corresponding elements.

The source term S is, in general, a function of ϕ; it can be expressed in the following form [4]:

$$S = S_C + S_P\phi \tag{3-6}$$

If the dependence of S on ϕ is non-linear, appropriate linearization techniques can be used to cast it in the form given by Eqn. (3-6). Such techniques are described and discussed in [4]. The values of S_C and S_P are stored at the centroids of the subelements and assumed to prevail over the corresponding subelements.

Interpolation functions for the general dependent variable ϕ

All integral terms appearing in Eqn. (3-4) contain the dependent variable ϕ. In the derivation of algebraic approximations to these different integrals, it is not necessary to use the same interpolation function for ϕ. Indeed, in the formulation of computationally efficient and stable numerical methods, it is usually necessary to use different interpolation functions to approximate the different integral

terms in the control-volume conservation equations [2,4]. In the proposed method, in the integral involving the source term S and in the integrals representing the convective transport of ϕ across cross-sectional faces, such as u_1 and d_1 shown in Fig. 3-4(a), the nodal values of ϕ are assumed to prevail over their associated subelement control volumes.

In the derivation of algebraic approximations to the integral terms which represent the convection-diffusion transport of ϕ across lateral faces, such as a and c shown in Fig. 3-4(a), more careful considerations are required in the choice of a suitable shape function for ϕ. In the absence of cross-stream velocity components (u=v=0), ϕ is interpolated linearly in each subelement. In the presence of cross-stream fluid flow, however, the use of linear interpolation functions could lead to physically unrealistic oscillatory solutions and cause iterative solution methods to diverge [1,2]. To overcome this difficulty, an element interpolation function proposed by Baliga and Patankar [1,2] is used. This function responds to the relative strengths of convection and diffusion in the cross-stream transport terms, and it also takes into account the direction of a subelement-averaged cross-section velocity vector.

Consider the subelement 165 shown in Fig. 3-6. The element-averaged cross-sectional velocity vector for this subelement is denoted by $\vec{v}_o$. A new subelement coordinate system (X,Y,Z) is introduced at this stage; its origin is located at the centroid o; the X-axis is aligned with the

element-averaged cross-sectional velocity vector $\vec{v}_o$; and the Z-axis is aligned with the duct axis or z-direction. Let $\vec{\ell}$ and $\vec{k}$ denote unit vectors in the X and Y directions, respectively, and U and V the corresponding velocity components. Then

$$\vec{v}_o = U_{av}\,\vec{\ell} \tag{3-7}$$

where

$$U_{av} = \left[\left(\frac{u_1+u_5+u_6}{3}\right)^2 + \left(\frac{v_1+v_5+v_6}{3}\right)^2\right]^{\frac{1}{2}} . \tag{3-8}$$

Let

$$X_{max} = \max(X_1,X_5,X_6); \quad X_{min} = \min(X_1,X_5,X_6) \tag{3-9}$$

and

$$Pe_\Delta = \rho U_{av}\left(\frac{X_{max} - X_{min}}{\Gamma}\right) \tag{3-10}$$

where Pe_Δ is a subelement Peclet number based on the magnitude of the element-averaged cross-sectional velocity vector $\vec{v}_o$. In terms of these variables, the interpolation function for ϕ in subelement 165 shown in Fig. 3-6 is given by

$$\phi = A\,\xi + BY + C \tag{3-11}$$

where

$$\xi = \frac{\Gamma}{\rho U_{av}} \left\{ \exp \left(\frac{Pe_{\Delta}\,(X - X_{max})}{X_{max} - X_{min}} \right) - 1 \right\} \qquad (3\text{-}12)$$

and A, B and C are constants that can be uniquely determined from the nodal values of ϕ (Appendix II). The rationale for using the interpolation function given in Eqn. (3-11) has been extensively discussed by Baliga and Patankar [1,2]. Briefly, the advantages of this practice are the following:

(1) the exponential function used in Eqn. (3-12) provides the appropriate amount of "upwinding";

(2) the "spinning" of the local (X,Y,Z) coordinate system to align it with the direction of the average cross-sectional velocity, $\vec{v}_o$, substantially reduces the numerical or false diffusion difficulty that plagues many of the currently-available upwind-type finite-difference and finite-element schemes [2,4];

(3) in the absence of cross-stream velocities (u=v=0), Eqn. (3-11) reduces to a linear interpolation function, and thus conforms to the standard practice for pure diffusion situations.

Interpolation functions for the velocity components u, v and w

The velocity components u, v and w are stored at all nodes, and interpolation functions for these variables are

prescribed in each subelement in the calculation domain. It is again emphasized that interpolation functions are required to obtain algebraic approximations to the different integral transport and source terms present in the control-volume conservation equations, and it is not necessary to use the same interpolation functions in all these different terms and equations [4].

In the derivation of algebraic approximations to the integral terms which represent convective transport of momentum across cross-sectional faces, such as u_1 and d_1 shown in Fig. 3-4(a), the nodal values of u, v and w are assumed to prevail over the surfaces of their associated subelement control volumes. In the derivation of algebraic approximations to the integral terms which represent the convection-diffusion transport of momentum across lateral faces, such as a and c shown in Fig. 3-4(a), u, v and w are interpolated by functions similar to the ϕ interpolation function given in Eqn. (3-11).

In the calculation of mass flow rates across cross-sectional faces, such as u_1 and d_1 shown in Fig. 3-4(a), nodal values of w are assumed to prevail over the surfaces of their associated subelement control volumes. In the derivation of algebraic approximations to mass flow rates across lateral faces, such as a and c in Fig. 3-4(a), u and v are assumed to vary linearly in the subelements.

Interpolation function for pressure

The pressure is stored at the vertices of the macroelements and interpolated linearly within each macroelement. Thus, the interpolation function can be expressed as

$$p = ax + by + c \tag{3-13}$$

where a, b and c are constants which can be uniquely determined from the nodal values of p (Appendix I).

3.4 DERIVATION OF THE DISCRETIZATION EQUATIONS

The discretization equations are algebraic approximations to the control-volume conservation equations such as Eqn. (3-4). They are obtained by first deriving such approximations to the corresponding element contributions and the boundary contributions, if applicable, and then assembling these contributions appropriately. In the following discussion, the derivation of the discretization equation for the general dependent variable ϕ is presented first. Then discretization analogues of the x-, y- and z-momentum equations are presented. Finally, discretized forms of the continuity and momentum equations are combined to obtain discretization equations for the pressure p and the axial pressure gradient $(d\bar{p}/dz)$.

3.4.1 Discretization Equations for ϕ

The following discussion pertains to node 1 of the subelement 165, shown in Fig. 3-4(a), and its associated subelement control volume; discretization equations associated with other subelement nodes are obtained analogously.

Element contributions

Using the interpolation functions presented earlier, the integral transport of ϕ across the upstream and downstream control volume faces u_1 and d_1 are approximated as follows:

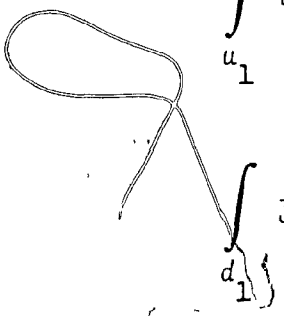

$$\int_{u_1} \vec{J} \cdot \vec{n} \, ds = - \frac{A_{165}}{3} [\rho w_1 \phi_1]^U \qquad (3\text{-}14)$$

$$\int_{d_1} \vec{J} \cdot \vec{n} \, ds = \frac{A_{165}}{3} [\rho w_1 \phi_1]^D \, , \qquad (3\text{-}15)$$

where the superscripts U and D refer to the upstream and downstream planes, respectively, and A_{165} is the area of triangle 165. The assumption that the values of ϕ and w at node 1 prevail over the control volume faces u_1 and d_1 has been employed in deriving Eqns. (3-14) and (3-15).

Simpson's rule and the fully-implicit formulation are used to approximate the integral transport of ϕ across the lateral faces a and c. Thus the convection-diffusion

transport of ϕ across the lateral surface a is approximated as follows [2]:

$$\int_a \vec{J}\cdot\vec{n}\, ds \simeq \frac{-Y_a \Delta z}{6}\left[(J_X)_o^D + 4(J_X)_r^D + (J_X)_a^D\right] + \frac{X_a \Delta z}{6}\left[(J_Y)_o^D + 4(J_Y)_r^D + (J_Y)_a^D\right] \qquad (3\text{-}16)$$

where J_X and J_Y are the components of $\vec{J}$ in the spun coordinate system X and Y, respectively. The interpolation functions given in Eqn. (3-11) are used to approximate J_X and J_Y:

$$\left.\begin{aligned} J_X &\simeq \rho(U - U_{av})A\xi + \rho U(BY + C) - \Gamma A \\ J_Y &\simeq \rho V A\xi + \rho V(BY + C) - \Gamma B \end{aligned}\right\} \qquad (3\text{-}17)$$

The subscripts o, r and a in Eqn. (3-16) refer to the locations shown in Fig. 3-6. U and V are the cross-sectional velocity components in the spun X and Y coordinate directions, respectively. The interpolation constants A, B and C can be expressed in terms of the coordinates of the nodes 1, 6 and 5 and the corresponding nodal values ϕ_1, ϕ_6 and ϕ_5; the exact expressions for these constants are given in Appendix II. Eqn. (3-16) can be compactly written as follows†:

---

† the derivation here is straightforward but quite lengthy; its details are reported in Appendix II.

$$\int_a \vec{J}\cdot\vec{n}\, ds \simeq -(A_1^a\, \phi_1^D + A_5^a\, \phi_5^D + A_6^a\, \phi_6^D) \qquad (3\text{-}18)$$

where A_1^a, A_5^a and A_6^a are constants that involve the fluid properties ρ and Γ and the nodal coordinates and velocity components. In Eqn. (3-18), the superscript a pertains to the integration across the control volume face a.

In a similar manner, the convection-diffusion transport of ϕ across face c can be expressed as:

$$\int_c \vec{J}\cdot\vec{n}\, ds = A_1^c\, \phi_1^D + A_5^c\, \phi_5^D + A_6^c\, \phi_6^D \qquad (3\text{-}19)$$

Again, details of this derivation are available in Appendix II.

The integral involving the source term is approximated as follows:

$$\int_V S\, dV = \int_V (S_C + S_P\, \phi)\, dV \simeq \frac{A_{165}}{3}\, \Delta z\, (S_C + S_P\, \phi_1^D) \qquad (3\text{-}20)$$

Adding up Eqns. (3-14), (3-15), (3-18), (3-19) and (3-20), the total contribution of subelement 165 to the integral conservation equation for the control volume surrounding node 1 is obtained:

$$\int_{u_1} \vec{J}\cdot\vec{n}\, ds + \int_{d_1} \vec{J}\cdot\vec{n}\, ds + \int_{a} \vec{J}\cdot\vec{n}\, ds + \int_{c} \vec{J}\cdot\vec{n}\, ds - \int_{v_1} S\, dV$$

$$= \{\frac{A_{165}}{3}\,[(\rho w_1)^D - S_p\,\Delta z\,] - A_1^a + A_1^c\}\,\phi_1^D$$

$$- \{A_5^a - A_5^c\}\,\phi_5^D - \{A_6^a - A_6^c\}\,\phi_6^D$$

$$- \{\frac{A_{165}}{3}\,(\rho w_1)^U\}\,\phi_1^U - \{\frac{A_{165}}{3}\,\Delta z\, S_c\} \qquad (3\text{-}21)$$

It can be shown that, if the element contribution to the mass conservation equation for the control volume associated with node 1 is multiplied by ϕ_1^D and then subtracted from Eqn. (3-21), the result is:

$$\text{CONT1} = \left[\int_{u_1} \vec{J}\cdot\vec{n}\, ds + \int_{d_1} \vec{J}\cdot\vec{n}\, ds + \int_{a} \vec{J}\cdot\vec{n}\, ds + \int_{c} \vec{J}\cdot\vec{n}\, ds - \int_{v_1} S\, dV\right]$$

$$- \phi_1^D \left[\int_{u_1} \rho\vec{v}\cdot\vec{n}\, ds + \int_{d_1} \rho\vec{v}\cdot\vec{n}\, ds + \int_{a} \rho\vec{v}\cdot\vec{n}\, ds + \int_{c} \rho\vec{v}\cdot\vec{n}\, ds\right]$$

$$= \{\frac{A_{165}}{3}\,[(\rho w_1)^U - S_p\,\Delta z] + A_5^a - A_5^c + A_6^a - A_6^c\}\,\phi_1^D$$

$$- \{A_5^a - A_5^c\}\,\phi_5^D \quad - \{A_6^a - A_6^c\}\,\phi_6^D$$

$$- \{\frac{A_{165}}{3}\,(\rho w_1)^U\}\,\phi_1^U \quad - \{\frac{A_{165}}{3}\,\Delta z\, S_c\} \qquad (3\text{-}22)$$

When similar contributions from all other elements associated with node 1 are added up, the net contribution from terms involving the mass flow integrals is zero; this is a requirement of the law of conservation of mass. Hence, Eqn. (3-22) can be regarded as the total contribution of the subelement 165 to the ϕ-conservation equation for the control volume surrounding node 1.

The motivation for using Eqn. (3-22) instead of (3-21) is the following [2]. In problems where the source term is absent ($S = 0$), if ϕ satisfies the governing equation, then (ϕ + constant) also satisfies this equation. Since the discretization equations are algebraic approximations to the governing equation, it is desirable that they too possess this property. It is seen that in Eqn. (3-22), with $S_C = S_P = 0$, the coefficient of ϕ_1^D is the negative sum of the coefficients of ϕ_5^D, ϕ_6^D and ϕ_1^U. Thus, Eqn. (3-22) has the aforementioned property. Eqn. (3-21) also exhibits this property, provided that the mass flow field satisfies the mass conservation law for the control volume surrounding node 1. This may not always be the case, however, especially during iterative solution of the various sets of discretization equations.

Eqn. (3-22) can be cast into the following compact form:

$$\text{CONT1} = C_{11}\,\phi_1^D + C_{15}\,\phi_5^D + C_{16}\,\phi_6^D + C_{11}^U\,\phi_1^U + B_1 \qquad (3\text{-}23)$$

where

$$\left.\begin{aligned} C_{11} &= -(C_{15} + C_{16} + C_{11}^{U}) \\ C_{15} &= -(A_5^a - A_5^c) \\ C_{16} &= -(A_6^a - A_6^c) \\ C_{11}^{U} &= -\frac{A_{165}}{3}(\rho w_1)^{U} \\ B_1 &= -\frac{A_{165}}{3}\Delta z\, S_C \end{aligned}\right\} \quad (3\text{-}24)$$

Similarly, the total element contributions to the discretization equations for nodes 5 and 6 can be expressed in the following compact forms:

$$\left.\begin{aligned} \text{CONT5} &= C_{51}\phi_1^D + C_{55}\phi_5^D + C_{56}\phi_6^D + C_{55}^U\phi_5^U + B_5 \\ \text{CONT6} &= C_{61}\phi_1^D + C_{65}\phi_5^D + C_{66}\phi_6^D + C_{66}^U\phi_6^U + B_6 \end{aligned}\right\} \quad (3\text{-}25)$$

Boundary contributions

When a node lies on the boundary, special attention is required in deriving its discretization equation. The control volume surrounding a boundary node possesses one or more domain boundary faces, as illustrated in Fig. 3-7. The normal fluxes of the dependent variable crossing these faces need to be integrated and added to the discretization

equation for the corresponding boundary node. Information regarding these fluxes is available from the boundary conditions on the variable of interest.

Typically, three kinds of boundary conditions are commonly encountered. They are:

(1) specified ϕ at the boundary,

(2) no flow, specified diffusion flux at the boundary, and

(3) the so-called outflow condition [4].

The procedures for treating such boundary conditions are outlined below.

Specified ϕ boundary condition: When the value of ϕ is specified at the boundary, there is no need to assemble its discretization equation. Rather, the discretization equation for such a boundary node i takes on the following trivial form:

$$\phi_i = \phi_{specified} \qquad (3\text{-}26)$$

No flow, specified diffusion flux boundary condition: Here, there is no flow crossing the boundary and hence the convection flux component of $\vec{J}$ is zero. The diffusion flux component on the other hand, is specified. Usually, only

the component of this flux normal to the boundary is given:

$$-(\Gamma \vec{\nabla} \phi) \cdot \vec{n} = q \text{ (specified)} \qquad (3\text{-}27)$$

where q is the specified outward normal component of the diffusion flux. A typical example of this type of boundary condition is the specified heat flux boundary; symmetry and adiabatic surfaces are particular cases of this boundary condition in which q = 0.

Referring to Fig. 3-7, the contribution of the sub-element 165 to the discretization equation for node 1 can be expressed as:

$$\begin{aligned} \text{CONT1} = &\left[\int_{u_1} \vec{J}\cdot\vec{n}\, ds + \int_{d_1} \vec{J}\cdot\vec{n}\, ds + \int_{a} \vec{J}\cdot\vec{n}\, ds + \int_{c} \vec{J}\cdot\vec{n}\, ds \right. \\ &\left. + \int_{1a} \vec{J}\cdot\vec{n}\, ds - \int_{v_1} S\, dV \right] \\ &- \phi_1 \left[\int_{u_1} \rho\vec{v}\cdot\vec{n}\, ds + \int_{d_1} \rho\vec{v}\cdot\vec{n}\, ds + \int_{a} \rho\vec{v}\cdot\vec{n}\, ds + \int_{c} \rho\vec{v}\cdot\vec{n}\, ds \right] \\ &= C_{11}\phi_1^D + C_{15}\phi_5^D + C_{16}\phi_6^D + C_1^U\phi_1^U + B_1 + \int_{1a} q\, ds \,. \end{aligned} \qquad (3\text{-}28)$$

Outflow boundary condition: At an "outflow" boundary, where the fluid leaves the calculation domain, it is common that neither the value of ϕ nor its flux is known. In duct flow problems, the last downstream plane of the calculation domain is an example of an outflow boundary. The assumption usually made in such situations is that the convection flux component of $\vec{J}$ is large enough to overwhelm its diffusion counterpart [4]. Thus, it is assumed that

$$- \Gamma \vec{\nabla} \phi \cdot \vec{n} = 0 \qquad (3\text{-}29)$$

An outflow boundary could be: (i) a cross-sectional surface, or (ii) a lateral face. In the former case, no special treatment is required: the streamwise transport of ϕ by diffusion has already been neglected in the parabolic problems of interest here; and the convective transport across downstream cross-sectional surfaces, such as d in Fig. 3-4(a), has already been included in the element contributions discussed earlier. In the latter case, however, the transport of ϕ by convection across the boundary faces, such as 1a and 1c in Fig. 3-7(b), must be integrated and included in the conservation equation for node 1. In a manner similar to the derivations in Appendix II, it can be shown that

$$\int_{1a} \vec{J} \cdot \vec{n} \, ds = A_1^{1a} \phi_1^D + A_5^{1a} \phi_5^D + A_6^{1a} \phi_6^D \qquad (3\text{-}30)$$

Thus, the total contribution of subelement 165 to the discretization equation for boundary node 1, shown in Fig. 3-7, is given by the following equation:

$$\begin{aligned}
\text{CONT1} = \{ & \int_{u_1} \vec{J}\cdot\vec{n}\, ds + \int_{d_1} \vec{J}\cdot\vec{n}\, ds + \int_{a} \vec{J}\cdot\vec{n}\, ds + \int_{c} \vec{J}\cdot\vec{n}\, ds \\
& + \int_{1a} \vec{J}\cdot\vec{n}\, ds - \int_{v_1} S\, dV \} \\
& - \phi_1^D \Big[\int_{u_1} \rho\vec{v}\cdot\vec{n}\, ds + \int_{d_1} \rho\vec{v}\cdot\vec{n}\, ds + \int_{a} \rho\vec{v}\cdot\vec{n}\, ds + \int_{c} \rho\vec{v}\cdot\vec{n}\, ds \\
& + \int_{1a} \rho\vec{v}\cdot\vec{n}\, ds \Big] \\
= & \ (C_{11} - A_5^{1a} - A_6^{1a})\phi_1^D + (C_{15} + A_5^{1a})\phi_5^D + (C_{16} + A_6^{1a})\phi_6^D \\
& + C_{11}^U \phi_1^U + B_1 \qquad (3\text{-}31)
\end{aligned}$$

The boundary contributions to the conservation equations associated with other boundary nodes are handled in a similar manner.

Assembly of the discretization equations

The discretization equation for ϕ at a node i is obtained by adding up the total (internal + boundary)

contributions of all subelements associated with the control volume surrounding node i. This is done by visiting all subelements one-by-one; in each subelement, the contributions CONT1, CONT5 and CONT6, discussed earlier, are calculated and added to the appropriate nodal discretization equations. The resulting discretization equation for ϕ at a node i can be cast into the following general form:

$$a_i \phi_i = \sum_{nb} a_{nb} \phi_{nb} + a_i^U \phi_i^U + b_i \qquad (3\text{-}32)$$

where the summation is done in the downstream plane over all nodes belonging to the subelements associated with node i. In Eqn. (3-32), it is to be noted that the superscript D for denoting downstream values of ϕ has been omitted for convenience in this presentation.

3.4.2 Momentum Discretization Equations

The momentum equations, Eqns. (2-9), (2-10) and (2-11), can be integrated over a fixed control volume V to obtain the following equations:

x-momentum

$$\int_{\partial V} [\rho \vec{v} u - \mu \vec{\nabla} u] \cdot \vec{n} \, ds = \int_V (-\frac{\partial p}{\partial x}) dV \qquad (3\text{-}33)$$

y-momentum

$$\int_{\partial V} [\rho \vec{v} v - \mu \vec{\nabla} v] \cdot \vec{n} \, ds = \int_{V} (-\frac{\partial p}{\partial y}) dV \qquad (3\text{-}34)$$

z-momentum

$$\int_{\partial V} [\rho \vec{v} w - \mu \vec{\nabla} w] \cdot \vec{n} \, ds = \int_{V} (-\frac{d\bar{p}}{dz}) dV \qquad (3\text{-}35)$$

In Eqns. (3-33) - (3-35), the integral terms representing the convection-diffusion transport of u, v and w are similar to the corresponding integral transport term in the conservation equation for ϕ, Eqn. (3-3). The derivation of algebraic approximations to these integral transport terms has already been described in previous sections of this chapter, and so it will not be repeated here.

The integrals involving the pressure gradient terms, $(\partial p/\partial x)$ and $(\partial p/\partial y)$ can be expressed in terms of nodal pressure values, using the macroelement interpolation function given in Eqn. (3-13). Thus, within a macroelement:

$$\frac{\partial p}{\partial x} = a \,, \qquad \frac{\partial p}{\partial y} = b. \qquad (3\text{-}36)$$

Therefore, with reference to Fig. 3-3(a), the contributions of the macroelement 123 to the pressure gradient integrals over the subelement control volume surrounding node 1 can be expressed as follows:

$$\int_{V_1} \left(-\frac{\partial p}{\partial x}\right) dV = -v_1 a = D_1^u p_1 + D_2^u p_2 + D_3^u p_3 \qquad (3\text{-}37)$$

and

$$\int_{V_1} \left(-\frac{\partial p}{\partial y}\right) dV = -v_1 b = D_1^v p_1 + D_2^v p_2 + D_3^v p_3 \qquad (3\text{-}38)$$

The fully-implicit formulation is used to obtain Eqns. (3-37) and (3-38), so the nodal pressure values in these equations pertain to the downstream plane of macroelement 123. It should also be noted that the coefficients D_j^u and D_j^v in these equations depend only on the geometry of macroelement 123. Details of the derivation of Eqns. (3-37) and (3-38) are given in Appendix I. Similar contributions from other macroelements associated with node 1 can be approximated analogously.

The axial gradient of the cross-sectional averaged pressure, $(d\bar{p}/dz)$, is assumed to be constant over the axial step size Δz. Therefore, for node i,

$$\int_{V_i} \left(-\frac{d\bar{p}}{dz}\right) dV = v_i \left(-\frac{d\bar{p}}{dz}\right) \qquad (3\text{-}39)$$

where v_i is the volume of the subelement control volume associated with node i.

Discretization analogues of the portion of the integral momentum equations which do not involve the pressure gradient terms are assembled by using the procedure described in the last subsection. The pressure-gradient integrals are assembled on a macroelement-by-macroelement basis, using Eqns. (3-37) - (3-39). The resulting u, v and w discretization equations for a node i can be cast into the following general forms:

$$a_i^u u_i = \sum_{nb} a_{nb}^u u_{nb} + a_i^{u,U} u_i^U + b_i^u + \sum_j \lambda_j^u p_j \qquad (3\text{-}40)$$

$$a_i^v v_i = \sum_{nb} a_{nb}^v v_{nb} + a_i^{v,U} v_i^U + b_i^v + \sum_j \lambda_j^v p_j \qquad (3\text{-}41)$$

$$a_i^w w_i = \sum_{nb} a_{nb}^w w_{nb} + a_i^{w,U} w_i^U + b_i^w + \nu_i \left(-\frac{d\bar{p}}{dz}\right) \qquad (3\text{-}42)$$

where λ_j^u and λ_j^v are constant coefficients containing combinations of D_j^u and D_j^v, respectively. In Eqns. (3-40) and (3-41), the summations involving the velocity neighbours are done over all downstream nodes belonging to the subelements associated with node i. The summations involving pressures, however, pertain to the downstream vertices of the macroelements associated with node i. It is again emphasized that the fully-implicit formulation is used in the derivation of Eqns. (3-40) to (3-42); nodal velocities and pressures which appear in these equations without superscripts are values stored in the downstream plane.

Representation in terms of pseudovelocities: Eqns. (3-40) - (3-42) can be expressed compactly in terms of pseudovelocities $\hat{u}$, $\hat{v}$ and $\hat{w}$ defined as follows:

$$\hat{u}_i = \frac{\sum_{nb} a^u_{nb} u_{nb} + a^{u,U}_i u^U_i + b^u_i}{a^u_i} \tag{3-43}$$

$$\hat{v}_i = \frac{\sum_{nb} a^v_{nb} v_{nb} + a^{v,U}_i v^U_i + b^v_i}{a^v_i} \tag{3-44}$$

$$\hat{w}_i = \frac{\sum_{nb} a^w_{nb} w_{nb} + a^{w,U}_i w^U_i + b^w_i}{a^w_i} \tag{3-45}$$

It is to be noted that these pseudovelocities at node i are defined in terms of upstream and downstream neighbouring velocities, but they do not depend directly on p and $(d\bar{p}/dz)$. Thus, given a velocity field at a downstream cross-sectional plane, the corresponding pseudovelocities can be calculated without an explicit knowledge of the pressure distribution.

Using these pseudovelocities, Eqns. (3-40) to (3-42) can be rewritten as follows:

$$u_i = \hat{u}_i + \sum_j \lambda^u_j p_j / a^u_i \tag{3-46}$$

$$v_i = \hat{v}_i + \sum_j \lambda^v_j p_j / a^v_i \tag{3-47}$$

$$w_i = \hat{w}_i + v_i \left(-\frac{d\bar{p}}{dz}\right)/a_i^w \qquad (3\text{-}48)$$

These compact representations of the discretized momentum equations are used in the derivation of the discretization equations for p and $(d\bar{p}/dz)$.

If u, v or w are specified at a boundary node i, the corresponding momentum discretization equations associated with that node reduce to:

$$\begin{aligned} u_i &= \hat{u}_i = u_{specified} \\ v_i &= \hat{v}_i = v_{specified} \\ w_i &= \hat{w}_i = w_{specified} \end{aligned} \qquad (3\text{-}49)$$

3.4.3 Discretization Equation for Cross-Sectional Pressure p

A discretization equation for the cross-sectional pressure p can be obtained by substituting Eqns.(3-46) and (3-47) into a discretized mass conservation equation. The key ideas of this derivation are presented concisely in this section; the details are presented in Appendix III.

Consider the macroelements and control volume surrounding node 1 in Fig. 3-3(c). With reference to the notation in this figure and to Eqn. (3-5), the contribution of macroelement 123 to the integral mass conservation equation associated with node 1 can be approximated using Simpson's rule and the velocity interpolation functions described in section 3.3. Thus,

$$\text{PCONT1} = \left[\int_{U_1} \rho\vec{v}\cdot\vec{n}\, ds + \int_{D_1} \rho\vec{v}\cdot\vec{n}\, ds + \int_{A} \rho\vec{v}\cdot\vec{n}\, ds + \int_{C} \rho\vec{v}\cdot\vec{n}\, ds\right]$$

$$= MU_4^1\, u_4 + MU_5^1\, u_5 + MU_6^1\, u_6$$

$$+ MV_4^1\, v_4 + MV_5^1\, v_5 + MV_6^1\, v_6$$

$$+ \text{MWCON1} \qquad (3\text{-}50)$$

where

$$\text{MWCON1} = MW_1^1\, w_1 + MW_5^1\, w_5 + MW_6^1\, w_6$$

$$+ MW_1^{1,U}\, w_1^U + MW_5^{1,U}\, w_5^U + MW_6^{1,U}\, w_6^U \qquad (3\text{-}51)$$

In Eqn. (3-51), all values of w and w^U are treated as known or already calculated.

The subelement control volumes associated with nodes 4, 5 and 6 lie totally within the region enclosed by macroelement 123 and a maximum of three associated macroelements, as illustrated in Fig. 3-8. Therefore, the discretization equations for the velocity components u_4, u_5, u_6, v_4, v_5 and v_6 which appear in Eqn. (3-50) involve a maximum of four nodal pressure values each. With reference to Fig. 3-8, the pseudo-velocity representations of these discretization equations are the following:

$$u_4 = \hat{u}_4 + (\lambda_1^u\, p_1 + \lambda_2^u\, p_2 + \lambda_3^u\, p_3 + \lambda_{o1}^u\, p_{o1})/a_4^u \qquad (3\text{-}52)$$

$$u_5 = \hat{u}_5 + (\lambda_1^u p_1 + \lambda_2^u p_2 + \lambda_3^u p_3 + \lambda_{o2}^u p_{o2})/a_5^u \qquad (3\text{-}53)$$

$$u_6 = \hat{u}_6 + (\lambda_1^u p_1 + \lambda_2^u p_2 + \lambda_3^u p_3 + \lambda_{o3}^u p_{o3})/a_6^u \qquad (3\text{-}54)$$

and

$$v_4 = \hat{v}_4 + (\lambda_1^v p_1 + \lambda_2^v p_2 + \lambda_3^v p_3 + \lambda_{o1}^v p_{o1})/a_4^v \qquad (3\text{-}55)$$

$$v_5 = \hat{v}_5 + (\lambda_1^v p_1 + \lambda_2^v p_2 + \lambda_3^v p_3 + \lambda_{o2}^v p_{o2})/a_5^v \qquad (3\text{-}56)$$

$$v_6 = \hat{v}_6 + (\lambda_1^v p_1 + \lambda_2^v p_2 + \lambda_3^v p_3 + \lambda_{o3}^v p_{o3})/a_6^v \qquad (3\text{-}57)$$

Eqns. (3-52) to (3-57) can be substituted into Eqn. (3-50) to obtain the following representation of the contribution of macroelement 123 to the integral mass conservation equation associated with node 1:

$$\text{PCONT1} = MP_1^1 p_1 + MP_2^1 p_2 + MP_3^1 p_3 + MP_{o1}^1 p_{o1} + MP_{o2}^1 p_{o2} + MP_{o3}^1 p_{o3} + \text{MPCON1} \qquad (3\text{-}58)$$

where the term MPCON1 is a linear combination of the values of the pseudovelocity components, $\hat{u}$ and $\hat{v}$, at the nodes 4, 5, and 6

in the downstream cross-sectional plane of macroelement 123, and the axial velocity component, w, at the nodes 1, 5 and 6 in the downstream and upstream cross-sectional planes of macroelement 123.

Similarly, the contributions of the macroelement 123 to the integral mass conservation equations associated with nodes 2 and 3 can be expressed in the following forms:

$$\text{PCONT2} = MP_1^2\, p_1 + MP_2^2\, p_2 + MP_3^2\, p_3 + MP_{o1}^2\, p_{o1} + MP_{o2}^2\, p_{o2} + MP_{o3}^2\, p_{o3} + \text{MPCON2} \quad (3\text{-}59)$$

$$\text{PCONT3} = MP_1^3\, p_1 + MP_2^3\, p_2 + MP_3^3\, p_3 + MP_{o1}^3\, p_{o1} + MP_{o2}^3\, p_{o2} + MP_{o3}^3\, p_{o3} + \text{MPCON3}. \quad (3\text{-}60)$$

The derivation of these equations is analogous to that of Eqn. (3-58) presented in Appendix III.

Eqns. (3-59) and (3-60) represent the total internal contributions of the macroelement 123 to the integral mass conservation equations associated with nodes 2 and 3, respectively. If one or more lateral faces of the macroelement coincide with the domain boundary, the mass flow rates across these surfaces must be integrated and added to the internal macroelement contributions to complete the assembly of the discretized mass conservation equations. In this thesis, however, since only ducts with impermeable walls are considered, the mass flow across the duct walls is zero.

The discretization equations for the nodal values of the cross-sectional pressure p are obtained by a macroelement-by-macroelement assembly of the corresponding integral mass conservation equations: all macroelements are visited one-by-one, and in each one, the algebraic expressions for PCONT1, PCONT2 and PCONT3, presented earlier, are assembled appropriately. The complete discretization equation for pressure at a macroelement vertex i can be cast into the following general form:

$$a_i^p \, p_i = \sum_{nb} a_{nb}^p \, p_{nb} + b_i^p \qquad (3\text{-}61)$$

The summation in this equation is taken over all the downstream vertices of all macroelements and associated-macroelements connected with the pressure node i. Collectively, these neighbour pressure nodes form the star-like cluster shown in Fig. 3-9.

The term b_i^p in Eqn. (3-61) is a linear combination of the pseudovelocity components $\hat{u}$ and $\hat{v}$, stored at the velocity nodes marked with a cross-mark (x) in Fig. 3-9, and the corresponding axial velocity components w and w^U. Therefore, given a velocity field, the set of pressure equations, such as Eqn. (3-61), can be assembled and solved to get the corresponding cross-sectional pressure field.

If the cross-sectional pressure at a boundary node i is specified, the corresponding discretization equation reduces to

$$p_i = (p_i)_{\text{specified}} \tag{3-62}$$

3.4.4 Discretization Equation for $(d\bar{p}/dz)$

For steady flow in a duct with impermeable walls, the total mass flow rate crossing any cross-sectional plane of the duct is a constant:

$$\dot{m} = \int_{\substack{\text{cross-sectional} \\ \text{area of the duct}}} \rho w \, d A = \text{constant} \tag{2-12}$$

Assuming that the nodal values of w prevail over the polygonal cross-sections of their associated subelement control volumes, the mass flow rate $\dot{m}$ can be approximated as follows:

$$\dot{m} = \sum_i \rho A_i w_i \tag{3-63}$$

where A_i is the total area of the polygonal cross-section of the subelement control volume surrounding node i, and the summation is taken over all nodes in the duct cross-section of interest.

The pseudovelocity representation of the z-momentum equation associated with node i is given by Eqn. (3-48). This equation can be substituted into Eqn. (3-63) to obtain:

$$\dot{m} = \sum_i \rho A_i \{\hat{w}_i + \nu_i (-\frac{d\bar{p}}{dz})/a_i^w\} \tag{3-64}$$

This equation can be rewritten as follows:

$$(-\frac{d\bar{p}}{dz}) = \frac{\dot{m} - \sum_i \rho A_i \hat{w}_i}{\sum_i \rho A_i \nu_i / a_i^w} \tag{3-65}$$

At any axial station $(z + \Delta z)$, if the velocity field is known, the value of $(d\bar{p}/dz)$ pertaining to the region between z and $(z + \Delta z)$ can be obtained by using Eqn. (3-65).

3.5 SOLUTION OF THE DISCRETIZATION EQUATIONS

3.5.1 Marching Integration

As was discussed in earlier chapters, in parabolic duct flow and heat transfer problems, conditions at a point in the duct can only influence the conditions at a downstream point,

not vice-versa. The discretization equations presented in the last section possess this characteristic too. Thus the discretization equation associated with a node in any cross-sectional plane of the duct of interest may depend on and involve values of the dependent variables at nodes in the same and the adjacent upstream cross-sectional planes, but they are in no way connected to the values of the dependent variables at downstream nodes. Therefore, the assembly and solution of the discretization equations associated with the nodes in any given cross-sectional plane, or axial station, require the values of dependent variables at the adjacent upstream cross-sectional plane only: once this is done, the same procedure can be repeated to advance the solution to the next downstream plane, then the next one, and so on. In other words, starting with the known initial conditions at the inlet cross-sectional plane of the duct, a plane-by-plane marching integration procedure can be used to determine the values of the dependent variables at all nodes of the calculation domain.

An iterative method similar to the SIMPLER procedure of Patankar [4] is used to advance the solution from one cross-sectional plane to the next downstream one. In this procedure, at the end of each iteration, the calculated velocity components are corrected via suitable pressure corrections so that the overall and local mass conservation equations are satisfied. In addition, to ensure convergence of this procedure, it is necessary to slow down the changes in the coefficients of the discretization equations from iteration to

iteration by the use of under-relaxation. These matters are discussed in the following subsections. A summary of the overall calculation procedure is presented at the end of this section.

3.5.2 Velocity and Pressure Correction Equations

At any stage of the aforementioned SIMPLER-type iterative procedure, upstream values of the dependent variables and guessed, or tentative, values of these variables at the nodes in the cross-sectional plane of interest can be used to calculate the coefficients of the discretized momentum equations. These coefficients can then be used in Eqns. (3-43) to (3-45) to obtain the pseudovelocities $\hat{u}$, $\hat{v}$ and $\hat{w}$. Then, these pseudovelocities can be used in Eqns. (3-65) and (3-61) to calculate the corresponding values of the axial gradient of the cross-sectional averaged pressure and the cross-section pressure; they are denoted by $(d\bar{p}/dz)^{\#}$ and $p^{\#}$, respectively. Using $(d\bar{p}/dz)^{\#}$ and $p^{\#}$, the discretized momentum equations can be solved to obtain the velocity components; these calculated velocity components are denoted by $u^{\#}$, $v^{\#}$ and $w^{\#}$. In general, $u^{\#}$, $v^{\#}$ and $w^{\#}$ will not satisfy the overall and local mass conservation equations. One way to ensure that they do satisfy mass conservation requirements is to correct them via suitably calculated corrections to $(d\bar{p}/dz)^{\#}$ and $p^{\#}$. Let the correct values of these variables be given by

$$\frac{d\bar{p}}{dz} = \left(\frac{d\bar{p}}{dz}\right)^{\#} + \left(\frac{d\bar{p}}{dz}\right)' \qquad (3\text{-}66)$$

and

$$p = p^{\#} + p' \tag{3-67}$$

where the superscripts $(\ )^{\#}$ and $(\ )'$ refer to tentative and correction values, respectively. These corrected values can be substituted into the discretized momentum equations to obtain equations for the corresponding velocity corrections w', u' and v'. These equations can be simplified if the contributions of the neighbour-point velocity corrections, $\Sigma\ a^{w}_{nb}\ w'_{nb}$, $\Sigma\ a^{u}_{nb}\ u'_{nb}$ and $\Sigma\ a^{v}_{nb}\ v'_{nb}$ are considered negligible [4]: it is to be noted that, as the solution converges, these quantities do indeed become negligible. The resulting velocity correction equations are:

$$w_i = w_i^{\#} + \nu_i \left(-\frac{d\bar{p}}{dz}\right)' / a_i^{w} \tag{3-68}$$

$$u_i = u_i^{\#} + \sum_j \lambda_j^{u}\ p'_j\ /a_i^{u} \tag{3-69}$$

$$v_i = v_i^{\#} + \sum_j \lambda_j^{v}\ p'_j\ /a_i^{v} \tag{3-70}$$

Eqn. (3-68) can be substituted into Eqn. (3-63) to obtain an equation for $(d\bar{p}/dz)'$; the derivation of this equation is identical to the derivation of the equation for $(d\bar{p}/dz)$ presented earlier. The result is

$$\left(-\frac{d\bar{p}}{dz}\right)' = \frac{\dot{m} - \sum_i \rho A_i w_i^{\#}}{\sum_i \rho A_i \nu_i / a_i^w} \qquad (3\text{-}71)$$

Similarly, Eqn. (3-69) and (3-70) can be used in conjunction with the macroelement control volume mass conservation equation to obtain a pressure correction equation; the derivation of this equation is analogous to the derivation of the pressure equation presented in an earlier section. The result is:

$$a_i^P p_i' = \sum_{nb} a_{nb}^p p_{nb}' + b_i^p \qquad (3\text{-}72)$$

The coefficients in this equation are the same as those in Eqn. (3-61). However, the term b_i^p in Eqn. (3-61) is a function of the pseudovelocities $\hat{u}$ and $\hat{v}$ and the axial velocity component w, but in Eqn. (3-72), it is a function of $u^{\#}$, $v^{\#}$ and w.

If the pressure at a boundary node i is specified, then Eqn. (3-72) for that node is overwritten and reduced to

$$p_i' = 0. \qquad (3\text{-}73)$$

When the calculated velocity field satisfies overall and local mass conservation equations, as is the case when the overall iterative solution procedure converges, $(d\bar{p}/dz)'$ and p' reduce to zero.

It is to be noted that the objective of calculating $(d\bar{p}/dz)'$ and p' is to use them in Eqns. (3-68) to (3-70) to correct the velocity field so that it satisfies overall and local mass conservation requirements at the start of every iteration. Thus $(d\bar{p}/dz)$ and p are not updated or corrected using Eqns. (3-66) and (3-67); rather, they are calculated in every iteration using Eqns. (3-65) and (3-61). Further discussion on this feature of SIMPLER-like procedures for the solution of momentum and continuity equations is available in [4].

3.5.3 Under-relaxation

As was seen in Chapter II, the partial differential equations which govern parabolic duct flows are non-linear and coupled. Therefore, their discretization analogues are also non-linear and coupled. In the proposed SIMPLER-like iterative solution procedure, the coefficients in these equations are calculated using guessed values of the dependent variables or their values from the previous iteration. To ensure the convergence of this iterative procedure, it is often necessary to slow down the changes in the coefficients of the discretization equations from one iteration to the next one. This is done by under-relaxing the dependent variables, using the implicit under-relaxation technique proposed by Patankar [4]. Thus, for the general scalar dependent variable ϕ, under-relaxation is introduced by re-writing its discretization equation as follows:

$$\frac{a_i}{\alpha_\phi}\,\phi_i = \sum_{nb} a_{nb}\,\phi_{nb} + a_i^U\,\phi_i^U + b_i + \frac{(1-\alpha_\phi)}{\alpha_\phi}\,a_i\,\phi_i^* \qquad (3\text{-}74)$$

where ϕ_i^* is a guessed value of ϕ, or its value at the end of the previous iteration, and α_ϕ is the corresponding under-relaxation parameter. The under-relaxation of u, v, w and p is done similarly. The corrections to the axial pressure gradient and the cross-sectional pressure, $(d\bar{p}/dz)'$ and p', are not under-relaxed; otherwise, the objective of calculating $(d\bar{p}/dz)'$ and p', namely the correction of the velocity field so that it satisfies overall and local mass conservation requirements, will be defeated.

The following set of under-relaxation parameters has been found to be satisfactory in the solution of many duct flow and heat transfer problems: in the vicinity of the inlet or in regions where boundary conditions change abruptly:

$$\alpha_u = \alpha_v = \alpha_w = 0.5; \quad \alpha_p = 0.8; \quad \alpha_\phi = 1 \qquad (3\text{-}75)$$

and after a few axial steps (>5) downstream of points where the boundary conditions change abruptly:

$$\alpha_u = \alpha_v = 0.8; \quad \alpha_w = 1; \quad \alpha_p = 1; \quad \alpha_\phi = 1 \qquad (3\text{-}76)$$

A general prescription for the optimum selection of these under-relaxation parameters is not available.

3.5.4 Summary of the Overall Calculation Procedure

The details of some of the key ideas of the proposed procedure for solving the discretization equations were presented in the last couple of subsections. A summary of the various operations of this procedure and their exact sequence is given below:

(1) Start at the duct inlet; assign all given initial conditions to the dependent variables u, v, p, $\bar{p}$ and other ϕ's, if applicable.

(2) March one step down the duct: guess all unknown values of the dependent variables; normally, the known upstream values are good guesses.

(3) Calculate the coefficients of the discretization equation for w, Eqn. (3-42), and store them; in a computer implementation, temporary or scratch disk storage is recommended for this step.

(4) Calculate the pseudovelocity component $\hat{w}$, using Eqn. (3-45).

(5) Calculate $(d\bar{p}/dz)^{\#}$, using Eqn. (3-65).

(6) Form the complete discretization equation for w, using the coefficients stored in step (3) and the calculated value of $(d\bar{p}/dz)^{\#}$, and solve it to obtain $w^{\#}$.

(7) Solve for $(d\bar{p}/dz)'$, using Eqn. (3-71), and then correct $w^{\#}$, using Eqn. (3-68), to obtain w.

(8) Calculate the coefficients of the discretization equations for u and v, Eqns. (3-40) and (3-41), based on the currently-available velocity field and store these coefficients; again, scratch disk storage is recommended for this step in a computer implementation.

(9) Calculate the pseudovelocity components $\hat{u}$ and $\hat{v}$, using Eqns. (3-43) and (3-44).

(10) Calculate the coefficients of the pressure equation, Eqn. (3-61), and solve it to obtain $p^{\#}$; in a computer implementation, store the coefficients of this equation on a temporary disk unit.

(11) Compile the complete discretization equations for u and v, using the coefficients calculated in step (8) and the pressure $p^{\#}$ computed in step (10), and solve them to obtain $u^{\#}$ and $v^{\#}$.

(12) Assemble the pressure correction equation, Eqn. (3-72), using the coefficients calculated in step (10) and a recalculated value of b_1^p based on $u^{\#}$ and $v^{\#}$, and solve it to obtain p'.

(13) Correct $u^{\#}$ and $v^{\#}$, using the p' field in Eqns. (3-69) and (3-70), to obtain u and v.

(14) Assemble and solve the discretization equations for all ϕ's coupled to the flow equations.

(15) With the currently-available values of u, v, w and ϕ as new guessed values, return to step (3), and repeat steps (3) to (15) until some suitably chosen convergence criterion is satisfied.

(16) At this point, the values of u, v, w, p and $(d\bar{p}/dz)$ can be considered as converged. Assemble the discretization equations for other ϕ's and solve them.

(17) Do all other auxiliary computations, such as calculations of friction factor, bulk temperature and Nusselt number.

(18) Go back to step (2) and repeat this plane-by-plane marching integration procedure until the entire calculation domain has been "swept".

CHAPTER IV

COMPUTER IMPLEMENTATION OF THE PROPOSED METHOD

The formulation of a control volume finite-element method for three-dimensional parabolic flow and heat transfer in ducts was presented in the previous chapter. In order to test the validity of the proposed method and to apply it to practical problems, it has to be incorporated into an efficient computer program. Some of the major tasks in the development of this program are presented in this chapter.

The numerical prediction of three-dimensional parabolic flows in ducts is not an inexpensive task. Therefore, the emphasis in the computer implementation of the proposed method is on efficiency rather than complete generality. Furthermore, the computer program described in this chapter is not intended to be used as a "black-box" by persons who are not familiar with the formulation of the proposed method. Rather, it is a user-oriented program designed for persons with an understanding of the key ideas of the proposed method and the physics of the problems it is formulated to solve.

The computer implementation of a general finite-element method involves four major tasks: (i) domain discretization and node numbering or labelling schemes; (ii) calculation of the local contributions from each element to the discretization equations for the corresponding nodes; (iii) assembly of all

individual element contributions into a global matrix form; and (iv) solution of the global discretization equations. Each of these tasks in the computer implementation of the proposed control-volume finite-element method is described in the following discussion. The corresponding computer code and its description are presented in Appendix IV.

4.1 DOMAIN DISCRETIZATION, NODE NUMBERING AND LABELLING SCHEMES

Discretization schemes could be manual or automatic. Manual schemes are usually extremely tedious and error-prone and, therefore, unfit for general applications. In this thesis, an automatic scheme is employed to discretize the duct in the axial direction, and a semi-automatic technique is used to discretize the duct cross-section.

4.1.1 Discretization of the Duct Axis: Automatic Step-Size Selector

As was stated in earlier chapters, in the duct flow and heat transfer problems of interest in this thesis, the dependent variables change significantly with the axial coordinate z in the vicinity of the entrance region of the duct, and they become progressively invariant with z as the fully-developed region is approached[†]. Typical variations of the axial velocity compo-

[†] The temperature T will keep changing, even in the thermally fully-developed region; however, the similarity variables θ and χ as defined in Chapter II are invariant with z in the f.d. region, and they can be treated as dependent variables.

nent and the local Nusselt number with z are shown in Fig. 4-1. It is desirable, therefore, to start computations with a very small axial step size, and adjust it appropriately in response to the relative rate of change of the dependent variables as the solution is advanced downstream. A procedure to automatically adjust the step size in this manner is described in this section.

Referring to Fig. 4-1(a), it is aimed to obtain an estimated IDEAL number of marching steps, where IDEAL is related to the desired change in the value of w_{max} in each axial step by the following equation:

$$[\Delta w_{max}]_{desired} = \frac{(w_{max})_{f.d.} - \bar{w}}{IDEAL} \qquad (4\text{-}1)$$

The numerator in Eqn. (4-1) represents the total change of w_{max} in the developing flow region. The slope (dw_{max}/dz) at axial station $z = z(ISTEP)$ can be approximated by:

$$\frac{dw_{max}}{dz} \simeq \frac{w_{max}(ISTEP) - w_{max}(ISTEP-1)}{z(ISTEP) - z(ISTEP-1)} \qquad (4\text{-}2)$$

Using linear extrapolation and the slope given by Eqn. (4-2), the axial step size required to produce $(\Delta w_{max})_{desired}$ is given by

$$\Delta z = z(ISTEP+1) - z(ISTEP)$$

$$= \frac{z(ISTEP) - z(ISTEP-1)}{w_{max}(ISTEP) - w_{max}(ISTEP-1)} \left(\Delta w_{max}\right)_{desired}$$

(4-3)

As is illustrated in Fig. 4-2, the actual change in w_{max}, $(\Delta w_{max})_{actual}$, produced by Δz would always be smaller than $(\Delta w_{max})_{desired}$, if w_{max} and its axial derivative change monotonically with z. Therefore, when this condition is met, the step size calculated in Eqn. (4-3) is a conservative one.

The entire scheme is started by prescribing a very small value of Δz for the first three steps. Then, from the fourth step onwards, Δz is calculated according to Eqn. (4-3). As the fully-developed region is approached, however, Eqn. (4-3) can give rise to disproportionately large step sizes since the variation of w_{max} with z is nearly flat there, as shown in Fig. 4-2. This difficulty is handled by adjusting $(\Delta w)_{desired}$ and Δz as follows:

$$(\Delta w)_{desired} = \min[(\Delta w)_{desired}, ((w_{max})_{f.d.} - w_{max}(ISTEP))]$$

(4-4)

$$\Delta z = \min\left[(\Delta z \text{ obtained from Eqn. (4-3)}), (\Delta z)_{max}\right] \quad (4-5)$$

where $(\Delta z)_{max}$ is a prescribed maximum step size.

The step-by-step marching integration procedure is stopped when the following flow condition is satisfied:

$$w_{max}(ISTEP) \geq 0.99(w_{max})_{f.d.} \tag{4-6}$$

This criterion for determining the extent of the developing flow regime is due to Shah and London [7].

So far, for convenience, the change of w_{max} between two consecutive steps has been used in the automatic calculation of the axial step size. It should be noted, however, that the corresponding change in any other suitable flow variable, such as $(d\bar{p}/dz)$, could have been used for the same purpose as well.

When the flow is hydrodynamically fully-developed but thermally developing, the change in the local peripherally-averaged Nusselt number is used in the automatic axial step size selector. For the two thermal boundary conditions considered in this thesis, namely (T) and (H), it can be shown that the Nusselt number starts off at a relatively high value ($z \to 0$, $Nu_z \to \infty$), and drops off quite rapidly towards a fully-developed value, as shown in Fig. 4-2(b). For this case, the "ideal" change in Nu_z between steps is defined as

$$(\Delta Nu_z)_{desired} = \frac{Nu_{f.d.} - Nu_z(ISTEP=3)}{IDEAL} \tag{4-7}$$

and the corresponding estimated step size is

$$\Delta z = \frac{z(\text{ISTEP}) - z(\text{ISTEP-1})}{Nu_z(\text{ISTEP}) - Nu_z(\text{ISTEP-1})} \left(\Delta Nu_z\right)_{\text{desired}} \qquad (4\text{-}8)$$

Again, as the thermally fully-developed region is approached, care must be exercised to ensure that (Δz) does not get too large. This can be done by setting:

$$\left(\Delta Nu_z\right)_{\text{desired}} = \max\left[\left(\Delta Nu_z\right)_{\text{desired}} ;\ \left(Nu_{f.d.} - Nu_z(\text{ISTEP})\right)\right] \qquad (4\text{-}9)$$

$$(\Delta z) = \min\left[(\Delta z) \text{ calculated in Eqn. (4-8)};\ (\Delta z)_{max}\right] \qquad (4\text{-}10)$$

In Eqn. (4-9), the maximum is taken since all values in the square bracket are negative. The marching integration procedure is halted when the following thermal condition is reached:

$$Nu_z(\text{ISTEP}) \leq 1.05\, Nu_{f.d.} \qquad (4\text{-}11)$$

In problems where fluid flow and heat transfer develop simultaneously, the automatic axial step size selector could be tied to the change in w_{max} or Nu_z between steps. Alternatively, the minimum of the steps calculated by Eqns. (4-3) and (4-8) could be used to march ahead. The choice of one alternative or the other depends on the problem being solved.

The requirements, in this connection, are that the final results should be insensitive, within tolerances, to the axial step sizes used, and, at the same time, the axial step sizes should not be too small in order to keep the method from getting prohibitively expensive. In Chapter VI, numerical experiments are carried out in order to determine the "best" of the above-mentioned alternatives for the problem of simultaneously developing flow and heat transfer in rod-bundle geometries.

4.1.2 Discretization of the Duct Cross-Section

The discretization of the duct cross-section involves its division into six-node triangular macroelements, and then the sub-division of each macroelement into four three-node triangular subelements, as was described in Chapter III. Here, a simple semi-automatic domain discretization scheme, proposed by Baliga [2] is employed for this purpose. In this procedure, consideration is first given to a unit square which is sub-divided into (LP1-1)† x (MP1-1)† smaller squares, as shown in Fig. 4-3(a). Following this, each small square is further divided into two triangles by joining the lower left-hand corner node to the one in the upper right-hand corner. The unit square is then manually distorted so as to fit the duct cross-section shape. The original grid lines could be bent

† the variable names employed here correspond to those used in the FORTRAN computer code given in Appendix IV.

in this operation but they are kept piecewise-linear, and they are adjusted in order to obtain the desired density of nodes. The resulting grid is composed of triangular elements which are regarded as macroelements. The subelements are obtained by joining the midpoints of the sides of each macroelement together. Fig. 4-3 illustrates the application of this discretization technique to three different irregular duct cross-sections.

4.1.3 Node and Element Numbering Schemes

As can be seen from Fig. 4-3, in each cross-sectional plane of the domain discretization, every pressure node can be uniquely addressed to by two integer indices (IP,JP): IP=1,2,... LP1; JP=1,2...,MP1. In a similar manner, each velocity node can be uniquely identified by two integer indices (I,J): I=1,2,...,L1; J=1,2,...,M1. At the vertices of the macroelements, the (IP,JP) and (I,J) sets of indices are interrelated via

$$\begin{aligned} I &= 2 * IP - 1 \\ J &= 2 * JP - 1 \end{aligned} \qquad (4\text{-}12)$$

Typical macroelements and subelements, along with their pressure and velocity nodes and their respective addresses are illustrated in Fig. 4-4.

Each pair of (IP,JP) indices can also be used to uniquely identify the quadrilateral formed by nodes (IP,JP), (IP+1,JP),

(IP+1,JP+1), (IP,JP+1). As illustrated in Fig. 4-4(a), every such quadrilateral is divided into two types of triangular macroelements: the macroelement formed by nodes (IP,JP), (IP+1,JP) and (IP+1,JP+1) is called a "type-1" macroelement; and the macroelement formed by nodes (IP,JP), (IP+1,JP+1) and (IP,JP+1) is termed "type-2" macroelement. Thus the complete address of a macroelement consists of the three indices (IP,JP, type). Similarly, a subelement is identified by the set of indices (I,J,type), as illustrated in Fig. 4-4(b).

4.1.4 Geographic Node Labelling Scheme

The line-by-line structure of grid points produced by the present domain discretization scheme enables easy identification of all neighbours to any nodal point. All the possible neighbours of a pressure node (IP,JP) form a star-like cluster displayed in Fig. 4-5(a). Each pressure neighbour is named according to its geographic position with respect to the central pressure node (IP,JP). Thus, referring to Fig. 4-5(a), "N" is the "north" neighbour, "NE" is the "north-east" neighbour, and "NNE" is the "north of north-east" neighbour, and so on. In total, up to twelve pressure neighbours could be involved in the pressure discretization equation for node (IP,JP).

All the possible neighbours of a velocity node (I,J) are displayed in Fig. 4-5(b). They too are labelled according to their geographic positions with respect to the central node (I,J). As is seen in Fig. 4-5(b), up to six

neighbours could appear in the momentum and ϕ discretization equations for node (I,J).

4.1.5 Comments

The aforementioned node and element addressing schemes have been made possible by the arrangement of grid points in simple and consistent line-by-line patterns in the proposed discretization scheme. This arrangement of grid points eliminates the need for elaborate node numbering schemes and neighbour-node directories usually encountered in general finite-element computer codes. The geographic nodal labelling scheme presented in the previous section is also made possible by the line-by-line arrangement of grid points.

The proposed discretization scheme yields a maximum of twelve neighbours in each of the discretization equations for pressure and pressure correction, and the momentum and ϕ discretization equations have a maximum of six neighbours each. Therefore, for each of these sets of discretization equations, computer storage is only required for the coefficients corresponding to these neighbours. As a result, significant economy in core storage can be achieved. Furthermore, as will be shown in a subsequent section, the grid line arrangement of nodes also allows the use of powerful iterative line-by-line methods for the solution of the discretization equations [4].

The proposed semi-automatic scheme to discretize the duct cross-section is suitable for simple irregular geometries and singly-connected domains: the unit square shown in Fig. 4-3(a) cannot be conveniently distorted to fit highly irregular and multiply-connected domains. Furthermore, the recommended triangulation of the calculation domain obtained by first dividing the domain into quadrilaterals and then subdividing each quadrilateral into triangles may not always allow the optimum distribution of the nodes [2]. These drawbacks can be considerably alleviated by the merging of the present discretization scheme with a recently-developed patch-by-patch procedure [35]. Such an approach, however, is left as a possible extension of the present work.

4.2 CALCULATION OF ELEMENT CONTRIBUTIONS AND ASSEMBLY OF DISCRETIZATION EQUATIONS

The derivation of the discretization equations has already been presented in Chapter III. In this section, the computer implementation of the procedures to calculate and assemble the coefficients in these equations is outlined.

4.2.1 Discretization Equations for ϕ

Consider the type-1 prism subelement shown in Fig. 4-6(a). In Chapter III, it was shown that the contribution of this element to the discretization equation associated with node 1 can be compactly written as follows:

$$CONT1 = C_{11}\,\phi_1 + C_{15}\,\phi_5 + C_{16}\,\phi_6 + C_{11}^{U}\,\phi_1^{U} + B_1 \qquad (3\text{-}23)$$

Using the (I,J) node addressing scheme, this equation can be rewritten as

$$CONT1 = C_{11}\phi(I,J) + C_{15}\phi(I+1,J) + C_{16}\phi(I+1,J+1) + C_{11}^{U}\phi^{U}(I,J) + B_1 \qquad (4\text{-}13)$$

In the FORTRAN computer language, the complete discretization equation for node (I,J), Eqn. (3-32), can be expressed as

$$\begin{aligned} AC(I,J)*\phi(I,J) = {} & AE(I,J)*\phi(I+1,J) + ANE(I,J)*\phi(I+1,J+1) \\ & + AN(I,J)*\phi(I,J+1) + AW(I,J)*\phi(I-1,J) \\ & + ASW(I,J)*\phi(I-1,J-1) + AS(I,J)*\phi(I,J-1) \\ & + ACON(I,J) \end{aligned} \qquad (4\text{-}14)$$

where the coefficient names correspond to the geographic node labelling scheme illustrated in Fig. 4-5(b). It is to be noted that, in Eqn. (4-14), the term involving $\phi^{U}(I,J)$ has been included in the non-homogeneous term ACON(I,J); this can be done in the marching integration scheme employed here because $\phi^{U}(I,J)$ is known or available from calculations at the previous axial step.

Comparing Eqns. (4-13) and (4-14), the contribution of the subelement under consideration to the discretization equations can be assembled as follows:

- with respect to node (I,J)

$$\begin{aligned} AC(I,J) &= AC(I,J) + C_{11} \\ AE(I,J) &= AE(I,J) - C_{15} \\ ANE(I,J) &= ANE(I,J) - C_{16} \\ ACON(I,J) &= ACON(I,J) - C_{11}^{U}\phi^{U}(I,J) - B_1 \end{aligned} \tag{4-15}$$

Similarly, the contribution of subelement (I,J,1) to the discretization equations for nodes (I+1,J) and (I+1,J+1) can be assembled in the following manner:

- with respect to node (I+1,J)

$$\begin{aligned} AC(I+1,J) &= AC(I+1,J) + C_{55} \\ AN(I+1,J) &= AN(I+1,J) - C_{56} \\ AW(I+1,J) &= AW(I+1,J) - C_{51} \\ ACON(I+1,J) &= ACON(I+1,J) - C_{55}^{U}\phi^{U}(I+1,J) - B_5 \end{aligned} \tag{4-16}$$

. with respect to node (I+1,J+1)

$$
\begin{aligned}
AC(I+1,J+1) &= AC(I+1,J+1) + C_{66} \\
ASW(I+1,J+1) &= ASW(I+1,J+1) - C_{61} \\
AS(I+1,J+1) &= AS(I+1,J+1) - C_{65} \\
ACON(I+1,J+1) &= ACON(I+1,J+1) + C^{U}_{66}\phi^{U}(I+1,J+1) - B_{6}
\end{aligned}
\qquad (4\text{-}17)
$$

A similar procedure is used to assemble the contributions of type-2 subelements. The complete discretization equations, such as Eqn. (4-14), are obtained when all elements have been visited and their internal contributions and boundary contributions, if applicable, are assembled appropriately. Further details on this assembly procedure are available in the Subroutine COEFF of the computer code presented in Appendix IV.

4.2.2 Discretization Equation for Pressure

Attention is now directed to a typical macroelement of type-1, shown in Fig. 4-6(b). As was discussed in Chapter III, the contribution of this macroelement to the macroelement control volume surrounding node (IP,JP) can be expressed as:

$$
\begin{aligned}
PCONT1 = {} & MP^{1}_{1}\, p_1 + MP^{1}_{2}\, p_2 + MP^{1}_{3}\, p_3 \\
& + MP^{1}_{o1}\, p_{o1} + MP^{1}_{o2}\, p_{o2} + MP^{1}_{o3}\, p_{o3} + MPCON1
\end{aligned}
\qquad (3\text{-}58)
$$

In terms of the (IP,JP) node addressing scheme shown in Fig. 4-6(b), Eqn. (3-58) can be rewritten as:

$$\begin{aligned} PCONT1 = {} & MP_1^1\, p(IP,JP) + MP_2^1\, p(IP+1,JP) \\ & + MP_3^1\, p(IP+1,JP+1) + MP_{o1}^1\, p(IP+2,JP+1) \\ & + MP_{o2}^1\, p(IP,JP+2) + MP_{o3}^1\, p(IP,JP-1) \\ & + MPCON1 \end{aligned} \qquad (4\text{-}18)$$

With reference to the node addressing and labelling schemes shown in Fig. 4-5(a), the complete pressure discretization equation can be written as follows:

$$\begin{aligned} APC(IP,JP)*p(IP,JP) = {} & [APE(IP,JP)*p(IP+1,JP) \\ & + APNE(IP,JP)*p(IP+1,JP+1) \\ & + APN(IP,JP)*p(IP,JP+1) + APNW(IP,JP)*p(IP-1,JP+1) \\ & + APW(IP,JP)*p(IP-1,JP) + APSW(IP,JP)*p(IP-1,JP-1) \\ & + APS(IP,JP)*p(IP,JP-1) + APSE(IP,JP)*p(IP+1,JP-1) \\ & + APENE(IP,JP)*p(IP+2,JP+1) + APNNE(IP,JP)*p(IP+1,JP+2) \\ & + APWSW(IP,JP)*p(IP-2,JP-1) + APSSW(IP,JP)*p(IP-1,JP-2)] \\ & + APCON(IP,JP) \end{aligned} \qquad (4\text{-}19)$$

where the expression in square brackets is the full form of the term $(\sum_{nb} a_{nb}^{P}\, p_{nb})$ in Eqn. (3-61). Comparing Eqns. (4-18) and (4-19), the contribution of macroelement (IP,JP,1) to

the discretized continuity equation for node (IP,JP) can be assembled in the following manner:

<u>with respect to node (IP,JP)</u>

$$\left.\begin{aligned}
\text{APC(IP,JP)} &= \text{APC(IP,JP)} + MP^1_1 \\
\text{APE(IP,JP)} &= \text{APE(IP,JP)} - MP^1_2 \\
\text{APNE(IP,JP)} &= \text{APNE(IP,JP)} - MP^1_3 \\
\text{APENE(IP,JP)} &= \text{APENE(IP,JP)} - MP^1_{o1} \\
\text{APN(IP,JP)} &= \text{APN(IP,JP)} - MP^1_{o2} \\
\text{APS(IP,JP)} &= \text{APS(IP,JP)} - MP^1_{o3} \\
\text{APCON(IP,JP)} &= \text{APCON(IP,JP)} - \text{MPCON1}
\end{aligned}\right\} \quad (4\text{-}20)$$

The contributions of the macroelement under consideration to the pressure equations for nodes (IP+1,JP) and (IP+1,JP+1) are assembled in a similar way. In order to avoid repetitions, the details are omitted here.

It is to be noted that all the coefficients in the pressure discretization equation, except the non-homogeneous term APCON(IP,JP), are the same as those appearing in the discretization equation for pressure correction. Consequently, in each iteration during the computational process, they are stored on an external disk storage unit and reloaded back into core storage when the time comes to compile the pressure correction equation. Further details on the assembly of the pressure and pressure correction equations are available in the subroutine PAPC of the computer code presented in Appendix IV.

4.3 SOLUTION OF THE DISCRETIZATION EQUATIONS

As was described in Chapter III, a step-by-step marching integration is used to obtain the velocity, pressure and ϕ distributions in the duct flow problems of interest. At each axial step, the values of these dependent variables at the nodes in the cross-sectional plane being considered are obtained by using an iterative solution procedure akin to SIMPLER [4]. In each iteration of this procedure, it is necessary to obtain a sequential solution of nominally linear sets of algebraic equations which govern $(d\bar{p}/dz)$, w, p, u, v, p' and ϕ. In this section, the method used to solve these nominally linear sets of discretization equations is described.

Several methods for the solution of a set of linear algebraic equations are available in the literature. They can be classified into two main categories: direct and iterative methods. Experience with numerical methods for multi-dimensional fluid flow and heat transfer has shown that iterative methods, if applicable, are simpler and more economical than direct methods, in terms of programming effort and computing costs [4]. In this thesis, an iterative line-by-line method [3,4] is employed for solving nominally linear sets of discretization equations. It is to be noted that the use of this particular method is possible because the domain discretization scheme described in section 4-1 yields a line-by-line arrangement of the nodes in each cross-sectional plane of the duct.

4.3.1 Solution of the Discretization Equations for u, v, w and ϕ

Nominally linear and decoupled discretization equations for u, v, w and ϕ have the same general forms, so the same method can be used to solve them. For convenience in the following discussion, the description of this method is presented with reference to the general scalar dependent variable ϕ.

At the start, the whole ϕ-field in the cross-section of interest is assigned guessed values. Then, attention is focussed on one particular grid line, line 'I' for example. Referring to Figs. 4-3 and 4-5, if the values of ϕ on the neighbouring grid lines (I+1) and (I-1) are treated as known, with the latest available values of ϕ assigned to the nodes on these lines, then each unknown value $\phi(I,J)$ on the 'I' line under consideration is connected to a maximum of two unknown neighbours $\phi(I,J+1)$ and $\phi(I,J-1)$. Collectively, therefore, the ϕ discretization equations for the nodes on the 'I' line form a tridiagonal matrix system which can be solved by the standard TriDiagonal Matrix Algorithm (TDMA) [4]. Once the nodal values of ϕ on line 'I' are calculated in this manner, the procedure is repeated for line 'I+1', then line 'I+2', and so on, until the whole cross-sectional domain has been 'swept' line-by-line. In an analogous manner, the cross-sectional calculation domain is then 'swept' using 'J' grid lines. In the computer implementation of the proposed method, if no information is available to

ascertain an optimum or preferred sweep direction, back-and-forth I- and J-sweeps are used alternately. Each iteration of this procedure is assumed to consist of four such alternating-direction sweeps of the calculation domain.

Several of the aforementioned iterations may be required to obtain an adequately converged solution of the nominally linear set of discretization equations. In this connection, it should be noted that, during the solution of non-linear flow problems, it is not necessary to solve nominally linear and decoupled sets of discretization equations to complete convergence. Indeed, substantial savings of computer time are possible if such intermediate solutions are carried to only partial convergence [4]. Currently, however, no criterion is available for determining the optimum degree of convergence in the solution of nominally linear and decoupled sets of discretization equations encountered in each iteration of the overall SIMPLER-like procedure.

4.3.2 Solution of the Pressure and Pressure Correction Equations

The pressure and pressure correction are stored only at the vertices of the macroelements. The macroelement node addressing scheme and the geographic node labelling scheme associated with the neighbours of a pressure node are illustrated in Figs. 4-3 and 4-5(a).

A line-by-line iterative procedure similar to one described in the last sub-section is used to solve the sets of discretization equations for p and p'. Consider a particular macroelement grid line, say line 'IP'. The values of p (or p', whichever is appropriate) on this line are treated as unknowns and the corresponding values at nodes lying on neighbouring lines (IP+1), (IP+2), (IP-1) and (IP-2) are regarded as known. The unknown nodal values of p (or p') on the line 'IP' are then calculated by using the TDMA. This procedure is then repeated for the 'IP+1' line, then the (IP+2) line, and so on, until the entire calculation domain is 'swept'. A similar 'sweep' of the calculation domain is then done using 'JP' lines. Two 'IP'-sweeps (back-and-forth) and two 'JP'-sweeps are performed in each iteration cycle. The iterations are continued until a suitable convergence criterion is satisfied.

4.3.3 Comments

The convergence of the aforementioned line-by-line iterative methods is guaranteed only if the coefficient matrix of the set of nominally linear discretization equations exhibits diagonal dominance [4]; this is the Scarborough criterion. In the proposed control volume finite-element method, this criterion is not always satisfied, especially in the case of pressure and pressure correction equations obtained with highly nonuniform grids. The lack of diagonance results if negative coefficients are encountered in

the coefficient matrix. In the testing of the computer code incorporating the proposed method, negative coefficients were encountered; but in all the test and application problems investigated so far, the negative coefficient difficulty was not serious enough to cause divergence of the proposed line-by-line iterative methods. Thus, it may be concluded that, while the convergence of these line-by-line iterative methods cannot be ensured for all possible situations, divergence is unlikely.

4.4 CLOSING REMARKS

In this chapter, the main tasks in the computer implementation of the proposed control volume finite-element method have been described. The complete computer code written in the FORTRAN computer language, its flow diagram, and brief descriptions of its various subroutines are given in Appendix IV. To validate the computer code and demonstrate its capabilities, several test problems have been solved; some of these problems are presented in Chapter V. In addition, the proposed method has been successfully applied to the problem of laminar fluid flow and heat transfer in rod-bundle geometries; the results are presented in Chapter VI.

CHAPTER V

APPLICATION OF THE METHOD TO SOME TWO- AND THREE-DIMENSIONAL TEST PROBLEMS

The validity and capabilities of the proposed control-volume finite-element method (CVFEM), and its computer implementation, are demonstrated in this Chapter by the presentation of its application to three different test problems. Whenever possible, the results produced by the proposed CVFEM are compared with the results of independent numerical and experimental investigations available in the literature.

As was described in Chapter III, the proposed CVFEM incorporates a step-by-step marching integration procedure which advances the solution in the main stream direction. At each axial step, the discretization analogues of the governing equations, which are parabolic in the main flow direction and elliptic in the cross-sectional plane, are solved by a procedure akin to SIMPLER [4]. Thus, the solution of three-dimensional parabolic duct flows resembles the solution of a series of two-dimensional elliptic problems. This feature of the proposed CVFEM was taken advantage of in the development and construction of its computer implementation. First, a general computer program incorporating a CVFEM for two-dimensional elliptic flows [1,2] was developed and tested thoroughly. This computer

program was then extended to handle three-dimensional parabolic flows and applied to test problems. This two-stage program development and testing procedure provided considerable convenience and cost savings.

In the remainder of this Chapter, the formulation, objectives, computational details and results of three different test problems are presented. The first problem involves two-dimensional natural convection in a vertically-oriented rectangular cavity. Two-dimensional natural convection in a trapezoidal cavity is investigated in the second problem. Fully-developed and developing flow and heat transfer in a duct of square cross-section are studied in the third problem. The first two two-dimensional problems were used in the first stage of the aforementioned two-stage procedure for the development and testing of the computer implementation of the proposed CVFEM. In this connection, it should be noted that the proposed computer program for three-dimensional parabolic flows can be adapted for the solution of two-dimensional flows by simply dropping the terms pertaining to the axial, or z-direction, derivative. With reference to the discretization equations presented in Chapter III, this can be achieved by setting the axial step size to a very large value, $\Delta z \rightarrow \infty$.

All three test problems presented in this chapter were simulated on an AMDAHL V7 computer using a FORTRAN-H extended compiler.

5.1 NATURAL CONVECTION IN A RECTANGULAR CAVITY

5.1.1 Problem Statement

Steady, laminar, natural convection in an enclosed rectangular cavity of aspect ratio 5 (height-to-width ratio) is investigated in this problem, which is depicted in Fig. 5.1(a). The two horizontal walls are insulated, the left vertical wall is maintained at a constant temperature T_c, and the right vertical wall is maintained at a uniform temperature T_h; $T_h > T_c$. The fluid inside the cavity is Newtonian and its density decreases linearly with temperature. The acceleration due to gravity is directed vertically downwards.

This problem has been the subject of several in-depth investigations [36-39]. In particular, Jones [39] has studied this problem by employing a finite-difference method based on the so-called stream function-vorticity formulation and has compared his results with experimental data of Duxbury [39]. Both Jones's and Duxbury's results are used to check the results of this investigation.

5.1.2 Analysis

The Boussinesq approximation [28] is used in this analysis. Thus the mass density of the fluid is treated as a constant in all terms except the buoyancy term. In the buoyancy term, the density is assumed to vary linearly with

temperature:

$$\rho = \rho_o[1 - \beta(T-T_c)] \tag{5.1}$$

where ρ_o is the density at $T = T_c$, and β is the thermal volumetric expansion coefficient.

The following non-dimensional variables† are used in this analysis:

$$\xi = x/L;\ \eta = y/L;\ A = H/L$$

$$u^* = u/(\mu/\rho_o L);\ v^* = v/(\mu/\rho_o L) \tag{5.2}$$

$$\theta = (T-T_c)/(T_h-T_c);\ p^* = p/\rho_o(\mu/\rho_o L)^2$$

$$Gr = \frac{g\beta(T_h-T_c)L^3}{(\mu/\rho_o)^2};\ Pr = \frac{\mu c_p}{k};\ Ra = GrPr$$

where Gr is the Grashof number, Pr is the Prandtl number, and Ra is the Rayleigh number. In terms of these non-dimensional variables, the governing equations can be written as follows:

---

†It is to be noted that these non-dimensional variables are defined for the natural convection problems presented in this section and Section 5.2 only. For the 3D parabolic duct flow problems presented in Section 5.3 and in Chapter VI, the definitions presented in Chapter II apply.

x-momentum:

$$\frac{\partial}{\partial \xi}(u^*u^*) + \frac{\partial}{\partial \eta}(v^*u^*) = - \frac{\partial p^*}{\partial \xi} - Gr\theta + \frac{\partial^2 u^*}{\partial \xi^2} + \frac{\partial^2 u^*}{\partial \eta^2} \qquad (5.3)$$

y-momentum:

$$\frac{\partial}{\partial \xi}(u^*v^*) + \frac{\partial}{\partial \eta}(v^*v^*) = - \frac{\partial p^*}{\partial \eta} + \frac{\partial^2 v^*}{\partial \xi^2} + \frac{\partial^2 v^*}{\partial \eta^2} \qquad (5.4)$$

continuity:

$$\frac{\partial u^*}{\partial \xi} + \frac{\partial v^*}{\partial \eta} = 0 \qquad (5.5)$$

energy:

$$\frac{\partial}{\partial \xi}(u^*\theta) + \frac{\partial}{\partial \eta}(v^*\theta) = \frac{1}{Pr}\left(\frac{\partial^2 \theta}{\partial \xi^2} + \frac{\partial^2 \theta}{\partial \eta^2}\right) \qquad (5.6)$$

The boundary conditions are $u^* = 0$ and $v^* = 0$ on all walls; $\theta = 0$ on the $\eta = 0$ wall, $\theta = 1$ on the $\eta = 1$ wall; and $(\partial\theta/\partial\xi) = 0$ on the $\xi = 0$ and $\xi = A$ walls.

Once the solution for θ has been obtained, the local Nusselt numbers on the hot wall can be evaluated:

$$Nu = \left\{\frac{k(\partial T/\partial y)_{y=L}}{(T_h - T_c)}\right\} (L/k) = \left(\frac{\partial \theta}{\partial \eta}\right)_{\eta=1} \qquad (5.7)$$

Then the average Nusselt number for the hot wall can be calculated:

$$Nu_{av} = \frac{1}{A} \int_o^A \left(\frac{\partial \theta}{\partial \eta}\right)_{\eta=1} d\xi \tag{5.8}$$

In this problem, the total heat transfer from the hot wall to the fluid is equal to that gained by the cold wall from the fluid. Thus the average Nusselt number for the hot wall is equal to that for the cold wall.

Another quantity of interest which can be computed after the solution of Eqs. (5-3)-(5.6) is the non-dimensional stream function ψ

$$\frac{\partial \psi}{\partial \eta} = u^*; \quad \frac{\partial \psi}{\partial \xi} = - v^* \tag{5.9}$$

Using the continuity equation,

$$\frac{\partial^2 \psi}{\partial \xi^2} + \frac{\partial^2 \psi}{\partial \eta^2} = \Omega \tag{5.10}$$

where Ω is the non-dimensional vorticity:

$$\Omega = \frac{\partial u^*}{\partial \eta} - \frac{\partial v^*}{\partial \xi} \tag{5.11}$$

In this analysis, the stream function ψ is obtained by solving

the conduction-type problem posed by Eqn. (5-10) subject to the boundary condition $\psi = 0$ on the walls.

5.1.3 Computation Details

A 13x9 uniform macroelement grid, corresponding to a 25x17 subelement grid, was used to discretize the calculation domain, as shown in Fig. 5.1(b). This grid corresponds to a total of 768 triangular subelements.

In accordance with previous investigations [39], three values of Rayleigh number were considered:

$$Ra = 2.49 \times 10^3,\ 1.49 \times 10^4 \text{ and } 1.36 \times 10^5.$$

In all cases, the Prandtl number was maintained at 0.7.

The solution procedure was started by assigning initial, or guess, values to the velocity and temperature fields. These were obtained from a previous, or lower Rayleigh number solution; in the lowest Rayleigh number case, a pure conduction solution with no flow was used to start the computations.

In all cases considered in this problem, the following set of under-relaxation parameters were used:

$$\alpha_u = \alpha_v = 0.5;\ \alpha_p = 0.8;\ \alpha_T = 1.0$$

The iterations in the SIMPLER-type solution procedure were terminated when the average Nusselt number, Nu_{av}, had converged

to at least five significant figures.

5.1.4 Results

Average Nusselt numbers for the three cases studied are presented in Table 5.1. The corresponding numerical results of Jones [39], obtained using a stream function-vorticity formulation and a finite-difference method, and the experimental results of Duxbury [39] are also presented in Table 5.1. Jones used a uniform 32x16 node grid in his computations. The results of the present analysis match those of Jones very well. The comparison with Duxbury's experimental results is not as good. However, it should be noted that Duxbury's Nusselt numbers on the cold face are consistently higher than those on the hot face; this indicates that there could be unaccounted heat losses in his experimental data. Furthermore, the mean values of his hot and cold face Nusselt numbers, shown in the last column of Table 5.1, agree quite well with the present results and those of Jones.

Computed temperature distributions across the rectangular cavity, for five different locations along its height (ξ = 0.5, 1.5, 2.5, 3.5 and 4.5) are presented in Figs. 5.2(a)-(c); these three figures pertain to Ra = 2.49×10^3, 1.67×10^4, and 1.36×10^5, respectively. Also presented in these graphs are the numerical results of Jones [39], plotted in dashed lines, and the experimental results of Duxbury [39];

Jones's and Duxbury's results were obtained by digitizing the corresponding temperature graphs in [39].

For Ra = 2.49×10^3, the temperature profile in the centre of the cavity is almost linear. Conduction is therefore the dominant mechanism for heat transfer, and the Nusselt number for this case is very close to 1. For Ra = 1.67×10^4, the temperature profiles tend to become flat in the central region and vary steeply near the vertical walls. This is the so-called "boundary layer regime" [39]: most of the heat is transferred by convection through the boundary layers and very little of it is transfereed across the cavity, in the central region. Agreement between the present results and those of Jones and Duxbury is very satisfactory for these two Rayleigh numbers.

For Ra = 1.36×10^5, the results of the present analysis, shown by solid lines in Fig. 5.2(c), exhibit small negative temperature gradients in the central region of the cavity, and these indicate that some heat in this region is being transferred in the positive y-direction. Jones's results show similar trends, although there are considerable departures from the present profiles for ξ = 0.5 and 4.5. However, both Jones's and the present results do not quite match Duxbury's experimental results so that no definite assessment can be made here. It is to be also noted that for this high value of Rayleigh number, there could be considerable heat losses through the insulated surfaces in Duxbury's experiments, as was previously discussed.

Nevertheless, there is qualitative agreement between the results of the present analysis and those of Jones and Duxbury.

Isotherm contours are presented in Figs. 5.3(a)-(c) for Ra = 2.49×10^3, 1.67×10^4, and 1.36×10^5, respectively. As expected, at the lowest Rayleigh number, the isotherms deviate only slightly from the vertical and are fairly evenly spaced over much of the rectangular enclosure; this indicates that conduction is the dominant mode of heat transfer. As the Rayleigh number is increased, convection becomes the dominant mode of heat transfer and the isotherms become increasingly wavy and get crowded in the vicinity of the hot and cold walls. In all cases, there is a considerable concentration of the isotherms in the lower right and the upper left corners of the enclosure. Heat transfer is therefore highest in these regions.

Streamline plots are presented in Figs. 5.4(a)-(c) for Ra = 2.49×10^3, 1.67×10^4, and 1.36×10^5, respectively. In all figures, ψ increases from a minimum value of zero on the walls to a maximum value in the central region of the enclosure. These results are in good qualitative agreement with the numerical results of Jones [39] and the flow visualization data of Duxbury [39].

5.2 NATURAL CONVECTION IN A TRAPEZOIDAL CAVITY

5.2.1 Problem Statement

In this problem, steady, laminar natural convection in an enclosure of trapezoidal cross section is investigated. A schematic illustration of the problem is given in Fig. 5.5(a). The top and bottom walls of the enclosure make an angle of 15° with the horizontal and are considered to be adiabatic. The left and right walls are vertical and are maintained at constant temperatures of T_h and T_c, respectively; $T_h > T_c$. The height of the left, or hot, wall is $H = 0.0254$ m, and the perpendicular distance between the left and right walls is $L = 0.0768$ m. The acceleration due to gravity $\vec{g}$ is directed vertically downwards.

This problem is used to demonstrate the capability of the proposed CVFEM to solve recirculating cross-sectional flows in irregular-shaped calculation domains. Iyican *et al.* [40,41] have studied this problem experimentally. Their results are used to check those of this analysis.

5.2.2 Analysis

Equations (5-1) to (5-6), which were used in the mathematical description of the last test problem, apply to this problem too. The boundary conditions are $u^* = v^* = 0$ on all walls; $\theta = 0$ and $\theta = 1$ on the right and left walls, respectively; and the normal derivative of the temperature is

zero on the top and bottom adiabatic walls.

Once the solution for θ has been obtained, the average Nusselt number for the hot wall can be calculated using

$$Nu_{av} = \frac{1}{A} \left[\int \left(\frac{\partial \theta}{\partial \eta}\right) d\xi\right]_{\text{hot wall}} \tag{5.12}$$

Another quantity of interest is the stream function ψ defined by Eq. (5.9). It is obtained by solving Eq. (5.10), subject to the boundary condition $\psi = 0$ on the walls of the enclosure.

5.2.3 Computation Details

All computations were done using a grid consisting of 288 six-node triangular macroelements; the corresponding subelement grid, composed of 1152 three-node triangular elements, is illustrated in Fig. 5.5(b).

Four different Rayleigh numbers were considered in this problem: Ra = 10^3, 10^4, 10^5, and 10^6. The Prandtl number was maintained constant at 0.7 in all computations. As in the previous test problem, initial, or guess, values of the velocity and temperature distributions, required to start the computations, were obtained from the previous, or lower, Rayleigh number case; for the lowest Rayleigh number, the conduction solution was used as the initial distribution.

In all computations, the following set of under-relaxation parameters was used:

$$\alpha_u = \alpha_v = 0.5;\ \alpha_p = 0.8;\ \alpha_T = 1.0.$$

The iterations in the SIMPLER-type solution procedure [4] were terminated when the values of Nu_{av} had converged to at least five significant figures.

5.2.4 Results

The variation of the average Nusselt number with Rayleigh number is presented in Fig. 5.6. Also presented in this figure are the experimental results of Iyican *et al.* [41] and a graph of a correlation proposed by the same authors. It is seen that the agreement between the results of this analysis and those of Iyican *et al.* is very good over the entire range of Rayleigh number considered.

Isotherm contours are presented in Figs. 5.7(a)-(d) for Ra = 10^3, 10^4, 10^5, and 10^6, respectively. For Ra = 10^3, conduction is the dominant mode of heat transfer, and the isotherms in Fig. 5.7(a) are almost parallel to the vertical walls. As the Rayleigh number is increased, convection starts contributing significantly to the overall heat transfer, and it is the dominant mode at Ra = 10^6. For all Rayleigh numbers, there is a higher concentration of isotherms in the vicinity of the left wall than that adjacent to the right wall. This is because the area of the left wall is less than that of the right wall. Thus for the same total heat transfer, the temperature gradients in the vicinity

of the left wall have to be higher than those adjacent to the right wall.

The corresponding streamline plots are given in Figs. 5.8(a)-(d). In all the figures, the stream function ψ decreases from a maximum value of zero on the walls to a minimum value in the central region of the cavity. As is to be expected, the strength of the recirculating flow increases with increasing Rayleigh number. At $Ra = 10^6$, the flow displays a multicellular structure in the central portion of the trapezoidal enclosure.

5.3 LAMINAR FLUID FLOW AND HEAT TRANSFER IN DUCTS OF SQUARE CROSS-SECTION

In this section, the complete CVFEM for three-dimensional parabolic flows is used to study steady, laminar, forced convection in a straight duct of square cross-section. It is assumed that the fluid is Newtonian and its properties are constant. Two thermal boundary conditions are investigated in this study: (i) constant wall temperature (T), and (ii) uniform wall heat flux (H).

A detailed mathematical description of this problem has already been presented in Chapter II, so it is not repeated here. In the subsections that follow, only the computational details and results are presented. First, a study is undertaken of fully-developed flow and heat transfer in square ducts. Then, attention is focused on the thermally-

developing situation under fully-developed flow conditions. Lastly, simultaneously developing flow and heat transfer in a duct of square cross-section are investigated.

5.3.1 Fully-Developed Flow and Heat Transfer

This problem has been studied extensively by a number of researchers; a review of these works has been compiled by Shah and London [7]. The results reported in [7] are used in this subsection to check the results of this analysis. The fluid flow results are presented first. Then, the heat transfer results are discussed.

A. Fluid Flow

The fully-developed flow in this problem is governed by Eq. (2.28). This equation can be solved by the CVFEM described in Chapter III by setting $u = v = w = 0$, $\phi = W$, $\Gamma = 1$, $S = -1$ and $\Delta z \to \infty$. Once the W-field has been obtained, the mean velocity, $\bar{W}$, can be computed. It can then be used to obtain the friction factor - Reynolds number product (f.Re) and the normalized velocity field $(W/\bar{W})$. The latter is stored and used as an input to the heat transfer problems. A flowchart outlining the above operations is given in Fig. 5.9.

Computational Details

Figure 5.10 shows the geometry of the problem considered.

Due to symmetry, only one-quarter of the duct cross-section, shown by the shaded area in Fig. 5.10(a), needs to be analyzed. A non-uniform macroelement grid of 6x6 pressure nodes, corresponding to an 11x11 node subelement grid, was employed to discretize this domain for all runs, except those made to examine the effect of grid size. The grid used is shown in Fig. 5.10(b). The positions of the I- and J-lines in this grid are given by the following equations:

·For I = 1, 3, 5 ..., L1, and J = 1, 3, 5 ..., M1

$$\left.\begin{aligned} X(I,J) &= [(I-1)/(L1-1)]^{POWER} * (L/2) \\ Y(I,J) &= [(J-1)/(M1-1)]^{POWER} * (L/2) \end{aligned}\right\} \quad (5.13)$$

·For I = 2, 4, 6 ..., (L1-1), and J = 2, 4, 6 ..., (M1-1)

$$\left.\begin{aligned} X(I,J) &= 0.5*(X(I+1)+X(I-1)) \\ Y(I,J) &= 0.5*(Y(I+1)+Y(I-1)) \end{aligned}\right\} \quad (5.14)$$

where L1 and M1 are the total number of nodes in the x- and y-directions, respectively, and POWER is a number which can be adjusted so as to obtain the desired density of grid lines in the vicinity of the walls. POWER = 1 corresponds to a uniform grid. A value of POWER greater than 1 is desirable since the fully-developed velocity profile is

expected to change more rapidly near the wall than in the central region of the duct. In this study, POWER = 1.4 was used in all runs, except those made to test the effect of POWER on the results.

Results

Fully-developed velocity profiles along a symmetry line and along a diagonal are shown in Figs. 5.11(a) and (b). The experimental results of Goldstein and Kreid [42] are also shown in these figures. The agreement between the computed and experimental results is very good. The computed maximum velocity, $(W/\bar{W})_{max}$, which occurs at the duct centerline, is 2.123. This compares favorably with the value of 2.0962 computed by Lundgren *et al.* [7, p. 198].

The friction factor - Reynolds number product, f.Re, is a constant for fully-developed laminar flow in a square duct. The calculated value here is f.Re = 57.092; the corresponding value calculated analytically by Shah and London [7] is 56.908. This corresponds to a relative error of 0.32%.

The aforementioned results were obtained using a subelement grid of 11x11 nodes and a value of POWER of 1.4. The effects of refining the grid size and varying the value of POWER, which determines the distribution of grid lines, are shown in Table 5.2. As is to be expected, successive refinement of the grid systematically decreases the percentage

error. For the 19x19 node subelement grid and POWER = 1.4, the error in f.Re is as small as 0.01%. For a fixed number of nodes, there is an optimum value of POWER for which the percentage error is a minimum. This appears to correspond to POWER = 1.4 for the three grids tested. On the basis of the results presented in Table 5.2, it was concluded that a subelement grid of 11x11 nodes with POWER = 1.4 is sufficiently accurate for this problem.

B. Heat Transfer: (T) Boundary Condition

The governing equation in this case is Eq. (2.55). This can be considered as an eigenvalue problem, with λ as the eigenvalue and the dimensionless temperature Θ as the eigenfunction. An iterative solution procedure was used to solve this problem. First, initial, or guessed, values of Θ were assigned to all nodes inside the calculation domain. Then, λ was calculated using Eq. (2.57). Equation (2.55) was then solved numerically, using the proposed CVFEM with $u = v = w = 0$, $\phi = \Theta$, $\Gamma = 1$, $S = \lambda(W/\bar{W})\Theta$, and $\Delta z \to \infty$. This yielded a new distribution of Θ which, in turn, was used to recalculate a new value of λ. This sequence of operations was repeated until convergence. This iterative procedure is outlined in Fig. 5.12.

Computation Details

As in the fluid flow analysis, an 11x11 node sub-

element grid with POWER = 1.4 was employed. The aforementioned iterative procedure was repeated until the relative change in λ between two successive iterations was less than 0.001%.

Results

The overall Nusselt number, $Nu_{(T)}$, computed in this study is 2.9386. This agrees to within 1.26% with the value of 2.976 reported by Shah and London [7].

The effect of grid size on $Nu_{(T)}$ is shown in Table 5.3. Successive grid refinement drives $Nu_{(T)}$ closer to the value obtained by Shah and London [7]. The accuracy provided by an 11x11 node grid with POWER = 1.4 is considered adequate in this study.

C. Heat Transfer, (H) Boundary Condition

The governing equation in this problem is Eq. (2.70). This equation was solved numerically using the proposed CVFEM with $u = v = w = 0$, $\phi = \chi$, $\Gamma = 1$, $S = (-4W/\bar{W})$, and $\Delta z \to \infty$. The solution procedure is outlined in the flowchart shown in Fig. 5.13. Again, a subelement grid of 11x11 nodes with POWER = 1.4 was employed in the computations.

Results

The overall Nusselt number, $Nu_{(H)}$, for this case was computed to be 3.0475. This agrees to within 1.4% with

the value of 3.091 obtained by Shah and London [7].

The effect of grid size on $Nu_{(H)}$ is shown in Table 5.3. Again, the computed value of $Nu_{(H)}$ approaches the analytical result of Shah and London [7] as the grid is refined.

The wall temperature distribution around the periphery of the duct cross-section is not uniform in the present case. The maximum temperature occurs at the duct corners, and the minimum temperature occurs at the mid-points of the sides. Shah [7] computed normalized maximum and minimum temperatures which are defined as follows:

$$T^*_{w,max} = \frac{T_{w,max} - T_c}{\bar{T}_w - T_c}, \quad T^*_{w,min} = \frac{T_{w,min} - T_c}{\bar{T}_w - T_c} \tag{5.15}$$

where T_c is the temperature at the centerline and $\bar{T}_w$ is the peripheral average wall temperature. In Table 5.4, the results of this analysis are compared with those of Shah. Agreement within 0.5% is found.

5.3.2 Hydrodynamically Fully-Developed and Thermally Developing Flow

In this subsection, consideration is given to the problem in which the velocity profile is fully-developed and remains fixed while the temperature profile develops. Though solutions to such problems strictly apply only to

situations where a hydrodynamic starting length is provided, so that the velocity profile is fully-established before heat transfer starts, they are excellent approximations to entrance flows of high Prandtl number fluids [28]. They have, therefore, received considerable attention in the literature [7,28]. The published results pertaining to flow in a square cross-section duct are used in this subsection to check the results of this investigation.

The governing equation for this problem is Eq. (2.34). In this equation, the velocity field is treated as known, and it is obtained from the analysis of fully-developed flow presented in the last subsection. Two thermal boundary conditions are considered: (i) constant wall temperature (T), and (ii) uniform wall heat flux (H). At the inlet of the duct, the temperature of the fluid is assumed to be uniform, $T = T_i$.

The proposed CVFEM was used to solve this problem. The complete developing temperature field was obtained by marching plane-by-plane in the direction of the primary flow. At each axial station, except for the fist three, the automatic step size selector described in Chapter IV was employed to adjust the step size Δz; this step-size adjustment was based on a specified desired change in the local Nusselt number and on the z-direction slope of this Nusselt number at the previous upstream station. A very small value of Δz was used for the first three axial steps so as to accommodate the expected steep variation of Nusselt

number in the vicinity of the duct entrance. Figure 5.14 gives an overview of the solution procedure employed.

The treatment of the initial condition in this problem deserves special mention, since for the (T) boundary condition, the initial condition is singular at the duct wall. The singularity results from the assumption that the inlet temperature profile possess an infinite gradient at the wall, as is illustrated in Fig. 5.15. Obviously, the present method with its finite mesh spacing cannot handle such a severe variation of temperature without incurring large errors near the singularity. Fortunately, numerical experiments† have shown that these initial errors tend to decay rather rapidly as the solution is advanced downstream. Furthermore, by (i) having a high concentration of grid lines near the wall, and (ii) taking very small initial step sizes, it is believed that these starting errors do not have any appreciable effect on the results, except in the immediate vicinity of the entrance.

Computation Details

Table 5.5 shows three different sets of grid and step sizes used for calculating the developing temperature field. The basic grid is the same as that employed in the analysis of the fully-developed regime, namely, a subelement grid of 11x11 nodes with POWER = 1.4; this grid is shown in

†To be described in the discussion of results.

Fig. 5.10(b). With reference to the automatic step-size selector described in Chapter IV, a value of IDEAL = 25 was chosen; IDEAL represents the estimated ideal number of steps needed to produce an accurate solution over the region inbetween z = 0 to a location where fully-developed conditions are reached. About 39 axial steps are actually required to attain the fully-developed situation for both (T) and (H) boundary conditions. Two other sets of grid and step sizes (Runs B and C in Table 5.5) were employed for checking the accuracy of the computations with the basic grid. In all runs, the marching scheme was started by using $\Delta z' \sim 10^{-7}$ for the first three axial steps.

At each axial station, after the calculation of the temperature field, the local and surface-averaged values of Nusselt number were evaluated as follows:

$$Nu_{z,(T)} \triangleq \frac{\dot{m}c_p D_H}{Pk(T_w-T_b)} \frac{dT_b}{dz} \cong \frac{\dot{m}c_p D_H}{Pk(T_w-T_b^D)} \frac{(T_b^D-T_b^U)}{\Delta z} \qquad (5.16)$$

$$Nu_{z,(H)} \triangleq \frac{q_w D_H}{(\bar{T}_w-T_b)k} \cong \frac{q_w D_H}{(\bar{T}_w-T_b^D)k} \qquad (5.17)$$

For both (T) and (H) boundary conditions:

$$Nu_m = \frac{1}{z}\int_o^z Nu_z\, dz \cong \frac{1}{z}\left[\int_o^{z-\Delta z} Nu_z\, dz + Nu_z\, \Delta z\right] \qquad (5.18)$$

where the superscripts U and D denote values stored at upstream and downstream stations, respectively. It is to be noted that the above expressions for calculating Nu_z and Nu_m are consistent with the profile assumptions used in the fully-implicit formulation of the proposed method; in the main flow direction, downstream values of the dependent variables are assumed to prevail over the interval Δz.

Results

A. Constant Wall Temperature Boundary Condition: (T)

Figure 5.16 shows the variation of local Nusselt number, $Nu_{z,(T)}$, with axial distance for different sets of grid and step sizes. As expected, $Nu_{z,(T)}$ has a maximum at the inlet plane and decreases as z' ($= z/D_H RePr$) increases; $Nu_{z,(T)}$ is less than 1.05 times the fully-developed value, $Nu_{(T)}$, at $z' \cong 0.066$. In the mathematical problem, $Nu_{z,(T)}$ should approach infinity as $z' \to 0$. This is because for the prescribed initial condition, the temperature gradient at the wall is infinite at $z' = 0$, as mentioned before. In the numerical problem, however, due to the finite mesh spacing used, $Nu_{z,(T)}$ asymptotes to a finite value as $z' \to 0$. This limiting value increases as the grid and step sizes are refined, and this observation is consistent with expectations. Furthermore, it is to be noted that for $z' > 6 \times 10^{-5}$, the difference between the curves (A), (B), and (C) in Fig. 5.16 is almost indistinguishable. This indicates

that the results generated by the basic 11x11 node with POWER = 1.4 are accurate and reliable for z' greater than $6x10^{5}$.

The local Nusselt number, $Nu_{z,(T)}$, and surface-averaged Nusselt number, $Nu_{m,(T)}$, as functions of z' are shown in Fig. 5.17. For checking these results, the corresponding computed results of Chandrupatla and Sastri [43] are also shown in Fig. 5.17. As can be seen in the figure, agreement between these results is very satisfactory.

B. Uniform Wall Heat Flux Boundary Condition: (H)

The axial variation of local Nusselt number, $Nu_{z,(H)}$, for different grid and step sizes is illustrated in Fig. 5.18. As in the (T) condition, $Nu_{z,(H)}$ starts with a high value and gradually decreases to within 1.05 times its fully-developed value at $z' \cong 0.07$. For $z' > 5x10^{-5}$, the $Nu_{z,(H)}$ *vs* z' curves for the three sets of grid and step sizes used are virtually the same, so the results obtained with the basic grid ((A)) can be regarded as adequate. For $z' < 5x10^{-4}$, however, each curve asymptotes to a different limiting value as $z' \to 0$. Mathematically, the value of $Nu_{z,(H)}$ at $z' = 0$ should be infinite: this is because $(\bar{T}_w - T_b) = 0$ at $z' = 0$ and $Nu_{z,(H)} \triangleq (q_w D_H)/[k(\bar{T}_w - T_b)]$. In the numerical solution, however, the value of $Nu_{z,(H)}$ for the first axial step is based on $(\bar{T}_w - T_b)$ at $z' = \Delta z'$, and this value is assumed to prevail over the region $0 \leq z' \leq \Delta z'$.

Therefore, all three curves in Fig. 5.18 give finite values of $Nu_{z,(H)}$ at $z' = 0$. As is to be expected, when the grid is refined, and $\Delta z'$ is reduced, the value of $Nu_{z,(H)}$ for the first axial step increases.

The variation of local and mean Nusselt numbers, $Nu_{z,(H)}$, and $Nu_{m,(H)}$, with non-dimensional axial distance z' are displayed in Fig. 5.19, and are compared with the corresponding results of Chandrupatla and Sastri [43]. It can be seen that good agreement is obtained for $Nu_{z,(H)}$. The values of $Nu_{m,(H)}$ computed by Chandrupatla and Sastri are higher than those obtained in this investigation, but this difference tends to decrease as z' is increased. Moreover, it is to be noted that in both analyses, $Nu_{m,(H)}$ is obtained from the computed values of $Nu_{z,(H)}$ by using the following equation: $Nu_{m,(H)} \triangleq [\int_0^{z'} Nu_{z,(H)}\, dz']/z'$. Therefore, the difference between the present results and those in [43] is probably due to the differences in the numerical integration schemes and the number of data points used to approximate the integral in the aforementioned equation for $Nu_{m,(H)}$.

5.3.3 Simultaneously Developing Flow and Heat Transfer

In this subsection, simultaneously developing steady, laminar fluid flow and heat transfer in a square cross-section duct are investigated. At the inlet of the duct, the velocity and temperature distributions are assumed

to be uniform across the duct cross-section: $w = \bar{w}$, $u = v = 0$ and $T = T_i$. The duct walls are considered to be impermeable and the no-slip condition applies: therefore, $u = v = w = 0$ on the duct walls. Two thermal boundary conditions are considered: (i) constant duct wall temperature (T) and (ii) uniform wall heat flux (H).

The equations governing this problem are the continuity equation, Eq. (2.8), the x-, y- and z-momentum equations, Eqs. (2.9) to (2.11), and the energy equation, Eq. (2.34). The equations governing the flow are non-linear and coupled. The energy equation is linear, but it needs the fluid flow solution as an input. Therefore, this problem tests all features of the proposed step-by-step marching solution procedure for three-dimensional parabolic flows.

A flow chart outlining the step-by-step solution procedure employed to obtain the developing velocity and temperature fields is given in Fig. 5.20. At each axial step, the flow field is solved for first, and then the energy equation is solved. An iterative procedure akin to SIMPLER is used to handle the solution of the continuity and momentum equations. After the first three steps, the step sizes are internally calculated using the automatic step size algorithm discussed in Chapter IV; in the first three steps, very small step sizes are used to account for the steep changes in the dependent variables. Over most of the solution procedure, the automatic step-size selection is based on the specified change in the value of the centerline

axial velocity component; however, once the flow is fully-developed, a specified desired change in Nusselt number is used to calculate the step size. The marching integration procedure is terminated when both velocity and temperature distributions are fully-developed; the velocity field is considered to be fully-developed when the centerline axial velocity component is larger than 99% of its fully-developed value, and the temperature field is assumed to be fully-developed when the Nusselt number is lower than 1.05 times its fully-developed value.

Special attention is required in the treatment of initial conditions, since they are singular at the duct walls. The singularity is a result of the assumptions that (i) the inlet axial velocity changes suddenly from $\bar{w}$ to zero at the walls of the duct, as shown in Fig. 5.21(a), and, (ii) there is a steep change in the initial temperature distribution from T_i to T_w in the case of the (T) condition, shown in Fig. 5.15. Clearly, such severe changes in the dependent variables cannot be handled by the proposed CVFEM without incurring relatively large errors near the singularity. However, as was shown in the analysis of thermally developing flow in the last subsection, these initial errors tend to decay rather quickly and, at a small distance from the inlet, they may be regarded as negligible. Moreover, the magnitudes and effects of these starting errors are significantly alleviated in the present analysis by the use of: (i) higher density of nodes in the wall

region than in the central region, and (ii) small initial step sizes.

Computation Details

In the proposed numerical method, the aforementioned singularity in the specified axial velocity distribution at the inlet duct cross-section cannot be modelled exactly. As was stated in Chapter III, in any given duct cross-section, the nodal values of the axial velocity are assumed to prevail over their corresponding control volume surfaces. Thus at the duct inlet, if the axial velocity is set equal to $\bar{w}$ at internal nodes and assigned the value of zero at nodes on the duct walls, as shown by the dashed lines in Fig. 5.21(b), the numerically calculated mass flow rate in the duct will be less than the desired, or specified, mass flow rate. Furthermore, the errors caused by this mass flow rate deficit will persist in all of the computed results. To overcome this problem, the following procedure is used to assign axial velocity values at the nodes in the inlet plane. First, these values are set according to

$$w_j = \begin{cases} \bar{w} \text{ if } j \text{ is an internal node} \\ 0 \text{ if } j \text{ is a node on the duct walls} \end{cases}$$

Then a correction factor FAC is calculated as follows:

$$FAC = \frac{\bar{w} \sum_j \rho_j A_j}{\sum \rho_j A_j w_j}$$

where A_j is the portion of the control volume surface associated with node j that lies in the inlet plane of the duct. This correction factor is then used to augment all inlet nodal values of w:

$$(w_j)_{corrected} = w_j \times FAC$$

This corrected inlet axial velocity distribution is shown in Fig. 5.21(b) by the solid line. The resulting numerically calculated mass flow rate is exactly equal to the desired value.

The choice of a grid that is satisfactory, both from an accuracy viewpoint and with respect to computational cost and storage requirements, is more important in this problem than in those discussed earlier. This is because the computational effort involved in the solution of simultaneously developing flow and heat transfer is substantially greater than that required to solve hydrodynamically fully-developed and thermally developing flow. In this study, on the basis of several numerical trial runs, a macroelement grid of 6x6 nodes, which corresponds to an 11x11 node subelement grid, was chosen; with reference to Eqs. (5.13) and (5.14), the corresponding grid distribution yielded by setting POWER = 1.4 was considered satisfactory. The first three axial steps

were executed with $\Delta z^* \sim 10^{-7}$. Following that, the automatic step selector discussed in Chapter IV was used with IDEAL = 25; in the actual computations, this resulted in about 34 steps from the inlet to a position where fully-developed flow and heat transfer conditions were attained.

At each axial step, for the first 15-20 steps, the iterations in the SIMPLER-type solution procedure were terminated when the maximum relative changes in the values of u, v, w and $(d\bar{p}/dz)$, at four selected nodes distributed across the duct cross-section, were all less than 10^{-5}. After the first 15-20 steps, this convergence criterion was applied only to the relative changes in the values of w and $(d\bar{p}/dz)$; this was because the values of the cross-sectional velocities, u and v, approach zero in the vicinity of the fully-developed region.

The Prandtl number is a parameter in this problem. In all computations, this parameter was maintained at a constant value: Pr = 0.72.

Fluid Flow Results

The variation of the mean pressure with axial distance is shown in Fig. 5.22. In the vicinity of the duct inlet, the axial pressure gradient is very high. This high pressure gradient is required to overcome the high wall shear stresses caused by the very steep velocity gradients at the wall, close to the inlet plane. As the flow proceeds downstream,

the pressure gradient approaches a constant fully-developed value. The results of this study are in excellent agreement with the measurements made by Beavers *et al.* [44], as seen in Fig. 5.22.

In Fig. 5.23, the predicted variation of the centerline axial velocity with axial distance, and the corresponding experimental results of Goldstein and Kreid [42] are presented. In the entrance region, continuity requirements cause a rapid increase in the axial velocity of the fluid at the duct centerline in response to the sudden deceleration of the fluid near the duct walls. At larger z*, the centerline axial velocity asymptotes to a constant fully-developed value. Once again, the agreement between the calculated and experimental results is very good.

Figure 5.24 shows the development of the axial velocity profile along a symmetry line and along a diagonal. Also superimposed on these graphs are the measurements of Goldstein and Kreid [42]. The satisfactory agreement between these results establishes the validity of the proposed CVFEM and the accuracy of the present computations.

The cross-sectional flow field at various axial locations is displayed in Fig. 5.25. It can be seen that the cross-stream flow is quite significant initially, but it dies out rather quickly as the main flow proceeds downstream. Additional evidence of the consistency of the proposed CVFEM is provided by the observed symmetry in the distribution of the cross-sectional velocities with respect to the diagonal.

Heat Transfer Results: (T) Boundary Condition

The Nusselt numbers, $Nu_{z,(T)}$ and $Nu_{m,(T)}$, as functions of axial distance z* are displayed in Fig. 5.26. The relatively high starting values are due to the very steep gradients of the inlet temperature profile at the walls. For comparison purposes, the solution of $Nu_{m,(T)}$ computed by Montgomery and Wilbulwas [45] and those of Chandrupatla and Sastri [46] are also included in Fig. 5.26. Montgomery and Wibulwas [45] neglected the cross-stream velocities in their analysis; therefore, their mean Nusselt numbers are significantly lower than the present values, especially near the entrance. Excellent agreement is found between the present results and those of Chandrupatla and Sastri [46] who took full account of the cross-stream flow.

The temperature contours given in Fig. 5.27 illustrate the development of the thermal problem. In this figure, Contour no. 1 represents the edge of the thermal boundary layer, or the location where $T = 1.01\ T_i$. It is seen that the thermal boundary layers on the duct walls merge much before the flow becomes thermally fully-developed; as was stated earlier, the thermally fully-developed region is characterized by a constant value of $Nu_{z,(T)}$.

Heat Transfer Results: (H) Boundary Condition

The variation of local and mean Nusselt numbers, $Nu_{z,(H)}$ and $Nu_{m,(H)}$, with axial distance z* is shown in

Fig. 5.28. No published results pertaining to this case could be found in the literature, so the predicted values of Nusselt numbers presented in Fig. 5.28 may be regarded as new results. Based on the demonstrated accuracy attained in the previous subsections, the results in Fig. 5.28 may also be considered as reliable data.

Other thermal results for this problem displayed trends similar to those of the corresponding results discussed in the last subsection in the context of the (T) boundary condition.

5.4 CLOSING REMARKS

In this Chapter, the proposed numerical method has been applied to a number of two- and three-dimensional test problems, and the computed results have been compared with published data. Agreement is, in general, very satisfactory. This establishes the validity and accuracy of the proposed numerical method, and its computer implementation, and warrants its use in the investigation of new problems for which no published results are available. One such problem, involving steady, longitudinal, laminar flow and heat transfer in an infinite rod-bundle, is investigated in the next Chapter.

CHAPTER VI

APPLICATION OF THE METHOD TO LONGITUDINAL, LAMINAR, FLOW AND HEAT TRANSFER IN ROD-BUNDLE GEOMETRIES

Longitudinal, laminar fluid flow and heat transfer in the interstices of an infinite array of rods arranged in an equilateral triangular pattern are investigated in this Chapter. A schematic illustration of this problem is given in Fig. 6.1. Attention is limited to the flow of an incompressible, constant property, Newtonian fluid and two thermal boundary conditions: (a) prescribed constant temperature of the rods (T), and (b) prescribed uniform heat flux on the surface of the rods (H). These boundary conditions represent extreme or bounding cases of those encountered in practical problems [7,30]. Hydrodynamically and thermally fully-developed and developing conditions are studied in this Chapter. In the developing flow and heat transfer problems, uniform distributions of axial velocity and temperature are assumed at the inlet cross-section.

The discussion in this Chapter is divided into four main parts: (i) considerations regarding the calculation domain, computational grids and problem parameters; (ii) investigation of hydrodynamically and thermally fully-developed conditions; (iii) study of hydrodynamically fully-developed but thermally developing cases; and (iv)

investigation of simultaneously developing fluid flow and heat transfer. Most of the details pertaining to the mathematical formulation of these problems have already been presented in Chapters II and V; therefore, to avoid repetition, appropriate sections and equations in these earlier Chapters will be referenced, whenever necessary. All aspects of the formulation and solution methodology which have not already been discussed in earlier chapters will be discussed in detail in this Chapter.

Longitudinal, laminar fluid flow and heat transfer in rod-bundle geometries is encountered in nuclear power-generation equipment and in shell-and-tube heat exchangers. Despite its practical importance, however, there are not too many papers on this topic in the published literature [7,47]. Some analytical and numerical results for the hydrodynamically and thermally fully-developed situations are available [7] and will be used to check the results of this investigation. However, to the best knowledge of the author, there has been no in-depth investigation of the hydrodynamically and thermally developing situations. Thus, many of the results presented in this Chapter are new and they augment the collection of heat transfer data in the literature.

All computations in this investigation were done on an AMDAHL V7 computer using an IBM FORTRAN-H extended compiler.

6.1 CONSIDERATIONS PERTAINING TO THE CALCULATION DOMAIN, COMPUTATIONAL GRID AND PROBLEM PARAMETERS

Figure 6.2(a) shows a cross-sectional view of an array of rods arranged in an equilateral triangular pattern; the primary flow is in the direction normal to the plane of the paper. The diameters of the rods is d and the centre-to-centre spacing between any two neighbouring rods is denoted by s. Due to the symmetry of the infinite rod-array configuration, consideration need be given to only a representative subdomain, such as the shaded region in Fig. 6.2(a). Once the solution is obtained in such a calculation domain, the solution in the rest of the problem geometry can be obtained by an appropriate repetition of the basic solution. An enlarged view of the calculation domain used in this study is shown in Fig. 6.2(b), along with the appropriate boundary conditions. On the symmetry surfaces, the normal derivatives of the dependent variables are equal to zero.

In the selection of a suitable discretization of the calculation domain shown in Fig. 6.2(b), use is made of the experience gained in the computations performed for the square duct geometry discussed in the last Chapter. It was shown there that for a given number of grid points, it is computationally efficient to concentrate more grid points in the region near the wall than in the central part of the flow passage; this allows an adequate handling, at a reasonable

computing cost, of the high gradients of the dependent variables in the wall regions. In this study, therefore, a non-uniform subelement grid of (L1 x M1) nodes is employed to discretize the calculation domain. The (x,y) coordinates of a typical grid point (I,J) are determined as follows:

·Vertices of Macroelements

$$I = 1, 3, 5 \ldots, L1$$
$$J = 1, 3, 5 \ldots, M1 \qquad (6.1)$$
$$X(I,J) = R(I,J) * COS(\theta(J))$$
$$Y(I,J) = R(I,J) * SIN(\theta(J))$$

where

$$\theta(J) = (J-1) * (\pi/6)/(M1-1)$$

and

$$R(I,J) = ((I-1)/(L1-1))**POWER*0.5*(s*SEC(\theta(J))-d)$$

·Mid-Side Nodes of Macroelements

$$I = 2, 4, 6 \ldots, (L1-1)$$
$$J = 2, 4, 6 \ldots, (M1-1) \qquad (6.2)$$
$$X(I,J) = 0.5 * (X(I+1,J) + X(I-1,J))$$
$$Y(I,J) = 0.5 * (Y(I,J+1) + Y(I,J-1))$$

where POWER is a user-specified constant for determining the grid line distribution. In all cases, the grid lines are uniformly spaced in the θ-direction. A value of POWER equal to unity yields a uniform distribution of grid points along each radially oriented grid line; for values of POWER greater than 1, more grid points are employed near the surface of the rod than in the central region of the interstices. A typical discretization at the subelement level, using L1 = M1 = 11 and POWER = 1.4, for a calculation domain with a pitch-to-diameter ratio (s/d) = 1.5 is shown in Fig. 6.3; the approximation of the curved rod-boundary by a piecewise-linear grid line is clearly evident in this figure.

The geometry of the flow passage in this problem is characterized by the pitch-to-diameter ratio (s/d). Another non-dimensional parameter, which is encountered in simultaneously developing flow and heat transfer situations is the Prandtl number ($Pr = \mu c_p/k$). The present investigation is limited to twelve different values of (s/d) in the range 1.05 to 2.0; this range of (s/d) values is relevant to the design of nuclear reactor cores. In the analysis of simultaneously developing flow and heat transfer, attention is focused on two values of Prandtl numbers: Pr = 0.72 and 3, which are representative of air and water, respectively. In addition, limiting cases in which the Prandtl number approaches zero and infinity are also investigated.

6.2 FULLY-DEVELOPED FLUID FLOW AND HEAT TRANSFER

Longitudinal, fully-developed, laminar flow and heat transfer is studied in this section. As was stated earlier, this problem has been the subject of previous investigations [7]; the results compiled by Shah and London [7] will be used here for comparison purposes.

Analysis

The applicable governing equations are the axial momentum equation, Eq. (2.28), and the modified forms of the energy equation, Eqs. (2.55) and (2.70), for the (T) and (H) heat transfer problems, respectively. The numerical procedure for the solution of these equations has already been described at length in Section 5.3.1 in connection with the analysis of the hydrodynamically and thermally fully-developed flow in a square duct. The solution to the flow field is obtained in terms of a non-dimensional axial velocity W; the (T) heat transfer problem is formulated and solved to obtain a non-dimensional temperature Θ; and the solution to the (H) heat transfer problem is obtained in terms of a non-dimensional temperature χ; these non-dimensional variables are defined in Eqs. (2.27), (2.55) and (2.69). The boundary conditions are the following: on the surface of the rod in Fig. 6.2(b), $W = 0$, $\Theta = 0$ and $(\partial\chi/\partial n) = 1$; on other boundaries, all of which are symmetry surfaces, the normal derivatives of W, Θ and χ are zero.

The flow field was solved first, and the normalized axial velocity ($W/\bar{W}$) was stored on external disk devices to serve as an input to the heat transfer problems. Auxiliary computations were done to obtain overall results such as the friction factor - Reynolds number product, f.Re, and the average Nusselt numbers, $Nu_{(T)}$ and $Nu_{(H)}$.

Computational Details

The final computations were performed with a macro-element grid of 6x6 nodes, which corresponds to a subelement grid of 11x11 nodes; the distribution of grid points was based on the relations given in Eqs. (6.1) and (6.2), with POWER = 1.4. This grid was chosen based on the experience gained in the analysis of the square duct geometry and its adequacy was established by doing sample computations with finer grids and different values of POWER. The calculations were carried out for values of pitch-to-diameter ratio of 1.05, 1.07, and 1.1 to 2 in steps of 0.1

The (T) heat transfer problem requires the solution to an eigenvalue problem posed by Eq. (2.55). The iterative procedure described in Section 5.3.1 was used to solve this problem. The iterations in this procedure were terminated when the change in the eigenvalue λ between successive iterations was less than 0.001%.

For each value of (s/d), the typical computer time required to obtain the W, Θ and χ fields and do all necessary

auxiliary computations was about 30 execute units†.

Fluid Flow Results

The friction factor - Reynolds number product, f.Re, as a function of (s/d) is given in Fig. 6.4. The solid line represents the results of this analysis and the dashed line denotes the analytical results reported in [7]. It can be seen that agreement between these results is very good throughout the range of (s/d) investigated. The f.Re product increases monotonically with the pitch-to-diameter ratio. This variation of f.Re with (s/d) reflects the simultaneous influences of the pressure gradient and the magnitude of the hydraulic diameter:

$$f.Re = \frac{(-d\bar{p}/dz)D_H}{\frac{1}{2}\rho\bar{w}^2} \cdot \frac{\rho\bar{w}D_H}{\mu} \qquad (6.3)$$

For a fixed mass flow rate and constant rod diameter, as the intercylinder spacing increases, the axial pressure gradient decreases but the hydraulic diameter increases. These opposing tendencies lead to the trend displayed in Fig. 6.4. For large values of (s/d), f.Re tends to infinity because D_H tends to infinity.

The effects of the number and distribution of grid points on the f.Re product for different pitch-to-diameter

†One execute unit on an AMDAHL V7 is the machine time required to perform one million operations.

ratios are summarized in Table 6.1. For POWER = 1.4, successive refinements of the grid size drive the f.Re factor closer to the analytical value reported in [7]. This trend is observed for the three spacing ratios presented in Table 6.1, and it is in accord with expectations. The effect of varying the value of POWER is illustrated in Table 6.1 for s/d = 1.05 and a subelement grid of 11x11 nodes. It appears there that a uniform grid (POWER = 1) yields the most accurate solution if the analytical value of [7] is taken as a reference. It is to be noted, however, that in the fully-developed regime, the velocity gradients at the rod surface are not as steep as those encountered in the developing region, especially in the vicinity of the inlet. As was discussed in Chapter V, the fully-developed results serve as reference values in the automatic axial step size selection algorithm used in the analysis of the developing region. It is, therefore, desirable to devise an optimum grid that provides adequate accuracy of the results in the fully-developed and in the developing flow regimes. With this consideration in mind, the value of POWER = 1.4 was retained for determining the distribution of grid lines in all subsequent computations.

Heat Transfer Results

The average Nusselt numbers, $Nu_{\textcircled{T}}$ and $Nu_{\textcircled{H}}$, are presented in Fig. 6.5 as functions of the pitch-to-diameter

ratio (s/d). Both $Nu_{(T)}$ and $Nu_{(H)}$ increase with increasing intercylinder spacing; this is a consequence of the dependence of the Nusselt numbers on the hydraulic diameter. For (s/d) $\gtrsim$ 1.17, it can be seen that the average Nusselt number for the (H) boundary condition is consistently higher than that for the (T) boundary condition. This trend can be explained on physical grounds as follows: for large (s/d) and the (H) boundary condition, the rod surface temperature distribution along its periphery is not influenced much by the presence of neighbouring rods and it tends to be uniform. Thus, for large values of (s/d), the (H) boundary condition approaches a condition of constant axial wall heat flux and uniform peripheral wall temperature; it can be shown, Shah and London [7], that the Nusselt number under such conditions is always higher than that for the (T) boundary condition. For small (s/d) values, however, the rod surface temperature varies markedly along its periphery. The highest value of T_w[†] occurs at the points where the lines joining the centers of adjacent cylinders intersect the rod surface. These "hot spots" increase the value of the surface-averaged temperature $\bar{T}_w$ which, in turn, decreases $Nu_{(H)}$. Thus, for s/d $\lesssim$ 1.17, the peripheral temperature distribution on the rod surface is highly non-uniform and $Nu_{(H)}$ is smaller than $Nu_{(T)}$.

In Fig. 6.5, the values of $Nu_{(H)}$ tabulated in [7] are plotted as a dashed line. As is evident, they match the

---

[†]This discussion is based on the viewpoint that the cylinder surface is hotter than the fluid.

present results extremely well. No published results for $Nu_{(T)}$ are available in the literature; therefore, the computed values reported here may be considered as new results.

The effects of the number and distribution of grid points on the values of $Nu_{(T)}$ and $Nu_{(H)}$, for three values of (s/d), are shown in Table 6.1. On the basis of these results, it was concluded that a subelement grid of 11x11 nodes with POWER = 1.4 yields adequate accuracy while not demanding an excessive amount of computer time.

6.3 HYDRODYNAMICALLY FULLY-DEVELOPED AND THERMALLY DEVELOPING FLOW

Attention in this section is focused on laminar flow which is hydrodynamically fully-developed and thermally developing. This situation is typically encountered in problems involving fluids with very large Prandtl numbers ($Pr \to \infty$). The velocity distribution remains invariant throughout the calculation domain; the fully-developed flow solution discussed in the last section is used as an input to this problem. The temperature distribution is assumed to be uniform in the inlet cross-section of the calculation domain, and it develops as the flow proceeds down the rod bundle.

Analysis

A detailed mathematical formulation of this problem

has already been presented in Chapter II. Therefore, only the applicable governing equations and boundary conditions are stated in this subsection. The development of the temperature field is governed by the energy equation, Eq. (2.34). The corresponding boundary conditions, with reference to the calculation domain shown in Fig. 6.2(b), are the following: on the surface of the rod, $T = T_w$ = constant in the (T) problem, and $(-k \frac{\partial T}{\partial r}) = q_w$ = constant in the (H) problem; on all other boundaries of the calculation domain, which are symmetry surfaces, the normal derivatives of T are zero. At the inlet cross-section of the calculation domain, the temperature distribution is taken as uniform.

The numerical procedure employed to solve the present problem is analogous to that described in Section 5.3.2 for the square duct geometry, so it is not repeated in this section. Furthermore, the discussion in Section 5.3.2 regarding the treatment of the initial condition also applies to this problem.

Computation Details

The final computations were conducted with a sub-element grid of 11x11 nodes; Eqs. (6.1) and (6.2) with POWER = 1.4 were used to obtain the desired distribution of the grid points. For the first three marching steps, a step size $\Delta z' \sim 10^{-7}$ was used so as to accommodate the large gradients of the dependent variables encountered in the

vicinity of the inlet cross-section. The step sizes at subsequent axial stations were determined using the automatic step size selection algorithm discussed in Section 4.1.1; the value of IDEAL was set equal to 25. In the actual computations, about 50 axial steps were required to attain fully-developed conditions. Additional runs with a sub-element grid of 19x19 nodes, POWER = 1.4 and IDEAL = 50 steps were made to check the validity and accuracy of the results obtained with the aforementioned basic grid. In all runs, the velocity distributions needed for the thermal solutions were obtained from the fully-developed flow analysis presented previously.

For each of the final runs, the computer times needed for a complete solution of the thermal entrance region averaged around 100 execute units.

Results: (T) Boundary Condition

Local Nusselt number, $Nu_{z,(T)}$, results for (s/d) = 1.05 and 2, and for two different grid and step size combinations, are shown in Fig. 6.6. In the vicinity of the inlet cross-section, the discrepancy between the results obtained with the two different grids is large; this reflects the inability of the numerical method, with its finite number and spacing of grid points, to adequately handle the singularity in temperature distribution at the inlet, as was discussed in Chapter V. However, it can be seen that

the differences in the results of the two grids decay quite rapidly and they can be regarded as negligible for $z' > 10^{-4}$. Thus, the Nusselt number results obtained with the 11x11 subelement grid with POWER = 1.4 and IDEAL = 25 may be considered as grid-independent for $z' > 10^{-4}$.

The local Nusselt number, $Nu_{z,\textcircled{T}}$, is defined by Eq. (2.41):

$$Nu_{z,\textcircled{T}} \triangleq \frac{q_z D_H}{(T_w - T_b)k} \tag{2.41}$$

where q_z is the average rod surface heat flux and T_b is the fluid bulk temperature. In the vicinity of the duct inlet, q_z is relatively high, but it decreases rapidly with axial distance; the fluid bulk temperature increases with axial distance, so $(T_w - T_b)$ decreases. The heat transfer coefficient h, which is the ratio $q_z/(T_w - T_b)$, decreases in the developing region and asymptotes to a constant value in the fully-developed region. This behaviour is evident in the $Nu_{z,\textcircled{T}}$ *vs* z' curves presented in Fig. 6.6.

Also of interest in Fig. 6.6 is the difference in trends displayed by the axial variation of $Nu_{z,\textcircled{T}}$ for small and large spacing ratios. For (s/d) = 1.05, the $Nu_{z,\textcircled{T}}$ *vs* z' curve experiences a change in its rate of decrease around $z' = 10^{-3}$, before asymptoting to the fully-developed value. On the other hand, this behaviour is not observed for (s/d) = 2. This difference in trends is caused by the

disparity in the fully-developed velocity distributions for small and large spacing ratios, and the corresponding differences in the variations of q_z and (T_w-T_b) with axial distance. The fully-developed velocity profile is non-uniform across the cross-section of the calculation domain, and this non-uniformity is more pronounced for (s/d) = 1.05 than for s/d = 2.0. With reference to the calculation domain shown in Fig. 6.2 and its discretization presented in Fig. 6.3, the fluid velocity is zero on the rod surface and maximum at the grid point (I = L1, J = M1); furthermore, as the fluid seeks the path of least resistance, its velocity in the vicinity of $\theta = 0$ is lower than that adjacent to $\theta = \pi/6$. The fluid bulk temperature rises steeply very close to the inlet, because of the high values of q_z and the rapid heating of the fluid adjacent to $\theta = 0$. However, once the low velocity fluid around $\theta = 0$ heats up to temperatures close to T_w, the rate of rise of T_b decreases because the high velocity fluid around $\theta = \pi/6$ heats up relatively slowly. This change in the rate of rise of T_b with axial distance is stronger for (s/d) = 1.05 than for (s/d) = 2.0. The corresponding effect on the rate of decrease of q_z with axial distance is not as pronounced because q_z is an area-averaged quantity, whereas T_b is a flow rate averaged quantity. These differences in the axial variations of q_z and T_b for (s/d) = 1.05 and (s/d) = 2.0 are reflected in the corresponding $Nu_{z,(T)}$ *vs* z' curves in Fig. 6.6.

Figure 6.7 shows the variation of the local Nusselt

number $Nu_{z,(T)}$ with axial distance z' for twelve different pitch-to-diameter ratios in the range $1.05 \leq (s/d) \leq 2.0$. The aforementioned difference in trends displayed by the axial variation of $Nu_{z,(T)}$ for large and small spacing ratios is also evident in Fig. 6.7, although not as clearly as in Fig. 6.6. To the best knowledge of the author, these are new results.

Results: (H) Boundary Condition

Figure 6.8 illustrates how the local Nusselt number, $Nu_{z,(H)}$, varies with axial distance for (s/d) = 1.05 and 2.0; the results obtained with two different grids are presented. These results show that for $z' > 10^{-4}$, the results obtained with the basic grid (11x11 subelement vertices and IDEAL = 25) are essentially grid independent. At smaller z', there are relatively large discrepancies between the results of the two grids used; this is because the thermal boundary layer thickness is very small for $z' < 10^{-4}$, and a very fine grid in the vicinity of the rod surface is required for accurate computations, as was discussed in Section 5.3.2.

The Nusselt number curve for (s/d) = 1.05 in Fig. 6.8 portrays a behaviour quite different from that for (s/d) = 2.0. As in the (T) problem, this difference is caused by the disparity in the velocity distributions across the cross-section for different intercylinder spacings and the

consequent differences in the axial variations of T_b. In the present case, the local Nusselt number is defined by Eq. (2.65):

$$Nu_{z,\textcircled{H}} \triangleq \frac{q_w D_H}{(\bar{T}_w - T_b)k} \tag{2.65}$$

where q_w is the specified constant heat flux at the rod surface, $\bar{T}_w$ is the average rod wall temperature and T_b is the fluid bulk temperature in the cross-section of interest. The temperature difference $(\bar{T}_w - T_b)$ rises in the developing region and eventually asymptotes to a constant value in the fully-developed region. For small spacing ratios, (s/d) $\sim$ 1.05, the highly non-uniform velocity distribution in the calculation domain could lead to significant differences in the axial variations of $\bar{T}_w$ and T_b in the developing region. These differences, in turn, lead to the change in the rate of decrease of the $Nu_{z,\textcircled{H}}$ *vs* z' curve for (s/d) = 1.05 in Fig. 6.8. The detailed explanation is very similar to that advanced in the last subsection for the Ⓣ problem, so it is not repeated here.

$Nu_{z,\textcircled{H}}$ *vs* z' curves for twelve different (s/d) ratios in the range $1.05 \leq (s/d) \leq 2.0$ are presented in Fig. 6.9. Similar results are not available in the published literature, so the results of this investigation may be considered to be new.

6.4 SIMULTANEOUSLY DEVELOPING FLUID FLOW AND HEAT TRANSFER

Attention is now turned to the situation in which both velocity and temperature profiles are uniform at the entrance and develop simultaneously. There are only a few papers in the literature which deal with simultaneously developing laminar flow and heat transfer in infinite rod-bundle geometries. The only works known to the author are those of Del Giudice *et al.* [24-26] who solved the hydrodynamic and thermal entry problems using a linearized procedure akin to that proposed by Sparrow *et al.* [8,9]. Del Giudice *et al.* have reported results for spacing ratios (s/d) = 1.5 and 2, and Pr = 1. As the Pr = 1 case is not treated here, only the hydrodynamic results of [24] will be used for comparison purposes in this study.

Analysis

Details of the equations which govern this problem have already been presented in Chapter II: the fluid flow problem is governed by the continuity equation, Eq. (2.8), and the momentum equations, Eqs. (2.9)-(2.11); and the temperature is governed by the energy equation, Eq. (2.34). As noted before, the momentum equations are non-linear and coupled to each other and the continuity equation; the energy equation is linear, but it requires the solution to the flow problem as an input.

With regard to boundary conditions, reference is

made to the enlarged view of the sub-channel of interest pictured in Fig. 6.2(b). As shown there, for fluid flow, the no-slip condition prevails over the impermeable rod surface: $u = v = w = 0$. Over the other surfaces of the calculation domain, all of which are symmetry surfaces, the following conditions apply: the velocity component normal to the surface is zero and the normal derivatives of the tangential velocity components are zero. Using the coordinate systems shown in Fig. 6.2(b), these conditions can be expressed as follows: at $y = 0$, $(\partial u/\partial y) = 0$, $v = 0$ and $(\partial w/\partial y) = 0$; at $x = s/2$, $u = 0$, $(\partial v/\partial x) = 0$, $(\partial w/\partial x) = 0$; at $\theta = 30°$, $v_n = 0$, $(\partial v_t/\partial n) = 0$ and $(\partial w/\partial n) = 0$, where n and t denote the normal and tangential directions to the face at $\theta = 30°$, respectively. The thermal boundary conditions, on the other hand, can be written as follows: on the wall surface, $T = T_w$ = constant for the (T) condition, and $(-k\ \partial T/\partial r) = q_w$ = constant for the (H) condition; on the symmetry surfaces, the normal derivative of the temperature $(\partial T/\partial n) = 0$.

Adaptation of the Proposed Solution Method

In Section 5.3.2, the use of the proposed method for the solution of simultaneously developing velocity and temperature fields was described in the context of fluid flow and heat transfer in a duct of square cross-section. All the details presented there are applicable to the present problem too, and so they are not repeated here. There is,

however, one specific aspect of the rod-bundle problem which deserves special mention. It relates to the imposition of appropriate boundary conditions on the cross-sectional velocity components at the inclined symmetry surface $\theta = 30°$. These conditions are:

$$\frac{\partial v_t}{\partial n} = \frac{\partial}{\partial n}(u \cos 30° + v \sin 30°) = 0 \qquad (6.4a)$$

$$v_n = - u \sin 30° + v \cos 30° = 0 \qquad (6.4b)$$

Thus, it can be seen that the boundary condition for u is indirectly specified through v, and *vice-versa*. This indirect specification is computationally inconvenient because the momentum equations for u and v are solved sequentially in the overall iterative solution procedure used in the proposed method. Hence, explicit boundary conditions for u and v on the inclined symmetry boundary are required.

Explicit boundary conditions on u and v at $\theta = 30°$ can be obtained by rewriting Eqs. (6.4a) and (6.4b) as follows:

$$\frac{\partial u}{\partial n} = 0 \qquad (6.5a)$$

$$v = u \tan 30° \qquad (6.5b)$$

In each iteration of the overall solution procedure, Eq. (6.5a)

and the boundary conditions at the remaining faces of the calculation domain allow a unique and computationally convenient solution of the u-field. Once this is done, Eq. (6.5b) can be used to obtain an explicit boundary condition for v. The iterations in the overall solution procedure are continued till convergence. Since Eqs. (6.5a) and (6.5b) are equivalent to Eqs. (6.4a) and (6.4b), the resulting cross-sectional velocities satisfy both Eqs. (6.4) and (6.5).

It is to be noted that in the implementation of the boundary conditions given by Eqs. (6.5a) and (6.5b), special care must be exercised in the calculation of the pseudo-velocity $\hat{v}$ at the inclined symmetry boundary. Equation (6.5b) implies that

$$v_i = u_i \tan 30° = \{\hat{u}_i + (\sum_j \lambda_j^u p_j)/a_j^u\} \tan 30° \qquad (6.6)$$

Therefore,

$$\hat{v}_i = \hat{u}_i \tan 30° \qquad (6.7)$$

and

$$v_i = \hat{v}_i + \sum_j (\lambda_j^u \tan 30°) p_j/a_i^u \qquad (6.8)$$

For a node i located on the inclined symmetry boundary, Eqs. (6.7) and (6.8) replace Eqs. (3.44) and (3.47), respectively. All other details of the proposed calculation

procedure are as described in Chapter III.

Computational Details

The results presented in Chapter V and in the previous sections of this Chapter have shown that the basic grid employed so far, a subelement grid of 11x11 nodes with POWER = 1.4 and IDEAL = 25 steps, yields adequate accuracy, except in the region very close to the entrance where starting errors dominate. This basic grid was also used in the investigation of this problem. At each axial step after the first three, the step size for marching ahead was determined by the automatic step-size algorithm discussed in Section 4.2.1; a specified desired change in the maximum axial velocity Δw_{max} was used to determine the appropriate values of Δz. A constant value of $\Delta z^* = 10^{-6}$ was used for the first three steps.

Flow and heat transfer results were obtained with the basic grid for the following pitch-to-diameter ratios: (s/d) = 1.05, 1.07, 1.1, 1.2, 1.3, 1.4, 1.5 and 2. Two values of Prandtl numbers were used in the computations: Pr = 0.72 and 3, which are representative of air and water, respectively. Additional computations with different grids and step sizes were also done for (s/d) = 1.05 and 1.5 in order to check the accuracy of the basic grid computations.

Since the equations governing the flow field are non-linear and coupled, it was necessary to use under-

relaxation in the computations for u, v, w and p. For the first three axial steps, the following under-relaxation parameters were used: $\alpha_u = \alpha_v = 0.5$, $\alpha_w = 0.8$, $\alpha_p = 0.8$. Following that, they were changed to $\alpha_u = \alpha_v = 0.8$, $\alpha_w = \alpha_p = 1$.

At each axial step, the iterative solution procedure for calculating the flow field was stopped when the maximum of the relative changes in u, v, w and $d\bar{p}/dz$ between consecutive iterations was less than 0.001%; the changes in u, v and w were calculated at four selected nodes in the calculation domain. The changes in u and v were not included in this convergence criterion in the vicinity of the fully-developed region where these cross-sectional velocity components approach zero.

Typically, about 50 axial steps and 2000 execute units of computing time on an AMDAHL V7 were needed to obtain the complete hydrodynamic and thermal solutions for each spacing ratio considered.

Fluid Flow Results

The presentation and discussion of results in this subsection is done in three parts. The first part is devoted to the effects of grid and step size details on the results. In the second part, attention is turned to the comparison of the present solutions with those reported by Del Giudice *et al.* [24]. The third part is concerned with the presentation and discussion of detailed solutions for the various pitch-to-diameter ratios investigated.

Since no bench-mark entry-flow solutions exist for the rod-bundle geometry, special care was taken to ensure that the final results of this investigation, obtained with a subelement grid of 11x11 nodes, POWER = 1.4 and IDEAL = 25, are, for all practical purposes, grid independent. This was achieved by doing additional computations with fine grids and small step sizes and comparing the results with those of the basic grid. Unfortunately, as noted earlier, the computational effort involved in the calculation of the developing flow is relatively high. Therefore, the extent to which grid and step size effects were explored was limited by the available resources. As a result, the grid verification computations were only done for two representative spacing ratios: (s/d) = 1.05 and 1.5. Furthermore, the calculations were carried out only in the initial part of the developing region; it is to be noted that the solutions near the entrance are a more stringent test of the accuracy and grid independence of the results than those in the remainder of the calculation domain. The effects of changing the axial step sizes were studied by varying the value of IDEAL, which determines the minimum number of steps required for attaining fully-developed conditions. In addition, the effects of tying the automatic step size selection to a specified change in the Nusselt number ($\Delta Nu_{z,\textcircled{T}}$) between successive axial steps, rather than the corresponding change in maximum axial velocity Δw_{max}, were also studied.

Figures 6.10 and 6.11 show the results of the aforementioned grid checks for (s/d) = 1.05 and 1.5, respectively, in the form of the axial variation of the maximum velocity, $(w/\bar{w})_{max}$; with reference to the grid shown in Fig. 6.3, the maximum velocity occurs at the point (I = L1, J = M1). As is evident from Figs. 6.10 and 6.11, the $(w/\bar{w})_{max}$ results obtained with the basic grid are, for all practical purposes, grid independent. The corresponding axial distributions of the mean pressure are not presented here, but they support this conclusion. It is to be noted that the grid check results in Figs. 6.10 and 6.11 apply only to a relatively small range of z*, but an indication on how well the basic grid performs at higher z* can be readily obtained from an inspection of the fully-developed results presented in Table 6.1. Thus, it may be concluded that sufficiently accurate, grid independent results can be obtained with the basic grid over the entire developing flow regime.

The focus of the discussion is now directed to the comparison of the present solutions with published data. As was noted in the introduction of this section, only the results of Del Giudice *et al.* [24-26] are available. Here, the data for (s/d) = 2.0, read-off from graphs in [24], are used.

The results of this investigation are compared with the corresponding results of [24] in Figs. 6.12 and 6.13. The variation of the mean pressure with axial distance is

displayed by the curves in Fig. 6.12, and those in Fig. 6.13 show the axial variation of $(w/\bar{w})_{max}$. The results of Del Giudice *et al.* [24] are based on a linearized formulation of the inertia terms in the axial momentum equation, and their computations were done with a 15x5 grid. Furthermore, as was discussed in Section 6.3, the singularities in the initial conditions at the duct inlet cross-section and the extremely thin boundary layers in the immediate vicinity of the inlet make it very difficult and costly, if not impossible, to get accurate numerical solutions. With these considerations in mind, it may be concluded that the results of this investigation and those of Del Giudice *et al.* [24] agree quite well.

Attention is now turned to the presentation of detailed results in Figs. 6.14 and 6.15, for eight different (s/d) values in the range $1.05 \leq (s/d) \leq 2.0$. The axial variation of mean pressure is given by the curves in Fig. 6.14. For all spacing ratios, the pressure gradients are higher near the entrance than in the developed flow region because of two effects: (i) the increase in the momentum of the fluid as the velocity field changes from a uniform to a non-uniform distribution; and (ii) the higher wall shear stress caused by higher transverse velocity gradients in the vicinity of the inlet. For a fixed z*, it can be seen that the slopes of the curves in Fig. 6.14 increase monotonically with spacing ratio. This, however, is because the hydraulic diameter increases with (s/d), and z* is inversely proportional

to the square of the hydraulic diameter. It does not represent an increase in pressure drop with (s/d). Indeed, if a $\bar{p}$ *vs* z curve were plotted for a fixed $\bar{w}$ and rod diameter, it would show a decrease in the axial pressure gradient with an increase in (s/d).

The axial variation of $(w/\bar{w})_{max}$ for eight different values of (s/d) ranging from 1.05 to 2.0 are plotted in Fig. 6.15. Inspection of this figure indicates that the hydrodynamic development is very rapid near the inlet and then proceeds more slowly with increasing downstream distance. The fully-developed value of $(w/\bar{w})_{max}$ increases with decreasing cylinder spacings because higher velocities are required for keeping the mass flow rate constant as the dimensions of the flow passage are reduced. As is evident from Fig. 6.15, in terms of z*, the fully-developed conditions are reached earlier for increasing (s/d) ratios. This is because z* is inversely proportional to D_H^2 and it does not imply shorter physical development lengths for larger spacing ratio. Indeed, for fixed values of the mean axial velocity $\bar{w}$ and rod diameter d, the physical development length increases with increasing spacing between adjacent rods.

The cross-sectional flow fields at three different axial locations for (s/d) = 1.5 are illustrated in Fig. 6.16 in the form of vector plots of the cross-sectional velocity at the subelement grid points. At $z^* = 1.7 \times 10^{-7}$, there is significant transverse flow near the wall because of the

sudden decrease in the axial velocity in this region, and the associated increase in this velocity in the central region of the space between rods. These cross-sectional velocities decay quite rapidly away from the inlet. All the cross-sectional velocity vectors shown point away from the rod surface, and, as is to be expected, there is no evidence of any recirculation zones in the cross-sectional planes.

Heat Transfer Results: (T) Boundary Condition

Heat transfer results for the (T) condition are presented in this subsection in three parts. In the first part, the effects of grid details are examined, and the second part is devoted to the presentation and discussion of detailed results for several spacing ratios, and two values of Prandtl numbers. In the third part, attention is focused on the effects of the Prandtl number.

In all computations presented so far in this Chapter, an 11x11 node subelement grid with POWER = 1.4 yielded satisfactory solutions in both the developed and developing regions. So this grid was chosen for all computations presented in this subsection. The grid checks were limited to an investigation of the effect of different axial step size combinations.

In Figs. 6.17(a) and (b), the axial variation of $Nu_{z,(T)}$ for (s/d) = 1.5 and 1.05, respectively, are presented; the Prandtl number in these computations was set equal to

0.72. The different curves in this figure correspond to the results of grid checks made with various values of IDEAL and with the automatic step size algorithm tied to a specified value of $\Delta Nu_{z,(H)}$ rather than Δw_{max}. In all cases, the calculations were not carried out till the fully-developed conditions. As is evident in Fig. 6.17, the discrepancies in the results obtained with the different grids diminish rapidly with axial distance, and they may be regarded as negligible for $z^* > 5x10^{-4}$. Thus the results of the basic grid may be considered as grid independent, for all practical purposes, for $z^* > 5x10^{-4}$.

Attention is now focused on the Nusselt number solutions for eight different values of (s/d) in the range $1.05 \leq (s/d) \leq 2.0$. These results are presented in Figs. 6.18 and 6.19. Figure 6.18 exhibits the axial variation of $Nu_{z,(T)}$ for Pr = 0.72, and the corresponding results for Pr = 3.0 are displayed in Fig. 6.19. The Nusselt number variations below $z^* = 10^{-3}$ are not shown because they may not be very accurate and they may be influenced by starting errors, as was discussed in the earlier sections of this Chapter and in Chapter V.

An inspection of Figs. 6.18 and 6.19 reveals that the Nusselt number solutions for simultaneously developing flow and heat transfer are similar in many respects to the thermal entry solutions presented in Fig. 6.7. Therefore, many of the remarks made in the discussion of Fig. 6.7 are also valid here. However, there are a couple of interesting

aspects of the results in Figs. 6.18 and 6.19 which deserve a separate discussion.

It is observed that for values of $z^* < 10^{-2}$ in Figs. 6.18 and 6.19, the curves corresponding to different spacing ratios are closer to one another than they are in Fig. 6.7. The explanation for this result is that the hydrodynamic and thermal boundary layers on the rod surface are very thin in the immediate vicinity of the inlet cross-section; so for a fixed $\bar{w}$, T_w and d, the surface heat flux is relatively insensitive to the spacing between the rods. Nevertheless, the Nusselt number curves for the different (s/d) ratios do not merge as z^* is decreased because of the dependence of the Nusselt number on the hydraulic diameter.

Another aspect of interest is the difference in trends of the Nusselt number distributions for small and large spacing ratios. Each of the curves for $(s/d) \leq 1.2$ exhibits an inflection point. The mechanisms that cause this behaviour are believed to be of the same nature as those discussed in Section 6.3 in the context of hydrodynamically developed but thermally developing flow. It was argued there that the significant disparity that exists in the fully-developed velocity profiles for small and large spacings caused the aforementioned differences in the axial variation of Nusselt number. An examination of Figs. 6.18 and 6.19 shows that the inflection points in the $Nu_{z,\,(T)}$ *vs* z^* curves for $(s/d) \leq 1.2$ occur at axial locations that are not in the immediate vicinity of the entrance. It seems reasonable,

therefore, to assume that the velocity profiles are relatively non-uniform at the locations of the inflection points, and the explanation put forth in Section 6.3 applies here too.

Figure 6.20 provides further insight regarding the growth of the thermal boundary layer. In this figure, suitably non-dimensionalized temperature profiles at six different axial locations are presented in the form of isotherms or contour plots; they correspond to $(s/d) = 1.5$ and $Pr = 0.72$. The edge of the thermal boundary layer (taken as the position where $T = 1.01\ T_i$) is represented by contour 1. At $z^* = 1.685 \times 10^{-7}$, the thermal boundary is very thin and there is a high concentration of isotherms near the wall, corresponding to the high wall temperature gradients there. At $z^* = 5.2 \times 10^{-4}$, the isotherms are almost concentric with the circular surface of the rod, indicating that the boundary layers on adjacent rod surfaces have not yet merged, and the interaction between neighbouring rods is minimal. At $z^* = 1.6 \times 10^{-3}$, the thermal boundary layers on adjacent rods have merged, but there still exists a small pocket of unheated fluid around the upper right-hand corner of the calculation domain where $(w/\bar{w})$ is a maximum. The development of the temperature field after the thermal effect of the wall has been felt throughout the fluid flow is displayed in the remaining contour plots in Fig. 6.20.

Attention is now directed to the effect of Prandtl

number on the heat transfer results. As is well known, the Prandtl number determines the rate of development of the temperature field relative to that of the velocity field. Thus, for a fluid with a large Prandtl number, the velocity field develops much faster than the temperature field; in the limit, as $Pr \to \infty$, it may be assumed that hydrodynamically fully-developed conditions prevail as the flow develops thermally. The other extreme, $Pr \to 0$, pertains to the situation where the velocity profile may be assumed to be uniform over the entire cross-section of the duct as the flow develops thermally. Such a situation is commonly referred to as "slug flow".

In this investigation, the effect of Prandtl number on the axial variation of Nusselt number was examined for three different spacing ratios: $(s/d) = 1.05$, 1.5 and 2.0. For each spacing ratio, four different values of Prandtl number were considered: $Pr \to 0$, $Pr = 0.72$ and 3, and $Pr \to \infty$. The results are presented in Figs. 6.21 to 6.23 in terms of $Nu_{m,(T)}$ *vs* z' curves; $Nu_{m,(T)}$ is the length-averaged mean Nusselt number defined by Eq. (2.46). The mean Nusselt number $Nu_{m,(T)}$ rather than the local Nusselt number $Nu_{z,(T)}$ is used in the presentation of these results because the $Nu_{z,(T)}$ results for $Pr = 0.72$ and 3 have already been presented in Figs. 6.18 and 6.19 and discussed in this subsection.

As is evident in Figs. 6.21 to 6.23, which correspond to $(s/d) = 1.05$, 1.5 and 2.0, respectively, $Nu_{m,(T)}$ at a

fixed z'[†] increases with decreasing Prandtl number. This can be explained as follows: for a fixed spacing ratio and at any given z', the axial velocity distribution becomes increasingly uniform over the cross-section of the calculation domain as the Prandtl number is decreased; this causes the transverse velocity gradient at the wall to be steeper, thereby enhancing the convection rate. For a fixed spacing ratio, all $Nu_{m,(T)}$ *vs* z' curves asymptote to the same thermally developed value because the Prandtl number ceases to be a parameter in the fully-developed region; the curve corresponding to the slug-flow situation reaches the thermally fully-developed value much later ($z' \to \infty$) than the other curves.

Heat Transfer Results: (H) Boundary Condition

The discussion in this part will be kept brief because most of the results obtained for the (H) condition are qualitatively similar to those discussed in the last subsection for the (T) condition. Checks to establish the grid independence of the results are presented first. Detailed solutions pertaining to the axial variation of the Nusselt number for several spacing ratios and two different Prandtl numbers are presented next. Finally, results illustrating the effect of Prandtl number on the developing temperature field are presented.

Based on the results already presented in earlier

[†]Note that for comparing thermal entry solutions, the abscissae coordinate z' (= $z/(D_H RePr)$) has been used instead of z*.

sections of this Chapter, the basic grid of 11x11 subelement nodes and POWER = 1.4 was chosen for all computations in this study. Grid checks were limited to an exploration of the effects of various parameters used in the automatic step size selection algorithm. The results of these computations are presented in Figs. 5.24(a) and (b) for (s/d) = 1.5 and 1.05, respectively. These results show that for values of $z^* > 10^{-3}$, the solutions obtained with the basic grid can be considered to be grid independent, for all practical purposes.

Axial variations of the local Nusselt number, $Nu_{z,(H)}$, for eight different values of spacing ratios, in the range $1.05 \leq (s/d) \leq 2.0$, and two values of Prandtl numbers, Pr = 0.72 and 3, are shown in Figs. 6.25 and 6.26. The trends displayed by these curves are qualitatively similar to those displayed by the corresponding results for the (T) condition. Therefore, the discussion presented in the last subsection applies here too.

The effects of Prandtl number on the axial variation of $Nu_{m,(H)}$ for spacing ratios of 1.05, 1.5 and 2 are displayed in Figs. 6.27 to 6.29, respectively. Again, the results for $Pr \to 0$ pertain to the so-called slug flow condition, and the results for $Pr \to \infty$ apply to situations where the flow is hydrodynamically fully-developed and thermally developing. The discussion presented in the last subsection in the context of the (T) condition is qualitatively applicable to these results too.

CHAPTER VII

CONCLUSION

In the preceding chapters, a control-volume finite-element method for three-dimensional parabolic duct flows has been formulated, tested and applied to longitudinal laminar flow and heat transfer in an infinite array of circular cross-section rods arranged in an equilateral triangular pattern. In this chapter, first, the main features of the proposed method and the principal achievements of this thesis are briefly reviewed and commented upon; then, suggestions for possible improvements and extensions of this work are presented.

7.1 REVIEW OF THE THESIS

The method proposed in this thesis was formulated by merging and extending several key ideas of the finite-difference method of Patankar and Spalding [6] for three-dimensional parabolic flows and the control-volume finite-element method of Baliga and Patankar [2] for two-dimensional elliptic flows. The following steps are involved in the formulation of the proposed method: the calculation domain is first divided into prism-shaped macroelements and sub-elements of triangular cross-section; then, each node is associated with prism-shaped control volumes of polygonal cross-section; integral conservation equations are then

written for each of the control volumes; following that, appropriate element interpolation functions are prescribed for each of the dependent variables; using these interpolation functions, algebraic approximations to the integral conservation equations are derived and solved iteratively.

The control-volume finite-element method employed here allows the discretization of straight ducts with regular- or irregular-shaped cross-sections. A semi-automatic discretization scheme is used to generate the cross-sectional domain discretizations. This scheme leads to considerable ease in the assembly of discretization equations and enables efficient use of available computer storage. It also allows the use of a line-by-line iterative procedure based on the Tri-Diagonal-Matrix-Algorithm [4] for the solution of the discretization equations at each axial step. However, it can handle only singly-connected domains. Thus, the present computer implementation of the proposed method is not suitable for the solution of duct flow problems involving complex multiply-connected domains.

In the derivation of the discretization equations, downstream values of the dependent variables are assumed to prevail over the axial step. This formulation, which is analogous to the fully-implicit formulation employed in the numerical solution of parabolic problems [4], is used for avoiding stability-related restrictions on the axial step sizes. In the cross-sectional planes, all the dependent

variables, except pressure, are interpolated in each sub-element by functions which are exponential in the direction of an element-averaged cross-flow velocity vector and linear in the direction normal to it; the pressure is interpolated linearly in each macroelement. This interpolation practice allows the proposed method to solve problems involving significant cross-stream flows, without incurring (i) the stability difficulties that could plague standard finite-element methods based on the Galerkin formulation, and (ii) the false-diffusion problems that commonly afflict upwind-type finite-difference and finite-element methods [1,4].

The proposed method uses a step-by-step marching integration scheme to advance the solution from the given conditions at the inlet of the duct to the downstream outlet cross-section. At each axial step, the SIMPLER calculation procedure of Patankar [4] is used to handle the velocity-pressure coupling which exists between the continuity and cross-stream momentum equations. Another velocity-pressure coupling which exists between the overall mass continuity and the streamwise momentum equations is handled by a new scheme akin to SIMPLER. These iterative solution procedures have worked well in all problems tested in this thesis.

Another key feature of the proposed method is an automatic step-size selection algorithm. This algorithm provides considerable ease and efficiency in the computations by automatically adjusting the axial step size in response

to the prevailing axial gradients of the dependent variables: in portions of the duct where steep axial gradients are encountered, very small step sizes are used; and relatively large step sizes are used in regions where mild gradients are encountered.

The proposed method and its computer implementation have been successfully applied to many two- and three-dimensional test problems. The results of several test problems, including laminar flow and heat transfer in ducts of square cross-section, were presented in Chapter V. These results compare very well with corresponding analytical, numerical and experimental results in the published literature, and they serve to establish the validity and capabilities of the proposed method.

The present solution method has been adapted and applied to laminar incompressible fluid flow and heat transfer in an infinite equilateral triangular array of circular cross-section rods. Several pitch-to-diameter ratios ranging from 1.05 to 2.0 were investigated. The thermal boundary conditions considered were: (1) constant wall temperature both peripherally and axially (T); and (2) constant axial and peripheral wall heat flux (H). Three categories of this problem were extensively studied: (1) fully-developed flow and heat transfer; (2) hydrodynamically fully-developed and thermally developing flow; and (3) simultaneously developing flow and heat transfer. Numerous preliminary

computations were done to ensure that the final results would be grid-independent, for all practical purposes. Results of the fully-developed fluid flow problem and the thermally fully-developed problem pertaining to the (H) boundary condition were compared with the corresponding analytical results presented in [7]; the agreement between these results was found to be very good. The results of the fully-developed problem with the (T) thermal boundary condition and most of the results pertaining to the developing flow and heat transfer problems are new, in that they are not available in the published literature. A detailed discussion of all these results was presented in Chapter VI. In addition to augmenting the currently available repertoire of published heat transfer data, these results demonstrate that the proposed method can be successfully applied to laminar flow and heat transfer in straight ducts of irregular-shaped but uniform cross-sections.

7.2 SUGGESTIONS FOR IMPROVEMENTS AND EXTENSIONS OF THIS WORK

The work presented in this thesis could be improved and extended in several ways. Some suggestions in this regard are presented in this section.

The numerical method proposed in this thesis is based on a primitive-variables formulation. As was described in earlier chapters, if the velocity components and pressure are

stored at the same grid points and interpolated by similar functions, the resulting discretization equations could admit physically unrealistic checkerboard-type pressure fields as solutions. This difficulty is avoided in the proposed method by using unequal-order pressure-velocity interpolations: the cross-sectional planes of duct-like calculation domains are discretized into six-node triangular macroelements and three-node subelements; the velocity components are stored at all nodes and interpolated by special upwind-type functions in each subelement; and the pressure is stored only at the vertices of the macroelements and interpolated linearly in each macroelement. A commonly-used argument for the mathematical justification of this unequal-order interpolation practice is that the momentum equations involve second-order derivatives of the velocity components in the viscous terms and only first-order derivatives of the pressure. This is a valid argument in the computation of parabolic flows because the cross-sectional velocity components are usually not too large; therefore, the convective transport of momentum in the cross-sectional planes does not overwhelm the corresponding viscous transport.

Although the aforementioned unequal-order interpolation of pressure and velocity can be mathematically justified in parabolic-flows, it does have some shortcomings. For the same number of nodes, six-node triangular macro-

elements do not allow as accurate a representation of cross-sections involving curved boundaries as that provided by three-node triangular elements. Another difficulty is that methods using unequal-order interpolations usually lead to a large number of neighbours in the discretization equations for pressure and pressure correction; as a result, the convergence of iterative procedures for the solution of these equations could be rather slow. A related difficulty is that the presence of a large number of coefficients in the discretization equations complicates the coding and book-keeping in the corresponding computer implementations. These difficulties have stimulated renewed interest in equal-order formulations which avoid checkerboard-type pressure distributions. Schneider *et al.* [33] have proposed and critically examined several equal-order finite-element formulations for two-dimensional elliptic flows. The development and incorporation of a suitable equal-order formulation in the proposed method is highly desirable and recommended.

The computer program developed in this thesis incorporates a semi-automatic domain discretization scheme. This scheme has many advantages, but it only allows the discretization of singly-connected duct cross-sections. The other key ideas of the proposed method, however, are not in any way limited to singly-connected domains. Furthermore, the corresponding computer code has been developed so that

it can be easily fitted into a patch-by-patch procedure [35] for domain discretization, equation assembly and solution which allows the investigation of problems with multiply-connected domains. The incorporation of such a patch-by-patch procedure into the computer implementation of the proposed method would enhance its capabilities considerably.

The proposed method has been formulated for the analysis of three-dimensional parabolic duct flows. The extension of its key ideas to partially-parabolic [5] and fully-elliptic flows would be a worthwhile undertaking. Such extensions would enable the analysis of flows in curved ducts, ducts with obstacles, and expanding and contracting ducts. Further research along these lines would greatly enhance the available tools for the numerical prediction of practical fluid flow and heat transfer phenomena.

Only laminar fluid flow problems were considered in this work. This restriction was imposed because the testing and performance evaluation of new numerical methods is best done by applying them to problems with well-established mathematical models. Nevertheless, the proposed control-volume finite-element method does not have any intrinsic limitations which would prevent the incorporation of currently available mathematical models for turbulent flows and two-phase flows in its formulation. The demonstration of this capability is suggested as an extension of this work.

The proposed method has been successfully applied to

several test problems and to the problem of longitudinal laminar flow and heat transfer in a rod-bundle. The results are encouraging enough to warrant the application of the method to other practical fluid flow problems, including, as was suggested in the previous paragraph, turbulent and two-phase flows. Experimental verification of the results of selected test problems is necessary to further establish the validity and capabilities of the proposed method. The possibilities seem to be limited only by the imagination and ingenuity of the researcher.

REFERENCES

1. Baliga, B.R. and Patankar, S.V., A New Finite-Element Formulation for Convection-Diffusion Problems, *Numerical Heat Transfer*, Vol. 3, pp 393-409, 1980.

2. Baliga, B.R., A Control Volume Based Finite-Element Method for Convective Heat and Mass Transfer, Ph.D. Thesis, University of Minnesota, 1978.

3. Patankar, S.V., Numerical Prediction of Three-Dimensional Flows, in *Studies in Convection*, B.E. Launder (Ed.), Vol. 1, Academic, New York, 1975.

4. Patankar, S.V., *Numerical Heat Transfer and Fluid Flow*, Hemisphere Publishing Co., McGraw-Hill Book Co., 1980.

5. Pratap, V.S. and Spalding, D.B., Fluid Flow and Heat Transfer in Three-Dimensional Duct Flows, *Int. J. Heat and Mass Transfer*, Vol. 19, pp 1183-1188, 1976.

6. Patankar, S.V. and Spalding, D.B., A Calculation Procedure for Heat, Mass and Momentum Transfer in Three-Dimensional Parabolic Flows, *Int. J. Heat and Mass Transfer*, Vol. 15, pp 1787-1806, 1972.

7. Shah, R.K. and London, A.L., *Laminar Flow Forced Convection in Ducts*, Advances in Heat Transfer, Supplement 1, Academic Press, 1978.

8. Sparrow, E.M., Lin, S.H. and Lundgren, T.S., Flow Development in the Hydrodynamic Entrance Region of Tubes and Ducts, *The Physics of Fluids*, Vol. 7, pp 338-347, 1964.

9. Fleming, D.P. and Sparrow, E.M., Flow in the Hydrodynamic Entrance Region of Ducts of Arbitrary Cross-Section, *J. of Heat Transfer*, Trans. ASME, Vol. 91, pp 345-354, 1969.

10. Der, J., A Study of General Three-Dimensional Boundary Layer Problems by an Exact Numerical Method, *AIAA J.*, Vol. 9, p. 1294, 1974.

11. East, J.L. and Pierce, F.J., Explicit Numerical Solution of Three-Dimensional Incompressible Turbulent Boundary Layer Equations, *AIAA J.*, Vol. 10, p. 1216, 1972.

12. Patankar, S.V., Rafiinejad, D. and Spalding, D.B., Three-Dimensional Boundary Layer with Solution to All Three Momentum Equations, *Comp. Methods Appl. Mech. Eng.*, Vol. 6, p. 283, 1975.

13. Caretto, L.S., Curr, R.M. and Spalding, D.B., Two Numerical Methods for Three-Dimensional Boundary Layers, *Comp. Methods Appl. Mech. Eng.*, Vol. 1, p. 39, 1972.

14. Curr, R.M., Sharma, D. and Tatchell, D.G., Numerical Predictions of Some Three-Dimensional Boundary Layer in Ducts, *Comp. Methods Appl. Mech. Eng.*, Vol. 1, pp 143-158, 1972.

15. Carlson, G.A. and Hornbeck, R.W., A Numerical Solution of Laminar Entrance Flow in a Square Duct, *J. of Applied Mechanics*, Vol. 40, pp 25-30, 1973.

16. Briley, W.R., Numerical Method for Predicting Three-Dimensional Steady Viscous Flow in Ducts, *J. of Comp. Physics*, Vol. 14, pp 8-28, 1974.

17. Robert, D.W. and Forester, C.K., Parabolic Procedure for Flows in Ducts of Arbitrary Cross-Sections, *AIAA J.*, Vol. 17, pp 33-40, 1979.

18. Ghia, U. and Sathyanarayana, K., Analysis and Solution of Three-Dimensional Viscous Flow in Non-Rotating Ducts, in Flow in Primary Non-Rotating Passages in Turbomachines, presented in the *ASME Winter Annual Meeting*, 1979.

19. Taylor, C., Morgan, K. and Brebia, C.A. (Eds), *Numerical Methods in Laminar and Turbulent Flows*, Pentech, London, 1978.

20. Chung, T.J., *Finite Element Analysis in Fluid Dynamics*, McGraw-Hill, 1978.

21. Baker, A.J., Finite-Element Solution Theory for Three-Dimensional Boundary Flows, *Comp. Methods Appl. Mech. Eng.*, Vol. 4, pp 367-386, 1974.

22. Davids, N., Kandarpa, K. and Melville, J., A Generalized Finite-Element Model for Entrance Flow in Ducts of Arbitrary Cross-Section, *Comp. and Fluids*, Vol. 5, pp 73-86, 1977.

23. Strada, M., Del Giudice, S. and Comini, G., Finite Element Solutions for Laminar Forced Convection in the Thermal Region of Ducts, *Numerical Heat Transfer*, Vol. 1, pp 471-488, 1978.

24. Comini, G., Del Giudice, S. and Strada, M., Finite Element Analysis of Laminar Flow in the Entrance Region of Ducts, *Int. J. of Numerical Methods in Eng.*, Vol. 15, pp 507-517, 1980.

25. Del Giudice, S., Step-by-Step Analysis of Flow Development in Ducts, *Numerical Heat Transfer*, Vol. 2, pp 291-302, 1979.

26. Del Giudice, S., Strada, M. and Comini, G., Laminar Heat Transfer in the Entrance Region of Ducts, *Numerical Heat Transfer*, Vol. 2, pp 487-496, 1979.

27. Del Giudice, S., Strada, M. and Comini, G., Three-Dimensional Laminar Flow in Ducts, *Numerical Heat Transfer*, Vol. 4, pp 215-228, 1981.

28. Kays, W.M. and Crawford, M.E., *Convective Heat and Mass Transfer*, Second Edition, McGraw-Hill Book Co., 1980.

29. Schlichting, H., *Boundary Layer Theory*, Seventh Edition, McGraw-Hill Book Co., 1979.

30. Sparrow, E.M. and Patankar, S.V., Relationships among Boundary Conditions and Nusselt Numbers for Thermally Developed Duct Flows, *J. of Heat Transfer*, Trans. ASME, Vol. 99, pp 483-485, 1977.

31. Sparrow, E.M., Baliga, B.R. and Patankar, S.V., Forced Convection Heat Transfer from a Shrouded Fin Array With and Without Tip Clearance, *J. of Heat Transfer*, Trans. ASME, Vol. 100, p. 572, 1978.

32. Hood, P. and Taylor, C., Navier-Stokes Equations Using Mixed Interpolation, in *Finite-Element Methods in Flow Problems*, Eds. J.T. Oden *et al.*, VAH Press, Huntsville, pp 57-66, 1974.

33. Schneider, G.E., Raithby, G.D. and Yovanovich, M.M., Finite-Element Solution Procedures for Solving the Incompressible Navier-Stokes Equations Using Equal Order Variable Interpolation, *Numerical Heat Transfer*, Vol. 1, pp. 433-451, 1978.

34. Zienkiewicz, O.C., *The Finite-Element Method*, Third Edition, McGraw-Hill Book Co., 1977.

35. Khayat, R.E., A Patch-by-Patch Approach to Domain Discretization, Equation Assembly and Solution in General Two-Dimensional Finite-Element Methods, *B.Eng. Honours Thesis*, McGill University, 1980.

36. Eckert, E.R.G. and Carlson, W.O., Natural Convection in an Air Layer Enclosed within Rectangular Cavities, *Int. J. of Heat and Mass Transfer*, Vol. 2, pp 106-120, 1961.

37. Mallinson, G.D. and de Vahl Davis, G., Three-Dimensional Natural Convection in a Box: A Numerical Study, *J. of Fluid Mechanics*, Vol. 83, pp 1-31, 1977.

38. Jones, I.P., A Comparison Problem for Numerical Methods in Fluid Dynamics, the 'Double-Glazing' Problem, presented at the *Int. Conf. on Numerical Methods in Thermal Problems*, Swansea, 1979.

39. Jones, I.P., A Numerical Study of Natural Convection in an Air-Filled Cavity: Comparison with Experiment, *Numerical Heat Transfer*, Vol. 2, pp 193-213, 1979.

40. Iyican, L., Bayazitoglu, Y. and Witte, L.C., An Analytical Study of Natural Convection in Trapezoidal Enclosures, *Journal of Heat Transfer*, Trans. ASME, Vol. 102, pp 640-647, 1980.

41. Iyican, L., Witte, L.C. and Bayazitoglu, Y., An Experimental Study of Natural Convection in Trapezoidal Enclosures, *Journal of Heat Transfer*, Trans. ASME, Vol. 102, pp 648-653, 1980.

42. Goldstein, R.J. and Kreid, D.K., Measurements of Laminar Flow Development in a Square Duct Using Laser-Doppler Flowmeter, *Journal of Applied Mechanics*, Vol. 34, pp 813-818, 1967.

43. Chandrupatla, A.R. and Sastri, V.M.K., Laminar Forced Convection Heat Transfer of a Non-Newtonian Fluid in a Square Duct, *Int. J. of Heat and Mass Transfer*, Vol. 20, pp. 1315-1324, 1977.

44. Beavers, G.S., Sparrow, E.M. and Magnuson, R.A., Experiments on Hydrodynamically Developing Flow in Rectangular Ducts of Arbitrary Aspect Ratio, *Int. J. of Heat and Mass Transfer*, Vol. 13, pp 689-702, 1970.

45. Montgomery, S.R. and Wibulwas, P., Laminar Flow Heat Transfer for Simultaneously Developing Velocity and Temperature Profiles in Ducts of Rectangular Cross-Section, *Appl. Sci. Res.*, Vol. 18, pp 247-259, 1967.

46. Chandrupatla, A.R. and Sastri, V.M.K., Constant Wall Temperature Entry Length Laminar Flow of and Heat Transfer to a Non-Newtonian Fluid in a Square Duct, in *Proc. 6th Int. Heat Transfer Conf.*, Toronto, pp 323-328, 1978.

47. Yao, S.C. and Pfund, P.A. (Eds.), Fluid Flow and Heat Transfer over Rod or Tube Bundles, Symposium Proceedings presented at *The Winter Annual Meeting of the ASME*, New York, 1979.

FIGURES

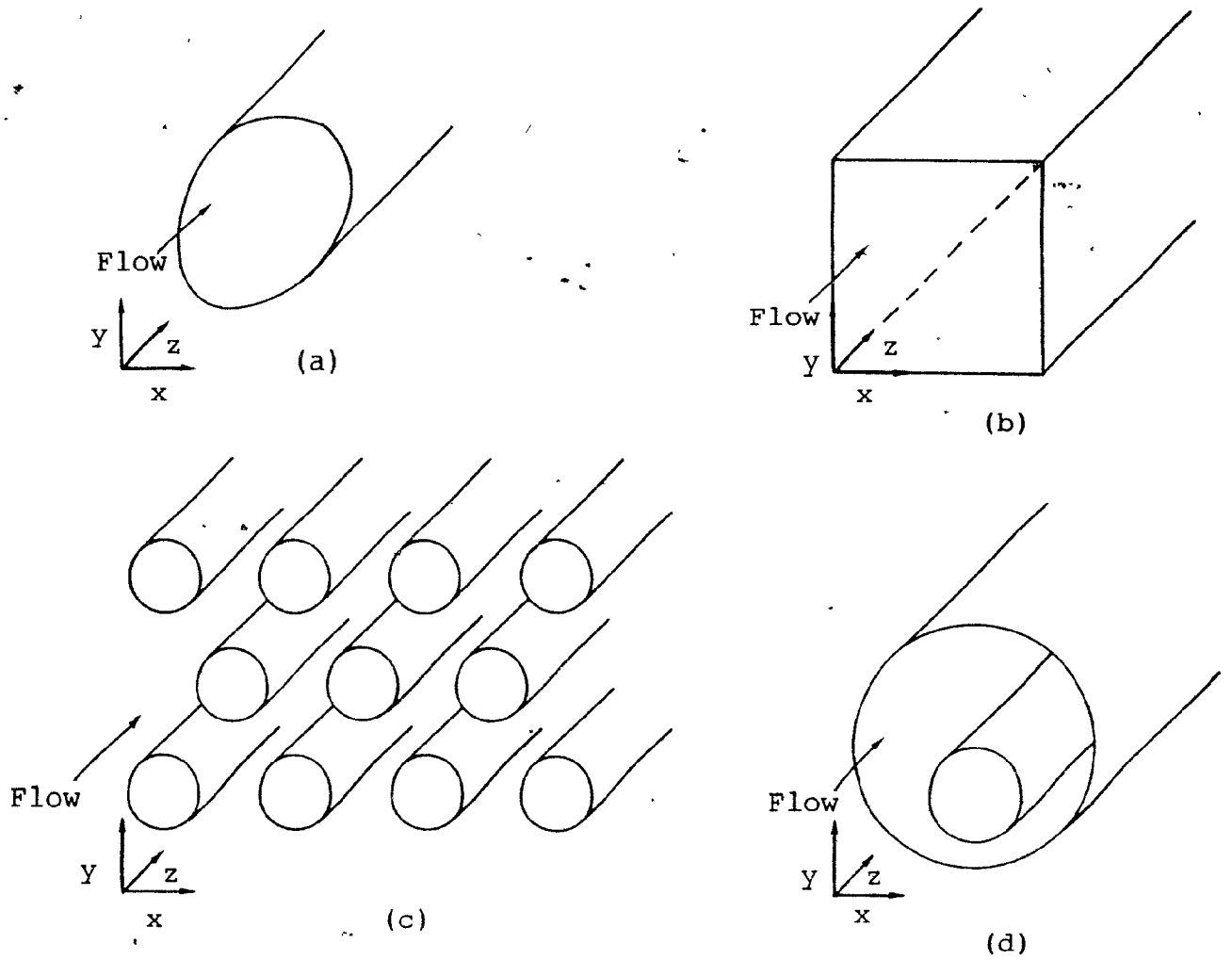

Fig. 2.1: Examples of three-dimensional parabolic flows in straight ducts of irregular-shaped cross-section.

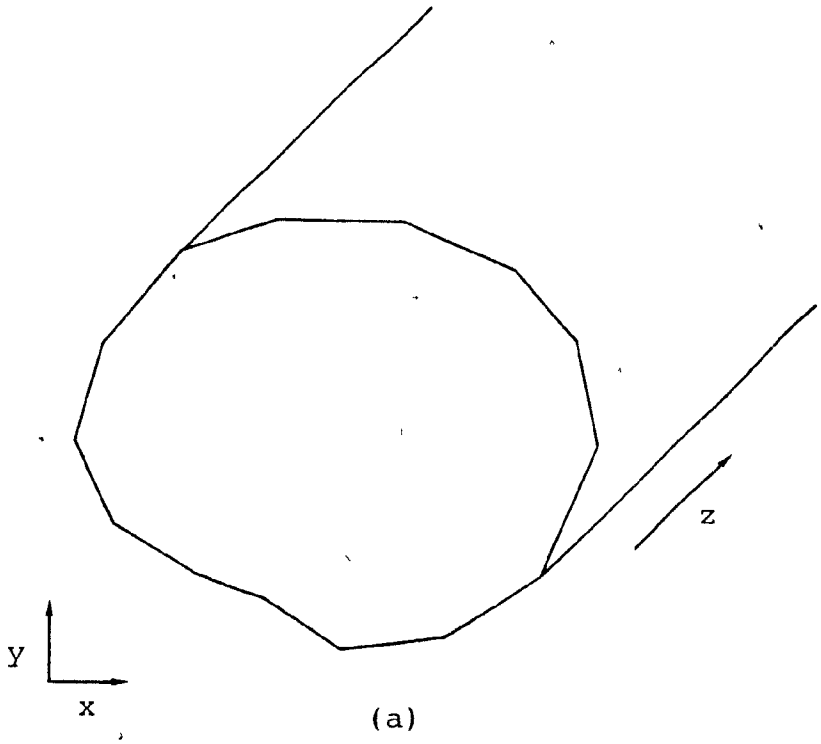

(a)

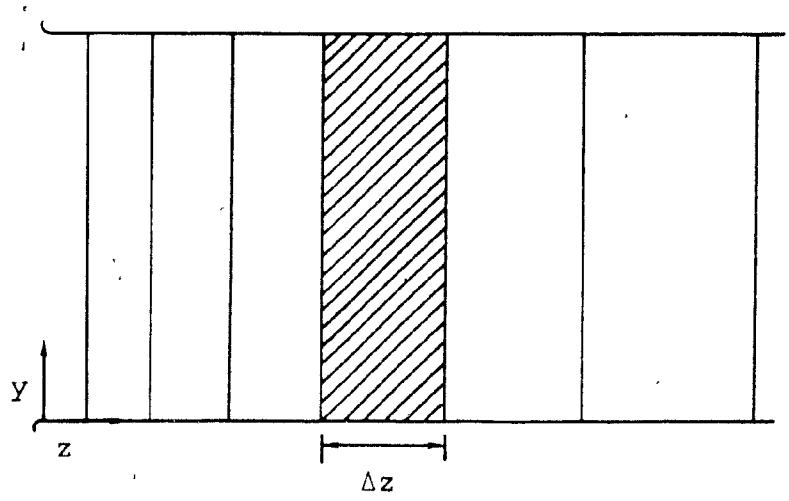

(b)

Fig. 3.1: Three-dimensional parabolic flow in a straight duct of irregular-shaped cross-section; (a) calculation domain; (b) discretization of the duct into slabs.

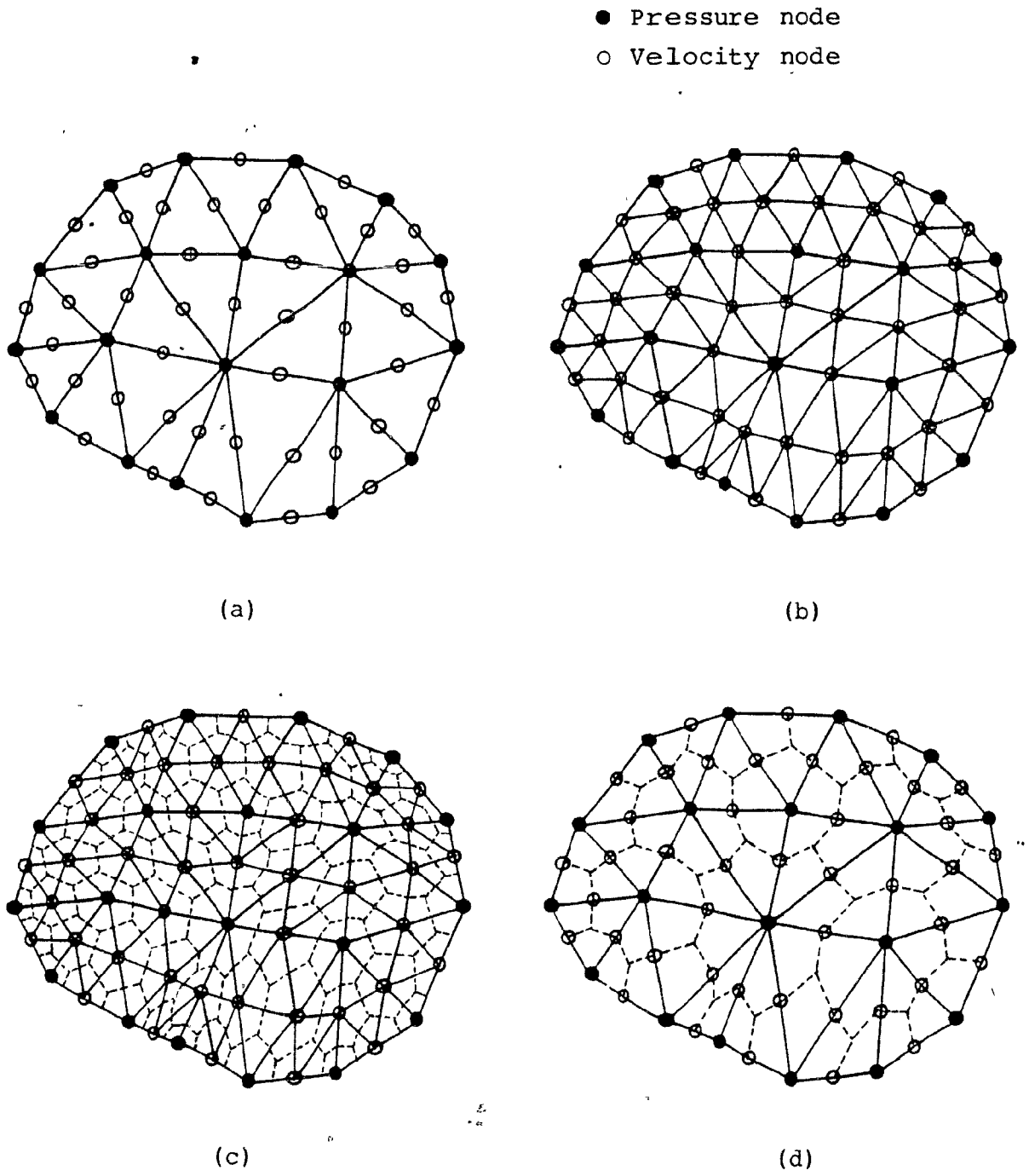

Fig. 3.2: Steps in the discretization of the duct cross-section: generation of (a) six-node triangular macroelements; (b) three-node triangular subelements; (c) subelement control volumes; and (d) macroelement control volumes.

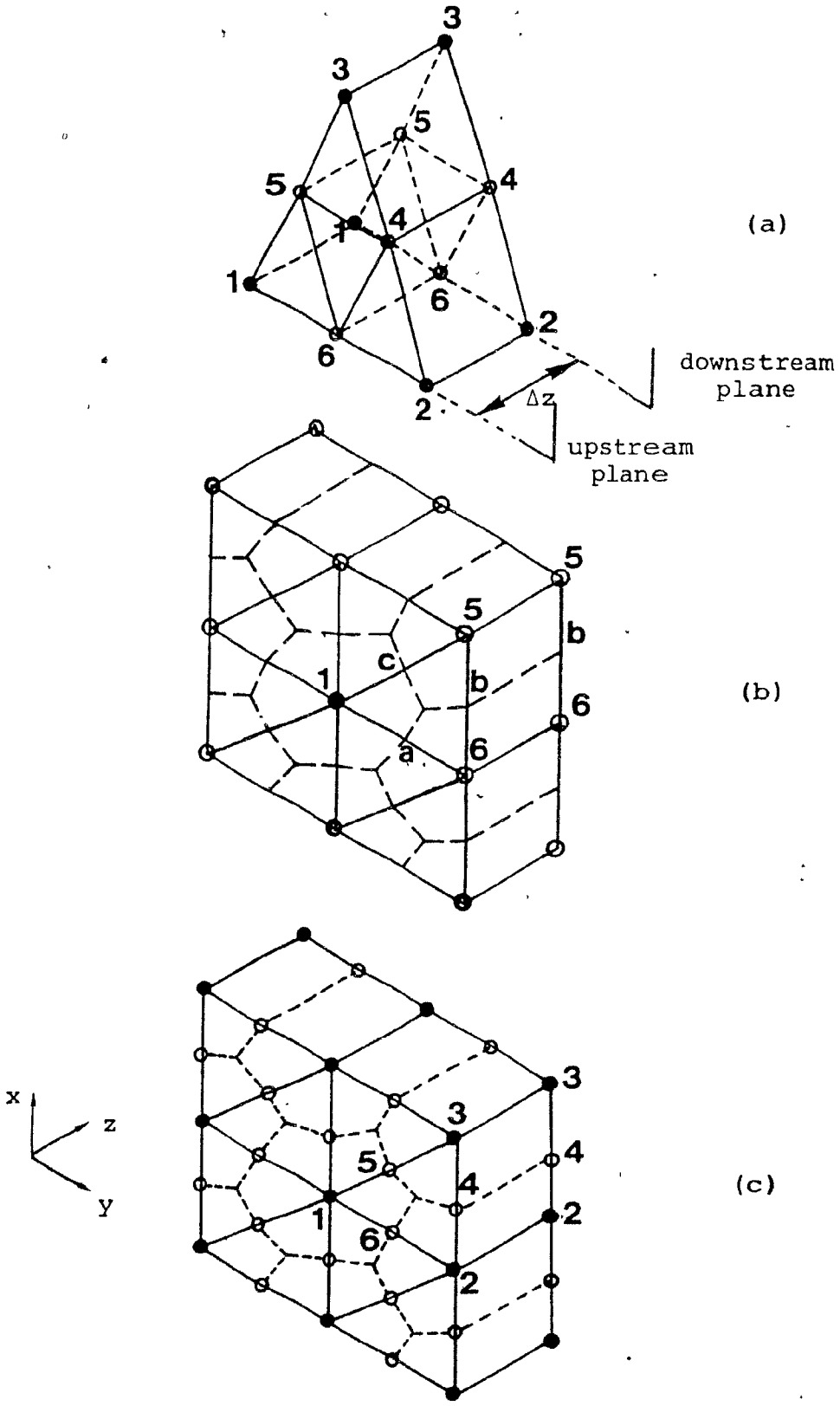

Fig. 3.3: Local node numbering and labelling schemes for (a) a typical prism macroelement and its four associated subelements; (b) a typical subelement control volume surrounding node 1; (c) a typical macroelement control volume surrounding node 1.

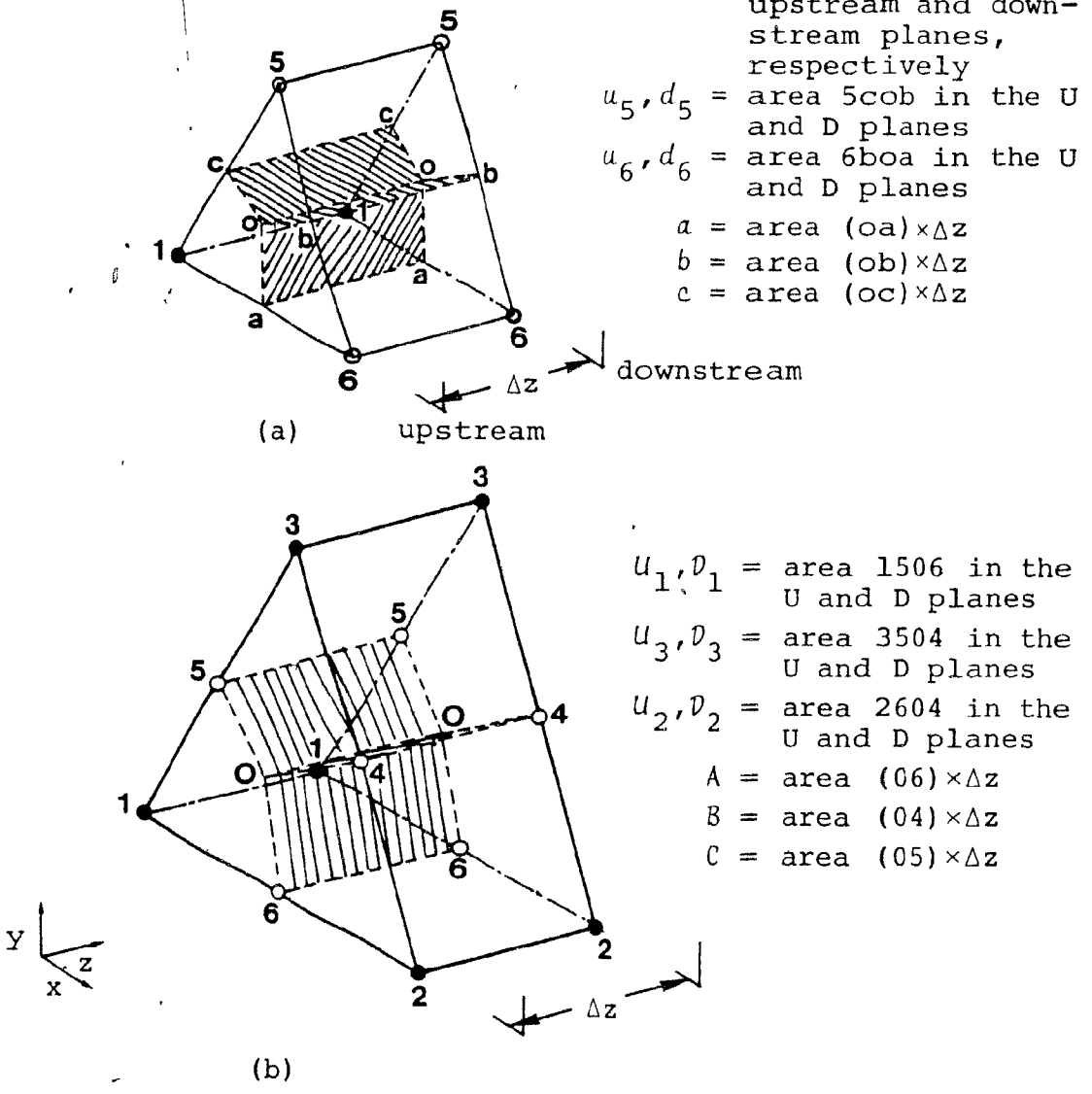

Fig. 3.4: Details of the control volume faces and related nomenclature: (a) a typical subelement control volume; (b) a typical macroelement control volume.

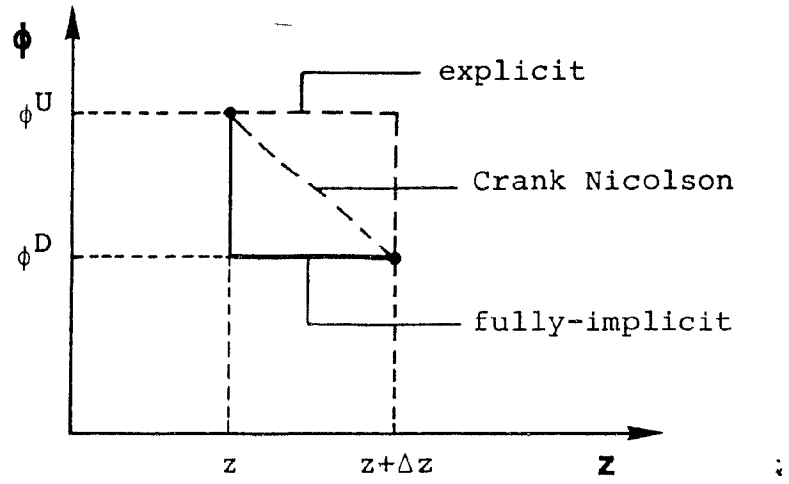

Fig. 3.5: Three different z-direction interpolation functions.

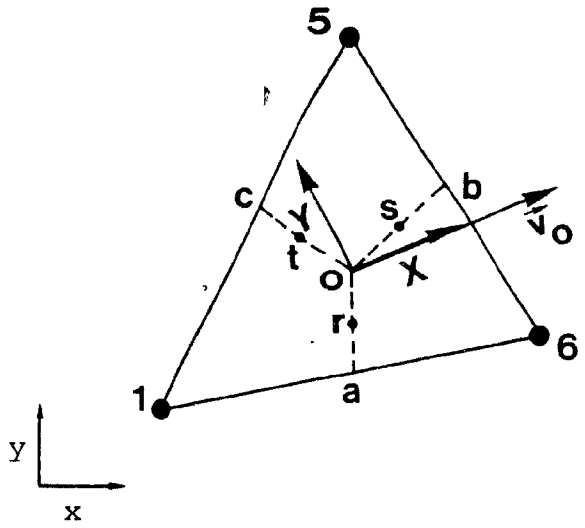

Fig. 3.6: A typical triangular subelement, the global (x,y) and local (X,Y) coordinate systems and related nomenclature.

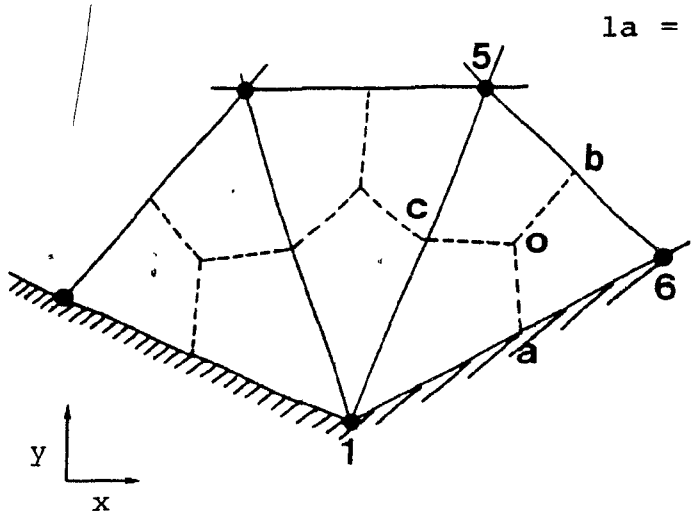

Fig. 3.7: A boundary node with its three associated sub-elements.

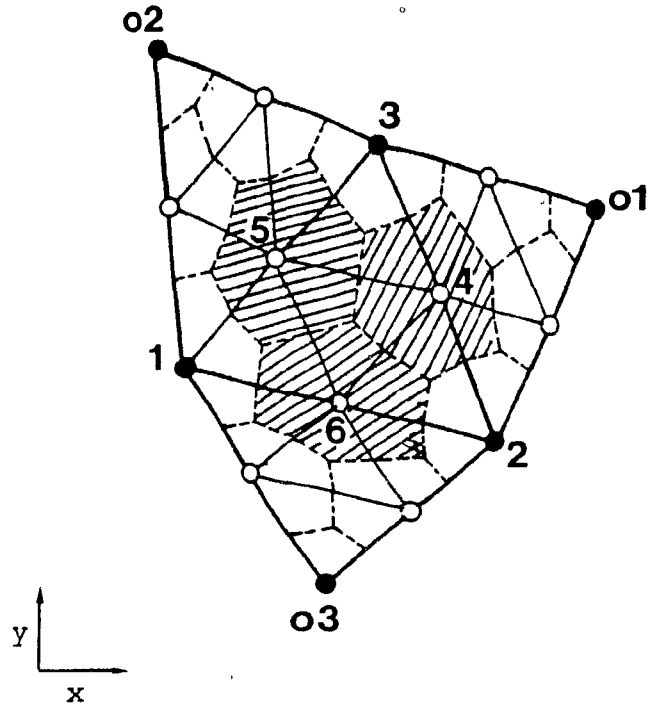

Fig. 3.8: Momentum control volumes associated with the mid-sides nodes of an internal macroelement.

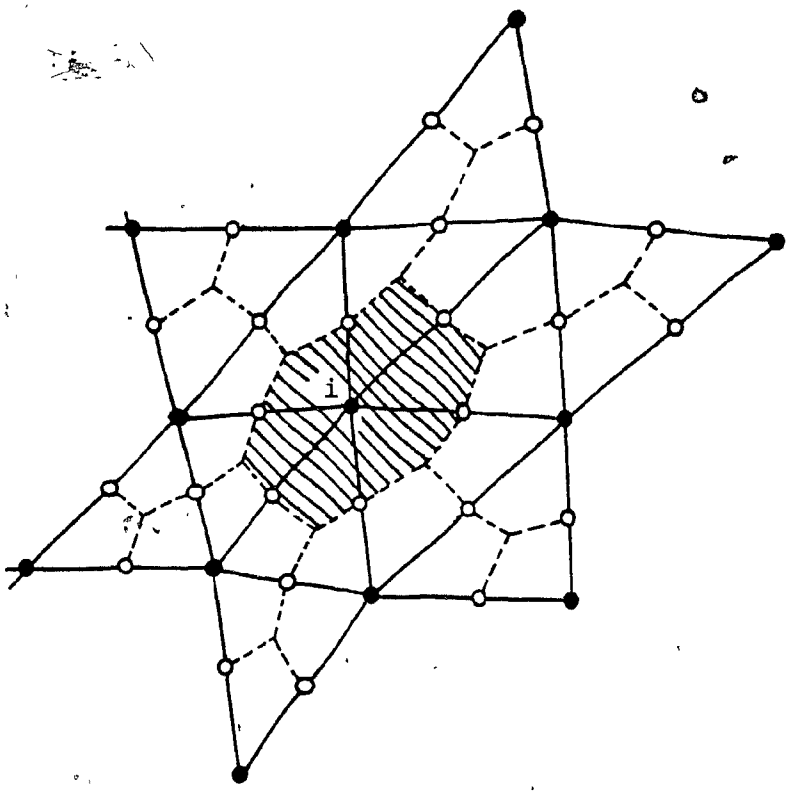

Fig. 3.9: An internal pressure node i and its cluster of neighbour nodes.

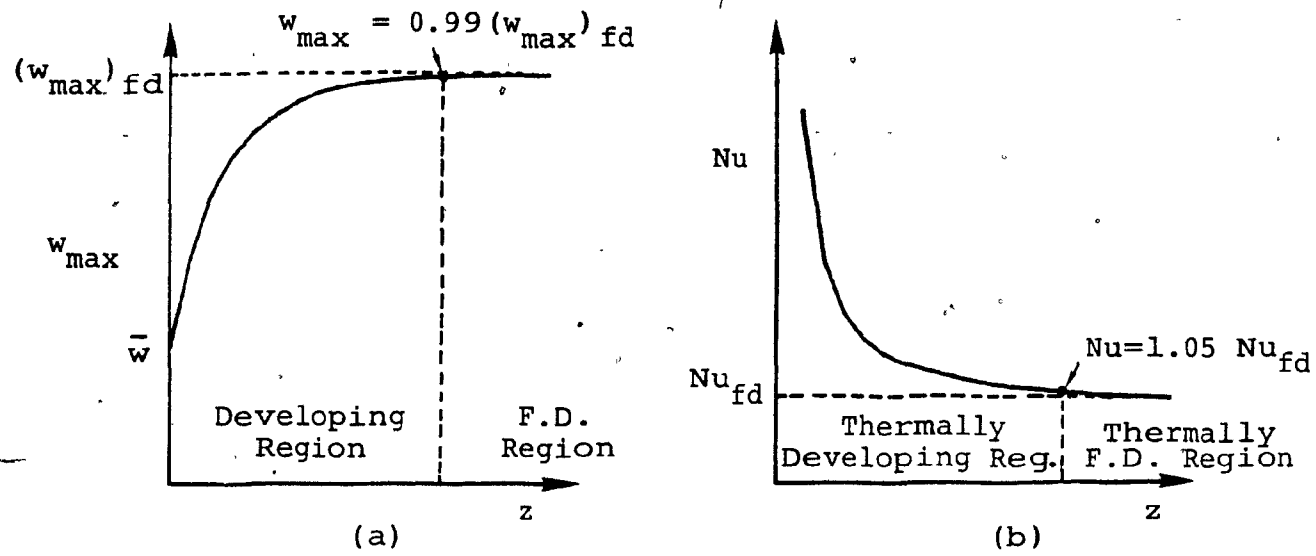

Fig. 4.1: Flow and heat transfer in ducts: (a) hydrodynamically developing and fully-developed regions; (b) thermally developing and fully-developed regions.

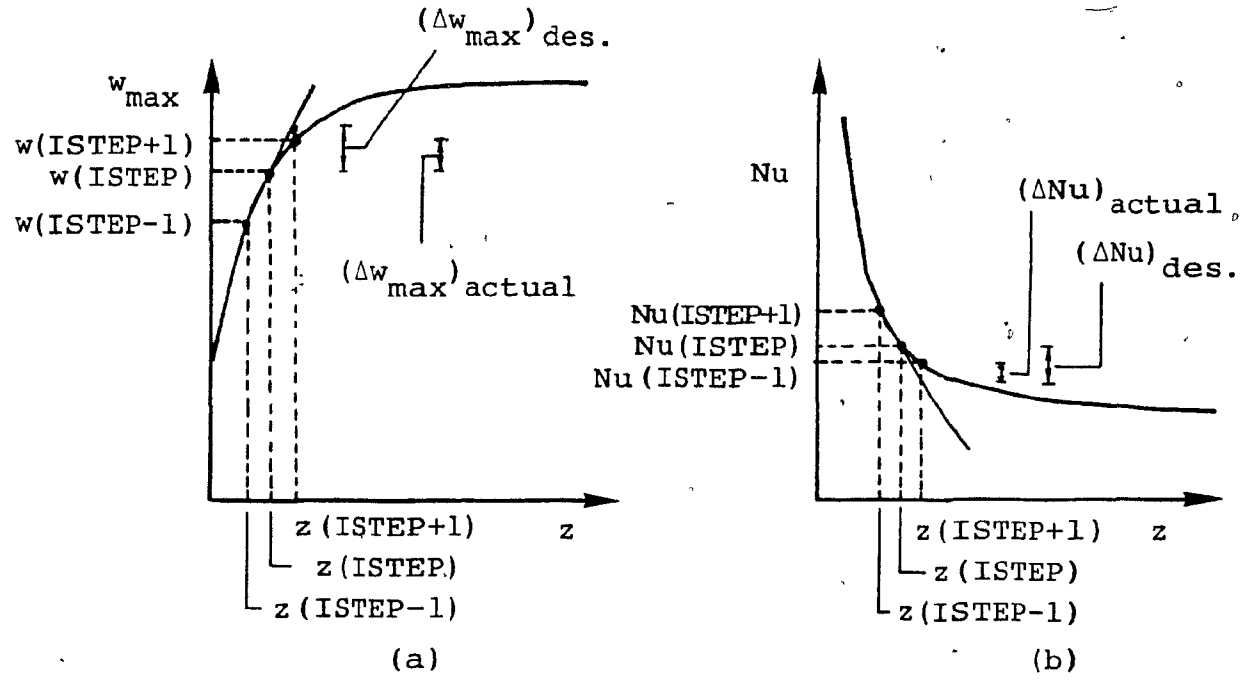

Fig. 4.2: Automatic step size selector algorithm based on: (a) $(\Delta w_{max}/\Delta z)$; (b) $(\Delta Nu/\Delta z)$.

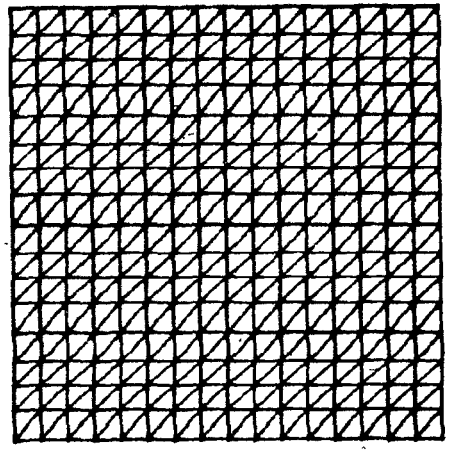

(a)

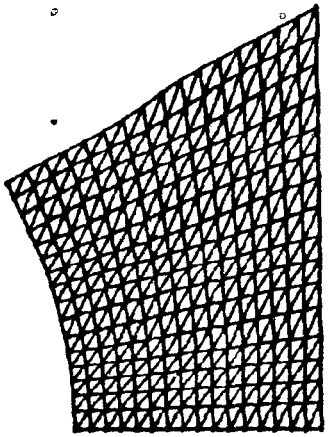

(b)

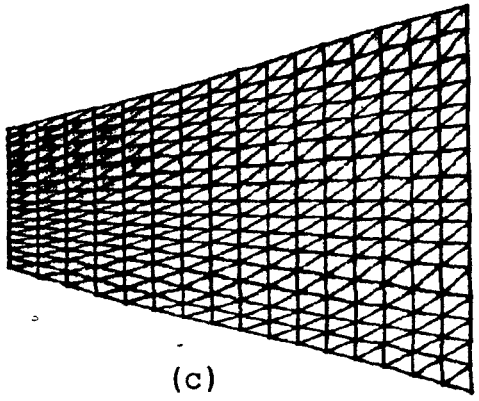

(c)

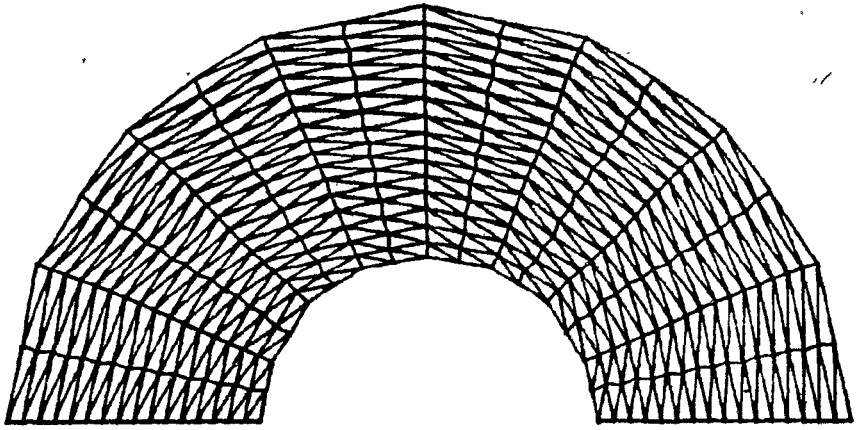

(d)

Fig. 4.3: Mapping of a unit square onto irregular-shaped domains.

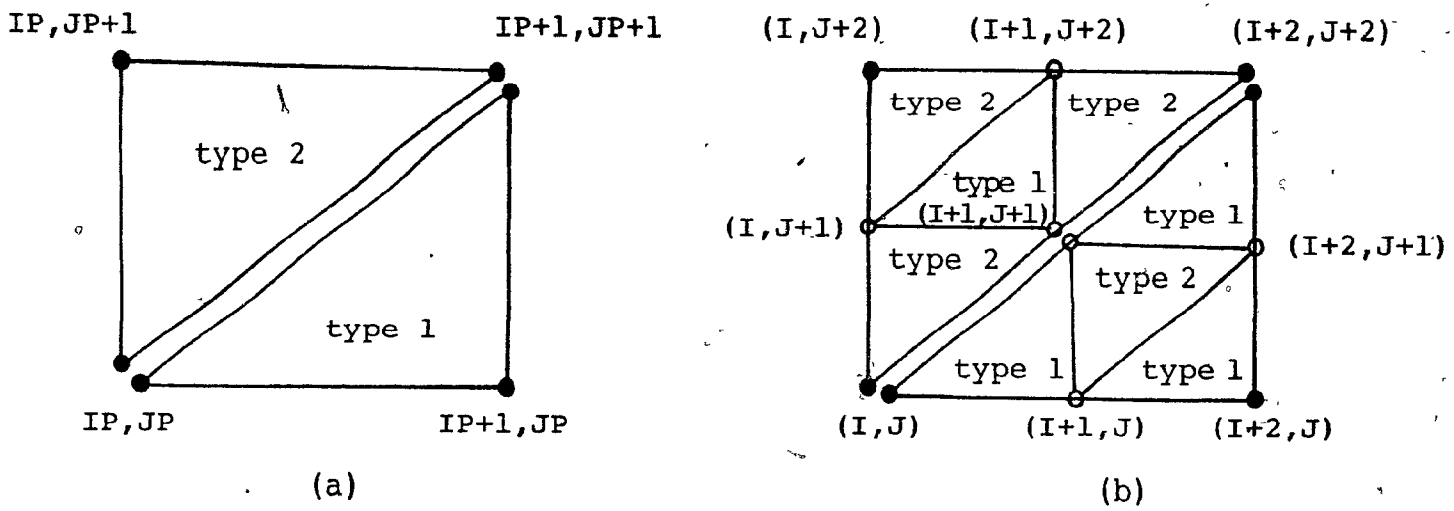

Fig. 4.4: (a) Typical macroelements of types 1 and 2, and associated (IP,JP) node addressing scheme; (b) corresponding subelements of types 1 and 2 and (I,J) node addressing scheme.

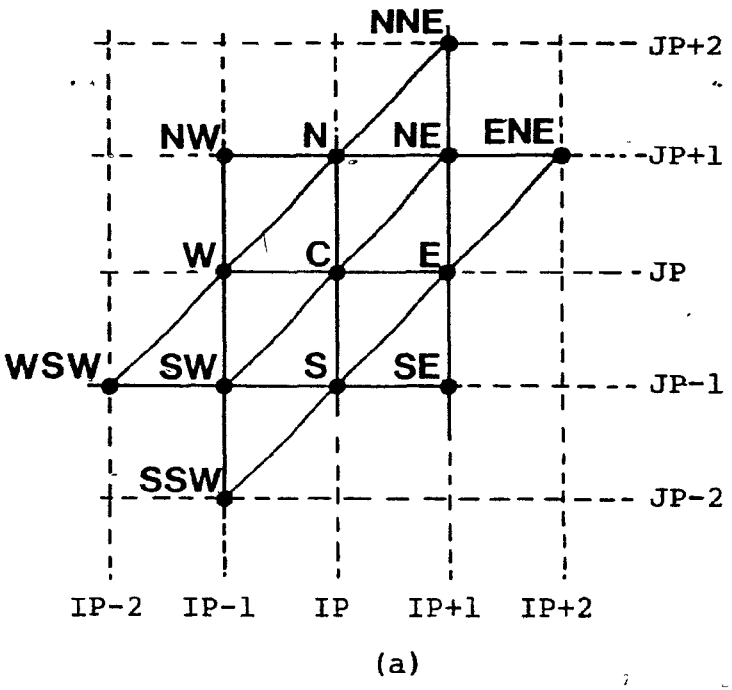

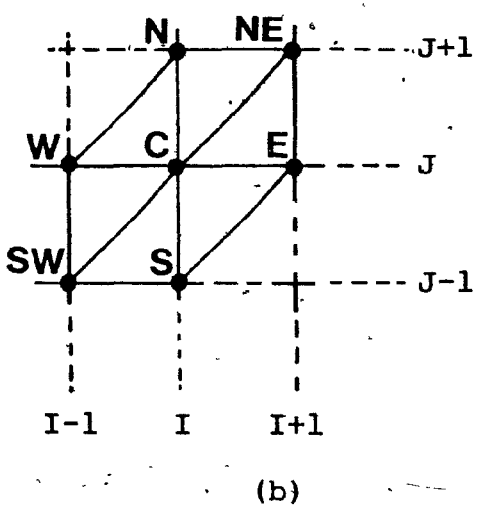

Fig. 4.5: Geographic node-labelling scheme: (a) macroelement vertices, C = (IP,JP), E = (IP+1,JP), N = (IP,JP+1) ... (b) subelement vertices, C = (I,J), E = I+1,J), N = (I,J+1) ... .

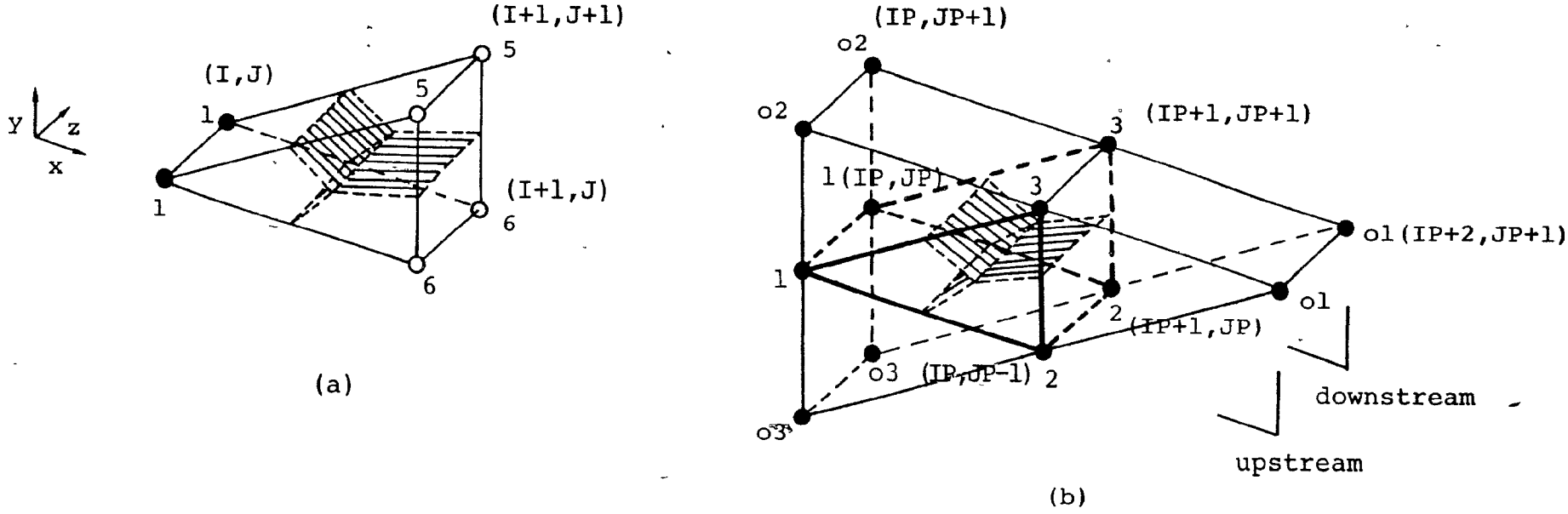

Fig. 4.6: Node addressing scheme for (a) a typical prism subelement of type-1; (b) a typical prism macroelement of type-1.

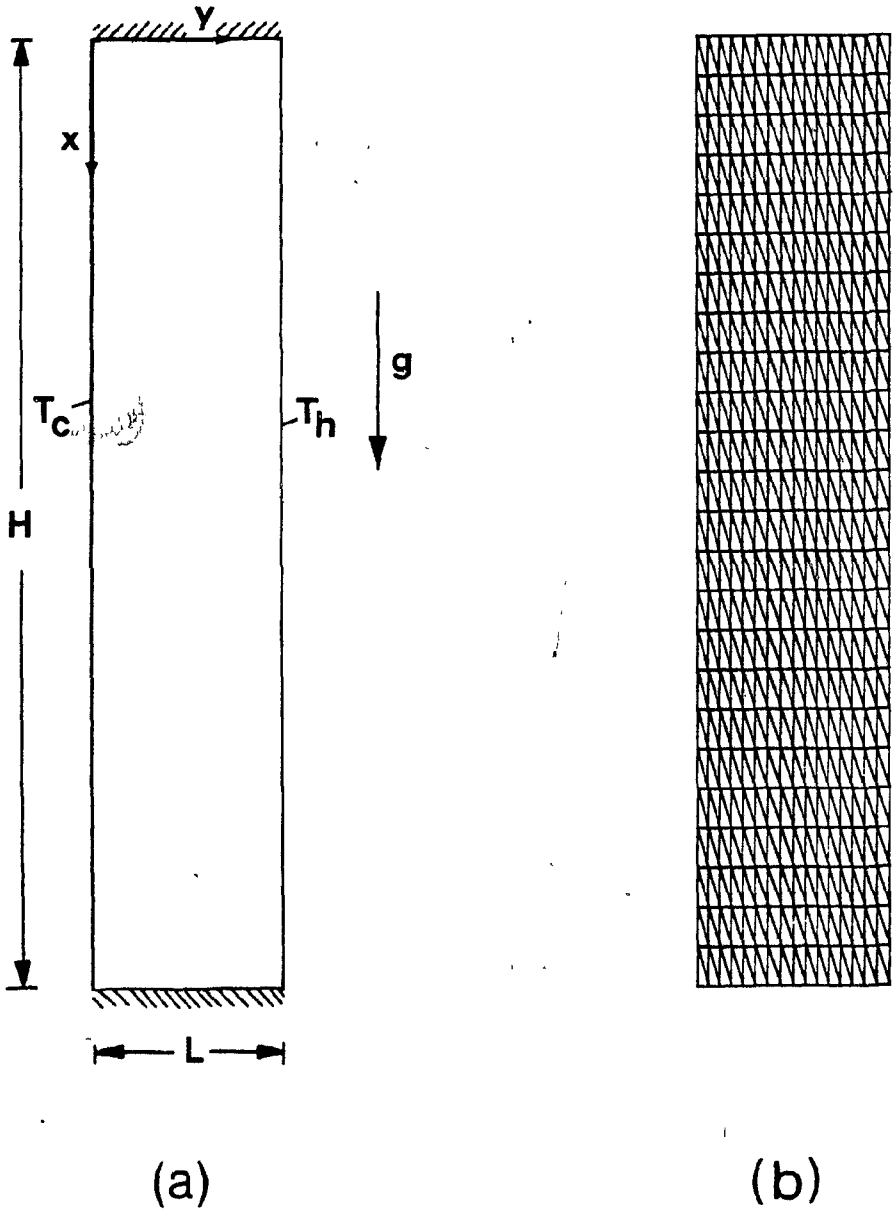

Fig. 5.1: Natural convection in a rectangular enclosure: (a) problem schematic; (b) domain discretization.

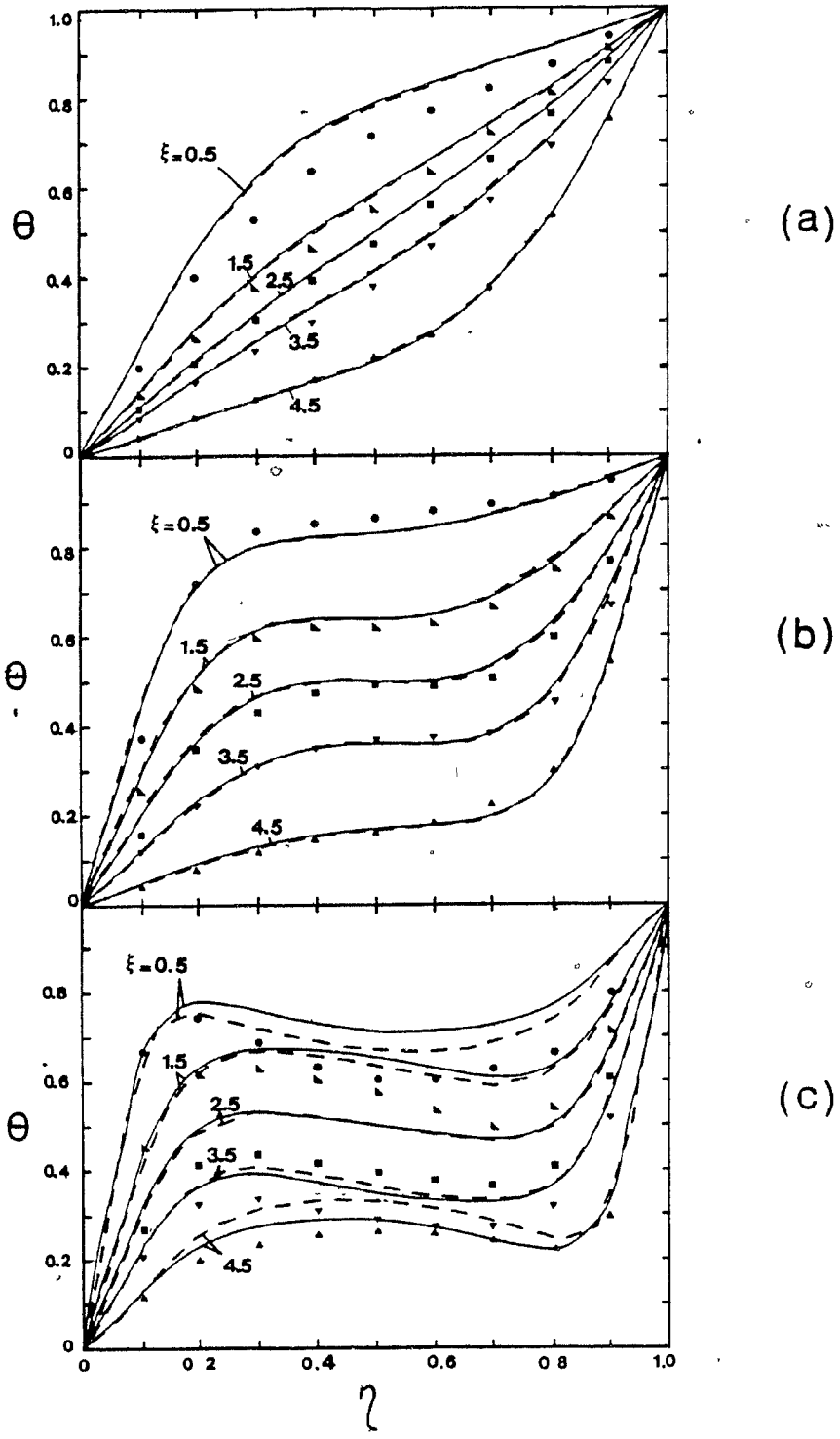

Fig. 5.2: Natural convection in a rectangular enclosure: temperature profiles for (a) Ra = 2.49×10^3, (b) Ra = 1.67×10^4, and (c) Ra = 1.36×10^5. Solid lines represent results produced by the CVFEM, dashed lines represent numerical results from Jones [39], and the symbols represent experimental results from Duxbury [39].

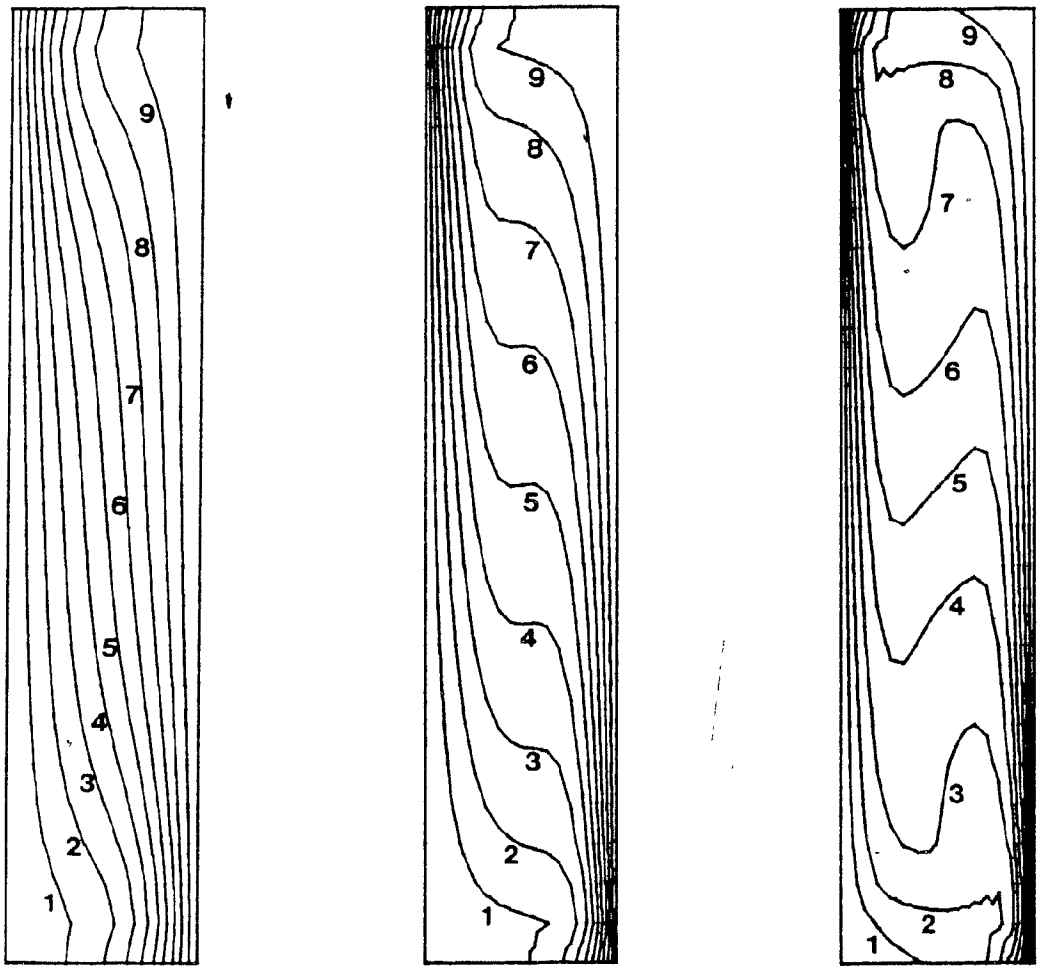

Fig. 5.3: Natural convection in a rectangular enclosure: isotherm contours for (a) Ra = 2.49×10^3, (b) Ra = 1.67×10^4, and (c) Ra = 1.36×10^5. The isotherm levels start with $\theta_1 = 0.1$ and increase to $\theta_9 = 0.9$ in equal steps of 0.1.

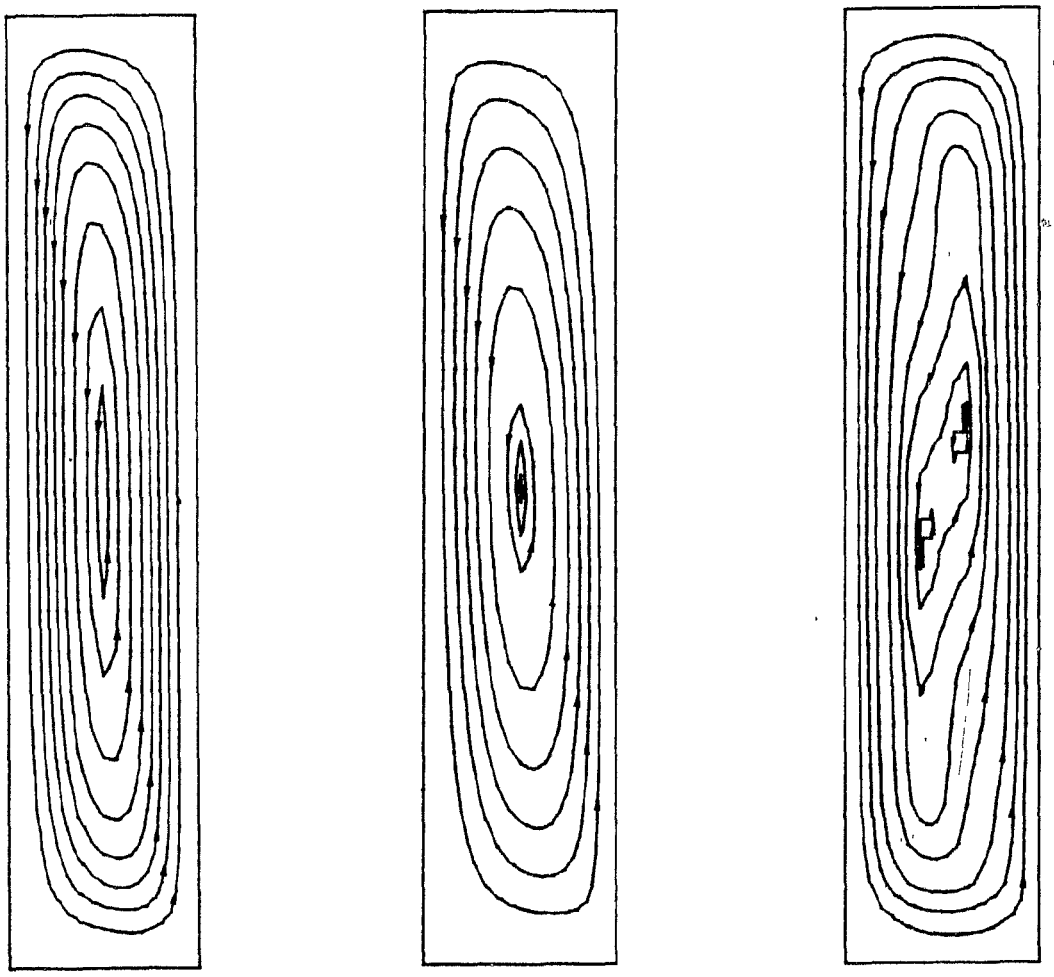

Fig. 5.4: Natural convection in a rectangular enclosure: streamline plots for (a) $Ra = 2.49 \times 10^3$ and ψ = 0, 1.08, 2.17, 3.26, 4.35, 5.43, 6.50, 7.22, 7.5; (b) $Ra = 1.67 \times 10^4$ and ψ = 0, 4.95, 9.89, 14.83, 19.78, 24.7, 28.9, 29.4, 29.7; (c) $Ra = 1.36 \times 10^5$ and ψ = 0, 9.86, 19.71, 29.57, 39.42, 44.35, 46.67, 48.06, 48.44.

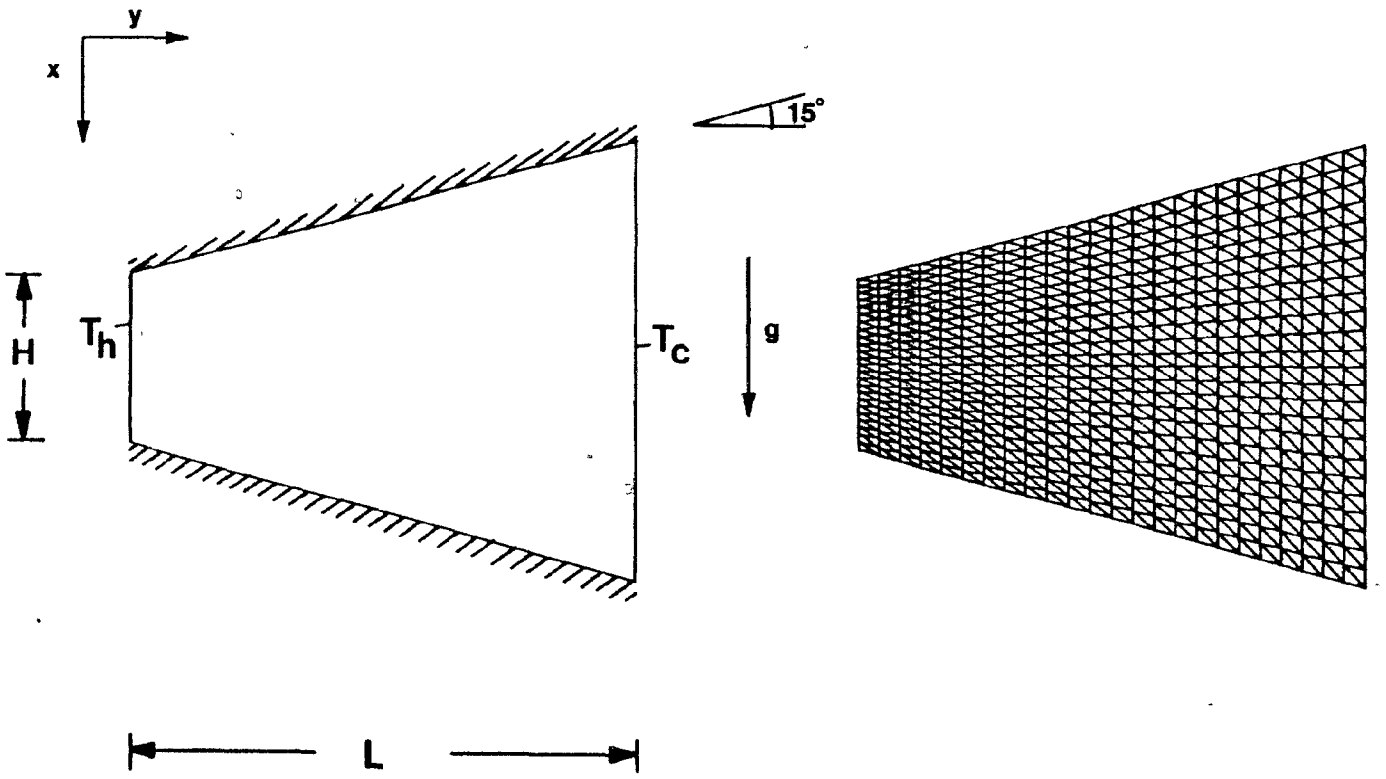

Fig. 5.5: Natural convection in a trapezoidal enclosure: (a) problem schematic; (b) domain discretization.

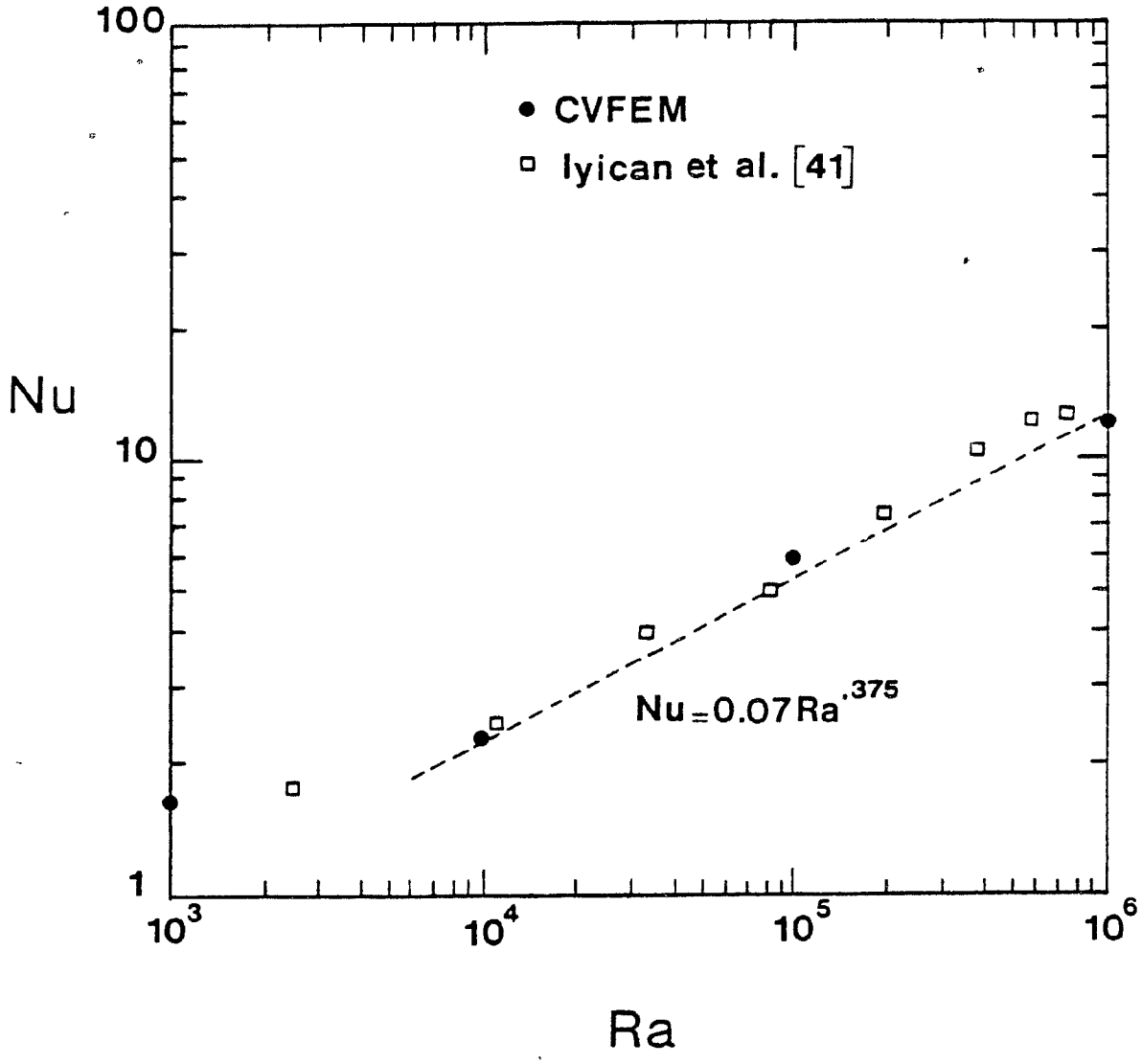

Fig. 5.6: Natural convection in a trapezoidal enclosure: variation of average Nusselt number with Rayleigh number.

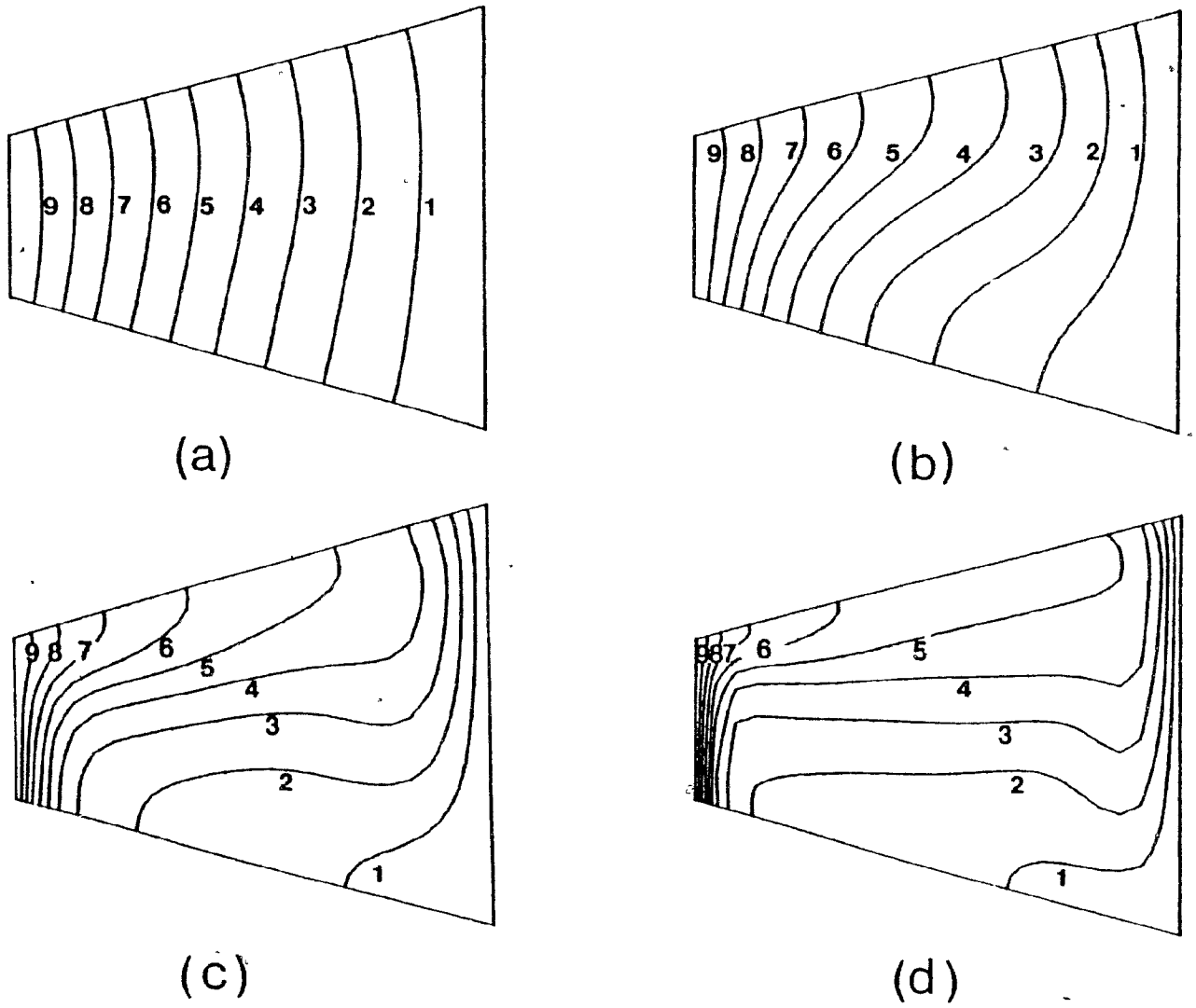

Fig. 5.7: Natural convection in a trapezoidal enclosure: isotherm contours for (a) Ra = 10^3; (b) Ra = 10^4; (c) Ra = 10^5; (d) Ra = 10^6. The isotherm levels start with $\theta_1 = 0.1$ and increase to $\theta_9 = 0.9$ in equal steps of 0.1.

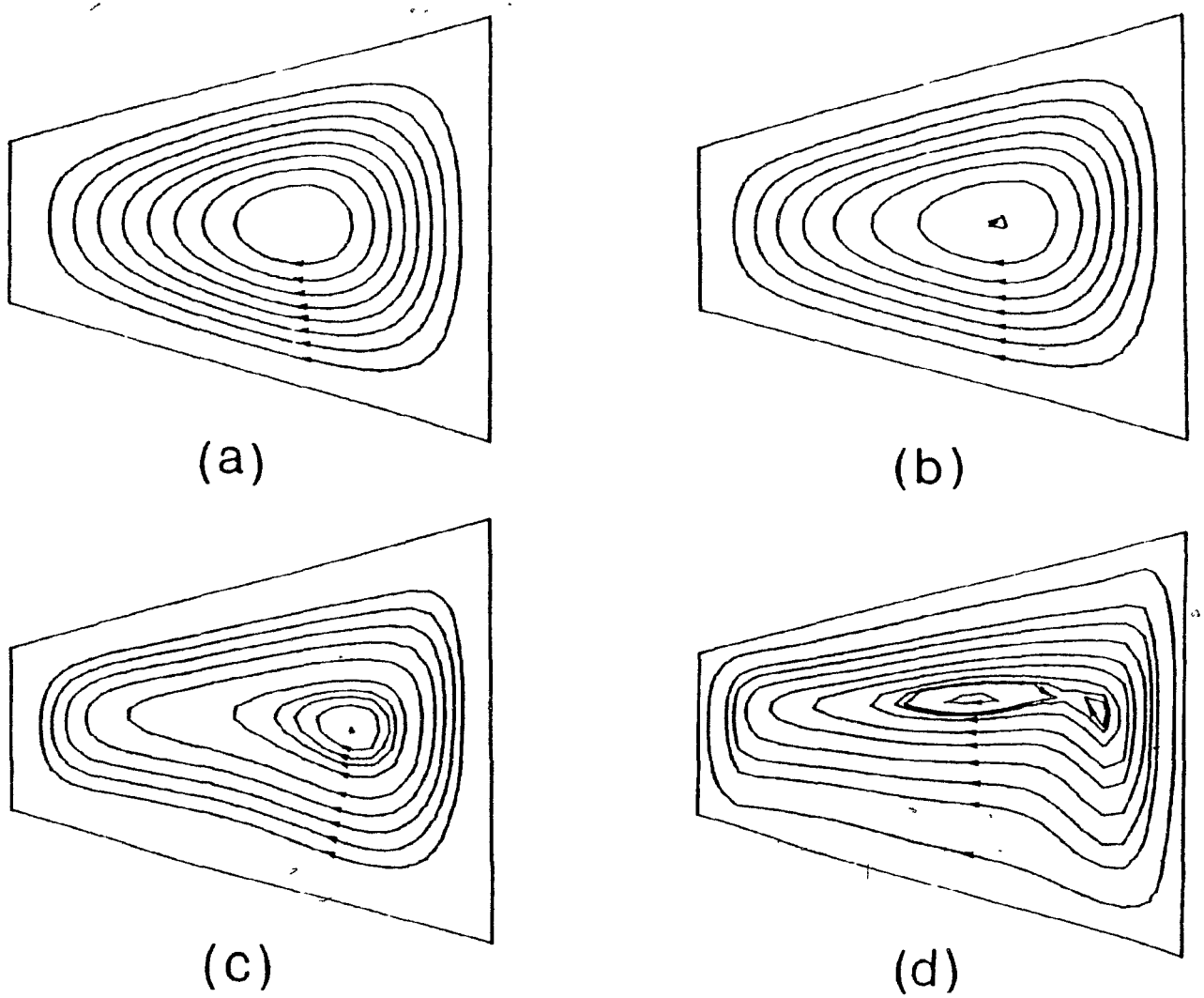

Fig. 5.8: Natural convection in a trapezoidal enclosure: streamline plots for (a) Ra = 10^3 and ψ = 0, -0.04, -0.81, -0.12, -0.16, -0.20, -0.24, -0.28, -0.32; (b) Ra = 10^4 and ψ = 0, -0.35, -0.69, -1.04, -1.39, -1.73, -2.08, -2.44, -2.77; (c) Ra = 10^5 and ψ = 0, -2.22, -3.33, -4.44, -5.55, -6.66, -7.77, -8.22, -8.44, -8.66, -8.88; (d) Ra = 10^6 and ψ = 0, -2.39, -7.17, -9.56, -11.94, -13.89, -15.00, -15.89, -16.22, -16.33, -16.67.

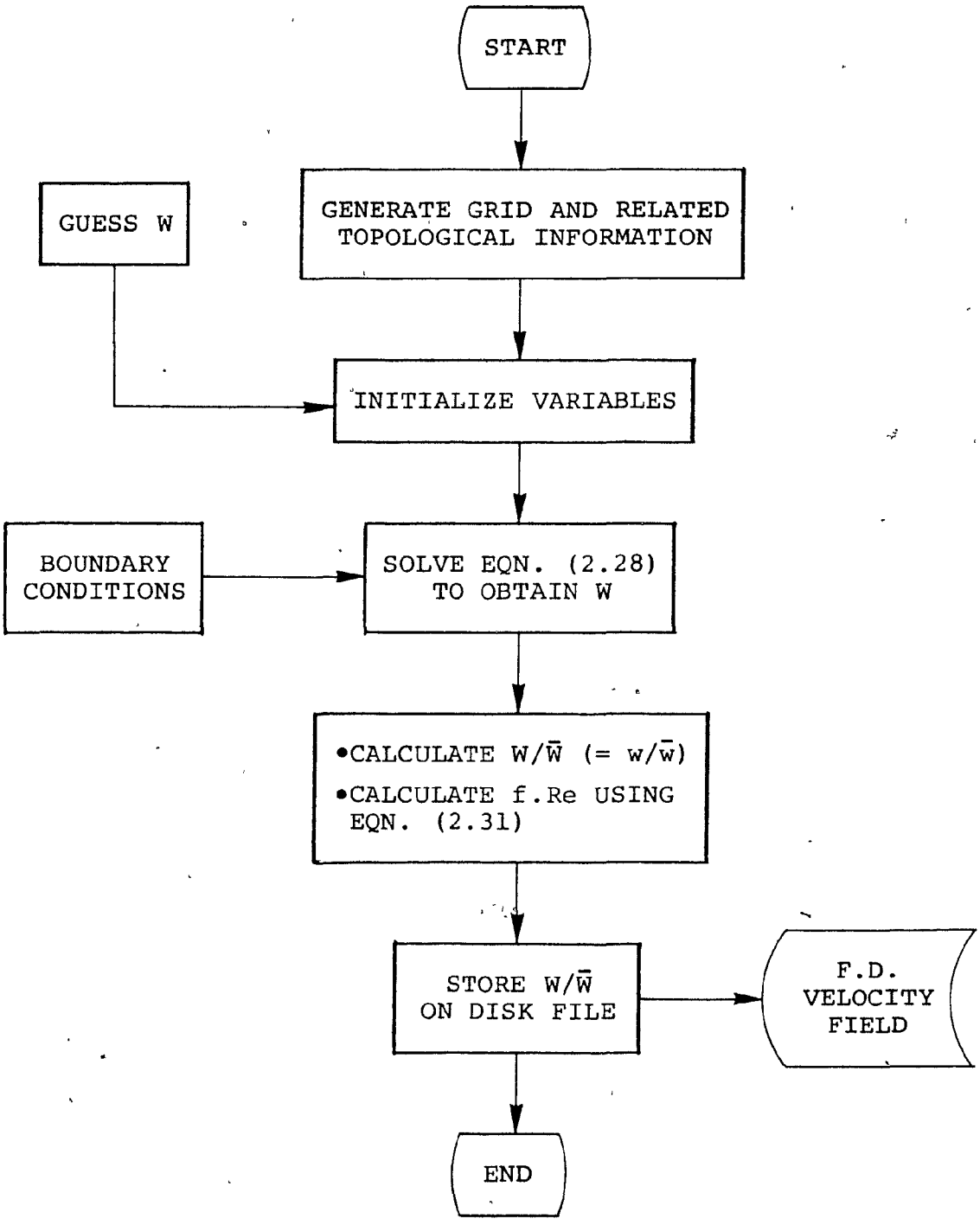

Fig. 5.9: Flowchart outlining the procedure used to solve the fully-developed flow problem

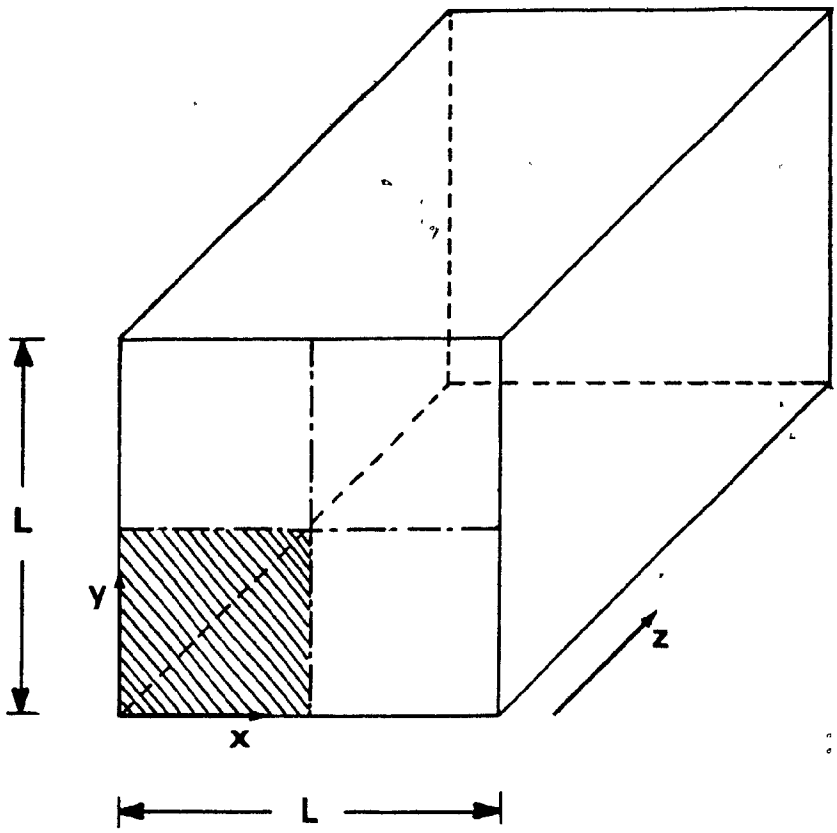

(a)

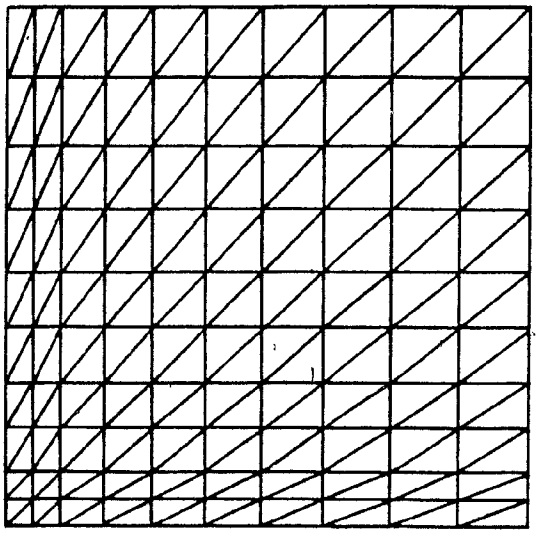

Ll = 11
Ml = 11
POWER = 1.4

(b)

Fig. 5.10: Laminar flow and heat transfer in a duct of square cross-section: (a) problem geometry with the shaded area indicating a typical cross-section of the calculation domain; (b) discretization of the calculation domain cross-section.

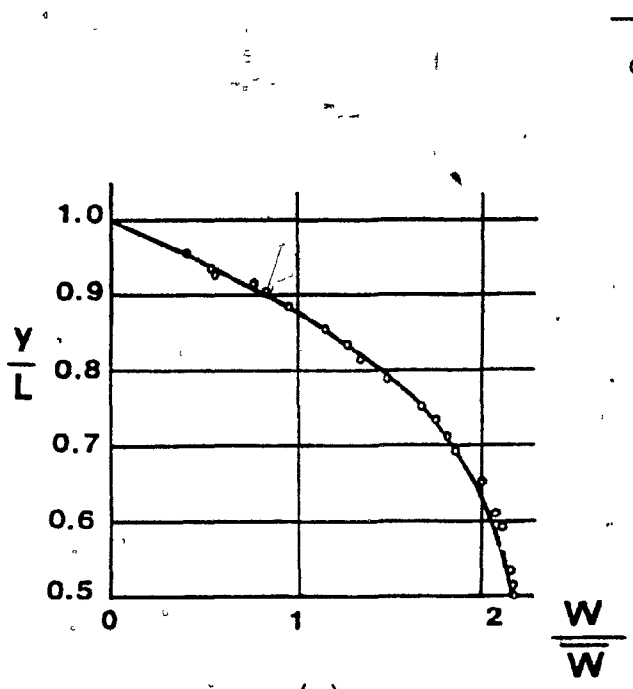

(a)

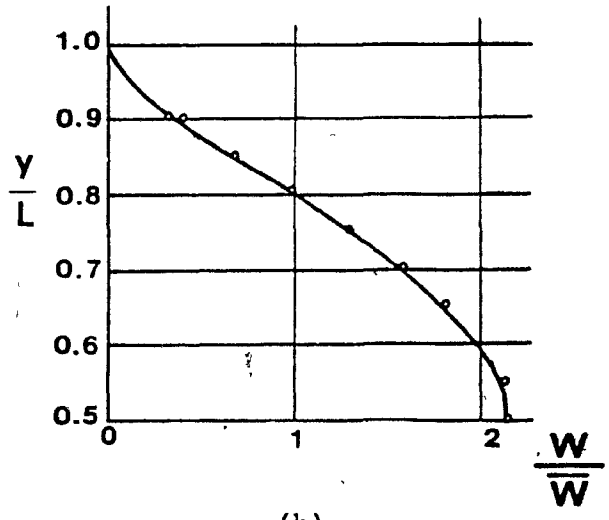

(b)

Fig. 5.11: Square duct problem: fully-developed axial velocity profiles along (a) a symmetry line; (b) a diagonal.

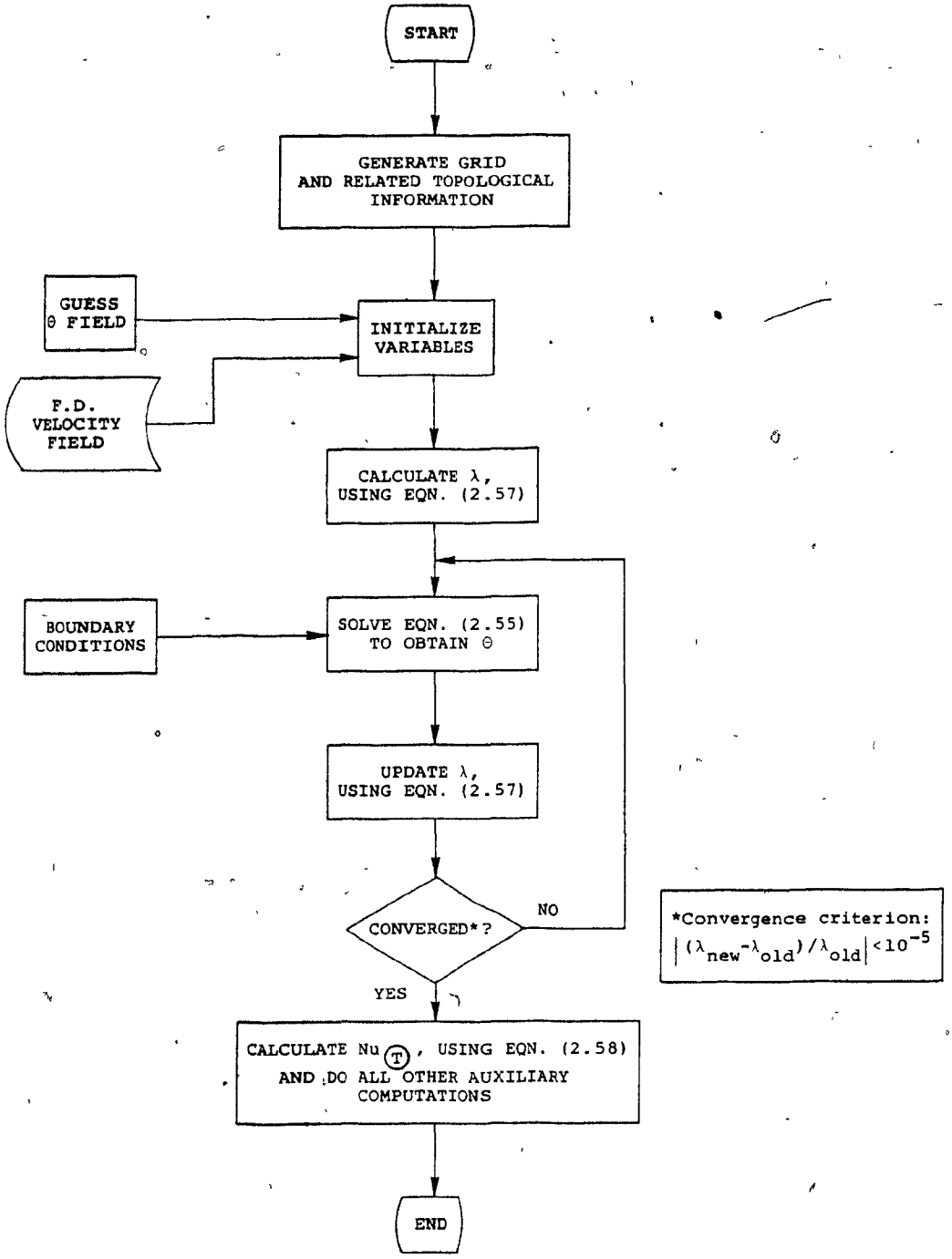

Fig. 5.12: Flowchart outlining the iterative procedure used to solve the problem of thermally developed flow in a square duct with (T) boundary condition.

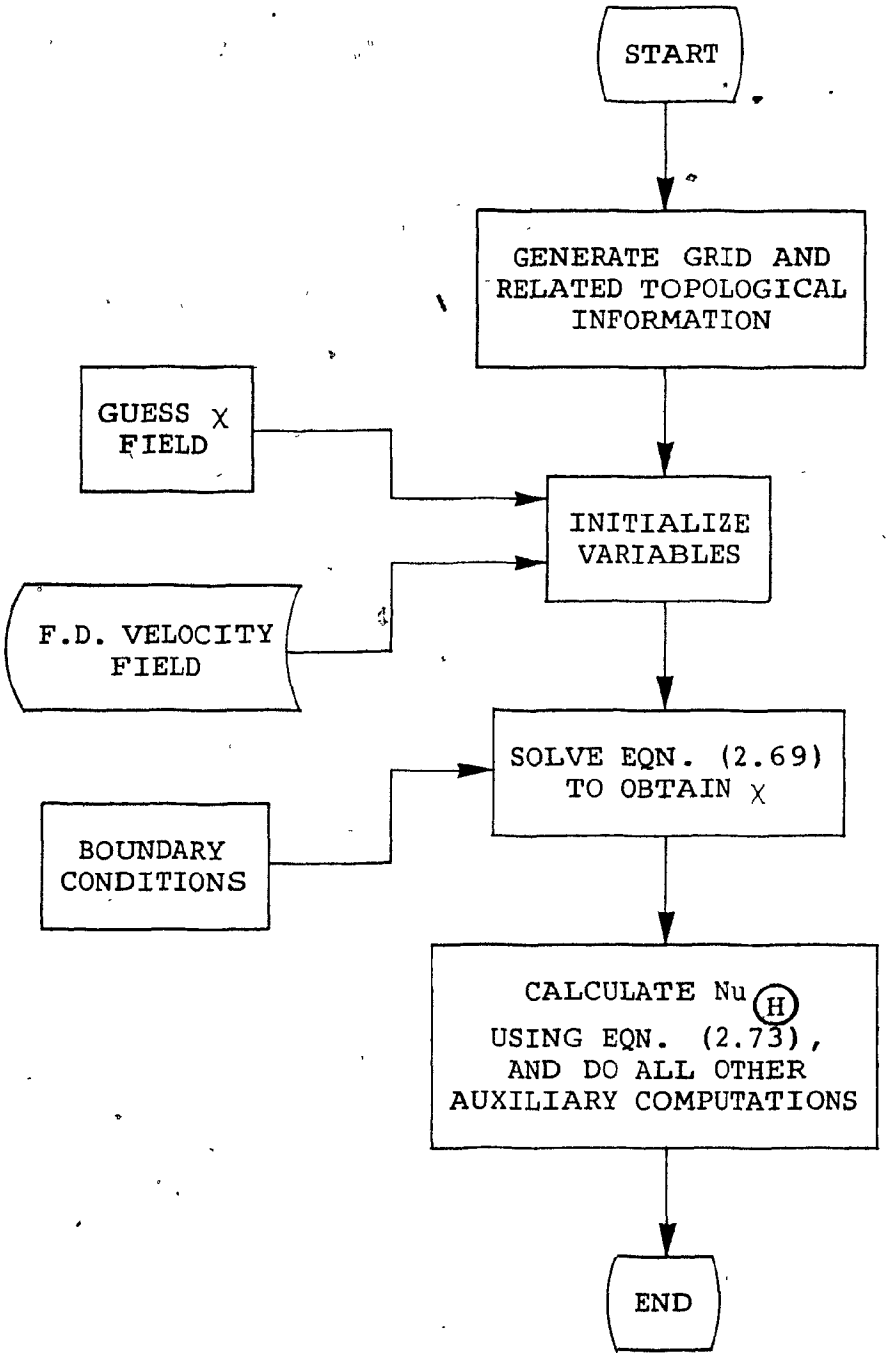

Fig. 5.13: Flowchart outlining the procedure used to solve the problem of thermally developed flow in a square duct with (H) boundary condition.

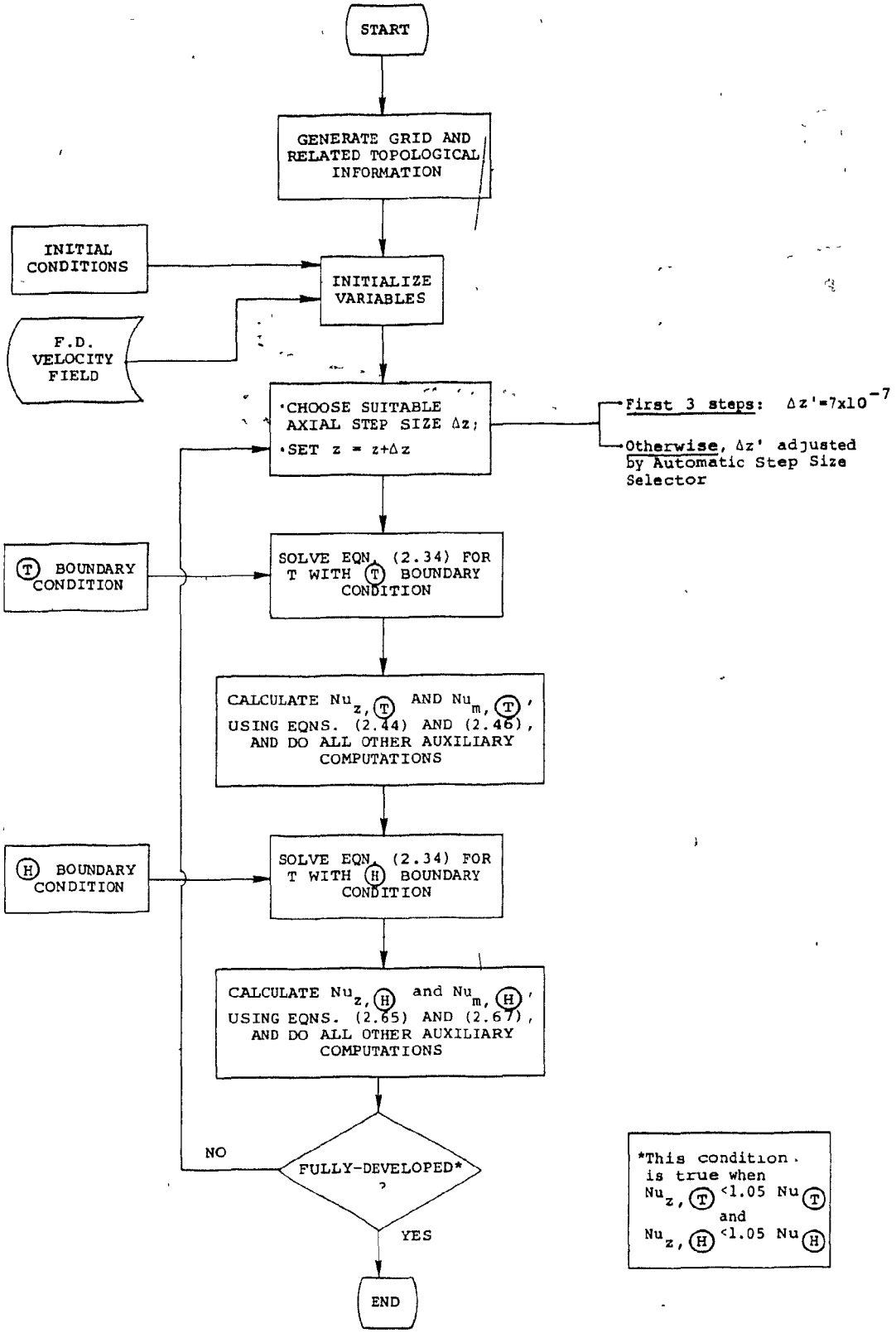

Fig. 5.14: Flowchart outlining the procedure used to solve the problem of hydrodynamically developed and thermally developing flow in a square duct.

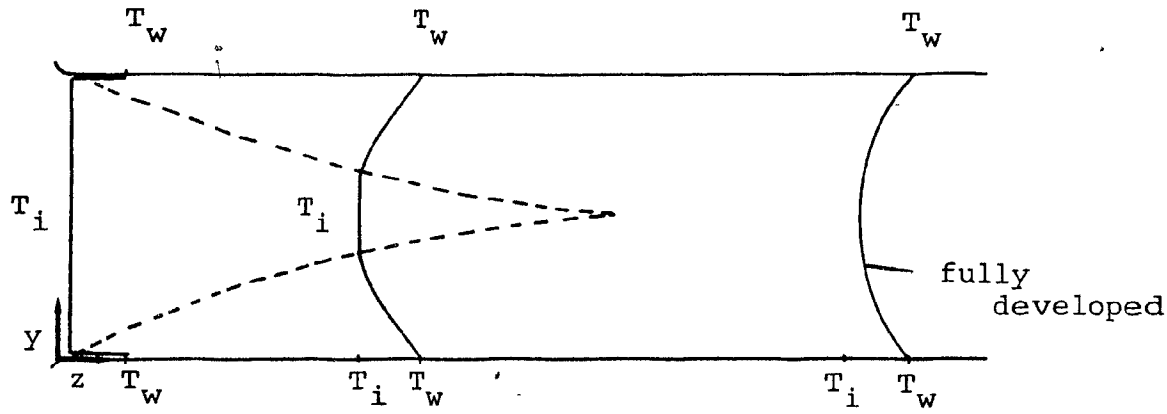

Fig. 5.15: Square duct problem: developing temperature profile for the (T) condition.

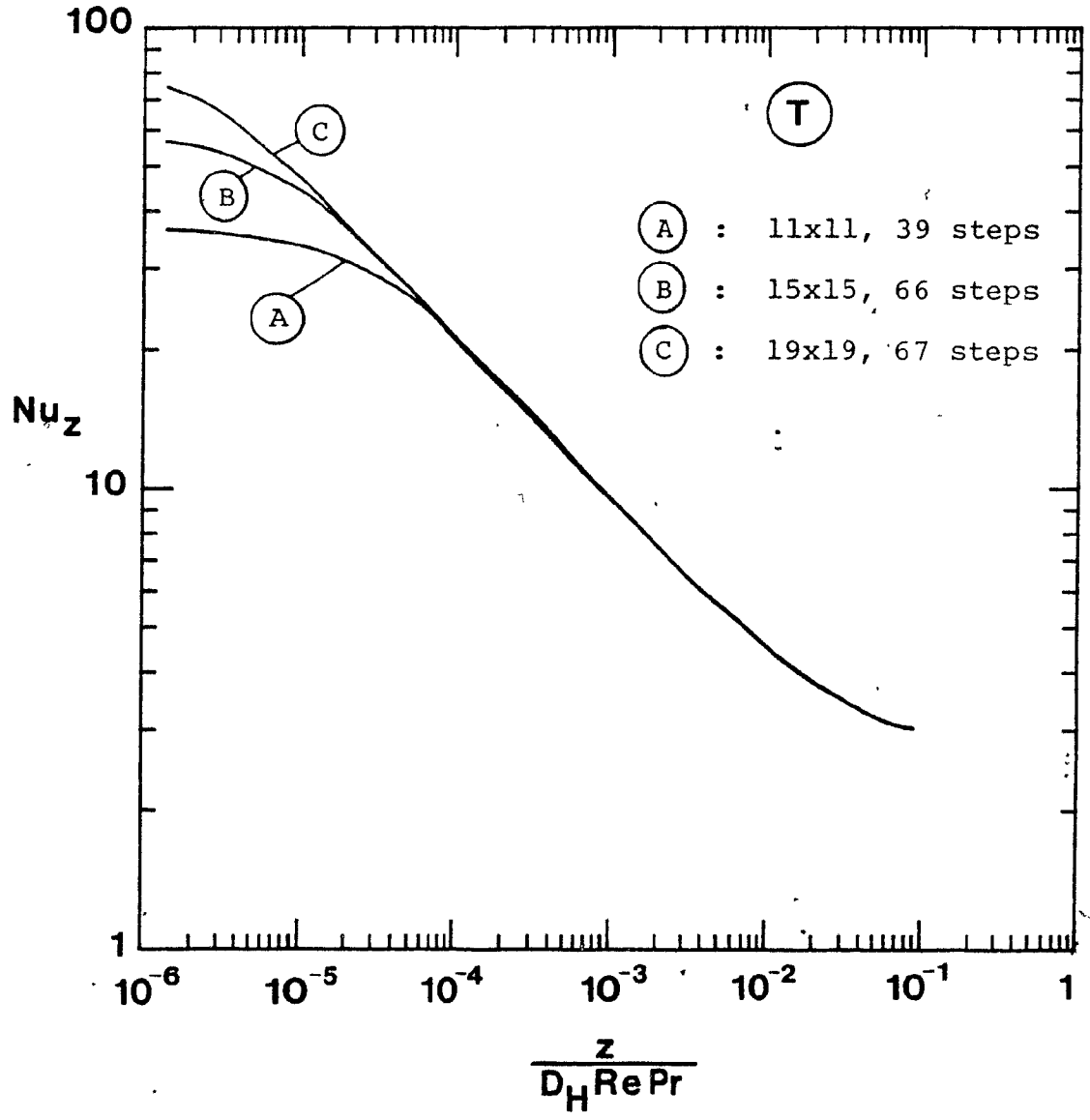

Fig. 5.16: Laminar fully-developed flow in a square duct with the (T) condition: local Nusselt number variation with axial distance for various grid and step sizes.

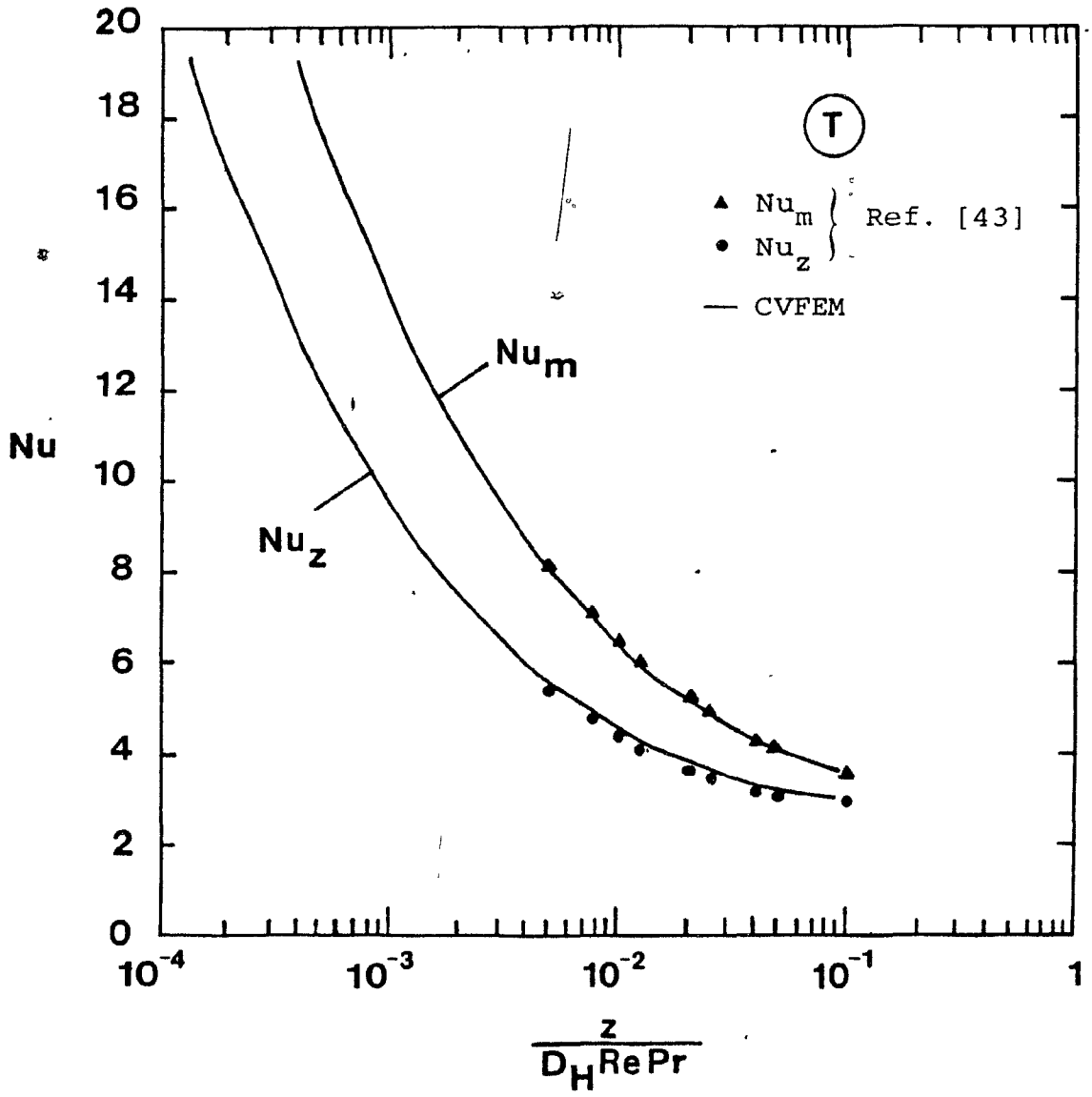

Fig. 5.17: Laminar fully-developed flow in a square duct with the (T) condition: local and mean Nusselt number variation with axial distance.

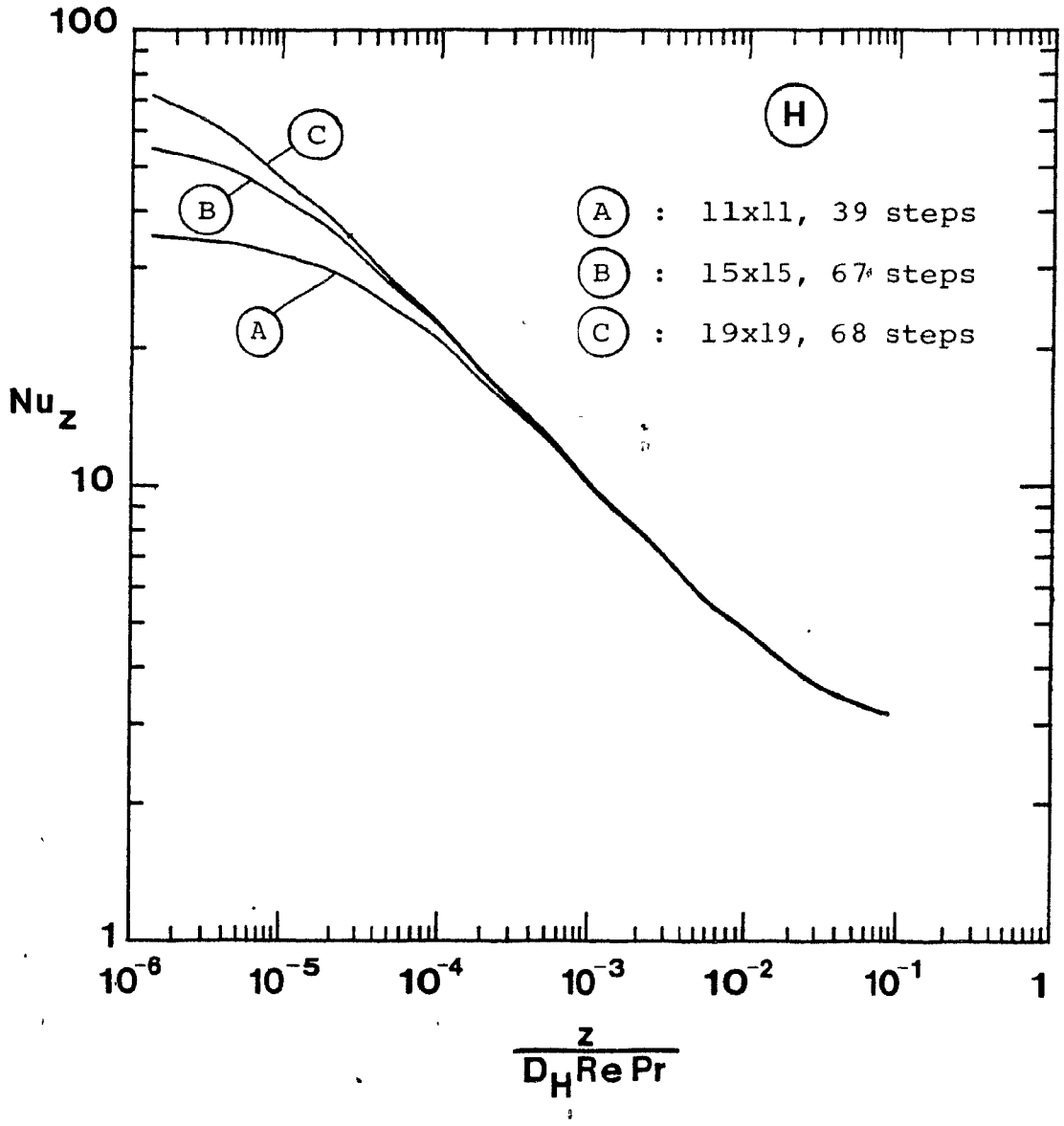

Fig. 5.18: Laminar fully-developed flow in a square duct with the (H) condition: local Nusselt number variation with axial distance for various grid and step sizes.

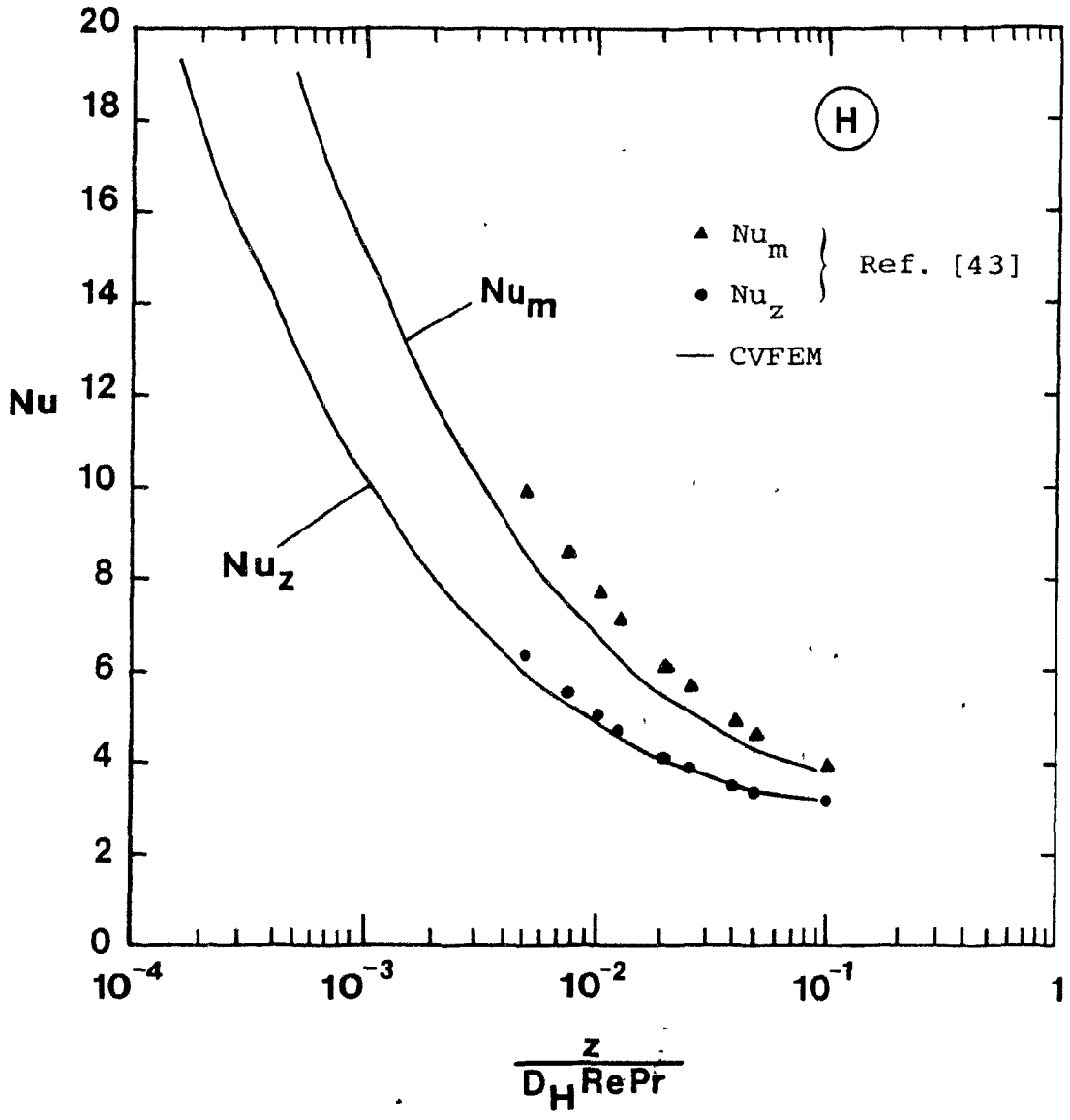

Fig. 5.19: Laminar fully-developed flow in a square duct with the (H) condition: local and mean Nusselt number variation with axial distance.

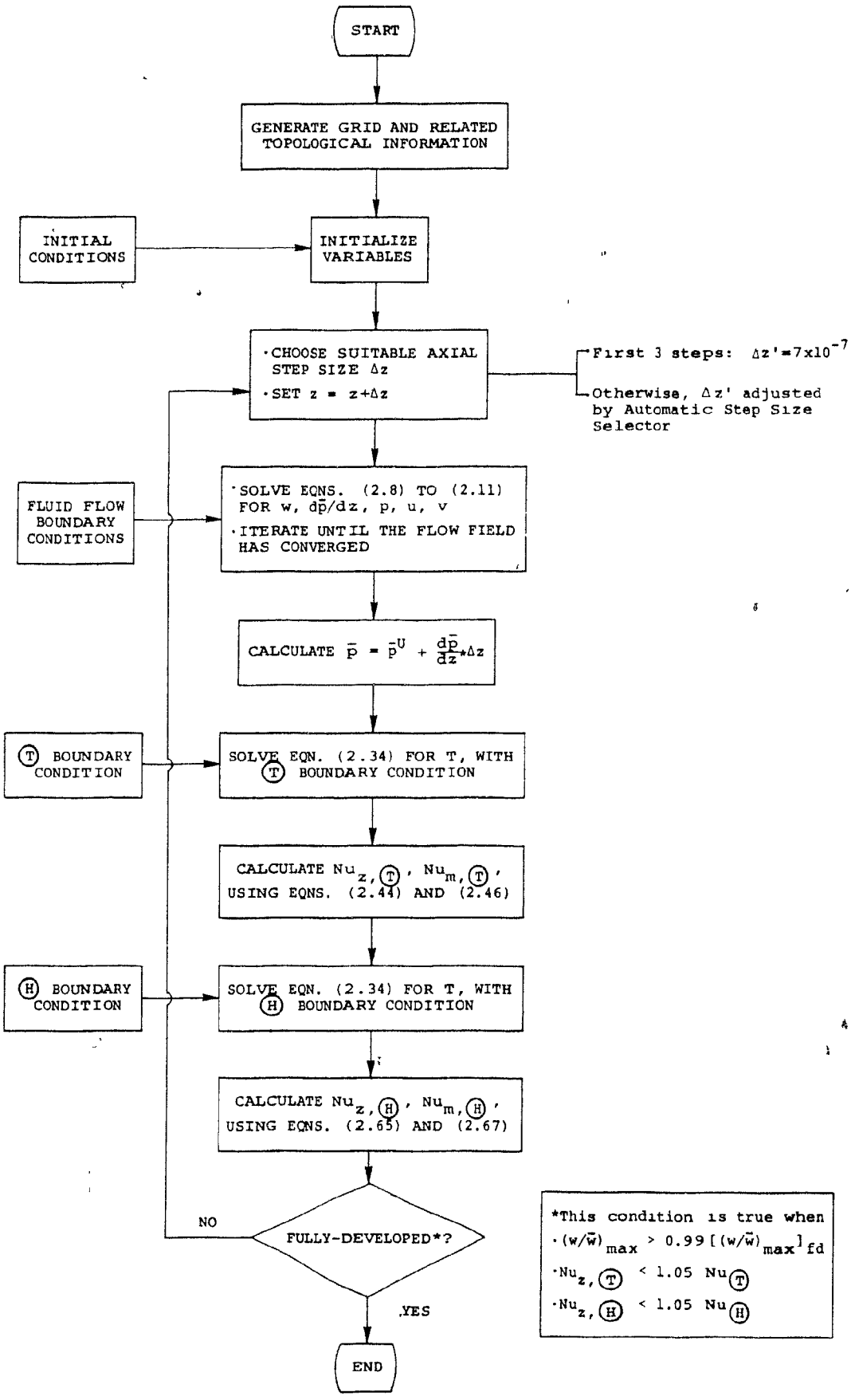

Fig. 5.20: Flowchart outlining the procedure used to solve the problem of simultaneously developing flow and heat transfer in a square duct.

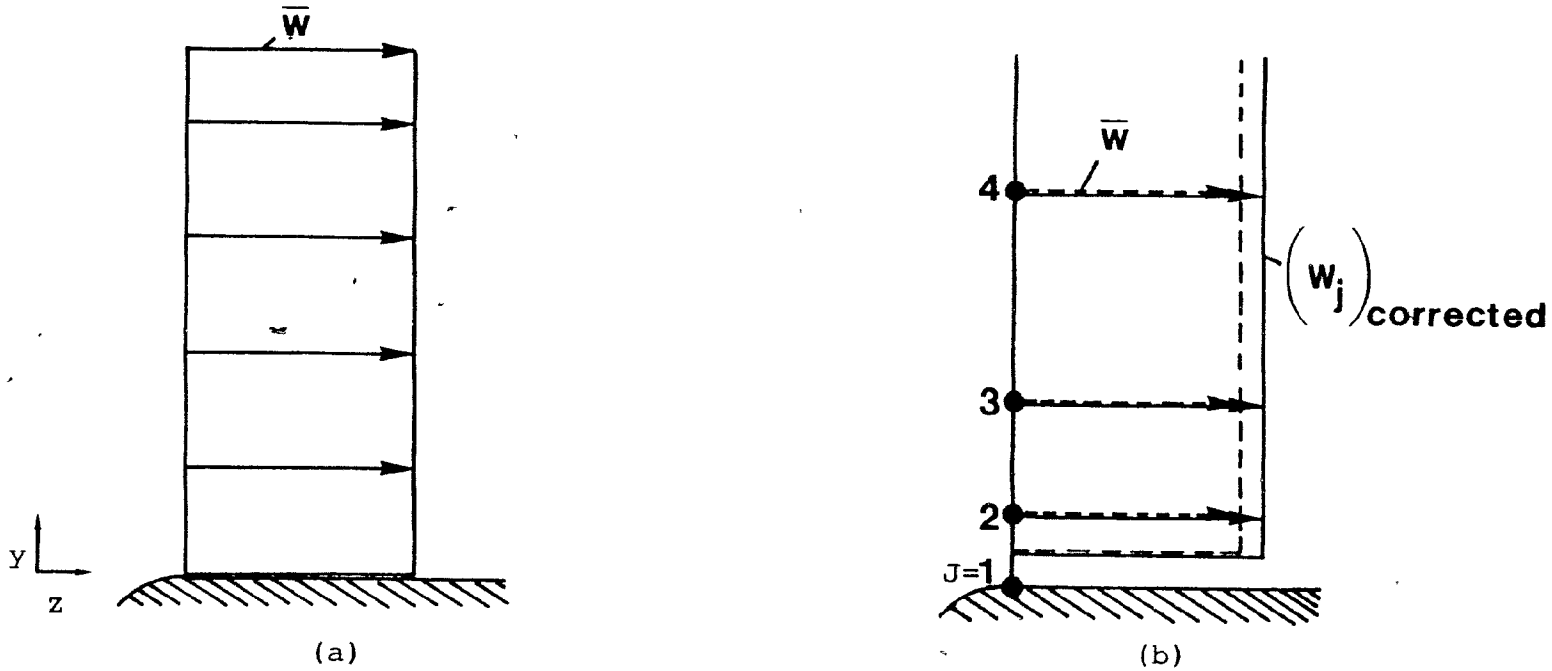

Fig. 5.21: Square duct problem: (a) desired uniform axial velocity distribution at the duct inlet; (b) uncorrected (---) and corrected (——) inlet axial velocity distributions used in the numerical analysis.

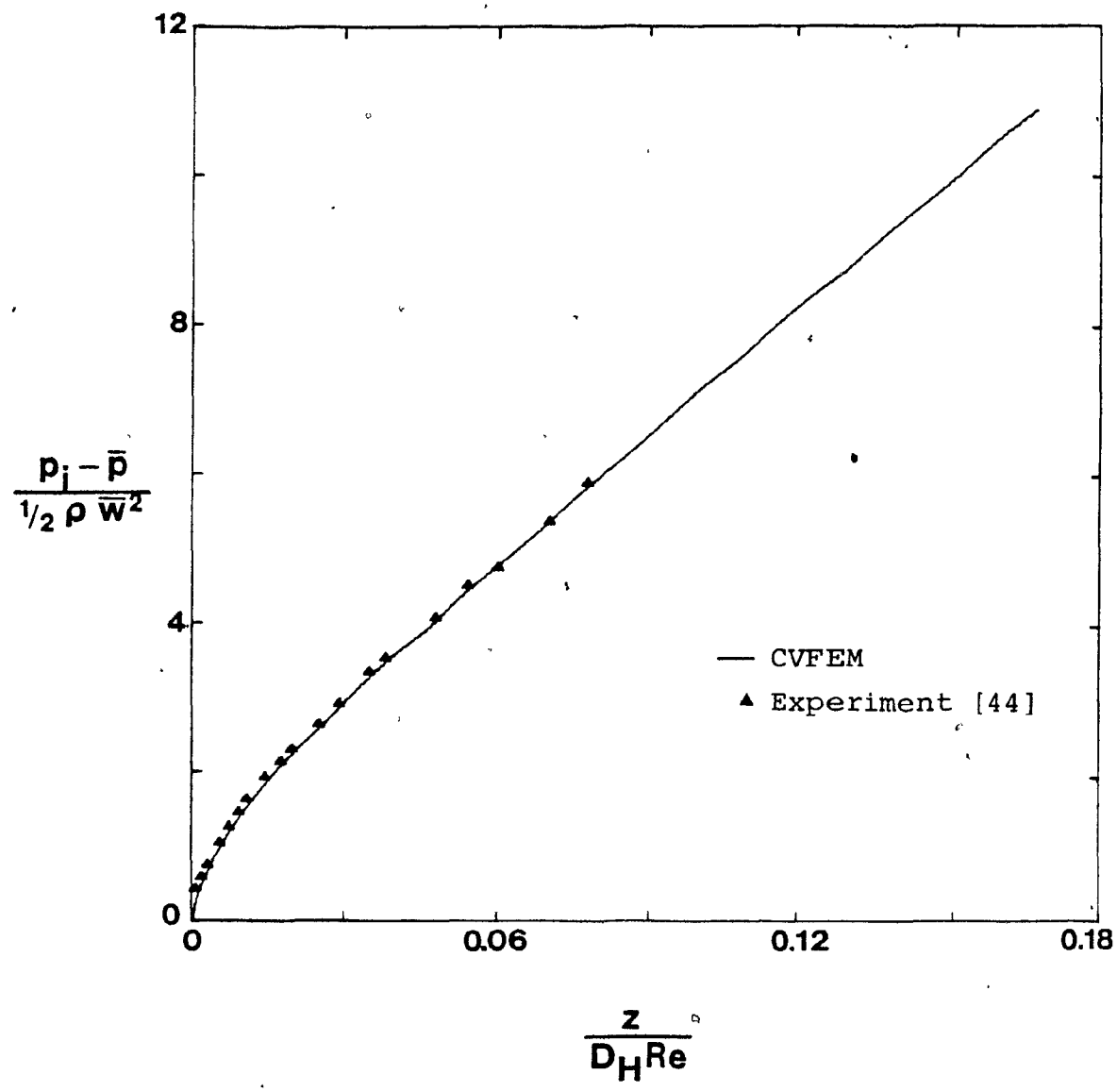

Fig. 5.22: Laminar developing flow in a square duct: variation of mean pressure with axial distance.

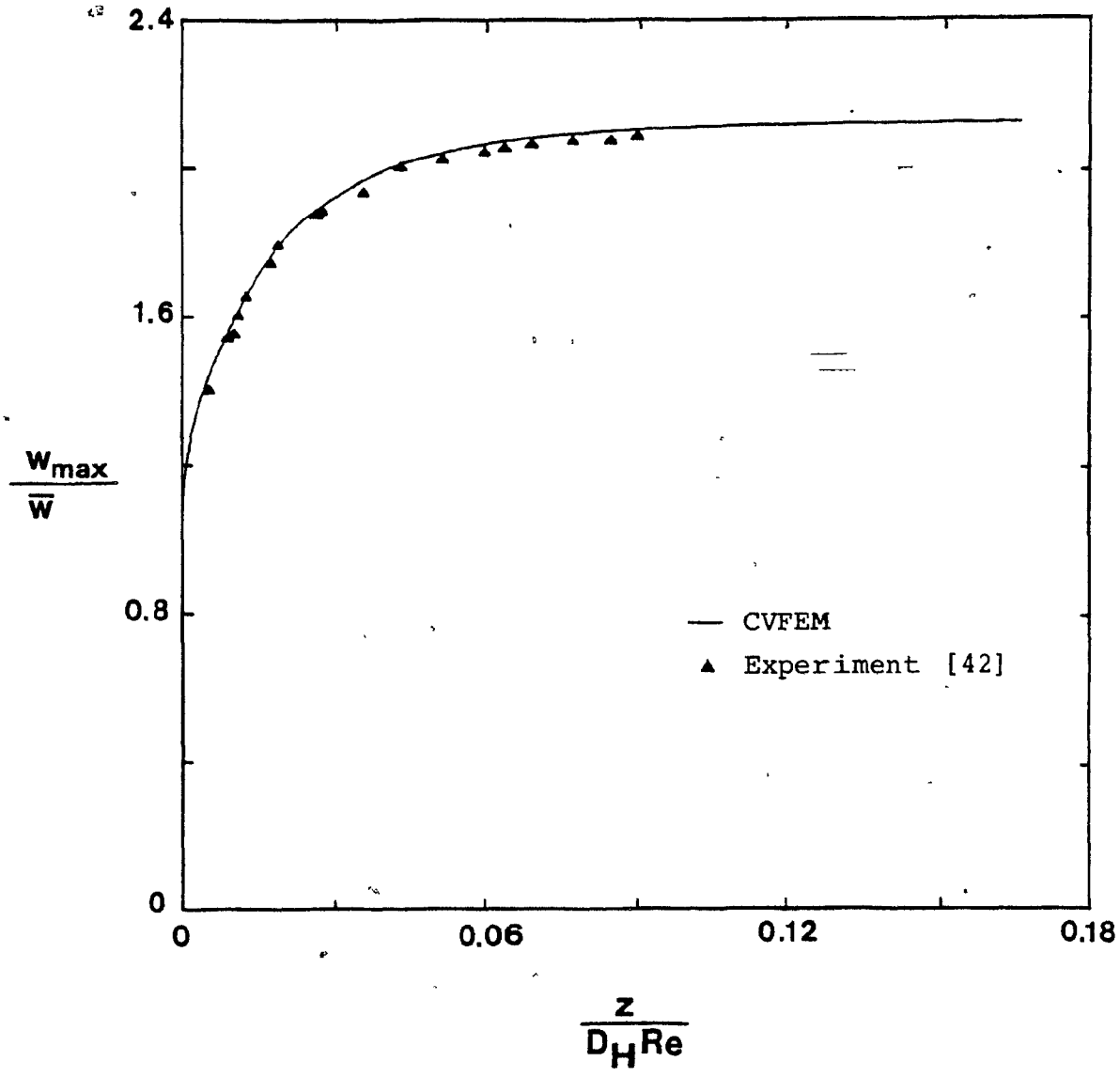

Fig. 5.23: Laminar developing flow in a square duct: variation of centerline axial velocity with axial distance.

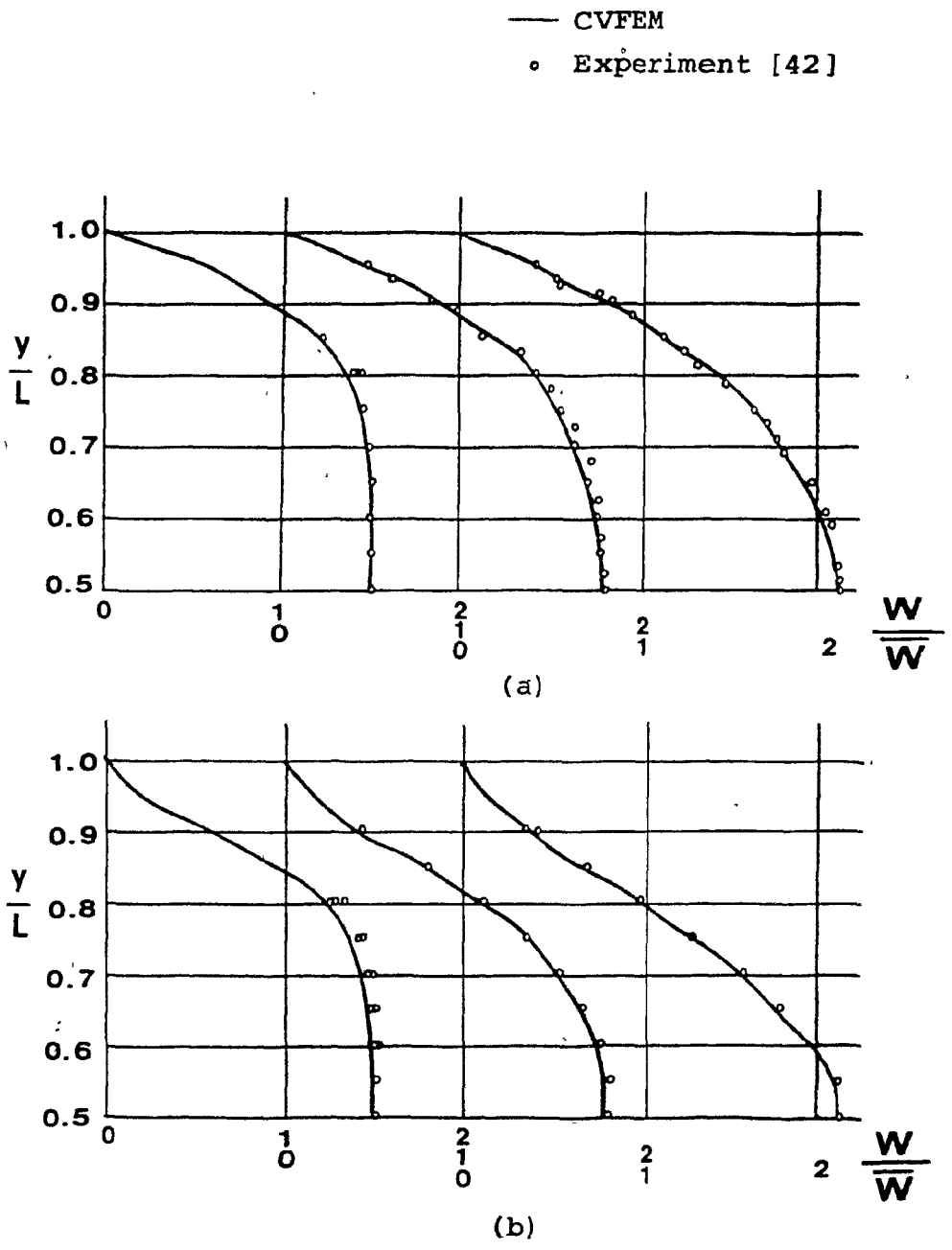

Fig. 5.24: Laminar developing flow in a square duct: axial velocity distributions along (a) a symmetry line; and (b) a diagonal.

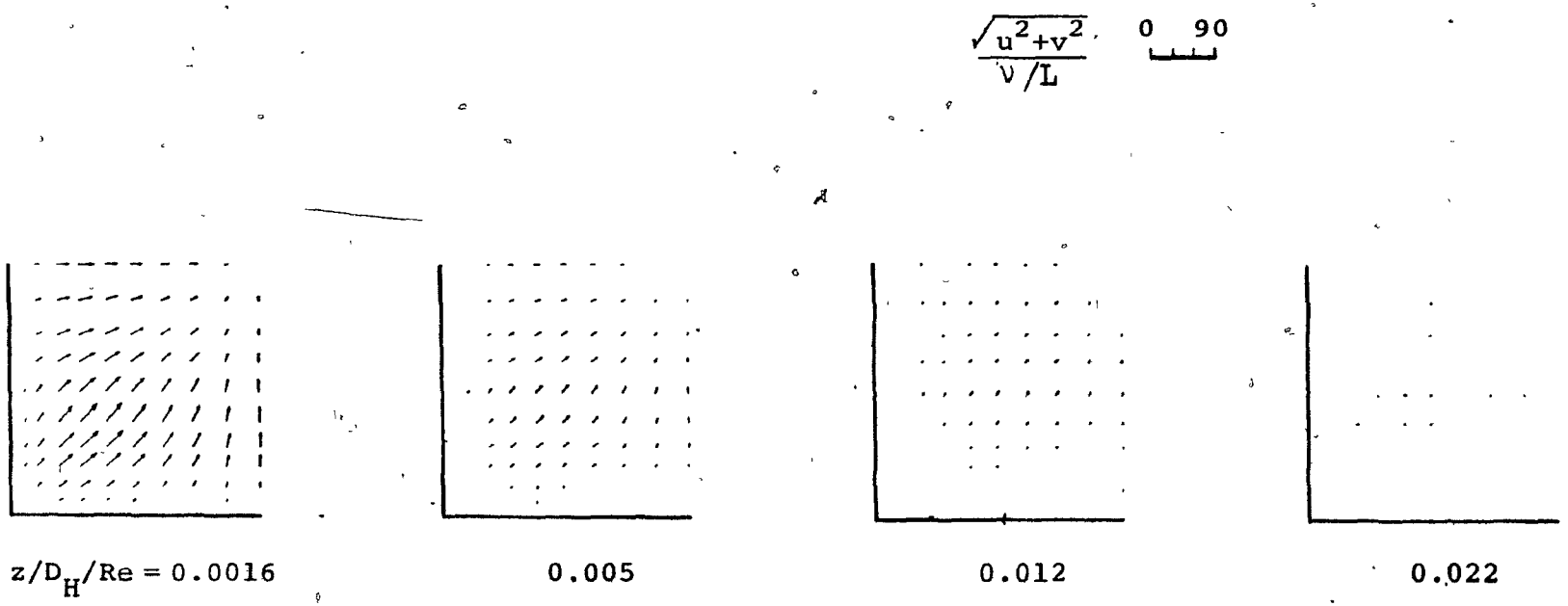

Fig. 5.25: Laminar developing flow in a square duct: cross-sectional velocity fields at four different axial locations.

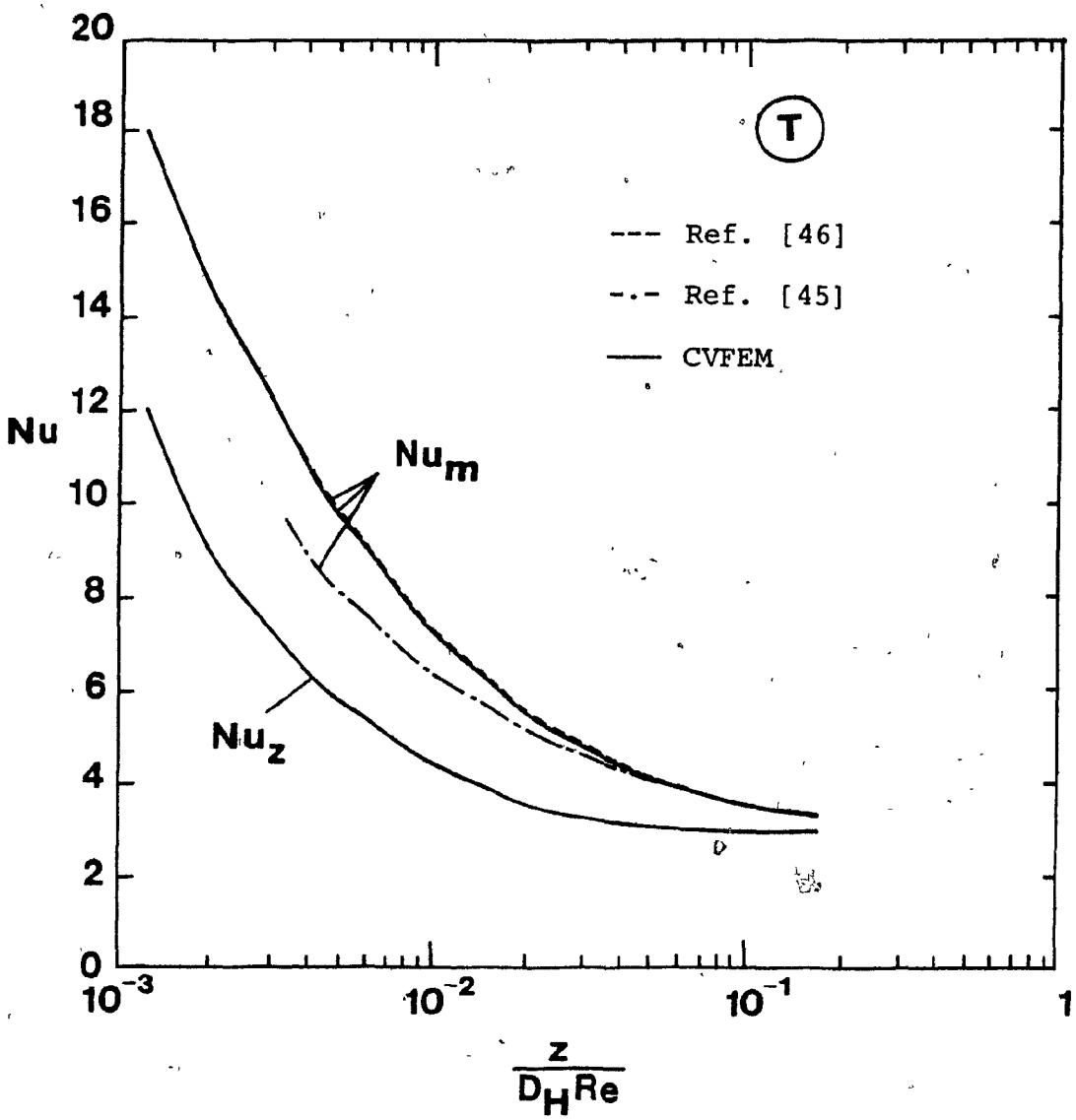

Fig. 5.26: Simultaneously developing flow and heat transfer in a square duct with the (T) boundary condition: variation of local and mean Nusselt numbers with axial distance.

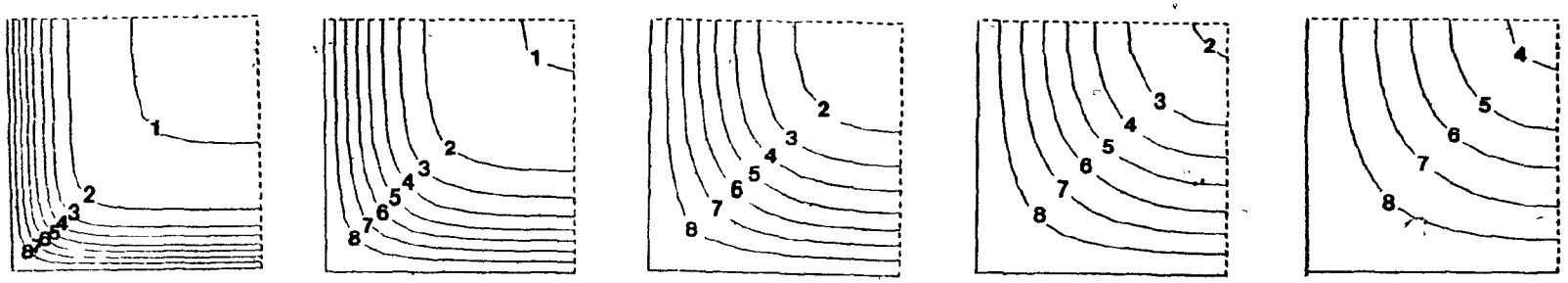

Fig. 5.27: Simultaneously developing flow and heat transfer in a square duct with the (T) boundary condition: non-dimensional temperature contours at five different axial locations; the contour levels are: $T_1^* = 0.005$, $T_2^* = 0.125$, $T_3^* = 0.250$, $T_4^* = 0.375$, $T_5^* = 0.500$, $T_6^* = 0.625$, $T_7^* = 0.750$, $T_8^* = 0.875$.

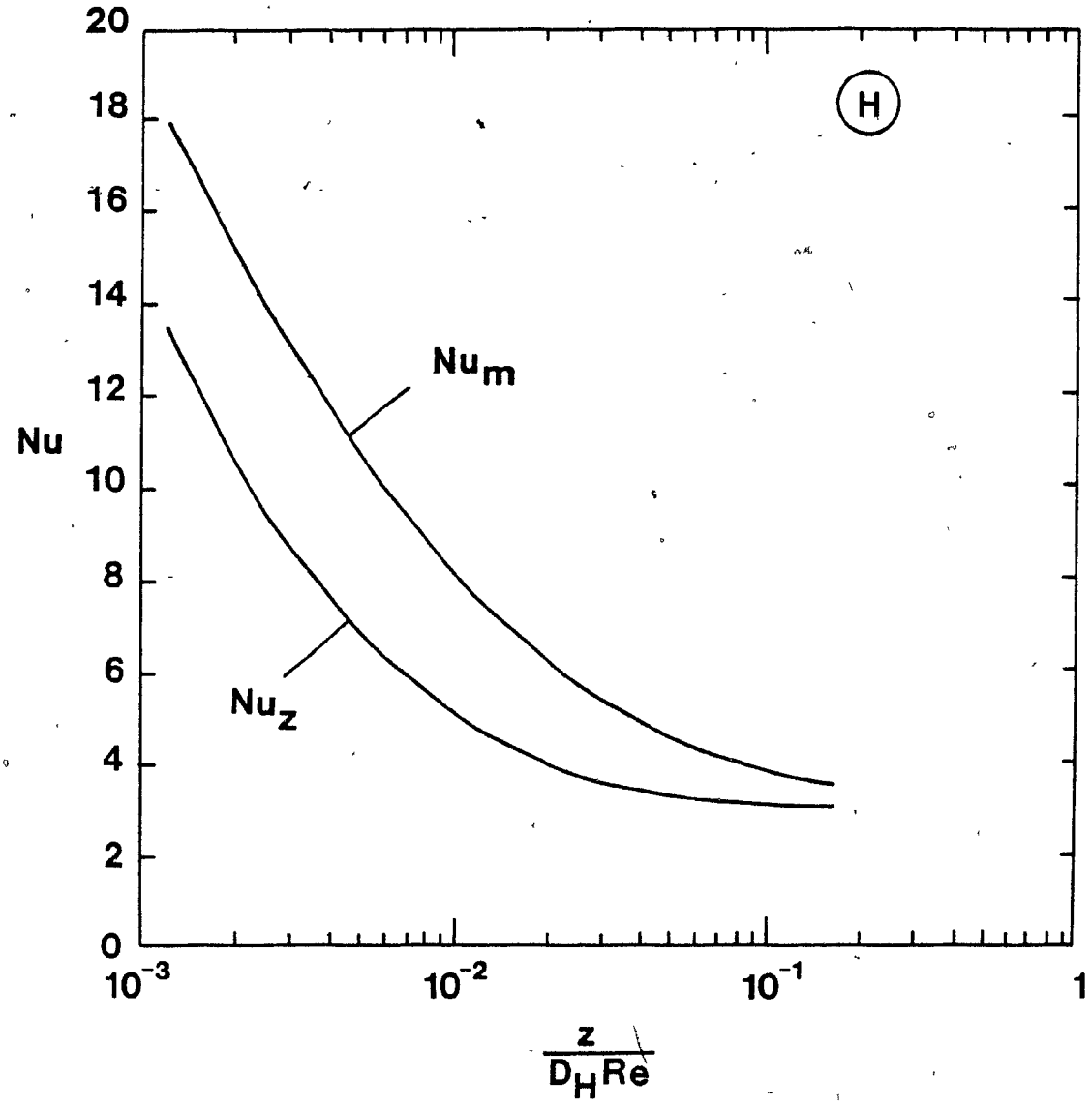

Fig. 5.28: Simultaneously developing flow and heat transfer in a square duct with the (H) condition: variation of local and mean Nusselt numbers with axial distance.

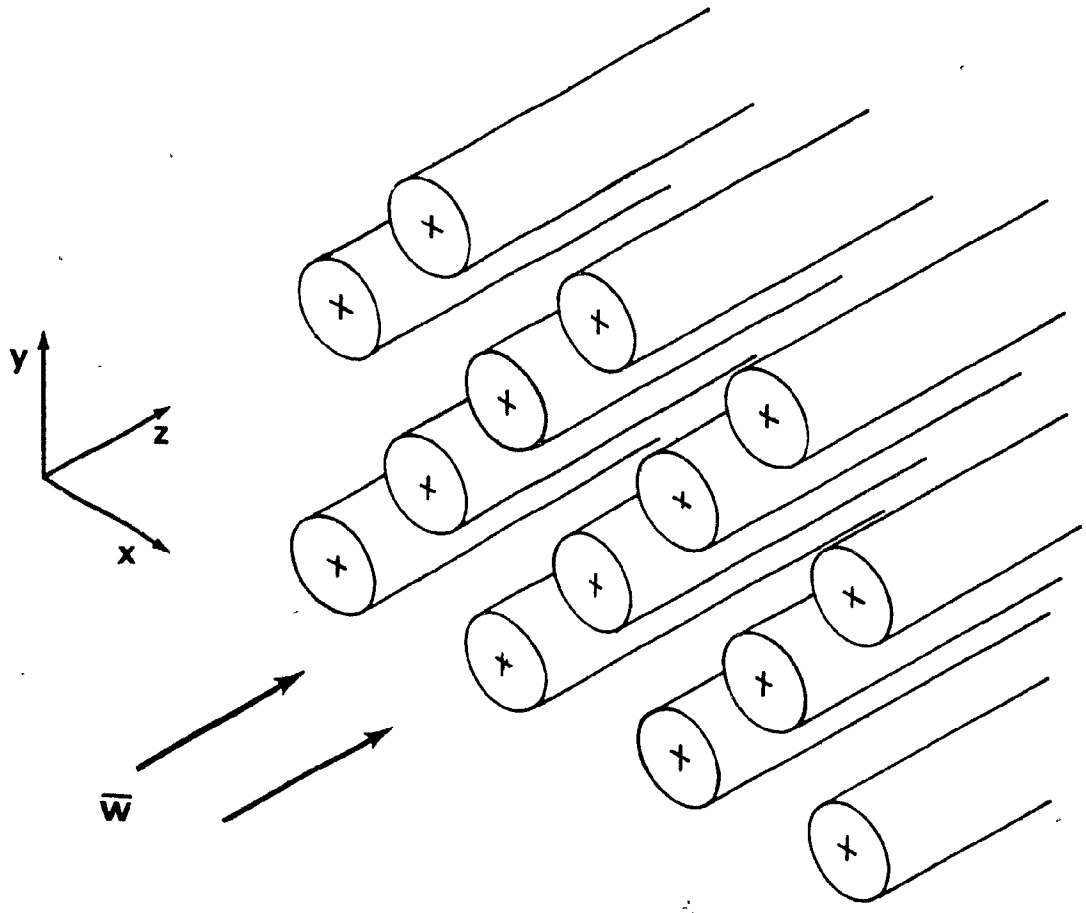

Fig. 6.1: Longitudinal flow between circular cross-section rods arranged in an equilateral triangular array: problem schematic.

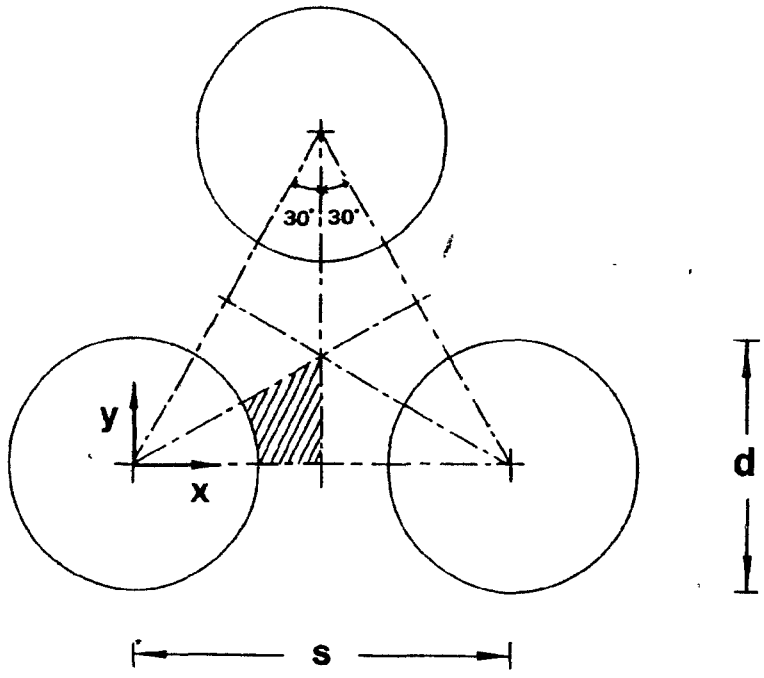

(a)

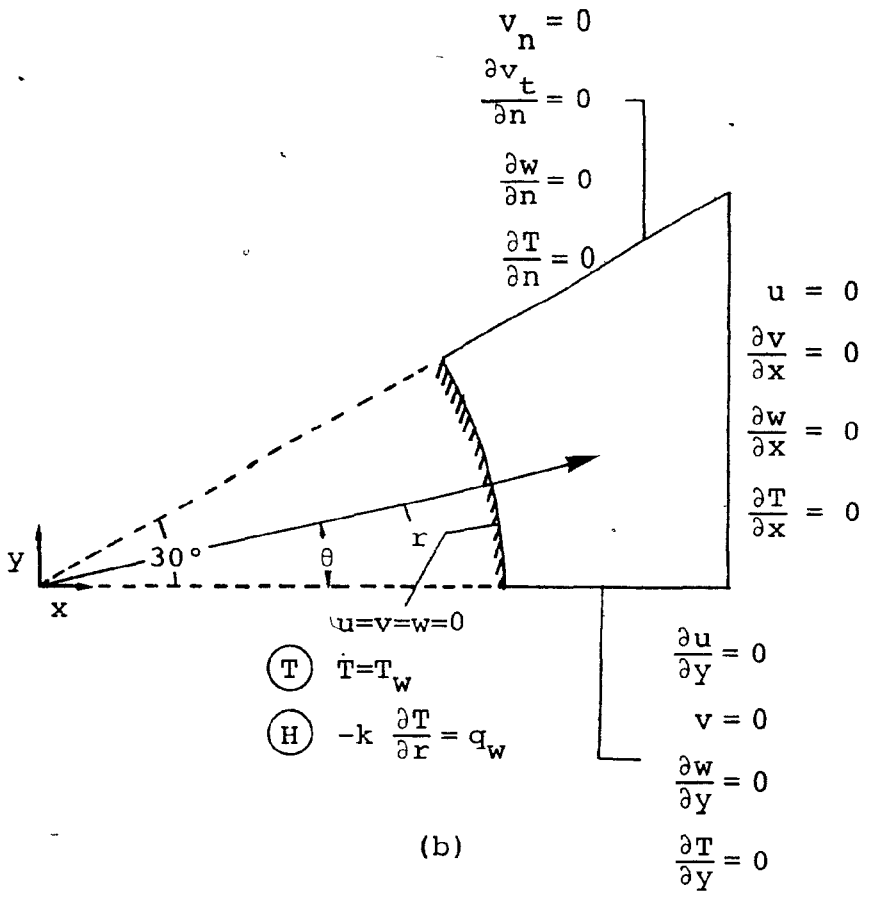

(b)

Fig. 6.2: Rod-bundle problem: (a) cross-sectional view of three of the rods; (b) calculation domain used in the analysis.

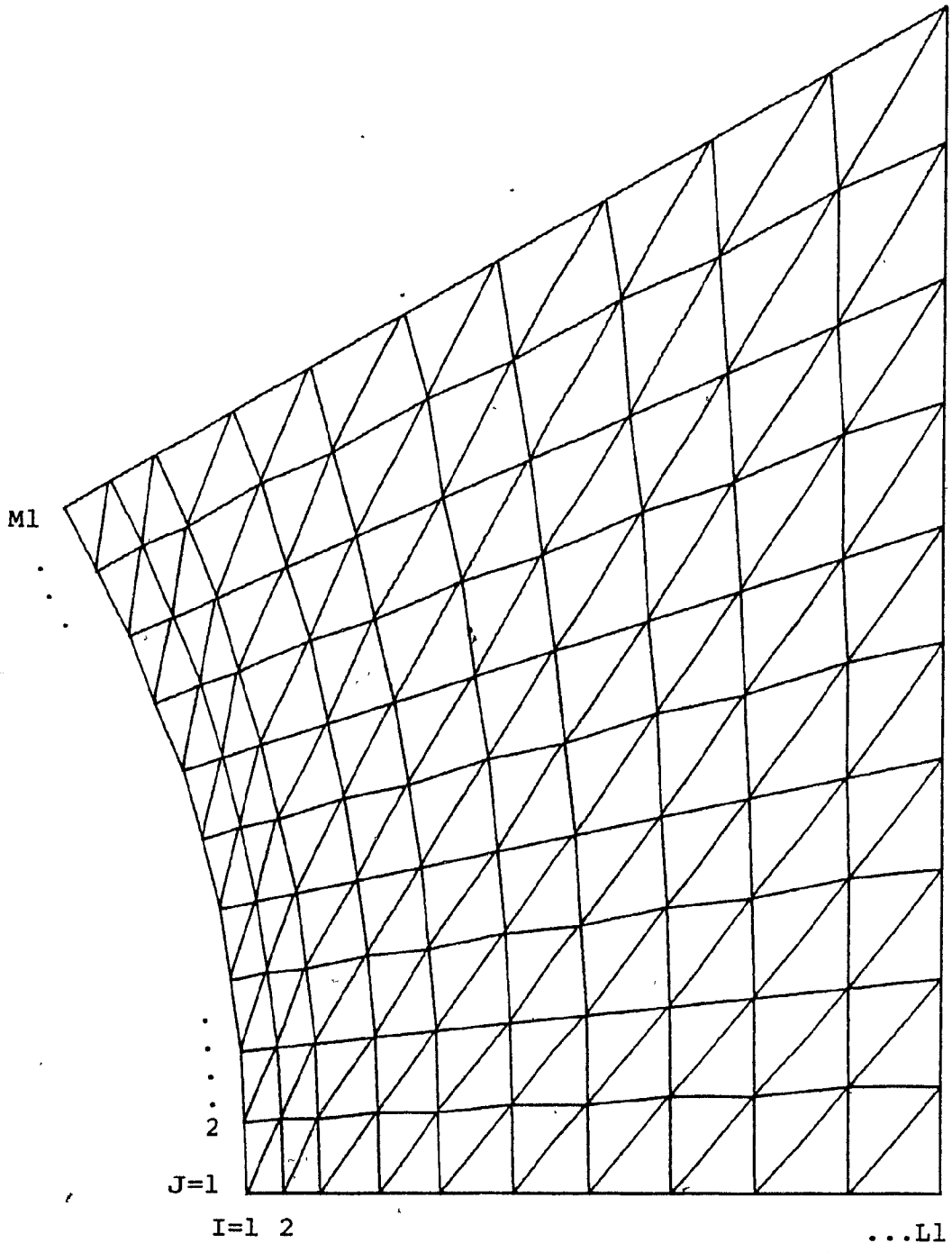

Fig. 6.3: Rod-bundle problem: discretization of the calculation domain using L1=M1=11, POWER = 1.4.

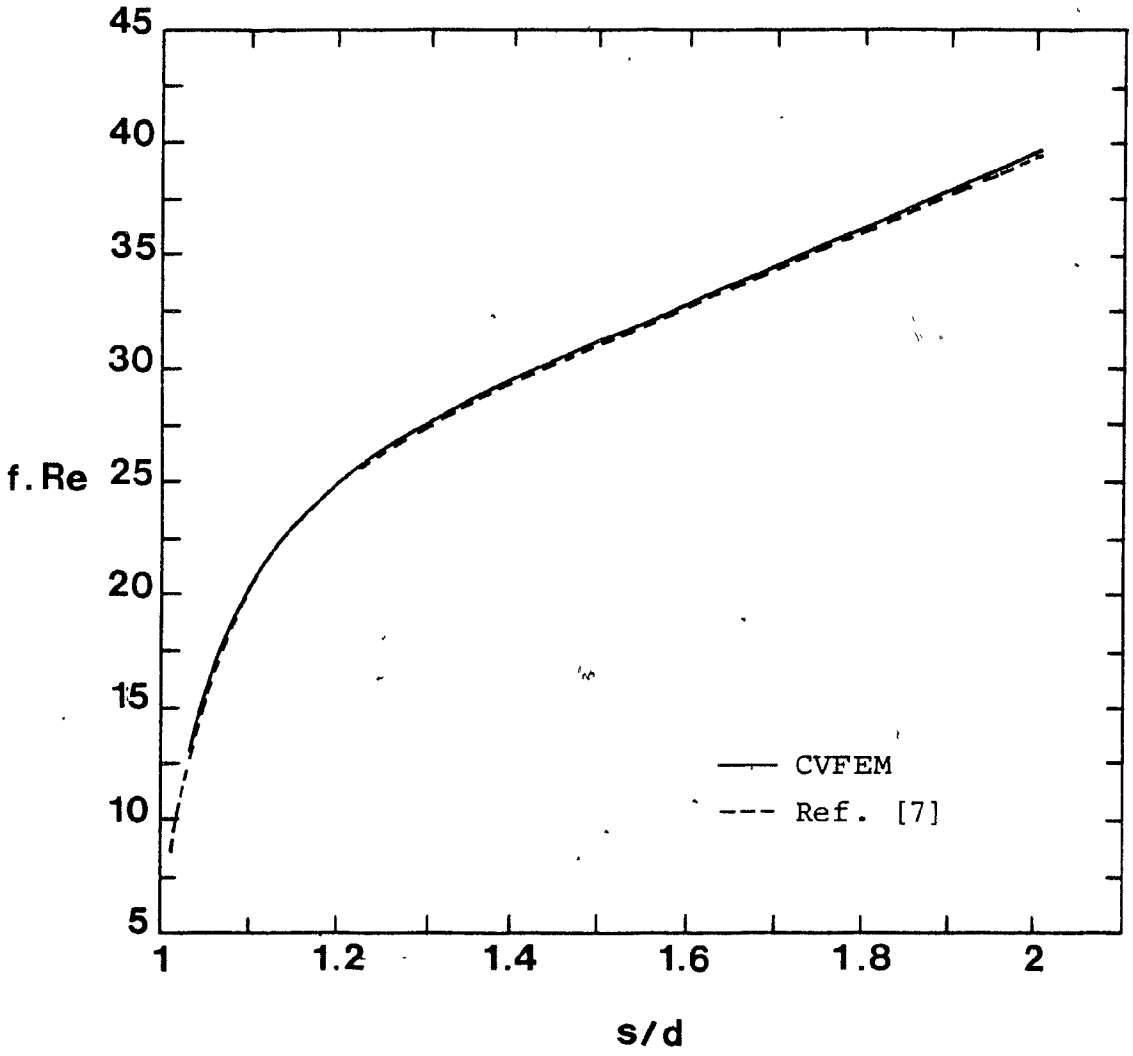

Fig. 6.4: Fully-developed flow over a rod-bundle: variation of friction factor-Reynolds number product with pitch-to-diameter ratio.

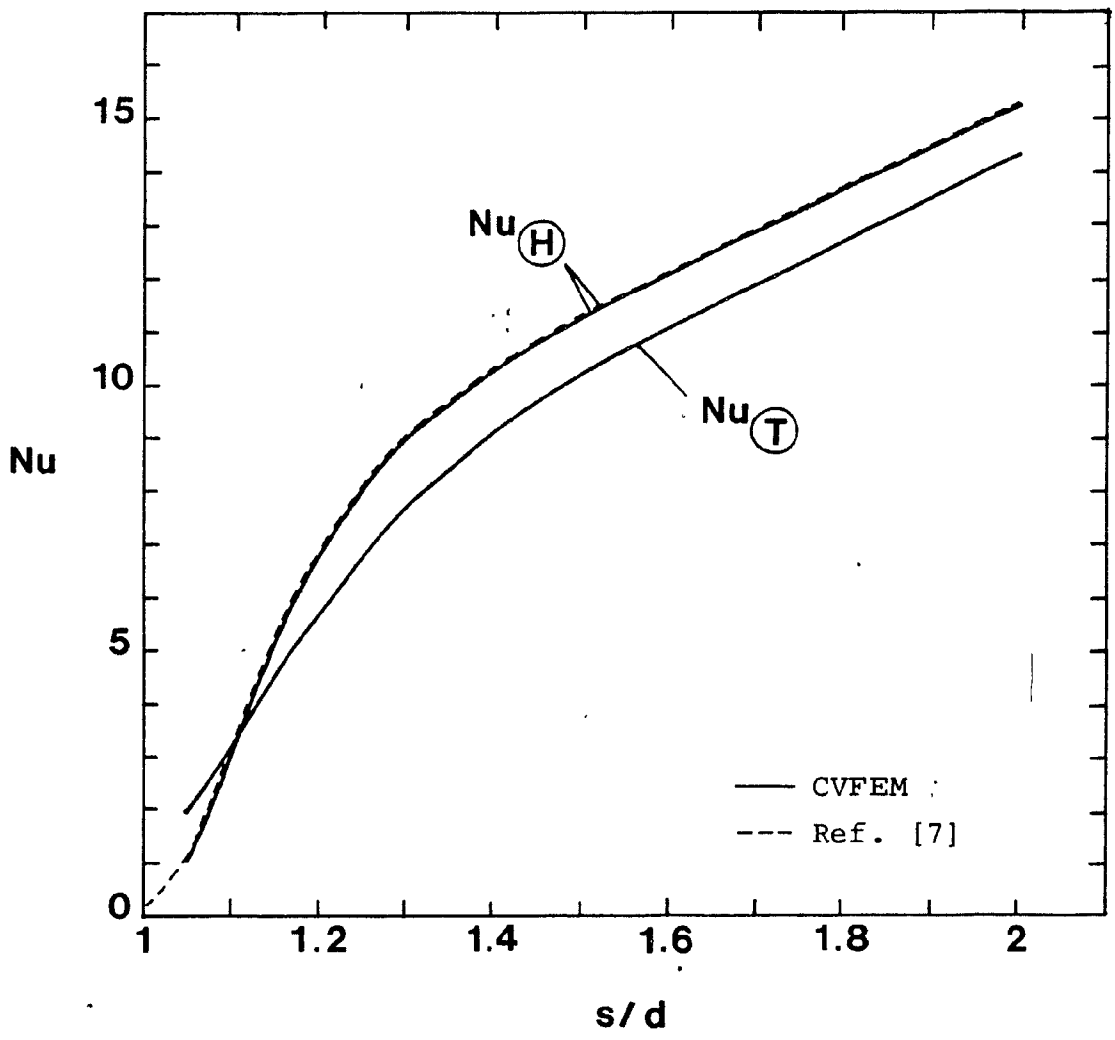

Fig. 6.5: Fully-developed flow and heat transfer over a rod-bundle: variation of average Nusselt number with pitch-to-diameter ratio.

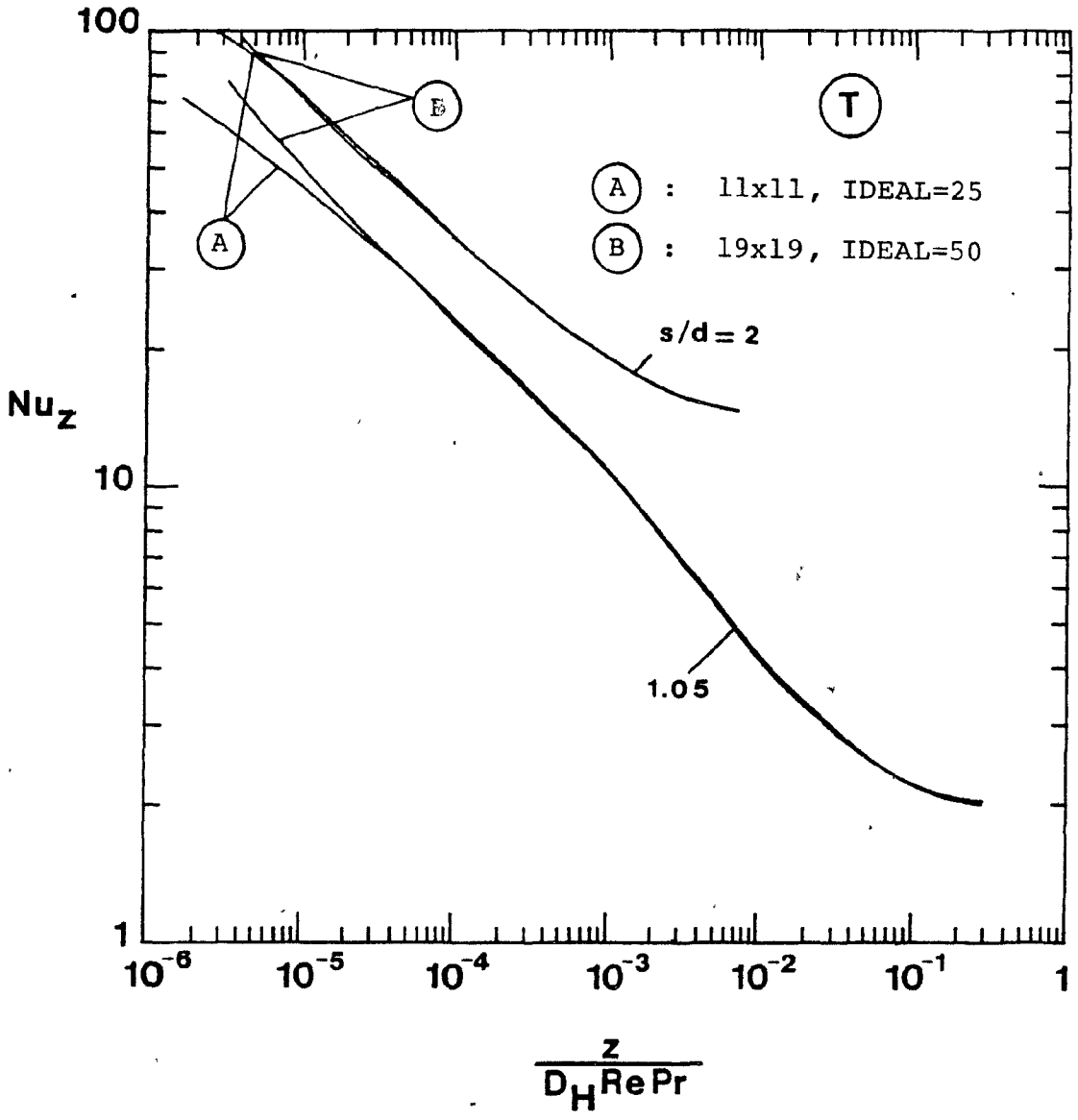

Fig. 6.6: Thermally-developing flow over a rod-bundle with the (T) condition: local Nusselt number variation with axial distance, for two grid and step sizes.

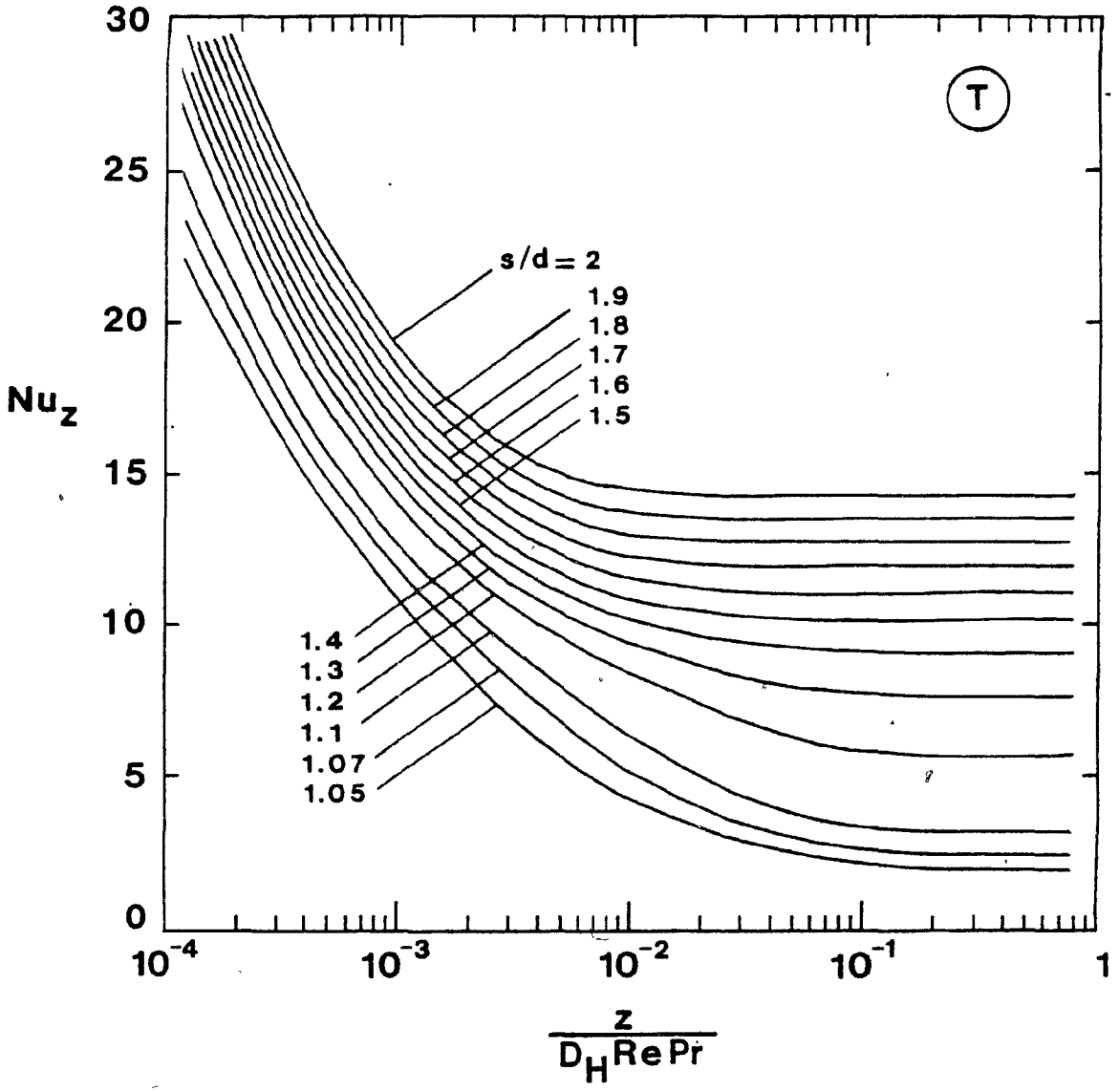

Fig. 6.7: Thermally-developing flow over a rod-bundle with the (T) condition: local Nusselt number variation with axial distance, for twelve pitch-to-diameter ratios.

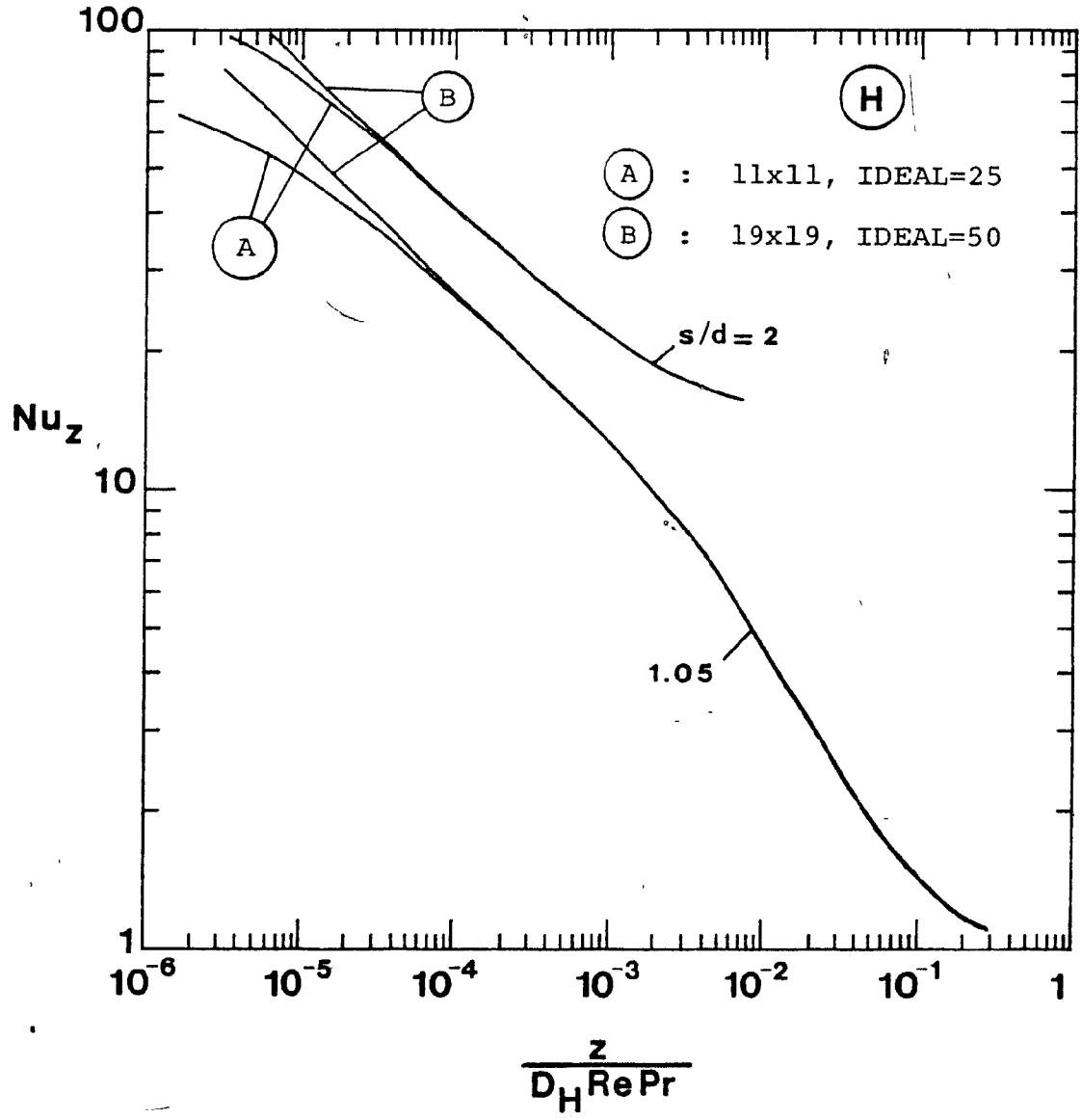

Fig. 6.8: Thermally-developing flow over a rod-bundle with the (H) condition: local Nusselt number variation with axial distance, for two grid and step sizes.

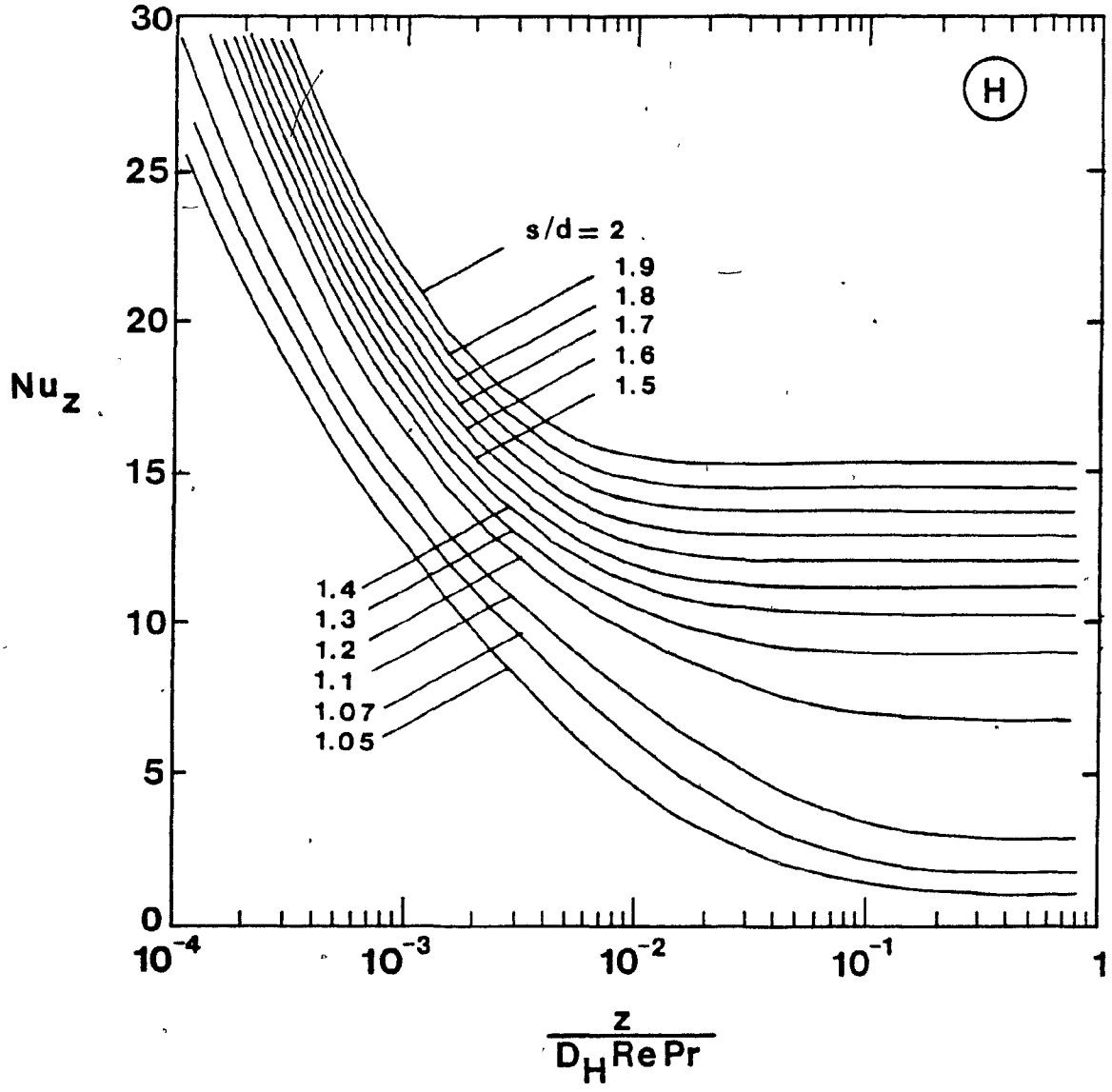

Fig. 6.9: Thermally-developing flow over a rod-bundle with the (H) condition: local Nusselt number variation with axial distance, for twelve pitch-to-diameter ratios.

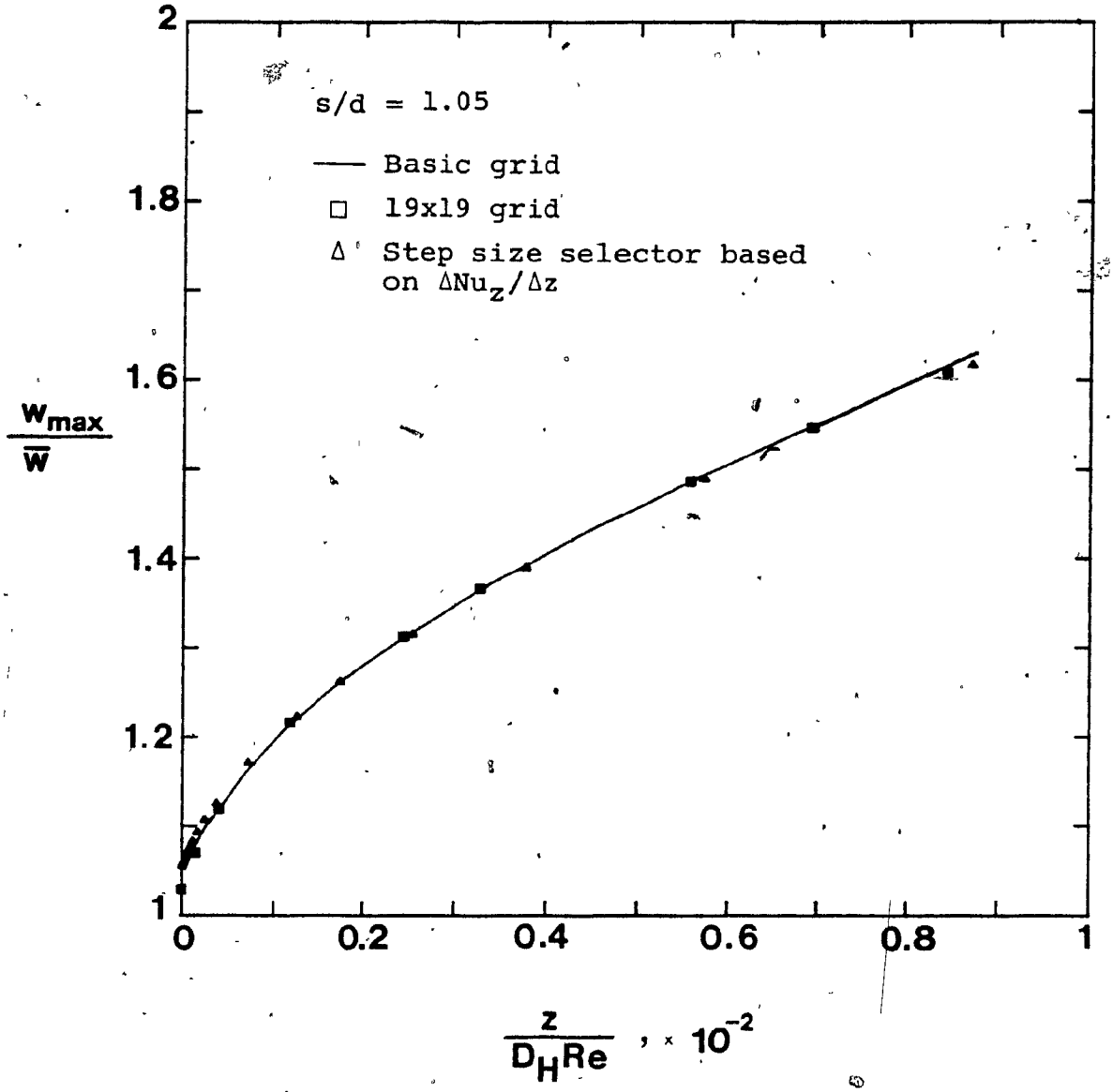

Fig. 6.10: Developing flow over a rod-bundle: grid checks for s/d = 1.05.

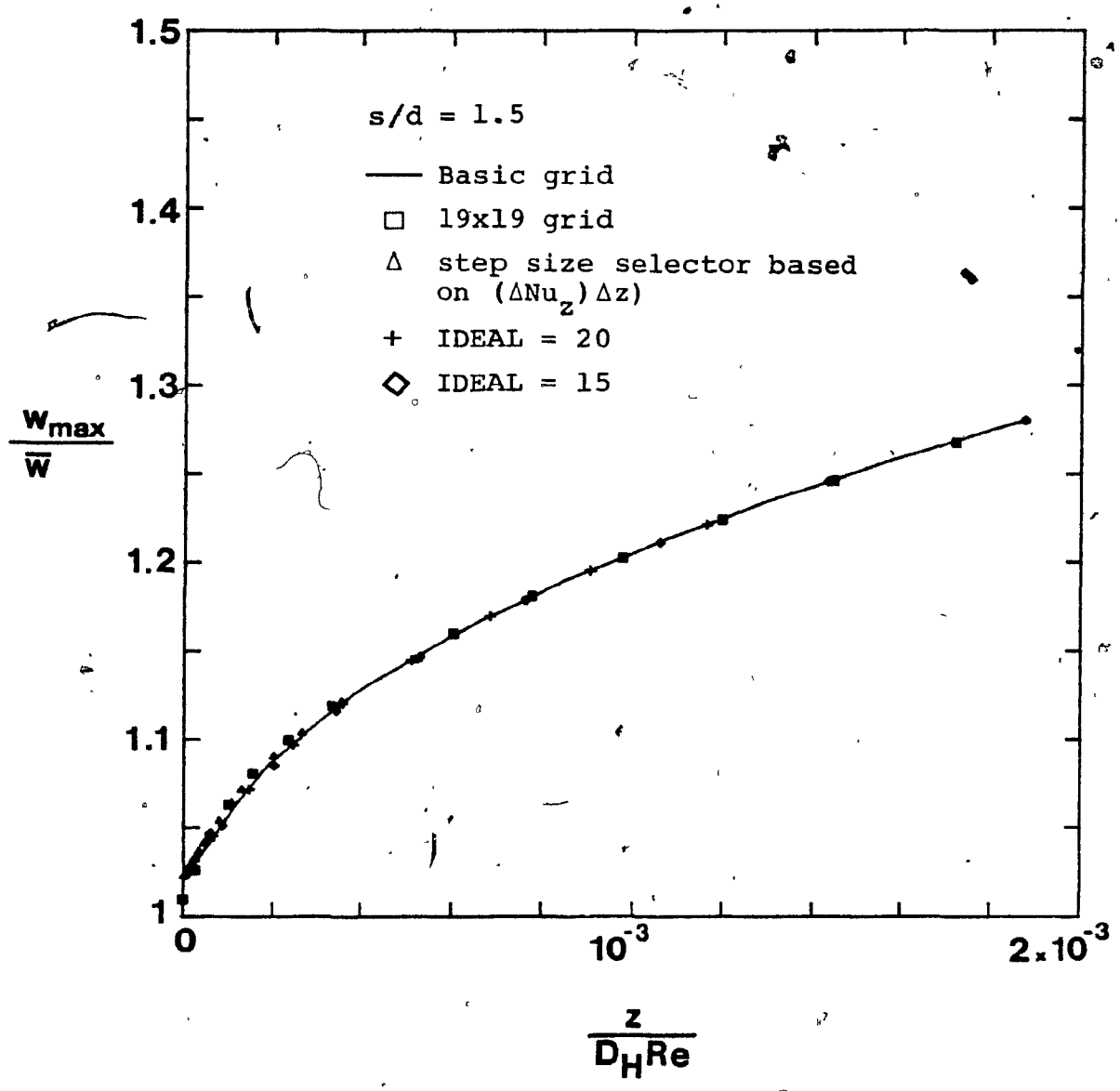

Fig. 6.11: Developing flow over a rod-bundle: grid checks for s/d = 1.5.

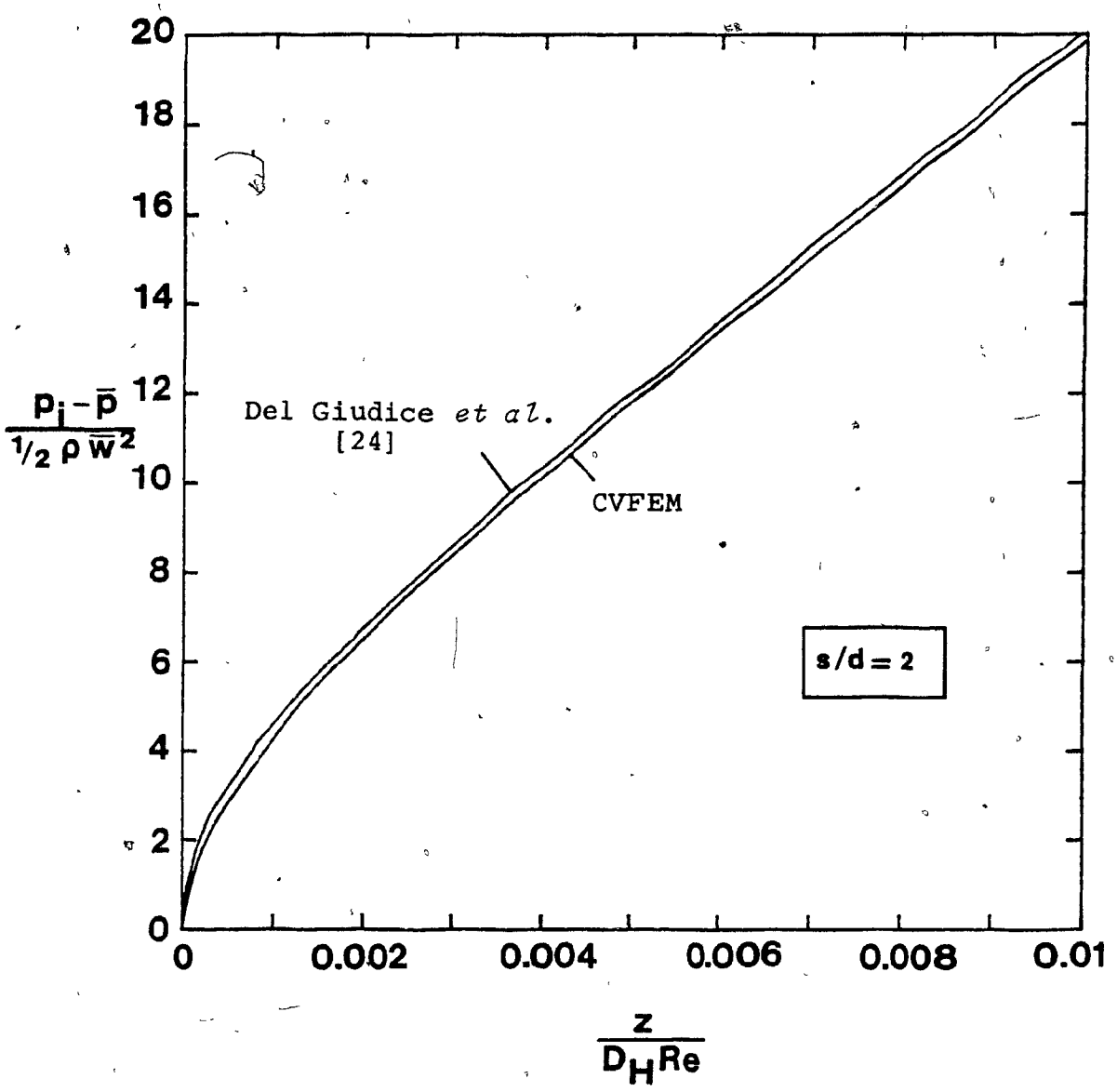

Fig. 6.12: Developing flow over a rod-bundle: variation of mean pressure with axial distance.

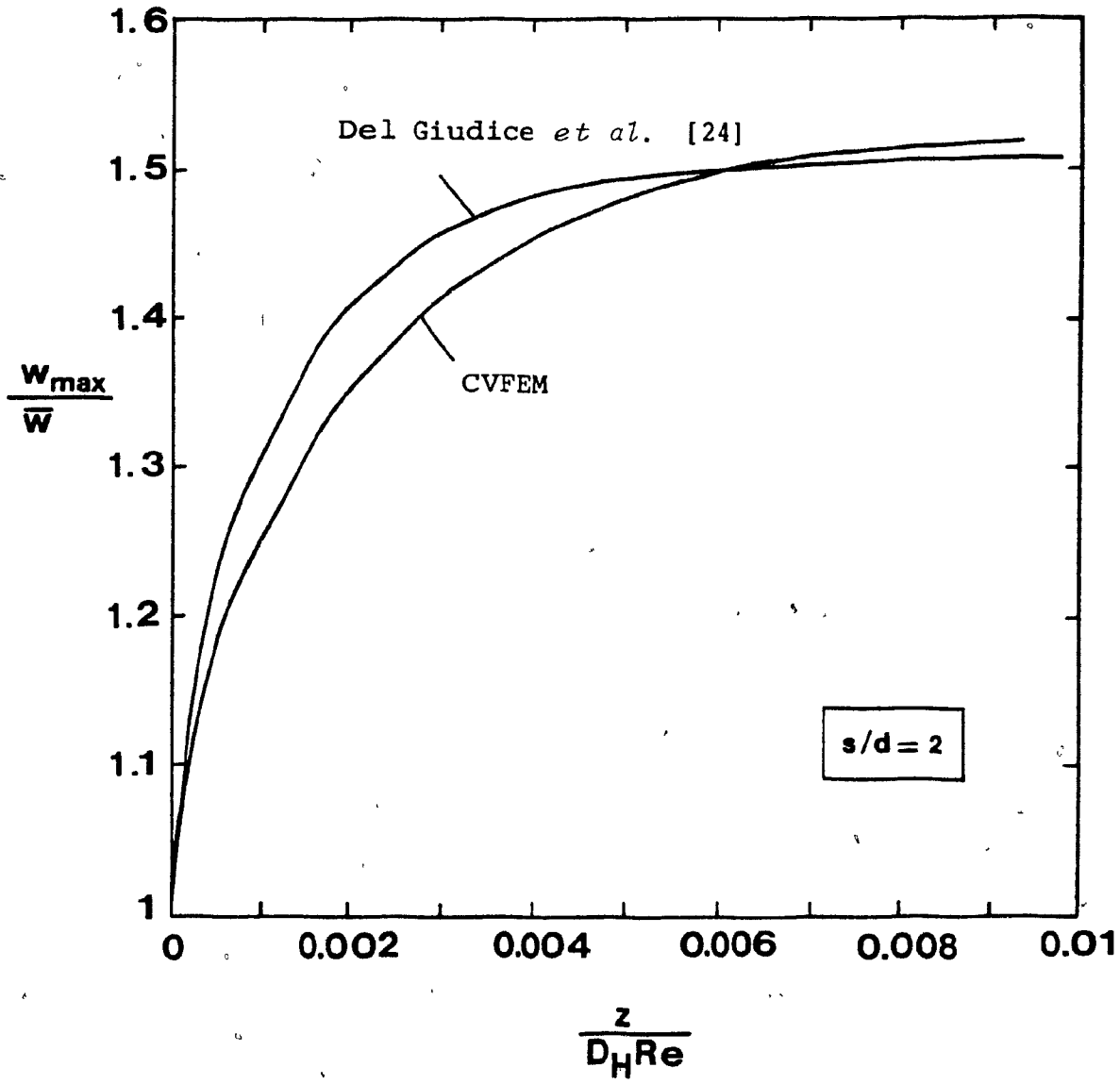

Fig. 6.13: Developing flow over a rod-bundle: variation of maximum axial velocity with axial distance.

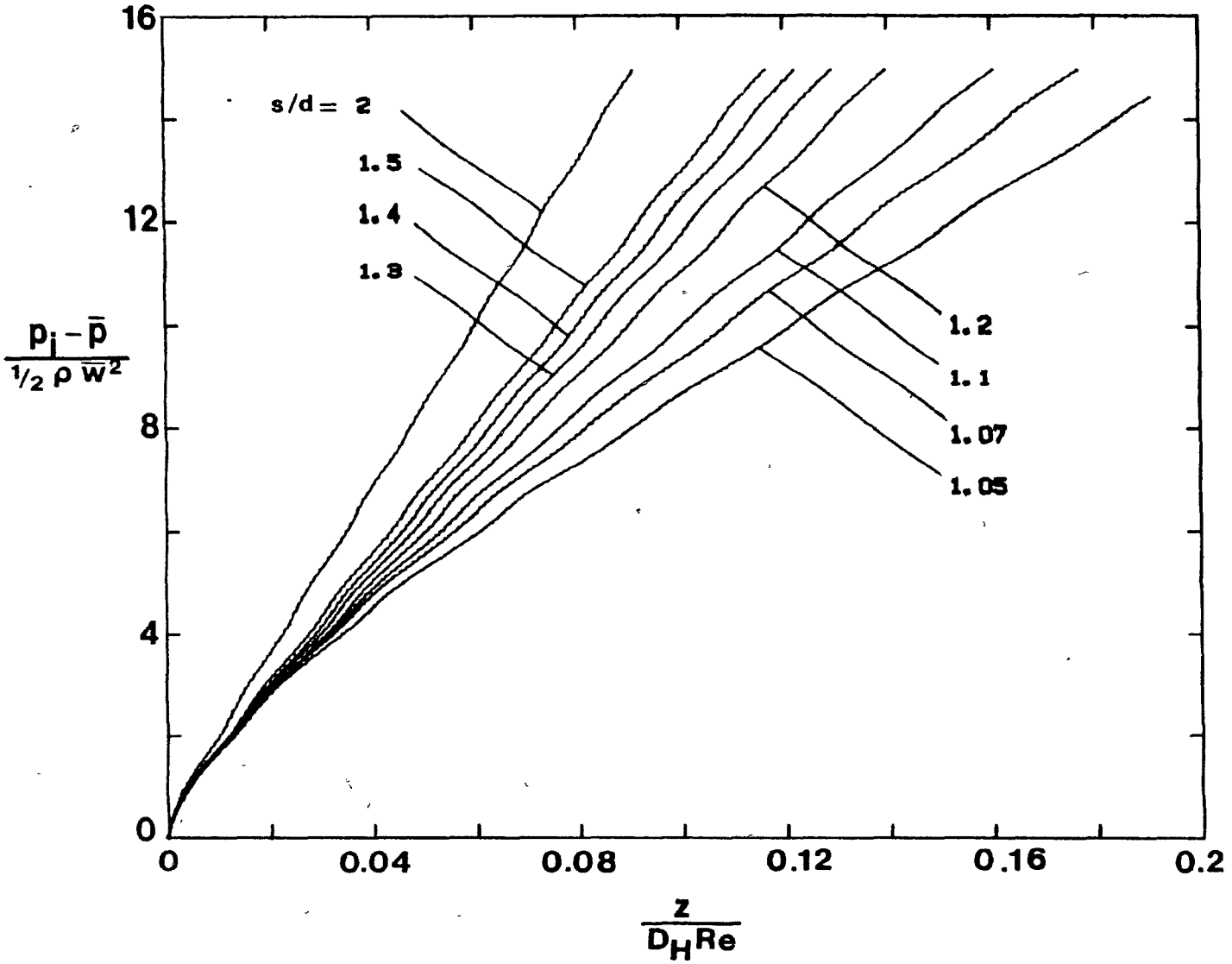

Fig. 6.14: Developing flow over a rod-bundle: variation of mean pressure with axial distance for eight pitch-to-diameter ratios.

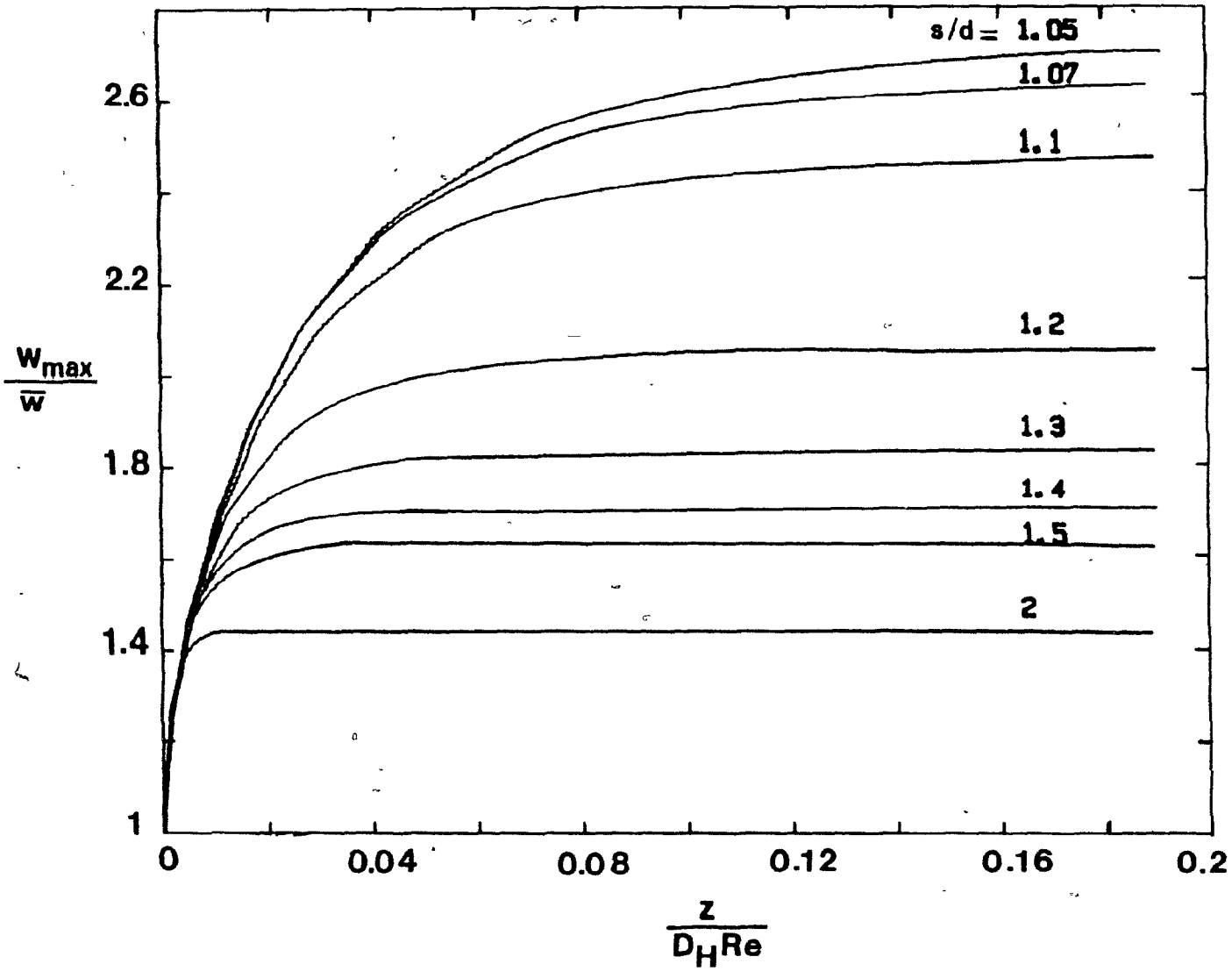

Fig. 6.15: Developing flow over a rod-bundle: variation of maximum axial velocity with axial distance for eight pitch-to-diameter ratios.

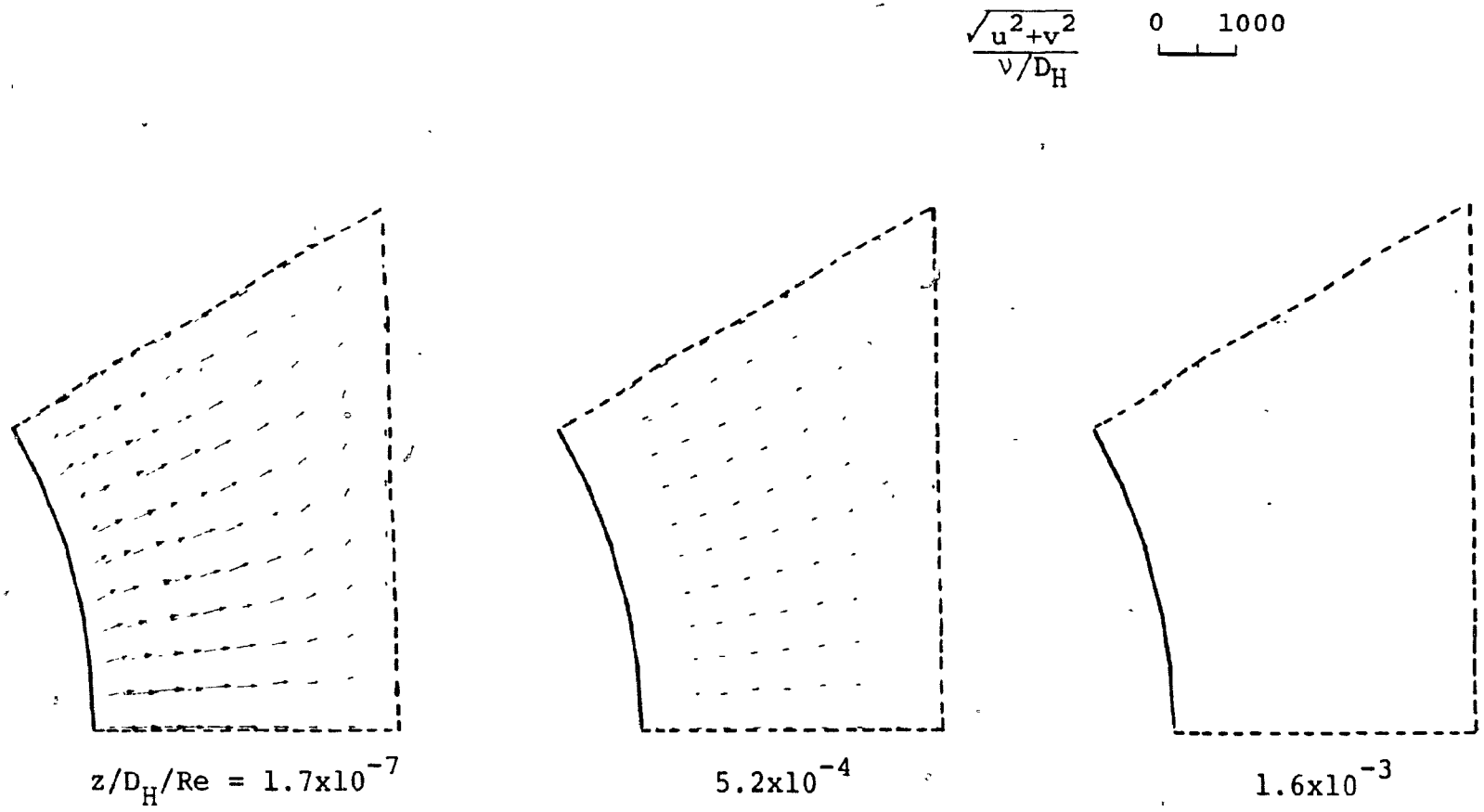

Fig. 6.16: Developing flow over a rod-bundle: cross-sectional velocity fields at three axial locations.

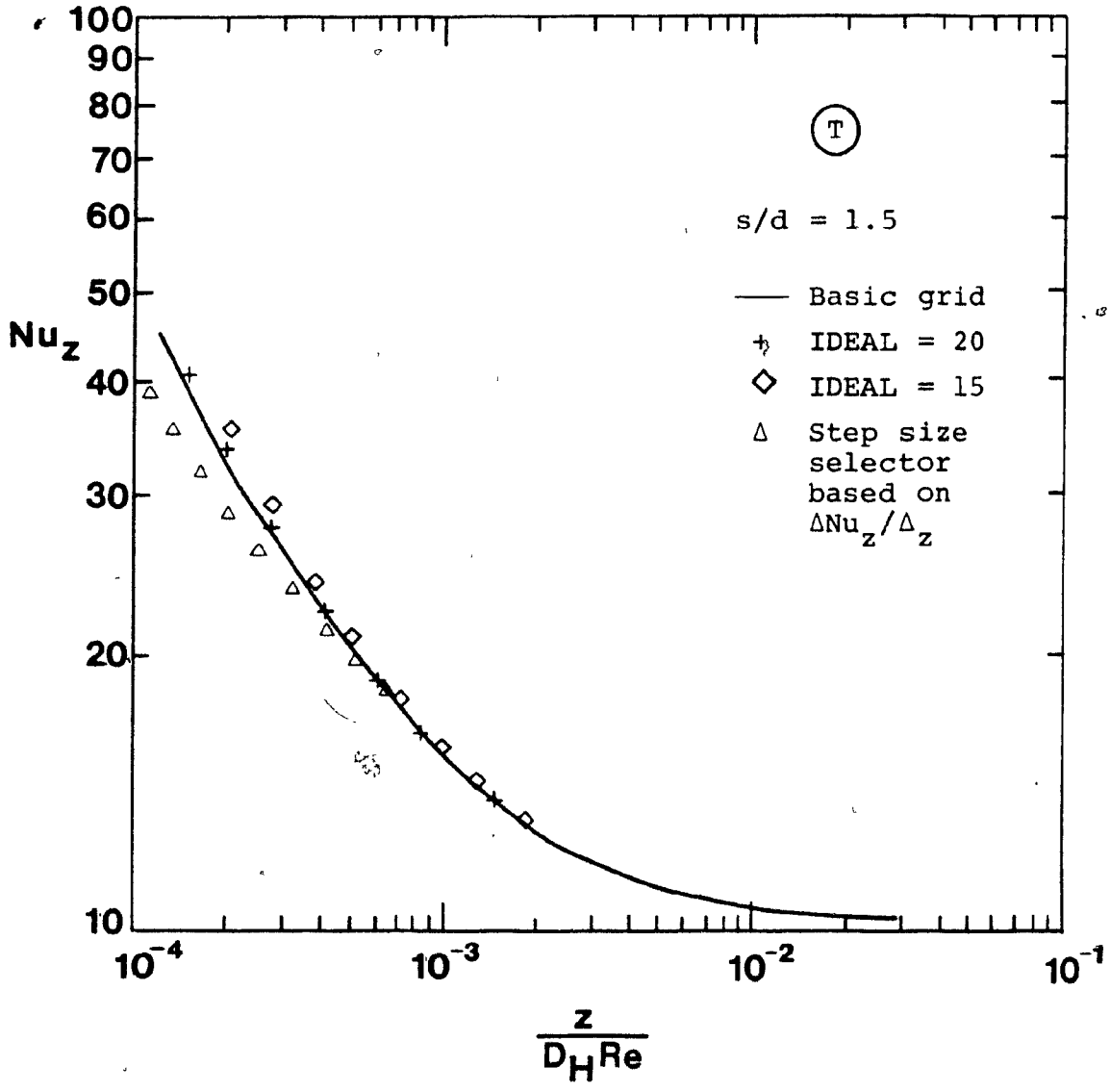

Fig. 6.17(a): Simultaneously developing flow and heat transfer over a rod-bundle with the (T) condition: grid check for s/d = 1.5.

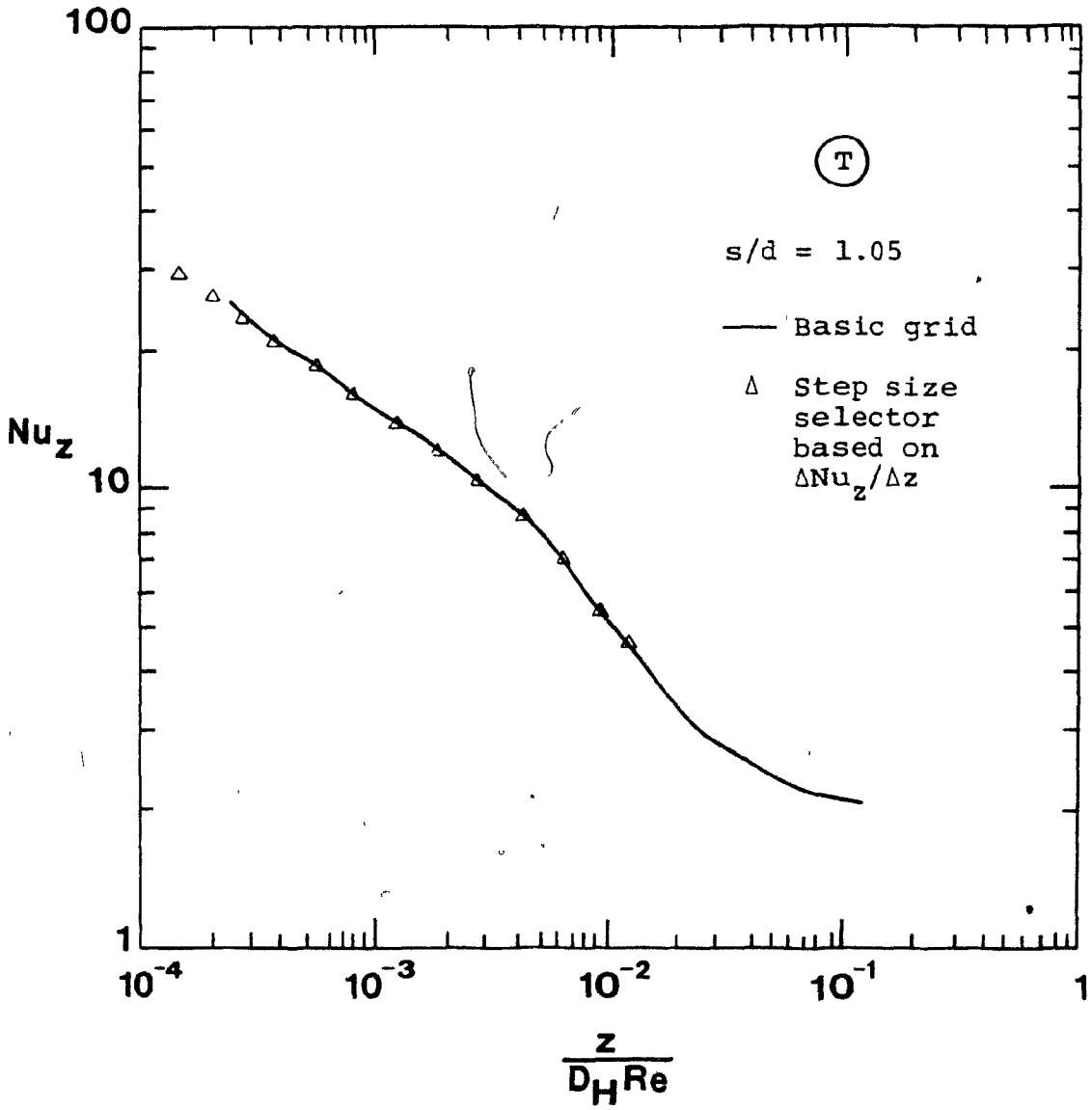

Fig. 6.17(b): Simultaneously developing flow and heat transfer over a rod-bundle with the (T) condition: grid check for s/d = 1.05.

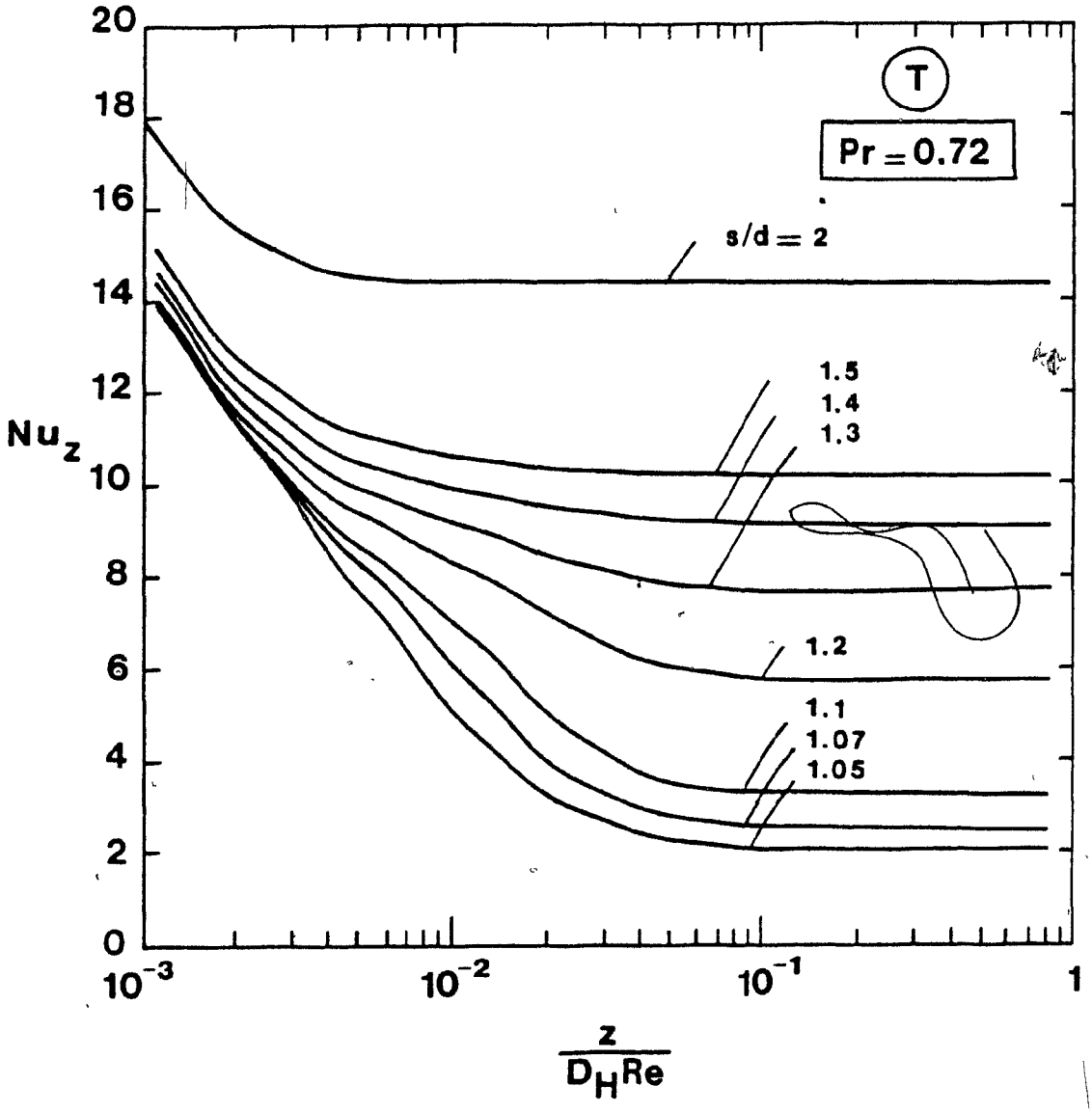

Fig. 6.18: Simultaneously developing flow and heat transfer over a rod-bundle with the (T) condition: variation of local Nusselt number with axial distance for eight pitch-to-diameter ratios and Pr = 0.72.

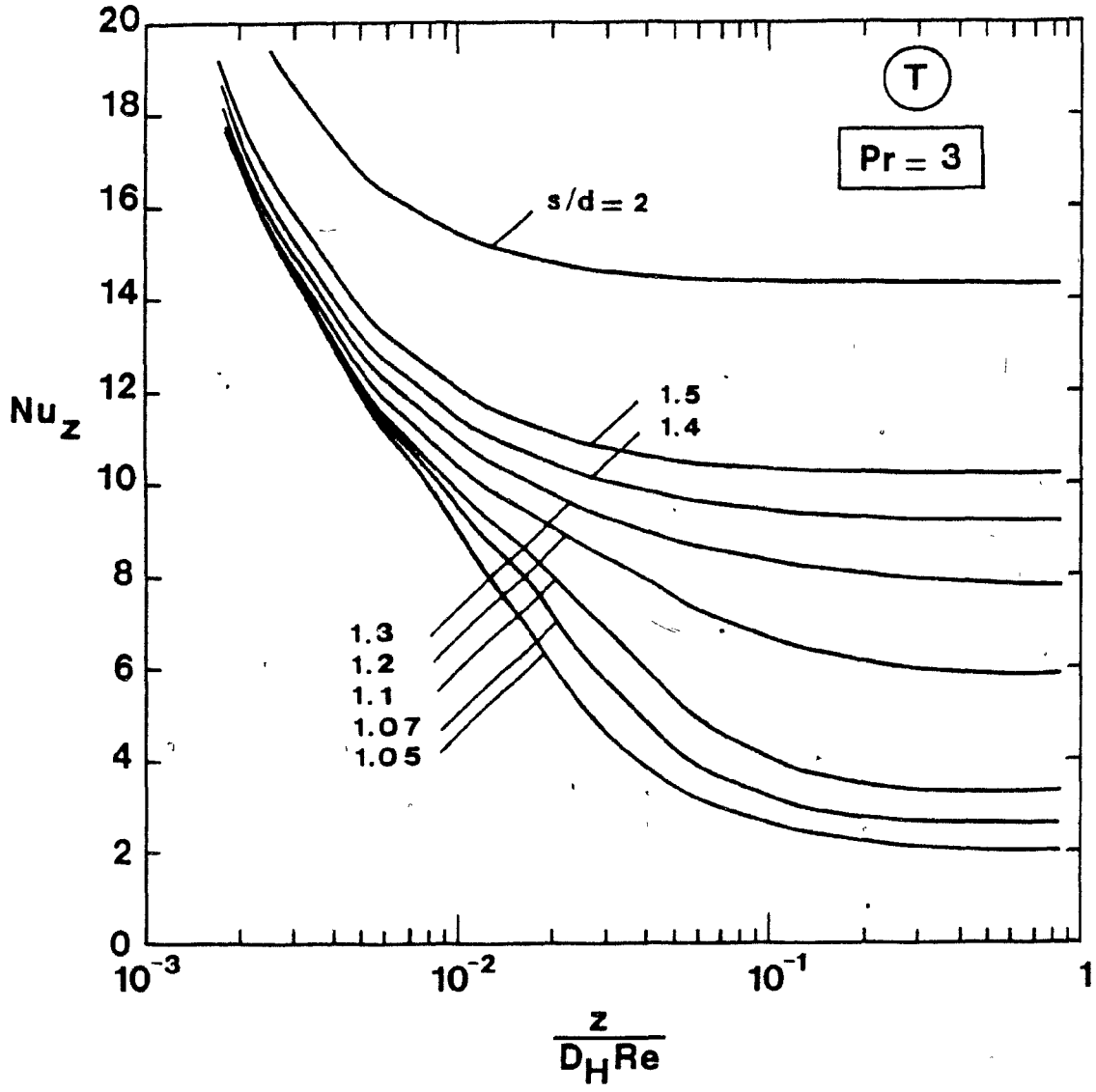

Fig. 6.19: Simultaneously developing flow and heat transfer over a rod-bundle with the (T) condition: variation of local Nusselt number with axial distance for eight pitch-to-diameter ratios and Pr = 3.0.

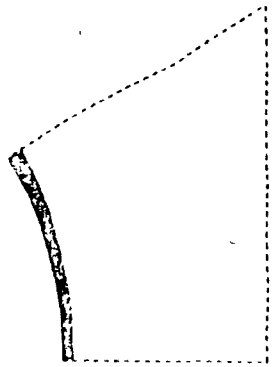

$3/D_H/Re = 1.7x10^{-7}$

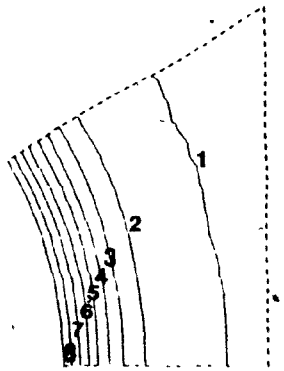

$5.2x10^{-4}$

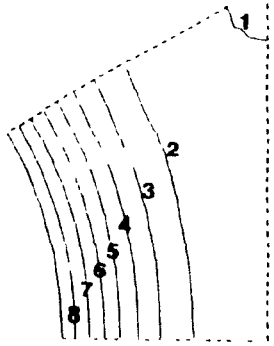

$1.6x10^{-3}$

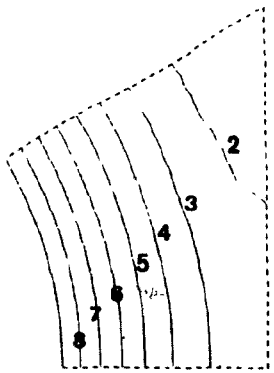

$3.9x10^{-3}$

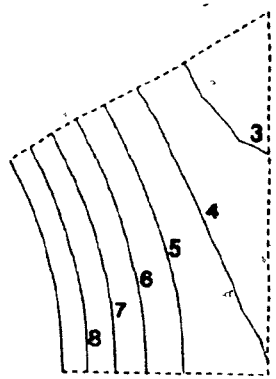

$7.4x10^{-3}$

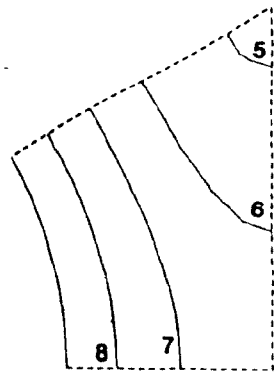

$1.8x10^{-2}$

Fig. 6.20: Simultaneously developing flow and heat transfer over a rod-bundle with the (T) condition: non-dimensional temperature contours at six different axial locations; the contour levels are: $T^*_1 = 0.005$, $T^*_2 = 0.125$. $T^*_3 = 0.250$, $T^*_4 = 0.375$, $T^*_5 = 0.500$, $T^*_6 = 0.625$, $T^*_7 = 0.750$, $T^*_8 = 0.875$.

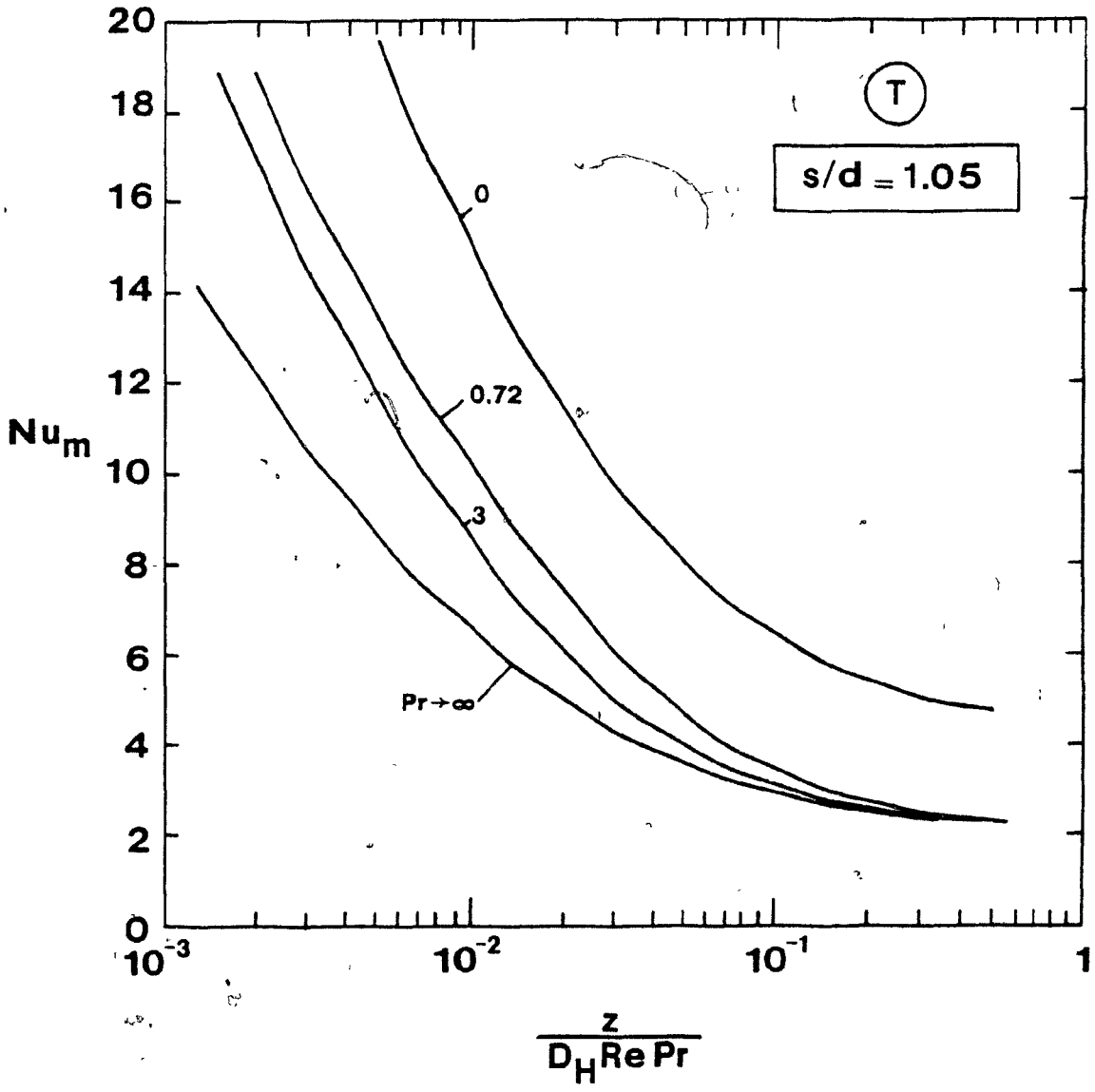

Fig. 6.21: Simultaneously developing flow and heat transfer over a rod-bundle with the (T) condition: variation of mean Nusselt number with axial distance for four Prandtl numbers and s/d = 1.05.

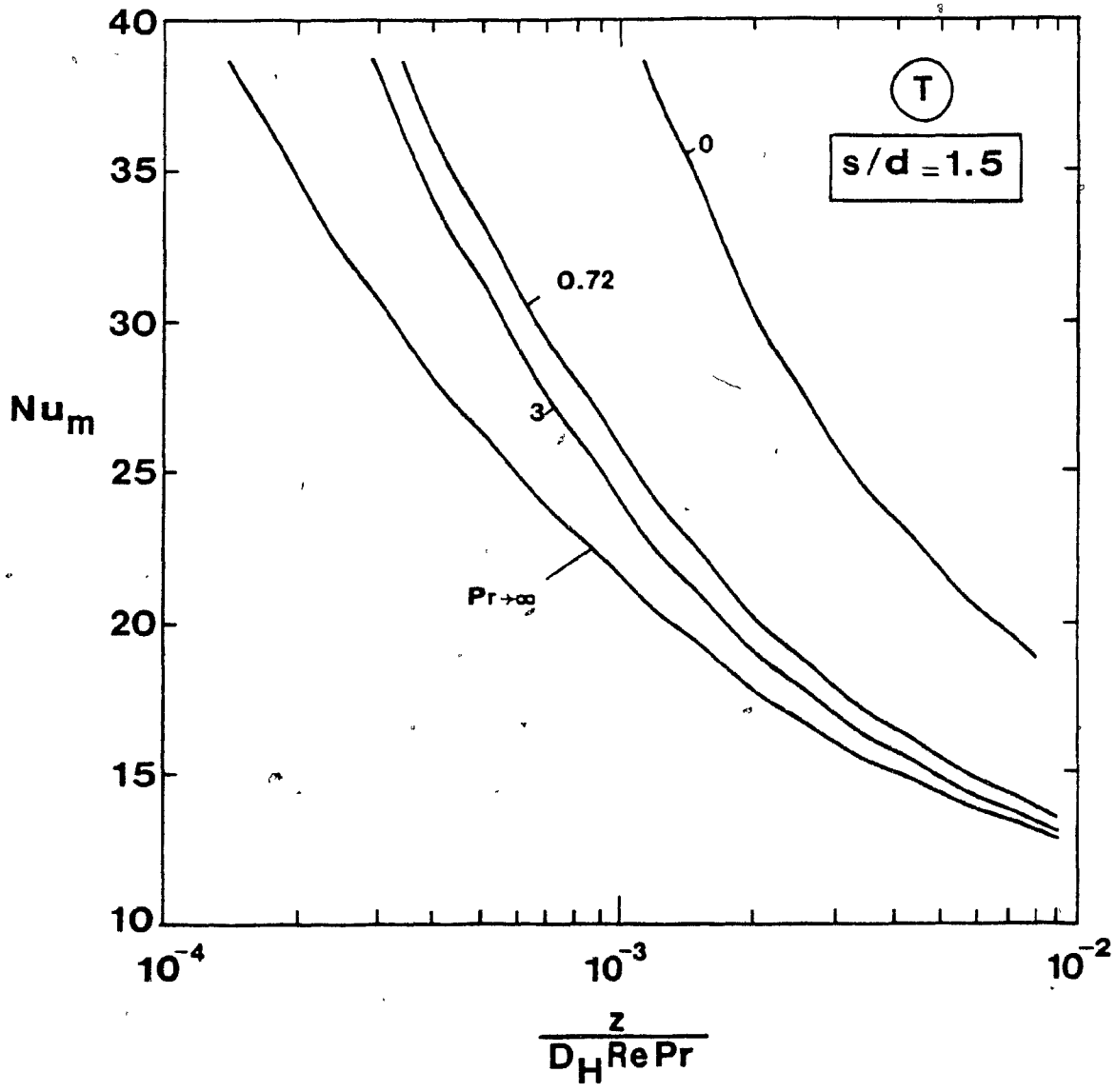

Fig. 6.22: Simultaneously developing flow and heat transfer over a rod-bundle with the (T) condition: variation of mean Nusselt number with axial distance for four Prandtl numbers and s/d = 1.5.

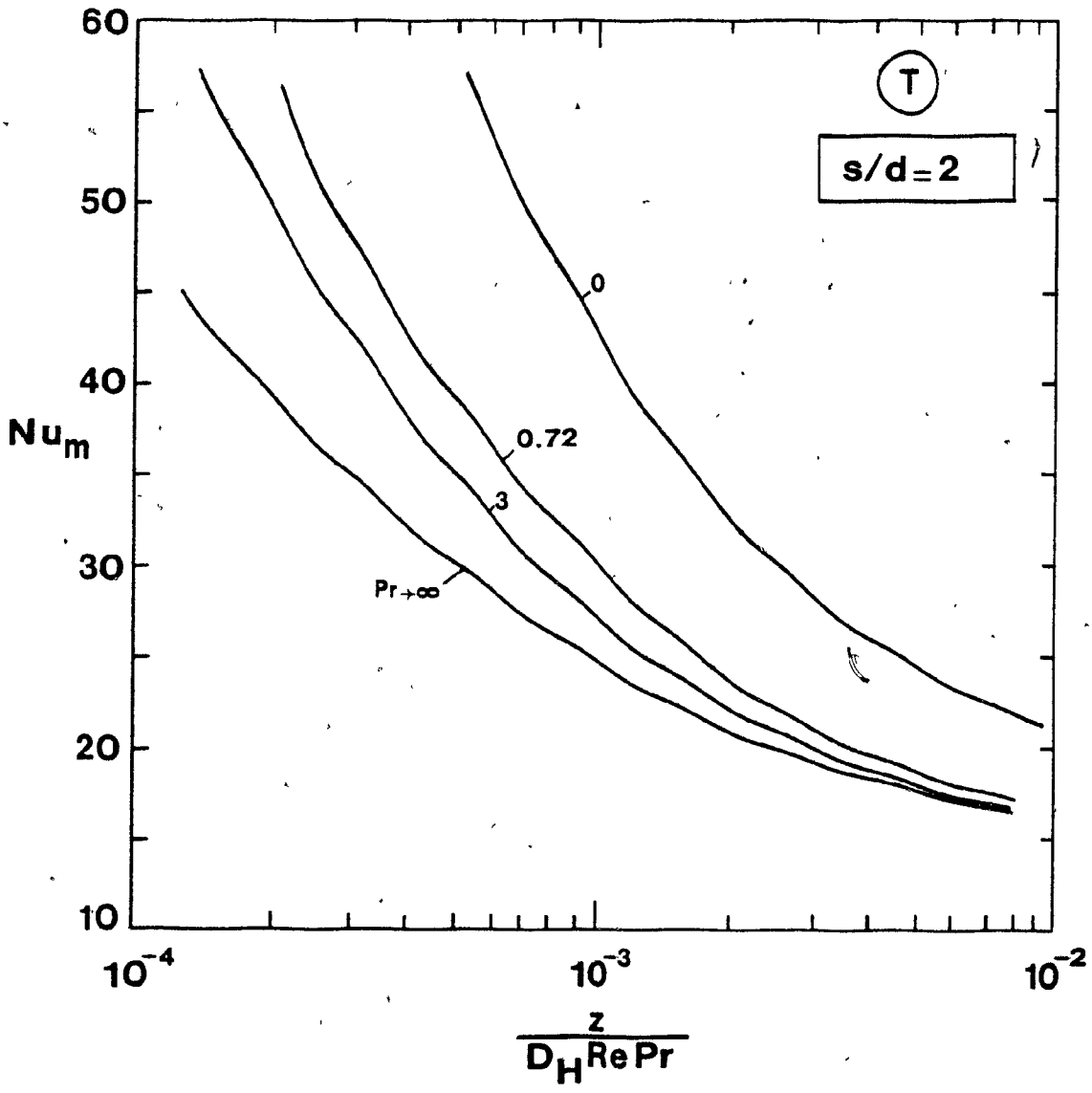

Fig. 6.23: Simultaneously developing flow and heat transfer over a rod-bundle with the (T) condition: variation of mean Nusselt number with axial distance for four Prandtl numbers and s/d = 2.0.

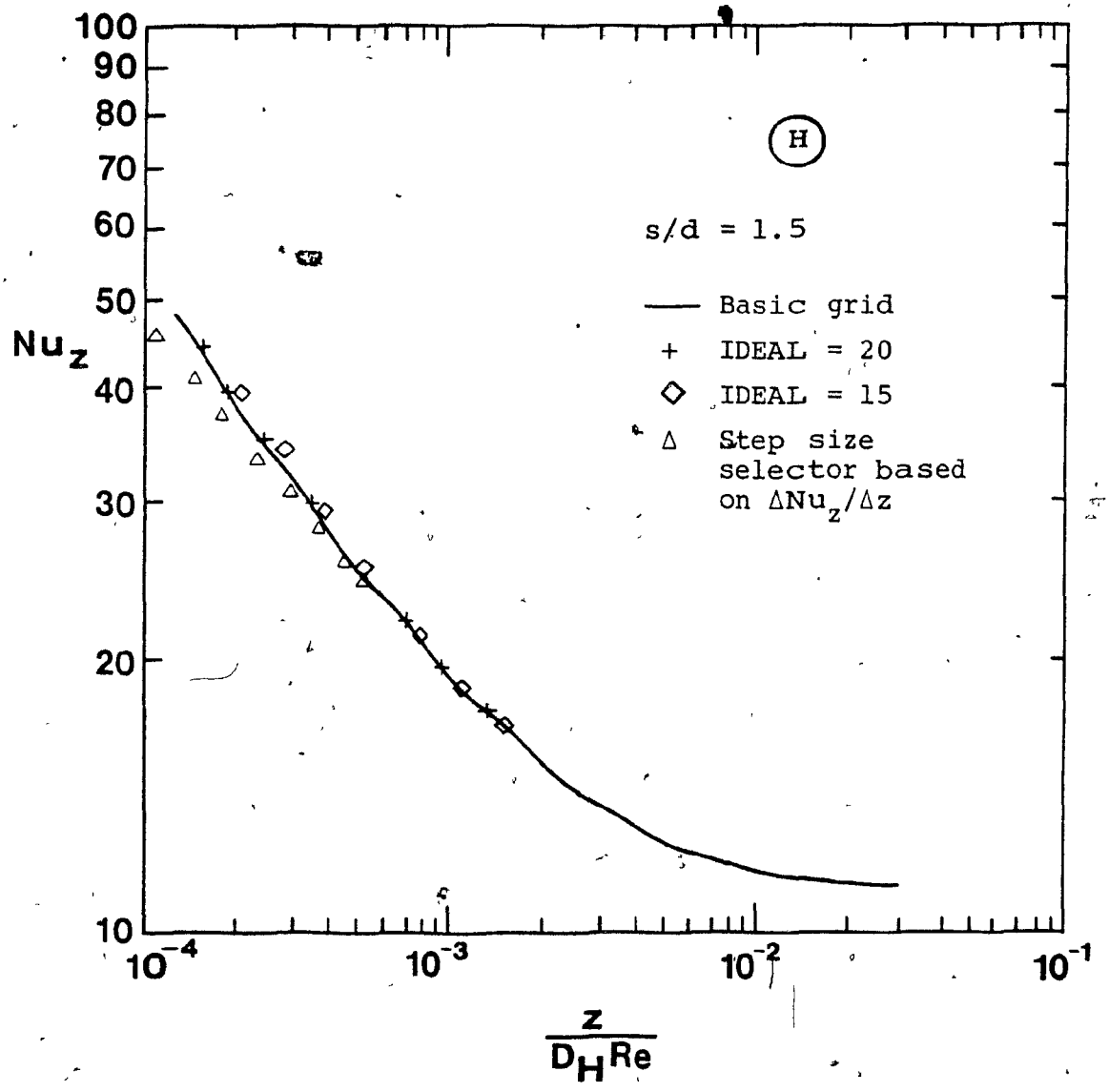

Fig. 6.24(a): Simultaneously developing flow and heat transfer over a rod-bundle with the (H) condition: grid check for s/d = 1.5.

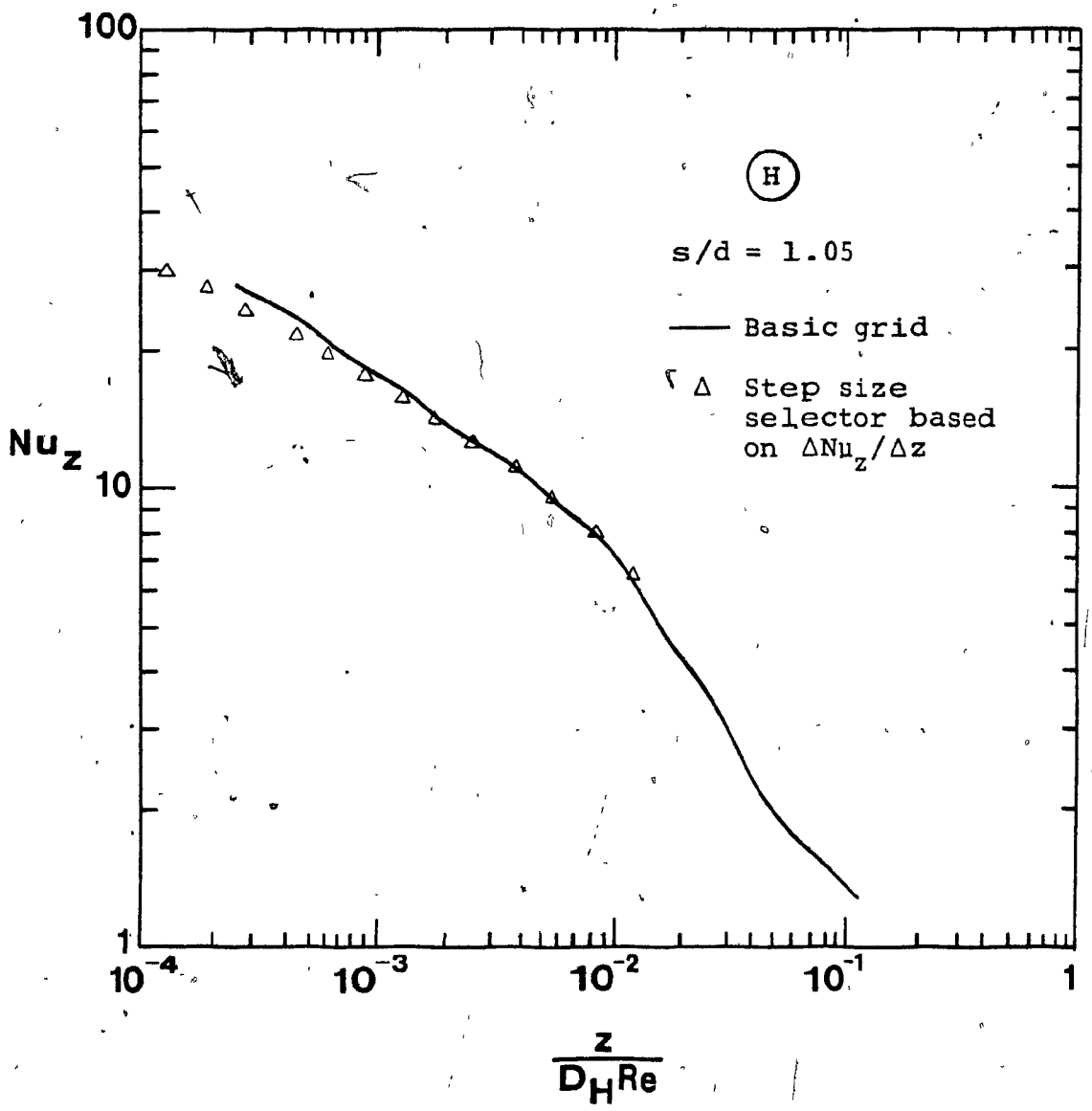

Fig. 6.24(b): Simultaneously developing flow and heat transfer over a rod-bundle with the (H) condition: grid check for s/d = 1.05.

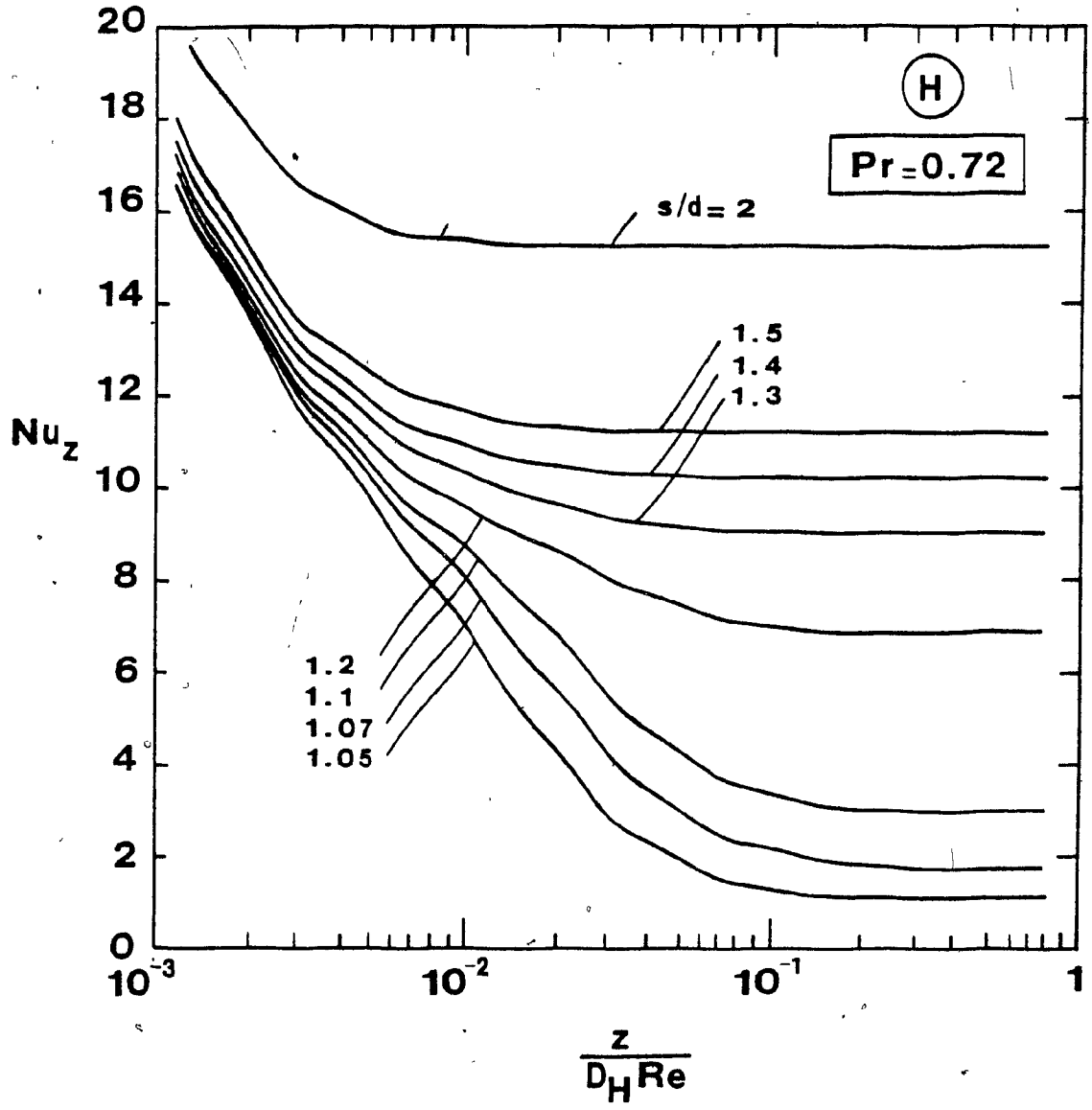

Fig. 6.25: Simultaneously developing flow and heat transfer over a rod-bundle with the (H) condition: variation of local Nusselt number with axial distance for eight pitch-to-diameter ratios and Pr = 0.72.

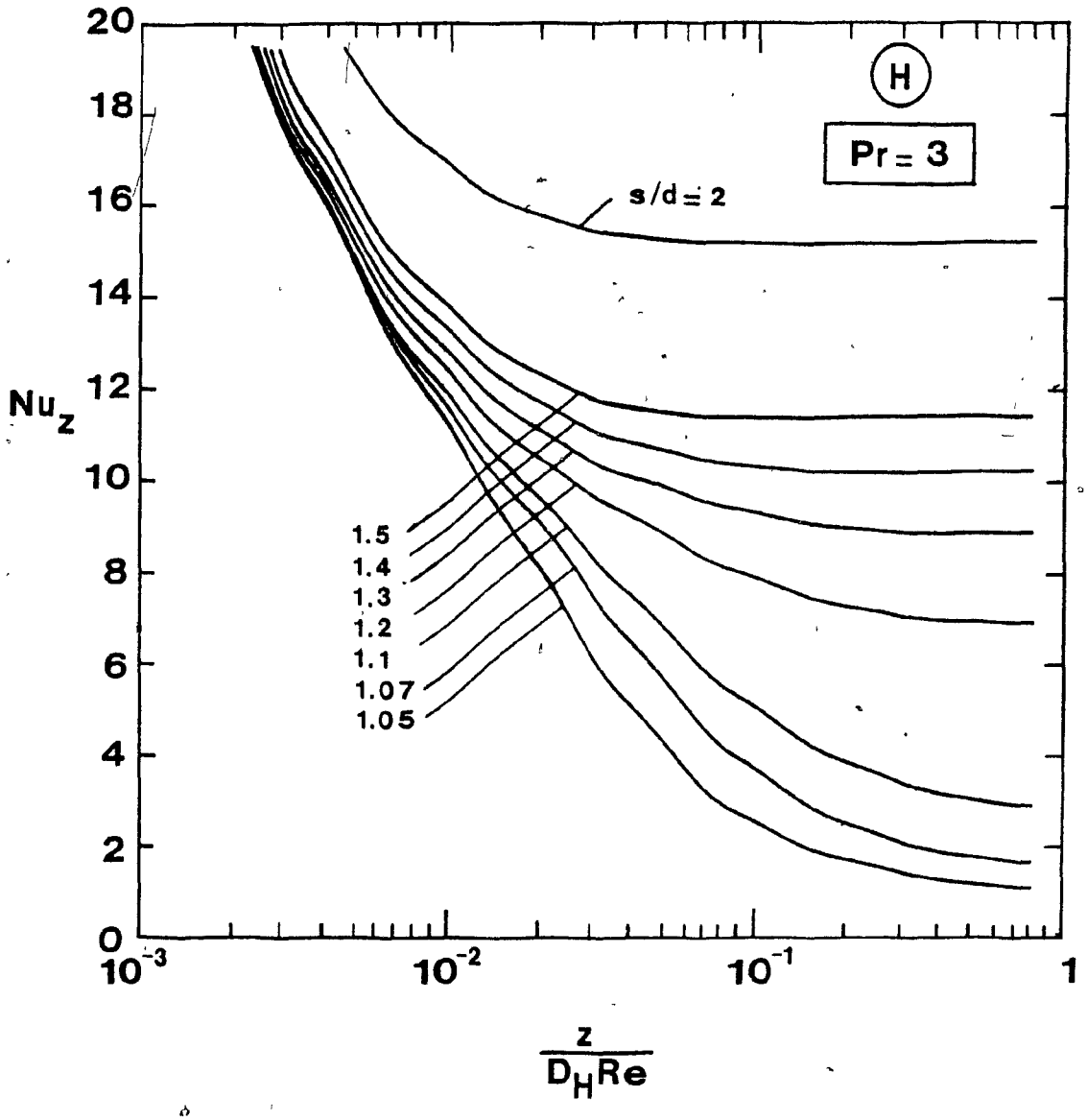

Fig. 6.26: Simultaneously developing flow and heat transfer over a rod-bundle with the (H) condition: variation of local Nusselt number with axial distance for eight pitch-to-diameter ratios and Pr = 3.0.

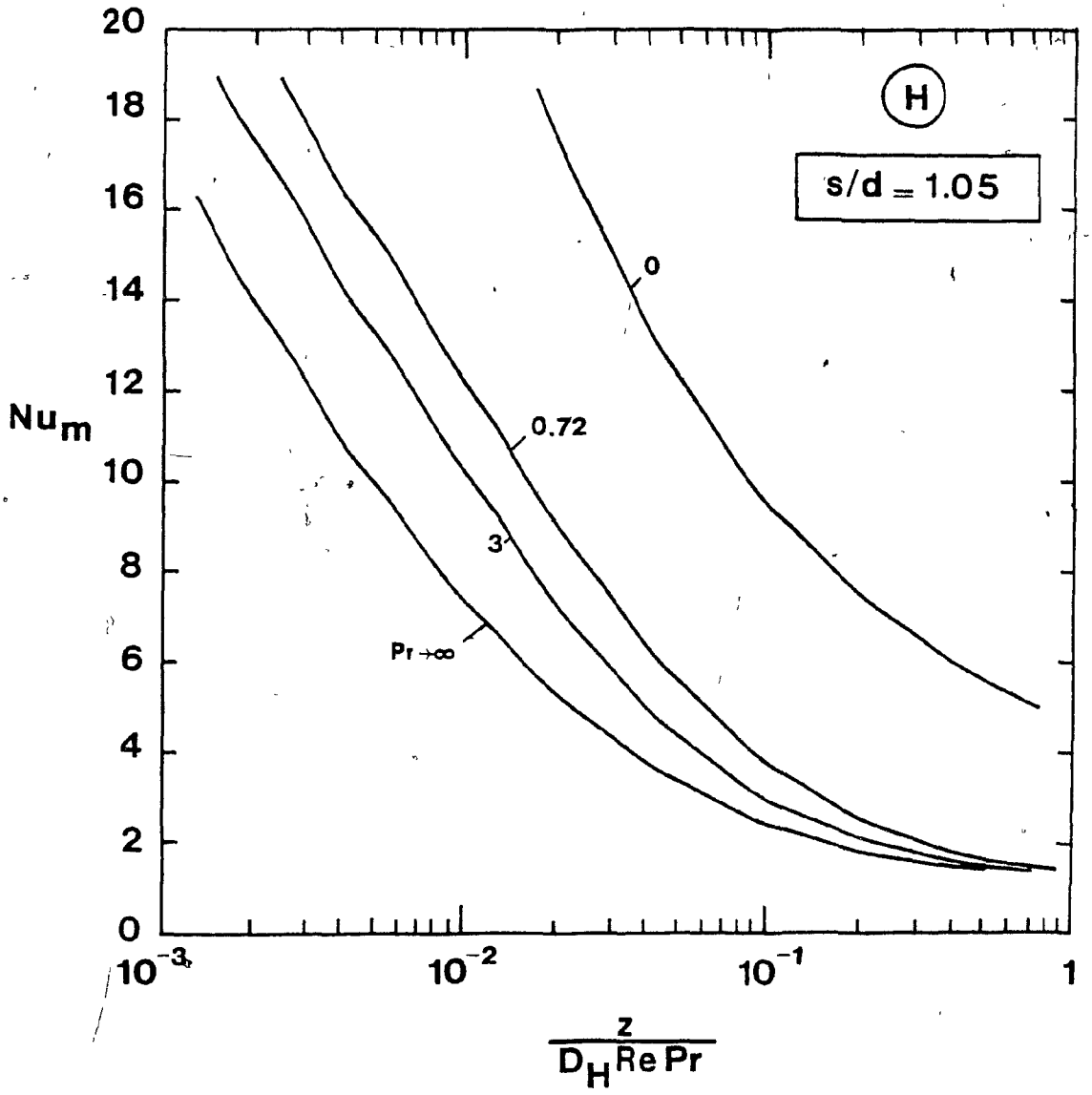

Fig. 6.27: Simultaneously developing flow and heat transfer over a rod-bundle with the (H) condition: variation of mean Nusselt number with axial distance for four Prandtl numbers and s/d = 1.05.

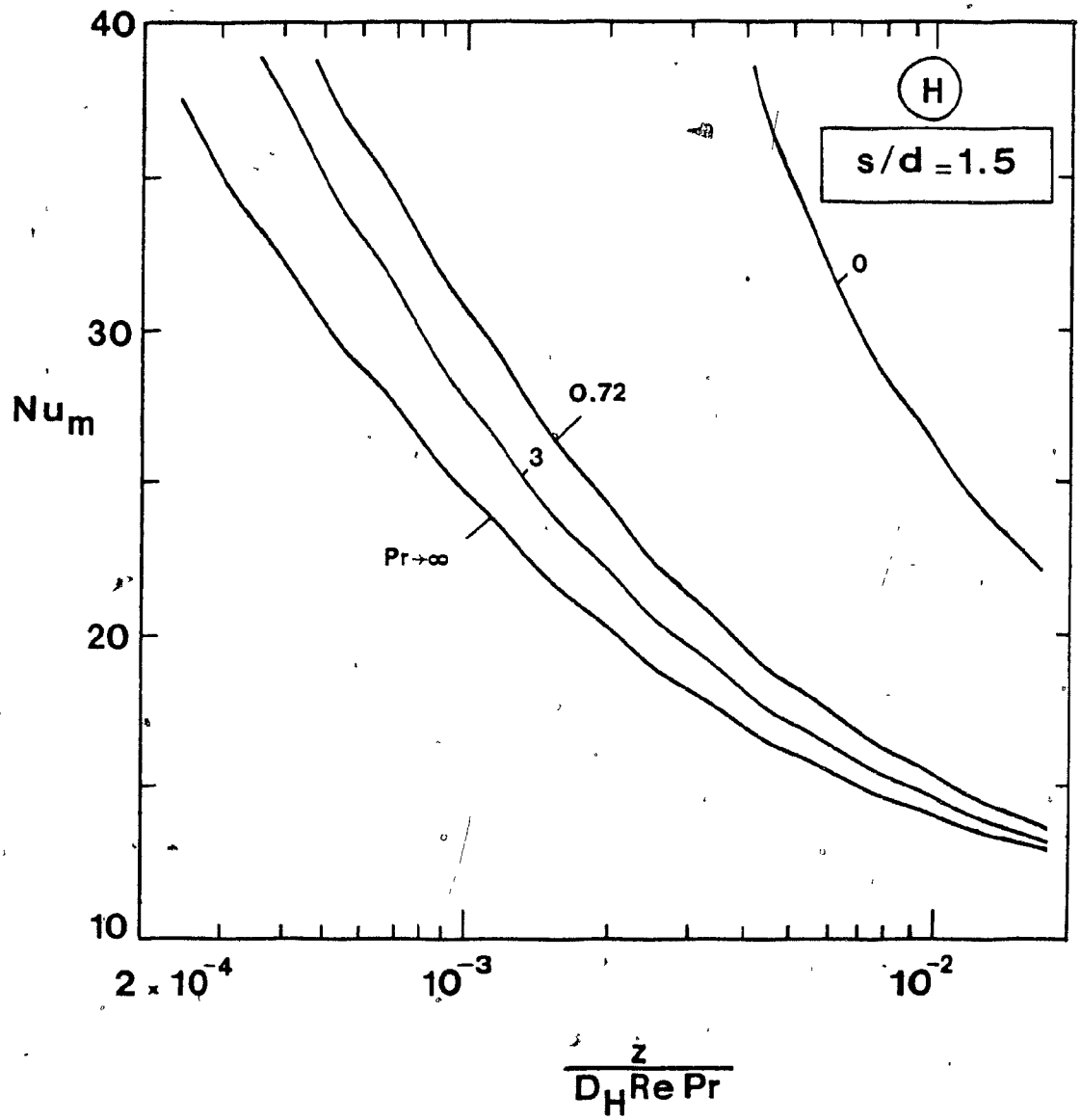

Fig. 6.28: Simultaneously developing flow and heat transfer over a rod-bundle with the (H) condition: variation of mean Nusselt number with axial distance for four Prandtl numbers and s/d = 1.15.

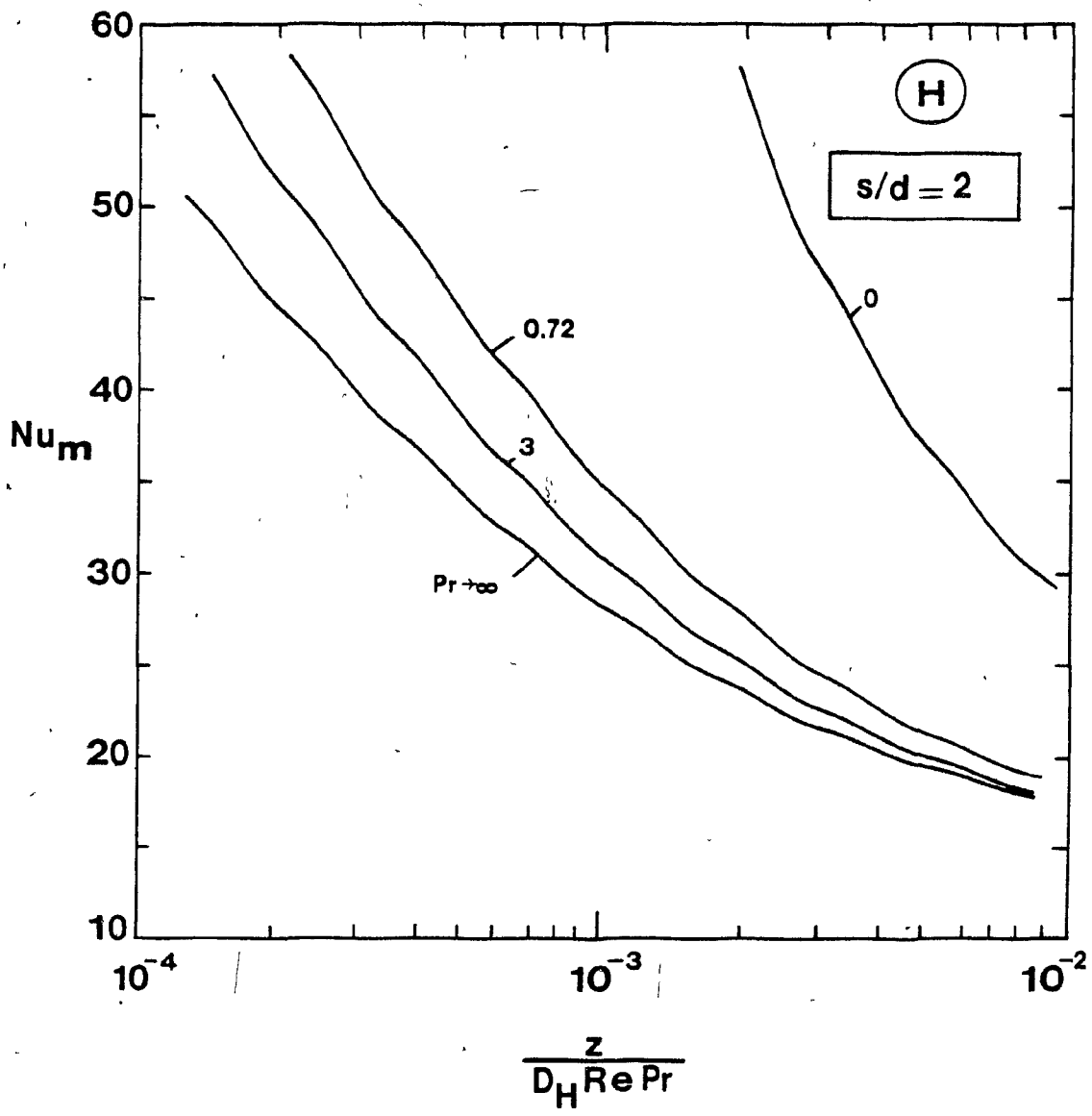

Fig. 6.29: Simultaneously developing flow and heat transfer over a rod-bundle with the (H) condition: variation of mean Nusselt number with axial distance for four Prandtl numbers and s/d = 2.0.

TABLES

Table 2.1

Interpretation of ϕ, Γ and S

Equation number	Description	ϕ	Γ	S
(2.8)	Continuity	1	0	0
(2.9)	x-momentum	u	μ	$-\frac{\partial p}{\partial x}$
(2.10)	y-momentum	v	μ	$-\frac{\partial p}{\partial y}$
(2.11)	z-momentum	w	μ	$-\frac{d\bar{p}}{dz}$
(2.20)	continuity	1	0	0
(2.21)	x-momentum	u*	1	$-\frac{\partial p^*}{\partial x^*}$
(2.22)	y-momentum	v*	1	$-\frac{\partial p^*}{\partial y^*}$
(2.23)	z-momentum	w*	1	$-\frac{d\bar{p}^*}{dz^*}$
(2.28)	z-momentum	W	1	1
(2.34)	energy	T	k/c_p	0
(2.38)	energy	T*	1/Pr	0
(2.55)	energy	Θ	1	$\frac{W}{\bar{W}} \lambda \Theta$
(2.62)	energy	t*	1/Pr	0
(2.70)	energy	χ	1	$-4\frac{W}{\bar{W}}$

Table 5.1

Laminar Natural Convection in a Rectangular Enclosure of Aspect Ratio 5:
Average Nusselt Numbers

Rayleigh Number	Nu_{av} CVFEM	Nu_{av} Jones[38,39]	Hot-face Nu_{av} Duxbury[39]	Cold-face Nu_{av} Duxbury[39]	Mean Nu_{av} Duxbury[39]
2.49×10^3	1.261	1.25	1.6	1.1	1.4
1.67×10^4	2.266	2.26	2.3	1.9	2.1
1.36×10^5	3.756	3.8	5.0	3.6	4.3

Table 5.2

Laminar Fully-Developed Flow in a Square Duct: Friction Factor Results for Various Grid Sizes and Grid-Line Distributions

Subelement Grid	POWER	f.Re	f.Re (Shah [7])	Error (%)
11x11	1.0	57.146	56.908	0.42
11x11	1.2	57.093		0.33
11x11	1.4	57.092		0.32
11x11	1.6	57.107		0.35
11x11	1.8	57.133		0.40
11x11	2.0	57.160		0.44
15x15	1.0	56.991		0.15
15x15	1.2	56.969		0.11
15x15	1.4	56.976		0.12
15x15	1.6	56.991		0.15
15x15	1.8	57.003		0.17
15x15	2.0	57.023		0.20
19x19	1.0	56.890		0.01
19x19	1.2	56.901		0.01
19x19	1.4	56.912		0.01
19x19	1.6	56.923		0.03
19x19	1.8	56.941		0.06
19x19	2.0	56.952		0.08

Table 5.3

Square Duct Problem: Fully-Developed Nusselt Numbers for Various Grid Sizes

Subelement Grid	POWER	$Nu_{(T)}$	$Nu_{(H)}$
11x11	1.4	2.9386	3.0475
15x15	1.4	2.9578	3.0670
19x19	1.4	2.9650	3.0743
Shah and London [7]	-	2.976	3.091

Table 5.4

Square Duct Problem: Normalized Minimum and Maximum Temperature on the Periphery

	$T^*_{w,max}$	$T^*_{w,min}$
CVFEM	1.3919	0.7722
Shah [7]	1.39	0.769
Error (%)	0.14	0.42

Table 5.5

Hydrodynamically Developed and Thermally Developing Flow in a Square Duct:
Discretization Details

Run	Subelement Grid	POWER	Initial $\Delta z'$	IDEAL	Actual Number of Steps Required for Reaching F-D Situation†	
					(T)	(H)
A (basic grid)	11x11	1.4	$7x10^{-7}$	25	39	39
B	15x15	1.4	$7x10^{-7}$	50	66	67
C	19x19	1.4	$7x10^{-7}$	50	67	68

†F.D. situation is regarded as reached when $Nu_z < 1.05\ Nu_{f.d.}$

Table 6.1

Rod-Bundle Problem: Fully-Developed Friction Factor and Nusselt Number Results

s/d	Subelement Grid	POWER	f.Re	f.Re [7]	Nu_T	Nu_H	Nu_H [7]
1.05	11x11	1.0	62.659	61.912	2.0045	1.0680	1.06
		1.2	62.670		2.0019	1.0684	
		1.4	62.685		1.9980	1.068	
		1.6	62.721		1.9934	1.0676	
		1.8	62.755		1.9882	1.0668	
	15x15	1.4	62.286		2.0249	1.0625	
	19x19	1.4	62.104		2.0348	1.0599	
1.5	6x6	1.4	124.72	124.14	10.190	11.195	11.22
	8x8	1.4	124.440		10.127	11.215	
	10x10	1.4	124.322		10.228	11.223	
2.0	6x6	1.4	158.366	157.536	14.33	15.25	15.26
	8x8	1.4	157.962		14.344	15.256	
	10x10	1.4	157.783		14.348	15.263	

APPENDICES

APPENDIX I

ALGEBRAIC EXPRESSIONS FOR THE PRESSURE GRADIENT INTEGRALS

Consider the following linear interpolation function for the pressure p:

$$p = ax + by + c \tag{I.1}$$

with the nodal conditions:

$$\left.\begin{aligned} p_1 &= ax_1 + by_1 + c \\ p_2 &= ax_2 + by_2 + c \\ p_3 &= ax_3 + by_3 + c \end{aligned}\right\} \tag{I.2}$$

The set of simultaneous linear equations (I.2) can be easily solved for the interpolation constants a, b and c, using the well-known Cramer's rule. Thus, let the determinant of the system of equations (I.2) be

$$DET = x_1y_2 + x_2y_3 + x_3y_1 - y_1x_2 - y_2x_3 - y_3x_1 \tag{I.3}$$

It follows that

$$a = \frac{1}{DET}\,[(y_2-y_3)p_1 + (y_3-y_1)p_2 + (y_1-y_2)p_3] \tag{I.4}$$

$$b = \frac{1}{DET}\,[(x_3-x_2)p_1 + (x_1-x_3)p_2 + (x_2-x_1)p_3] \tag{I.5}$$

$$c = \frac{1}{DET}\,[(x_2y_3-x_3y_2)p_1 + (x_3y_1-x_1y_3)p_2 + (x_1y_2-x_2y_1)p_3] \tag{I.6}$$

Since Eqn. (I.1) is linear in x and y, the pressure gradients in the x- and y-direction are constant within a macro-element 123. Hence,

$$\frac{\partial p}{\partial x} = a \tag{I.7}$$

$$\frac{\partial p}{\partial y} = b \tag{I.8}$$

Let v_1 denote the contribution of the macroelement 123 to the subelement control volume surrounding node 1. Then,

$$\int_{v_1} \left(-\frac{\partial p}{\partial x}\right) dV = -v_1\, a \tag{I.9}$$

$$\int_{v_1} \left(-\frac{\partial p}{\partial y}\right) dV = -v_1\, b \tag{I.10}$$

Let

$$D_1^u = \nu_1 \frac{(y_3-y_2)}{DET} \tag{I.11}$$

$$D_2^u = \nu_1 \frac{(y_1-y_3)}{DET} \tag{I.12}$$

$$D_3^u = \nu_1 \frac{(y_2-y_1)}{DET} \tag{I.13}$$

$$D_1^v = \nu_1 \frac{(x_2-x_3)}{DET} \tag{I.14}$$

$$D_2^v = \nu_1 \frac{(x_3-x_1)}{DET} \tag{I.15}$$

$$D_3^v = \nu_1 \frac{(x_1-x_2)}{DET} \tag{I.16}$$

Then, using Eqns. (I.4) to (I.6), Eqns. (I.9) and (I.10) can be rewritten as follows:

$$\int_{\nu_1} \left(-\frac{\partial p}{\partial x}\right) d\nu = D_1^u p_1 + D_2^u p_2 + D_3^u p_3 \tag{I.17}$$

$$\int_{\nu_1} \left(-\frac{\partial p}{\partial y}\right) d\nu = D_1^v p_1 + D_2^v p_2 + D_3^v p_3 \tag{I.18}$$

APPENDIX II

ALGEBRAIC EXPRESSIONS FOR THE CONVECTION-DIFFUSION TRANSPORT OF ϕ ACROSS LATERAL CONTROL-VOLUME SURFACES

The combined convection and diffusion flux of ϕ across the lateral control surface a in Fig. 3.4(a) can be written as follows [2]:

$$\int_a \vec{J}.\vec{n}\, ds \cong -\frac{Y_a \Delta z}{6}\left[(J_X)_o^D + 4(J_X)_r^D + (J_X)_a^D\right] + \frac{X_a \Delta z}{6}\left[(J_Y)_o^D + 4(J_Y)_r^D + (J_Y)_a^D\right] \qquad (II.1)$$

where

$$J_X = \rho U\phi - \Gamma \frac{\partial \phi}{\partial X} \qquad (II.2)$$

$$J_Y = \rho V\phi - \Gamma \frac{\partial \phi}{\partial Y} \qquad (II.3)$$

The element interpolation function for ϕ is:

$$\phi = A\xi + BY + C \qquad (II.4)$$

with

$$\xi = \frac{\Gamma}{\rho U_{av}}\left\{\exp\left[Pe_\Delta\left(\frac{X-X_{max}}{X_{max}-X_{min}}\right)\right]-1\right\} \qquad (II.5)$$

The interpolation constants A, B and C can be expressed in terms of the nodal values of ϕ as follows:

$$A = \frac{1}{DET}\left[(Y_5-Y_6)\phi_1 + (Y_6-Y_1)\phi_5 + (Y_1-Y_5)\phi_6\right] \qquad (II.6)$$

$$B = \frac{1}{DET}\left[(\xi_6-\xi_5)\phi_1 + (\xi_1-\xi_6)\phi_5 + (\xi_5-\xi_1)\phi_6\right] \qquad (II.7)$$

$$C = \frac{1}{DET}\left[(\xi_5Y_6-\xi_6Y_5)\phi_1 + (\xi_6Y_1-\xi_1Y_6)\phi_5 + (\xi_1Y_5-\xi_5Y_1)\phi_6\right] \qquad (II.8)$$

where

$$DET = \xi_1Y_5 + \xi_5Y_6 + \xi_6Y_1 - Y_1\xi_5 - Y_5\xi_6 - Y_6\xi_1$$

Substitution of Eqn. (II.4) into Eqns. (II.2) and (II.3) yields:

$$J_X = \rho(U-U_{av})A\xi + \rho U(BY+C) - \Gamma A \qquad (II.9)$$

$$J_Y = \rho VA\xi + \rho V(BY+C) - \Gamma B \qquad (II.10)$$

Substituting the expressions for A, B and C, Eqns. (II.6) to (II.8), into Eqns. (II.9) and (II.10), and re-arranging the resulting expressions gives:

$$J_X = \{ \frac{\rho}{DET} [f_1\phi_1 + f_5\phi_5 + f_6\phi_6] \}$$

$$+ \{ \frac{\Gamma}{DET} [(Y_6-Y_5)\phi_1 + (Y_1-Y_6)\phi_5 + (Y_5-Y_1)\phi_6] \} \quad \text{(II.11)}$$

$$J_Y = \{ \frac{\rho}{DET} [g_1\phi_1 + g_5\phi_5 + g_6\phi_6]$$

$$+ \{ \frac{\Gamma}{DET} [(\xi_5-\xi_6)\phi_1 + (\xi_6-\xi_1)\phi_5 + (\xi_1-\xi_5)\phi_6] \quad \text{(II.12)}$$

where

$$f_1 = (U-U_{av})(Y_5-Y_6)\xi + U(\xi_6-\xi_5)Y + U(\xi_5Y_6-\xi_6Y_5)$$

$$f_5 = (U-U_{av})(Y_6-Y_1)\xi + U(\xi_1-\xi_6)Y + U(\xi_6Y_1-\xi_1Y_6)$$

$$f_6 = (U-U_{av})(Y_1-Y_5)\xi + U(\xi_5-\xi_1)Y + U(\xi_1Y_5-\xi_5Y_1) \quad \text{(II.13)}$$

$$g_1 = V(Y_5-Y_6)\xi + V(\xi_6-\xi_5)Y + V(\xi_5Y_6-\xi_6Y_5)$$

$$g_5 = V(Y_6-Y_1)\xi + V(\xi_1-\xi_6)Y + V(\xi_6Y_1-\xi_1Y_6)$$

$$g_6 = V(Y_1-Y_5)\xi + V(\xi_5-\xi_1)Y + V(\xi_1Y_5-\xi_5Y_1)$$

Let

$$f_i^a = \frac{1}{6} \{ (f_i)_a + 4(f_i)_r + (f_i)_o \}; \quad \text{(II.14)}$$

$$g_i^a = \frac{1}{6} \{ (g_i)_a + 4(g_i)_r + (g_i)_o \}; \; i = 1, 5, 6$$

Then, Eqns. (II.11) and (II.12) can be substituted into Eqn. (II.1) to obtain the following equation:

$$\int_a \vec{J}.\vec{n}\, ds \;\cong\; -\,(A_1^a\,\phi_1 + A_5^a\,\phi_5 + A_6^a\,\phi_6) \qquad \text{(II.15)}$$

where

$$\left.\begin{aligned} A_1^a &= \frac{\rho\Delta z}{DET}(Y_a f_1^a - X_a g_1^a) + \frac{\Gamma\Delta z}{DET}\{Y_a(Y_6-Y_5) - X_a(\xi_5-\xi_6)\} \\ A_5^a &= \frac{\rho\Delta z}{DET}(Y_a f_5^a - X_a g_5^a) + \frac{\Gamma\Delta z}{DET}\{Y_a(Y_1-Y_6) - X_a(\xi_6-\xi_1)\} \\ A_6^a &= \frac{\rho\Delta z}{DET}(Y_a f_6^a - X_a g_6^a) + \frac{\Gamma\Delta z}{DET}\{Y_a(Y_5-Y_1) - X_a(\xi_1-\xi_5)\} \end{aligned}\right\} \text{(II.16)}$$

Similarly, the convection-diffusion flux of ϕ across the lateral surface c in Fig. 3.4(a), can be approximated by:

$$\int_c \vec{J}.\vec{n}\, ds \;\cong\; \frac{Y_c\Delta z}{6}\,[(J_X)_o^D + 4(J_X)_t^D + (J_X)_c^D] - \frac{X_c\Delta z}{6}\,[(J_Y)_o^D + 4(J_Y)_t^D + (J_Y)_c^D] \qquad \text{(II.17)}$$

Let

$$\left.\begin{aligned} f_i^c &= \frac{1}{6}\{(f_i)_c + 4(f_i)_t + (f_i)_o\}; \\ g_i^c &= \frac{1}{6}\{(g_i)_c + 4(g_i)_t + (g_i)_o\};\ i = 1, 5, 6 \end{aligned}\right\} \text{(II.18)}$$

Then Eqn. (II.17) can be rewritten as follows:

$$\int_C \vec{J}.\vec{n}\, ds \cong (A_1^c \phi_1 + A_5^c \phi_5 + A_6^c \phi_6) \qquad \text{(II.19)}$$

where

$$\left.\begin{aligned} A_1^c &= \frac{\rho\Delta z}{DET}(Y_c f_1^c - X_c g_1^c) + \frac{\Gamma\Delta z}{DET}\{Y_c(Y_6-Y_5) - X_c(\xi_5-\xi_6)\} \\ A_5^c &= \frac{\rho\Delta z}{DET}(Y_c f_5^c - X_c g_5^c) + \frac{\Gamma\Delta z}{DET}\{Y_c(Y_1-Y_6) - X_c(\xi_6-\xi_1)\} \\ A_6^c &= \frac{\rho\Delta z}{DET}(Y_c f_6^c - X_c g_6^c) + \frac{\Gamma\Delta z}{DET}\{Y_c(Y_5-Y_1) - X_c(\xi_1-\xi_5)\} \end{aligned}\right\} \qquad \text{(II.20)}$$

APPENDIX III

ALGEBRAIC EXPRESSIONS FOR THE MACROELEMENT CONTRIBUTION TO THE INTEGRAL MASS CONSERVATION EQUATION

Consider the macroelements and control volume surrounding node 1 in Fig. 3.3(c). The contribution of macroelement 123 to the integral mass conservation equation associated with node 1 can be written as follows:

$$PCONT1 = \left[\int_{U_1} \rho\, \vec{v}.\vec{n}\, ds + \int_{D_1} \rho\, \vec{v}.\vec{n}\, ds + \int_{A} \rho\, \vec{v}.\vec{n}\, ds + \int_{C} \rho\, \vec{v}.\vec{n}\, ds\right] \tag{III.1}$$

Using the interpolation functions for velocity introduced in Chapter III, the different integral terms in the above equation can be approximated as follows:

$$\int_{U_1} \rho\, \vec{v}.\vec{n}\, ds \cong -\frac{A_{123}}{3}\,[\rho w_1]^U \tag{III.2}$$

$$\int_{D_1} \rho\, \vec{v}.\vec{n}\, ds \cong \frac{A_{123}}{3}\,[\rho w_1] \tag{III.3}$$

$$\int_{A} \rho\, \vec{v}.\vec{n}\, ds \cong -\frac{\rho \Delta z}{6}\left[(y_6-y_0)(u_4+u_5+4u_6) - (x_6-x_0)(v_4+v_5+4v_6)\right] \tag{III.4}$$

$$\int_C \rho \vec{v}.\vec{n}\, ds \cong \frac{\rho\Delta z}{6}[(y_5-y_o)(u_4+4u_5+u_6) - (x_5-x_o)(v_4+4v_5+v_6)] \qquad \text{(III.5)}$$

With reference to Fig. 3.8, the pseudovelocity representation of the discretization equations for the velocity components u_4, u_5, u_6, v_4, v_5 and v_6 have the following forms:

$$u_4 = \hat{u}_4 + (\lambda^u_1 p_1 + \lambda^u_2 p_2 + \lambda^u_3 p_3 + \lambda^u_{o1} p_{o1})/a^u_4 \qquad \text{(III.6)}$$

$$u_5 = \hat{u}_5 + (\lambda^u_1 p_1 + \lambda^u_2 p_2 + \lambda^u_3 p_3 + \lambda^u_{o2} p_{o2})/a^u_5 \qquad \text{(III.7)}$$

$$u_6 = \hat{u}_6 + (\lambda^u_1 p_1 + \lambda^u_2 p_2 + \lambda^u_3 p_3 + \lambda^u_{o3} p_{o3})/a^u_6 \qquad \text{(III.8)}$$

and

$$v_4 = \hat{v}_4 + (\lambda^v_1 p_1 + \lambda^v_2 p_2 + \lambda^v_3 p_3 + \lambda^v_{o1} p_{o1})/a^v_4 \qquad \text{(III.9)}$$

$$v_5 = \hat{v}_5 + (\lambda^v_1 p_1 + \lambda^v_2 p_2 + \lambda^v_3 p_3 + \lambda^v_{o2} p_{o2})/a^v_5 \qquad \text{(III.10)}$$

$$v_6 = \hat{v}_6 + (\lambda^v_1 p_1 + \lambda^v_2 p_2 + \lambda^v_3 p_3 + \lambda^v_{o3} p_{o3})/a^v_6 \qquad \text{(III.11)}$$

Let

$$B_i^A = \frac{\rho\Delta z}{6}\left[(y_6-y_o)\left(\frac{\lambda_i^u}{a_4^u}+\frac{\lambda_i^u}{a_5^u}+\frac{4\lambda_i^u}{a_6^u}\right)\right.$$

$$\left. -(x_6-x_o)\left(\frac{\lambda_i^v}{a_4^v}+\frac{\lambda_i^v}{a_5^v}+\frac{4\lambda_i^v}{a_6^v}\right)\right] \qquad \text{(III.12)}$$

and

$$B_i^C = \frac{\rho\Delta z}{6}\left[(y_5-y_o)\left(\frac{\lambda_i^u}{a_4^u}+\frac{4\lambda_i^u}{a_5^u}+\frac{\lambda_i^u}{a_6^u}\right)\right.$$

$$\left. -(x_5-x_o)\left(\frac{\lambda_i^v}{a_4^v}+\frac{4\lambda_i^v}{a_5^v}+\frac{\lambda_i^v}{a_6^v}\right)\right] \qquad \text{(III.13)}$$

with i = 1, 2, and 3; and

$$BO_1^C = \frac{\rho\Delta z}{6}\left[(y_6-y_o)\left(\frac{\lambda_{o1}^u}{a_4^u}\right)-(x_6-x_o)\left(\frac{\lambda_{o1}^v}{a_4^v}\right)\right] \qquad \text{(III.14)}$$

$$BO_2^C = \frac{\rho\Delta z}{6}\left[(y_6-y_o)\left(\frac{\lambda_{o2}^u}{a_5^u}\right)-(x_6-x_o)\left(\frac{\lambda_{o2}^v}{a_5^v}\right)\right] \qquad \text{(III.15)}$$

$$BO_3^C = \frac{\rho\Delta z}{6}\left[(y_6-y_o)\left(\frac{4\lambda_{o3}^u}{a_6^u}\right)-(x_6-x_o)\left(\frac{4\lambda_{o3}^v}{a_6^v}\right)\right] \qquad \text{(III.16)}$$

$$BO_1^C = \frac{\rho\Delta z}{6}\left[(y_5-y_o)\left(\frac{\lambda_{o1}^u}{a_4^u}\right)-(x_5-x_o)\left(\frac{\lambda_{o1}^v}{a_4^v}\right)\right] \qquad \text{(III.17)}$$

$$BO_2^C = \frac{\rho\Delta z}{6}\left[(y_5-y_O)\left(\frac{4\lambda_{o2}^u}{a_5^u}\right) - (x_5-x_O)\left(\frac{\lambda_{o2}^v}{a_5^v}\right)\right] \qquad \text{(III.18)}$$

$$BO_3^C = \frac{\rho\Delta z}{6}\left[(y_5-y_O)\left(\frac{\lambda_{o3}^u}{a_6^u}\right) - (x_5-x_O)\left(\frac{\lambda_{o3}^v}{a_6^v}\right)\right] \qquad \text{(III.19)}$$

Further, let

$$G^A = \frac{\rho\Delta z}{6}\left[(y_6-y_O)(\hat{u}_4+\hat{u}_5+4\hat{u}_6) - (x_6-x_O)(\hat{v}_4+\hat{v}_5+4\hat{v}_6)\right] \qquad \text{(III.20)}$$

and

$$G^C = \frac{\rho\Delta z}{6}\left[(y_5-y_O)(\hat{u}_4+4\hat{u}_5+\hat{u}_6) + (x_5-x_O)(\hat{v}_4+4\hat{v}_5+\hat{v}_6)\right] \qquad \text{(III.21)}$$

Then Eqns. (III.6) to (III.11) can be substituted into Eqns. (III.4) and (III.5), and the resultant expression can be rearranged to yield:

$$\int_A \rho\,\vec{v}.\vec{n}\,ds = -\left[B_1^A p_1 + B_2^A p_2 + B_3^A p_3 + BO_1^A p_{o1} + BO_2^A p_{o2} + BO_3^A p_{o3} + G^A\right] \qquad \text{(III.22)}$$

and

$$\int_C \rho\,\vec{v}.\vec{n}\,ds = \left[B_1^C p_1 + B_2^C p_2 + B_3^C p_3 + BO_1^C p_{o1} + BO_2^C p_{o2} + BO_3^C p_{o3} + G^C\right] \qquad \text{(III.23)}$$

Summing up the different integral terms given in Eqns. (III.2), (III.3), (III.22) and (III.23), the total contribution of macroelement 123 to the integral mass conservation equation associated with node 1 can be compactly expressed as:

$$PCONT1 = MP_1^1 p_1 + MP_2^1 p_2 + MP_3^1 p_3 + MP_{o1}^1 p_{o1} + MP_{o2}^1 p_{o2} + MP_{o3}^1 p_{o3} + MPCON1 \qquad \text{(III.24)}$$

where

$$MP_1^1 = -B_1^A + B_1^C$$

$$MP_2^1 = -B_2^A + B_2^C$$

$$MP_3^1 = -B_3^A + B_3^C$$

$$MP_{o1}^1 = -BO_1^A + BO_1^C \qquad \text{(III.25)}$$

$$MP_{o2}^1 = -BO_2^A + BO_2^C$$

$$MP_{o3}^1 = -BO_3^A + BO_3^C$$

$$MPCON1 = -G^A + G^C + \frac{\rho A_{123}}{3}(w_1 - w_1^U)$$

The total contributions of macroelement 123 to the integral mass conservation equations associated with nodes 2 and 3 can be derived in a similar manner.

APPENDIX IV

SHORT DESCRIPTION AND LISTING OF THE COMPUTER PROGRAM

The computer program developed in this work has been given the name CVFEM3DP. In its present form, it can solve three-dimensional parabolic flow and heat transfer either in a rectangular duct or over an infinite triangular rod-bundle array; details of these problems can be found in Chapters V and VI.

A short description of CVFEM3DP and the main functions of its various subroutines are given below:

MAIN — Controls the program operations. It incorporates a dump/restart facility whereby the user may save the results of intermediate iterations, or steps, on external disk files. The impending operations can then be resumed later by retrieving the saved data.

USER — This subroutine allows the user to specify the details of the problem of interest. It is composed of the following entry points:

- GRID — Generates the duct cross-sectional grid and all other topological information.
- START — Specifies all control parameters and the initial conditions.
- OUTPUT — Prints out the intermediate and final results.

DENSE Specifies the fluid density in the calculation domain.

GAMSOR Specifies the diffusion coefficient Γ and the source term coefficients S_C and S_P.

BOUND Specifies the boundary conditions for all dependent variables.

BTSVEL Specifies the boundary conditions for the pseudovelocities $\hat{u}$, $\hat{v}$ and $\hat{w}$.

NUCALC Computes $Nu_{z,(T)}$ and $Nu_{z,(H)}$.

RESET Allows the user to reset the values of some control parameters when using the restart option.

SUPPLY Set of utility algorithms.

COEFF General subroutine which calculates the subelement contributions and assembles them to form the sets of discretization equations for u, v, w, T and ϕ.

PAPC General subroutine which calculates the macroelement contributions and assembles them to form the sets of discretization equations for the pressure p and the pressure correction p'.

SOLVE General subroutine which solves the sets of discretization equations for u, v, w, T and ϕ.

PSOLVE General subroutine which solves the sets of discretization equations for p and p'.

TEST Allows the printing of coefficients and intermediate results for testing purposes.

A complete listing of CVFEM3DP is given in the following pages. The program is written in the FORTRAN IV language and designed to be compiled by a FORTRAN-H extended compiler.

```
//ME68THRD JOB (ME68,000,040,0200,0000,30,,1),'TRI PHAM'
// EXEC FORTXCG
//FORT.SYSIN DD *
C-------------------------------------------------------------------C
C                                                                   C
C            C O N T R O L - V O L U M E                            C
C                                                                   C
C                 F I N I T E - E L E M E N T  M E T H O D          C
C                                                                   C
C                   F O R                                           C
C                                                                   C
C                         T H R E E - D I M E N S I O N A L         C
C                                                                   C
C                              P A R A B O L I C  F L O W S         C
C                                                                   C
C                   A N D                                           C
C                                                                   C
C                         H E A T  T R A N S F E R                  C
C                                                                   C
C                                                                   C
C                                                                   C
C     (CVFEM3DP)    COMPLETED AT  MCGILL UNIVERSITY  1983           C
C                                                                   C
C                                                                   C
C-------------------------------------------------------------------C
C     **********************
C     PROGRAM MAIN (CONTROL)
C     **********************
C
      IMPLICIT REAL*8(A-H,O-Z)
      LOGICAL LSOLVE,LCPRIN,LPRINT,LPPRIN
C-----------------------------------------------------------------------
      COMMON ASTORE(3528),X(21,21),Y(21,21),F(21,21,7),FU(21,21,7),
     1 FP(11,11,2),RHO(21,21),GAM(21,21),
     2 SC(21,21),SP(21,21),ACU(21,21),UHAT(21,21),
     3 D1T1(10,10,2),D2T1(10,10,2),D3T1(10,10,2),
     4 D1T2(10,10,2),D2T2(10,10,2),D3T2(10,10,2)
      COMMON /THRD/Z,DZ,DPDZ,DPDZC,PBAR,SPMF,WFD,CNUFD(4),LSTEP,ISTEP,
     1 ITMAX,ISTART,IPROB
      COMMON /PARM/RELAX(7),PRELAX
      COMMON /MONIT/LSOLVE(7),LCPRIN,LPRINT(7),LPPRIN
      COMMON /LABEL/TITLE(7),HDG(9)
      COMMON /INDX/NSWP(7),NPSWP(2),L1,L2,L3,M1,M2,M3,
     1 LP1,LP2,LP3,MP1,MP2,MP3,NFS,NFSMAX,NPS,NUME,IMONIT,LAST,
     2 LMID,MMID,LPMID,MPMID,IPREF,JPREF,ITER,IC(3),JC(3),IDEAL,
     3 IR,IRP1,IRM1,JR,JRP1,JRM1,IPR,IPRP1,IPRP2,IPRM1,IPRM2,JPR,JPRP1,
     4 JPRP2,JPRM1,JPRM2,NITMAX(7),NPITMX(2)
      COMMON /CONV/TOL(7),PTOL(2),DWDES,FCK(3,2),DPDZCK,CHGTOL,CHGCK
      COMMON /RODBUN/S,RAD,SDR,WBAR,FAREA,PERIM,PHY,DH,DHDR,XL,YL,TANPSI
     1 ,PSI,FBU4,FBU6,FB,FWAV,RHOA,CP1,DK1,DKDCP1,CP2,DK2,DKDCP2,
     2 RPOW,XPOW,YPOW,DMUA,REY,QW, TAUW(21),TW,TI
      COMMON /RESULT/TABLE(200,7)
C-----------------------------------------------------------------------
      DIMENSION W(21,21),WCK(3)
      DIMENSION P(11,11),PC(11,11)
      EQUIVALENCE (F(1,1,3),W(1)),(FP(1),P(1)),(FP(1,1,2),PC(1))
C-----------------------------------------------------------------------
C
```

```
C     RESTART FACILITY  ISTART = 1  -----> START FROM STEP 1, ITER 1
C                               2  -----> START FROM STEP=ISTEP
C                                         ITER=ITER+1
C                               3  -----> START FROM STEP=ISTEP+1,
C                                         ITER 1
      READ(5,5) ISTART
      GOTO (20,22,22),ISTART
C
C---  READ PREVIOUS ANALYSES DATA ON DISK (CHANNEL 9)
C
22    READ(9) X,Y,F,FU,FP,D1T1,D2T1,D3T1,D1T2,D2T2,D3T2,RELAX,PRELAX,
     1 Z,DZ,DPDZ,PBAR,SPMF,XL,YL,TITLE,TOL,PTOL,DWDES,CHGTOL,PR,ODPR,
     2 FBU4,FBU6,ZNM2,ZNM1,WNM2,WNM1,RHOA,CP1,DK1,DKDCP1,DMUA,REY,QW,
     3 CP2,DK2,DKDCP2,S,RAD,SDR,FAREA,PERIM,PHY,DH,DHDR,HDG,WFD,CNUFD,
     4 DNUDES,TW,TI,TABLE,PSI,TANPSI,IPROB,NSWP,NPSWP,L1,L2,L3,M1,M2,M3,
     5 LP1,LP2,LP3,MP1,MP2,MP3,NFSMAX,IMONIT,LAST,LMID,MMID,
     6 LPMID,MPMID,ITER,IPREF,JPREF,ISTEP,ITMAX,LSTEP,IC,JC,IDEAL,
     7 IR,IRP1,IRM1,JR,JRP1,JRM1,IPR,IPRP1,IPRP2,IPRM1,IPRM2,JPR,
     8 JPRP1,JPRP2,JPRM1,JPRM2,NITMAX,NPITMX,NFSMT,
     9 LSOLVE,LCPRIN,LPRINT,LPPRIN
C
C---  RESET CONTROL PARAMETERS
C
      CALL RESET
      CALL PRTINP
      IF (ISTART.EQ.3) GOTO 9
      GOTO 10
C
C---  NEW START (ISTEP=1;ITER=1)
C
20    CALL DEFVAL
      CALL GRID
      CALL START
      CALL PRTINP
C-----------------------------------------------------------------------
C
C---  START NEW STEP
C
9     ISTEP=ISTEP+1
C
C---  SOLVE FOR THE FLOW FIELD FIRST
C
      NFSMT=NFSMAX
      NFSMAX=3
C
C---  REDUCE P AND PC BY THEIR AVERAGE VALUE
C
      PAV=0.DO
      PCAV=0.DO
      DO 18 JP=1,MP1
      DO 18 IP=1,LP1
      PAV=PAV+P(IP,JP)
18    PCAV=PCAV+PC(IP,JP)
      PAV=PAV/DFLOAT(LP1*MP1)
      PCAV=PCAV/DFLOAT(LP1*MP1)
      DO 70 JP=1,MP1
      DO 70 IP=1,LP1
      P(IP,JP)=P(IP,JP)-PAV
```

```
70    PC(IP,JP)=PC(IP,JP)-PCAV
C
      DO 8 NF=1,NFSMT
      DO 8 J=1,M1
      DO 8 I=1,L1
8     FU(I,J,NF)=F(I,J,NF)
C
C---  DZ STEP SELECTOR
C
      IF (ISTEP.GT.3) CALL DZSEL
      Z=Z+DZ
15    WRITE(6,35) ISTEP,Z,DZ
      TABLE(ISTEP,1)=Z
      ITER=0
C
10    CONTINUE
      ITER=ITER+1
      WRITE(6,30) ITER
C
C---  OVERALL LOOP CONVERGENCE MONITOR
C
      DO 12 NF=1,2
      DO 12 N=1,3
12    FCK(N,NF)=F(IC(N),JC(N),NF)
      DO 16 N=1,3
16    WCK(N)=F(IC(N),JC(N),3)
      DPDZCK=DPDZ
C
C---  FORM DISCRETIZATION EQUATIONS AND SOLVE
C
      CALL COEFF
C
C
C---  CONVERGENCE CHECK (BASED ON THE MAXIMUM
C     CHANGE IN U, V, W  AND DP/DZ)
C
      IF (ISTEP.EQ.1.AND.ITER.EQ.1) GOTO 50
      CHGCK=0.D0
      DO 700 NF=1,2
      DO 700 N=1,2
700   CHGCK=DMAX1(CHGCK,DABS((F(IC(N),JC(N),NF)-FCK(N,NF))/FCK(N,NF)))
      DO 710 N=1,3
710   CHGCK=DMAX1(CHGCK,DABS((F(IC(N),JC(N),3)-WCK(N))/WCK(N)))
      CHGCK=DMAX1(CHGCK,DABS((DPDZ-DPDZCK)/DPDZCK))
      WRITE(6,300) CHGCK,W(L1,M1)
C
      IF (CHGCK.LE.CHGTOL) GOTO 14
C
50    IF (ITER.LT.ITMAX) GOTO 10
      GOTO 25
C
C---  AT THIS POINT, THE FLOW FIELD AT ISTEP MAY BE CONSIDERED CONVERGED
C---  TACKLE THE HEAT TRANSFER PROBLEMS NOW
C
14    CONTINUE
      PBAR=PBAR+DPDZ*DZ
      TABLE(ISTEP,2)=PBAR
      TABLE(ISTEP,3)=W(L1,M1)
```

```
C
      NFSMAX=NFSMT
      LSOLVE(1)=.FALSE.
      LSOLVE(2)=.FALSE.
      LSOLVE(3)=.FALSE.
C
C---  MONITOR THE TEMPERATURE PROBLEM
C
      IMONTT=IMONIT
      IMONIT=1
C
C---  FORM THE DISCRETIZATION EQUATIONS FOR TEMPERATURE AND SOLVE
C
      CALL COEFF
      IMONIT=IMONTT
C
C---  CALCULATE THE NUSSELT NUMBER CORRESPONDING TO THE DIFFERENT
C---  TEMPERATURE PROBLEMS
C
      CALL NUCALC
C
      CALL OUTPUT
C
C---  RESET CONTROL PARAMETERS FOR NEXT STEP . SOLVE FOR THE
C---  FLOW FIELD FIRST - THEN THE FOUR HEAT TRANSFER PROBLEMS
C
      LSOLVE(1)=.TRUE.
      LSOLVE(2)=.TRUE.
      LSOLVE(3)=.TRUE.
      IF (W(L1,M1).GE.(.99DO*WFD)) GOTO 27
      IF (ISTEP.LT.LSTEP) GOTO 9
C
C---  DUMP DATA ON DISK (CHANNEL 10)
C
27    WRITE(10)X,Y,F,FU,FP,D1T1,D2T1,D3T1,D1T2,D2T2,D3T2,RELAX,PRELAX,
     1 Z,DZ,DPDZ,PBAR,SPMF,XL,YL,TITLE,TOL,PTOL,DWDES,CHGTOL,PR,ODPR,
     2 FBU4,FBU6,ZNM2,ZNM1,WNM2,WNM1,RHOA,CP1,DK1,DKDCP1,DMUA,REY,QW,
     3 CP2,DK2,DKDCP2,S,RAD,SDR,FAREA,PERIM,PHY,DH,DHDR,HDG,WFD,CNUFD,
     4 DNUDES,TW,TI,TABLE,PSI,TANPSI,IPROB,NSWP,NPSWP,L1,L2,L3,M1,M2,M3,
     5 LP1,LP2,LP3,MP1,MP2,MP3,NFSMAX,IMONIT,LAST,LMID,MMID,
     6 LPMID,MPMID,ITER,IPREF,JPREF,ISTEP,ITMAX,LSTEP,IC,JC,IDEAL,
     7 IR,IRP1,IRM1,JR,JRP1,JRM1,IPR,IPRP1,IPRP2,IPRM1,IPRM2,JPR,
     8 JPRP1,JPRP2,JPRM1,JPRM2,NITMAX,NPITMX,NFSMT,
     9 LSOLVE,LCPRIN,LPRINT,LPPRIN
      WRITE (6,40) ISTEP,ITER
      STOP
C
C---  AFTER ITMAX ITERATIONS, THE FLOW FIELD HAS NOT CONVERGED
C---  DUMP IMPENDING DATA ON DISK FOR RESTART WITH MORE ITERATIONS
C
25    WRITE(6,100) ITMAX
      GOTO 27
C-----------------------------------------------------------------------
C
C---  FORMAT STATEMENTS
C
5     FORMAT(I1)
30    FORMAT(///,3X,'******************',/3X,
```

```
     1 '*',16X,'*',/3X,              '* ITERATION ',I4,' *',
     2 /3X,'*',16X,'*',/3X,18('*'))
35    FORMAT(//////,1X,131('='),//3X,'ISTEP = ',I3,//3X,'Z  = ',
     1 1PD15.7,//,3X,'DZ = ',1PD15.7,//)
40    FORMAT(////45X,44('*'),
     1 /,45X,'*',42X,'*',
     2 /,45X,'*',    'DATA DUMPED ON RECORD 10 FOR ISTEP = ',I3,2X,'*',
     3 /,45X,'*',    '                                    ITER  = ',I3,2X,'*',
     4 /,45X,'*',42X,'*',/,45X,44('*'))
100   FORMAT(///7X,'MAXIMUM NUMBER OF ITERATIONS = ',I3,' EXCEEDED')
300   FORMAT(/3X,'MAX. CHANGE IN (U, V ,W  , DP/DZ) = ',1PD15.7,
     1 2X,'CENTRE POINT W = ',1PD15.7)
      END
C*********************************************************************
      SUBROUTINE DZSEL
C*********************************************************************
      IMPLICIT REAL*8(A-H,O-Z)
      LOGICAL LSOLVE,LCPRIN,LPRINT,LPPRIN
C---------------------------------------------------------------------
      COMMON ASTORE(3528),X(21,21),Y(21,21),F(21,21,7),FU(21,21,7),
     1 FP(11,11,2),RHO(21,21),GAM(21,21),
     2 SC(21,21),SP(21,21),ACU(21,21),UHAT(21,21),
     3 D1T1(10,10,2),D2T1(10,10,2),D3T1(10,10,2),
     4 D1T2(10,10,2),D2T2(10,10,2),D3T2(10,10,2)
      COMMON /THRD/Z,DZ,DPDZ,DPDZC,PBAR,SPMF,WFD,CNUFD(4),LSTEP,ISTEP,
     1 ITMAX,ISTART,IPROB
      COMMON /PARM/RELAX(7),PRELAX
      COMMON /MONIT/LSOLVE(7),LCPRIN,LPRINT(7),LPPRIN
      COMMON /LABEL/TITLE(7),HDG(9)
      COMMON /INDX/NSWP(7),NPSWP(2),L1,L2,L3,M1,M2,M3,
     1 LP1,LP2,LP3,MP1,MP2,MP3,NFS,NFSMAX,NPS,NUME,IMONIT,LAST,
     2 LMID,MMID,LPMID,MPMID,IPREF,JPREF,ITER,IC(3),JC(3),IDEAL,
     3 IR,IRP1,IRM1,JR,JRP1,JRM1,IPR,IPRP1,IPRP2,IPRM1,IPRM2,JPR,JPRP1,
     4 JPRP2,JPRM1,JPRM2,NITMAX(7),NPITMX(2)
      COMMON /CONV/TOL(7),PTOL(2),DWDES,FCK(3,2),DPDZCK,CHGTOL,CHGCK
      COMMON /RODBUN/S,RAD,SDR,WBAR,FAREA,PERIM,PHY,DH,DHDR,XL,YL,TANPSI
     1 ,PSI,FBU4,FBU6,FB,FWAV,RHOA,CP1,DK1,DKDCP1,CP2,DK2,DKDCP2,
     2 RPOW,XPOW,YPOW,DMUA,REY,QW, TAUW(21),TW,TI
      COMMON /RESULT/TABLE(200,7)
C
C---  DZ SELECTION USING A LINEAR EXTRAPOLATION
C
      ZNM1=TABLE(ISTEP-1,1)
      ZNM2=TABLE(ISTEP-2,1)
      WNM1=TABLE(ISTEP-1,3)
      WNM2=TABLE(ISTEP-2,3)
      C1=(WNM2-WNM1)/(ZNM2-ZNM1)
      C2=WNM2-C1*ZNM2
      IF ((WNM1+DWDES).GT.WFD) DWDES=WFD-WNM1
      DZ=(WNM1+DWDES-C2)/C1-ZNM1
      RETURN
      END
C*********************************************************************
      SUBROUTINE USER
C*********************************************************************
C
C     USER SPECIFIED PROGRAM
C     ----------------------
```

```
C
C         NAME                    DESCRIPTION
C         ----                    -----------
C         GRID              GRID  SPECIFICATION
C         START             INPUT CONTROL PARAMETERS
C                           AND INITIALIZATION OF DEPENDENT VARIABLE
C                           ARRAYS (+INITIAL CONDITIONS)
C         OUTPUT            PRINTS OUTPUT
C         DENSE             SPECIFIES DENSITY VALUES FOR EACH SUBELEMENT
C         GAMSOR            SPECIFIES VALUES FOR GAMMA AND SC AND SP
C                           FOR EACH SUBELEMENT
C         BOUND             SPECIFIES THE BOUNDARY CONDITIONS
C         BTSVEL            TREATMENT OF PSEUDOVELOCITIES AT THE
C                           BOUNDARY
C         PBOUND            BOUNDARY CONDITIONS FOR PRESSURE
C         FLUX              CALCULATES THE FLUX AT WALL BOUNDARIES
C
C-----------------------------------------------------------------------
      IMPLICIT REAL*8(A-H,O-Z)
      LOGICAL LSOLVE,LCPRIN,LPRINT,LPPRIN
      COMMON ASTORE(3528),X(21,21),Y(21,21),F(21,21,7),FU(21,21,7),
     1 FP(11,11,2),RHO(21,21),GAM(21,21),
     2 SC(21,21),SP(21,21),ACU(21,21),UHAT(21,21),
     3 D1T1(10,10,2),D2T1(10,10,2),D3T1(10,10,2),
     4 D1T2(10,10,2),D2T2(10,10,2),D3T2(10,10,2)
      COMMON /THRD/Z,DZ,DPDZ,DPDZC,PBAR,SPMF,WFD,CNUFD(4),LSTEP,ISTEP,
     1 ITMAX,ISTART,IPROB
      COMMON /PARM/RELAX(7),PRELAX
      COMMON /MONIT/LSOLVE(7),LCPRIN,LPRINT(7),LPPRIN
      COMMON /LABEL/TITLE(7),HDG(9)
      COMMON /INDX/NSWP(7),NPSWP(2),L1,L2,L3,M1,M2,M3,
     1 LP1,LP2,LP3,MP1,MP2,MP3,NFS,NFSMAX,NPS,NUME,IMONIT,LAST,
     2 LMID,MMID,LPMID,MPMID,IPREF,JPREF,ITER,IC(3),JC(3),IDEAL,
     3 IR,IRP1,IRM1,JR,JRP1,JRM1,IPR,IPRP1,IPRP2,IPRM1,IPRM2,JPR,JPRP1,
     4 JPRP2,JPRM1,JPRM2,NITMAX(7),NPITMX(2)
      COMMON /CONV/TOL(7),PTOL(2),DWDES,FCK(3,2),DPDZCK,CHGTOL,CHGCK
      COMMON /RODBUN/S,RAD,SDR,WBAR,FAREA,PERIM,PHY,DH,DHDR,XL,YL,TANPSI
     1 ,PSI,FBU4,FBU6,FB,FWAV,RHOA,CP1,DK1,DKDCP1,CP2,DK2,DKDCP2,
     2 RPOW,XPOW,YPOW,DMUA,REY,QW, TAUW(21),TW,TI
      COMMON /RESULT/TABLE(200,7)
C---  DIMENSION AND EQUIVALENCE STATEMENTS
C
      DIMENSION AC(21,21),AE(21,21),ANE(21,21),AN(21,21),
     1 AW(21,21),ASW(21,21),AS(21,21),ACON(21,21)
      DIMENSION APC(11,11),APE(11,11),APNE(11,11),APN(11,11),
     1 APNW(11,11),APW(11,11),APSW(11,11),APS(11,11),APSE(11,11),
     2 APENE(11,11),APNNE(11,11),APWSW(11,11),APSSW(11,11),APCON(11,11)
      DIMENSION U(21,21),V(21,21),W(21,21),WU(21,21),P(11,11),PC(11,11),
     1 VHAT(21,21),ACV(21,21),WHAT(21,21)
      EQUIVALENCE (ASTORE(1),AC(1)),(ASTORE(442),AE(1)),(ASTORE( 883),
     1 ANE(1)),(ASTORE(1324),AN(1)),(ASTORE(1765),AW(1)),
     2 (ASTORE(2206),ASW(1)),(ASTORE(2647),AS(1)),(ASTORE(3088),
     3 ACON(1))
      EQUIVALENCE (ASTORE(1),APC(1)),(ASTORE(122),APE(1)),(ASTORE(243),
     1 APNE(1)),(ASTORE(364),APN(1)),(ASTORE(485),APNW(1)),
     2 (ASTORE(606),APW(1)),(ASTORE( 727),APSW(1)),(ASTORE( 848),
     3 APS(1)),(ASTORE( 969),APSE(1)),(ASTORE(1090),APENE(1)),
     4 (ASTORE(1211),APNNE(1)),(ASTORE(1332),APWSW(1)),
```

```
     5 (ASTORE(1453),APSSW(1)),(ASTORE(1574),APCON(1))
      EQUIVALENCE (F(1),U(1)),(F(1,1,2),V(1)),(F(1,1,3),W(1))
      EQUIVALENCE (FU(1,1,3),WU(1))
      EQUIVALENCE (FP(1),P(1)),(FP(1,1,2),PC(1))
      EQUIVALENCE (SC(1),VHAT(1)),(SP(1),ACV(1)),(SC(1),WHAT(1))
C
C---  ADDITIONAL DIMENSION AND EQUIVALENCE STATEMENTS
C
      DIMENSION ACB(21),AEB(21),ANEB(21),ANB(21),
     1 ASB(21),ACONB(21)
      DIMENSION CVAREA(21,21)
      EQUIVALENCE (ACU(1),CVAREA(1))
C-----------------------------------------------------------------------
C
C
C     **********
      ENTRY GRID
C     **********
C
C---  READ PROBLEM AND GRID SPECIFICATIONS (CHANNEL 5)
C
      READ(5,1010) HDG
      READ(5,1020) IPROB,LP1,MP1
      IF (IPROB.EQ.1) READ(5,1030) XL,YL,XPOW,YPOW
      IF (IPROB.EQ.2) READ(5,1030) RAD,SDR,PSI,RPOW
      READ(5,1040) (TITLE(NF),NF=1,7)
C
C---  CONVERT PSI TO RADIANS
C
      PHY=DATAN(1.0D0)*4.0D0
      PSI=PSI/180.D0*PHY
      CALL GRIDCT
      CALL DEFGRD
C
C---  GENERATE THE VELOCITY NODES AND D COEFFICIENTS
C
      CALL DCALC
      RETURN
C-----------------------------------------------------------------------
C     ***********
      ENTRY START
C     ***********
C
C---  PROBLEM SPECIFICATION
C
      WFD=2.123D0
      REY=1.D3
      DMUA=20.D-6
      WBAR=1.D0
      RHOA=REY*DMUA/WBAR/DH
      DK1=0.0265D0
      DK2=0.0651D0
      CP1=DK1*0.72D0/DMUA
      CP2=DK2*3.D0/DMUA
      DKDCP1=DK1/CP1
      DKDCP2=DK2/CP2
      QW=200.D0
      SPMF=RHOA*FAREA
```

```
      TW=60.DO
      TI=20.DO
C
C---  INITIAL STEP SIZE
C
      DZ=1.7511905D-5
      IDEAL=25
      Z=O.DO
      ISTEP=0
C
C---  CONTROL PARAMETERS
C
      LSTEP=1
      ITMAX=10
      LSOLVE(1)=.TRUE.
      LSOLVE(2)=.TRUE.
      LSOLVE(3)=.TRUE.
      LSOLVE(4)=.TRUE.
      LSOLVE(5)=.TRUE.
      LSOLVE(6)=.TRUE.
      LSOLVE(7)=.TRUE.
      NFSMAX=7
      LPRINT(1)=.TRUE.
      LPRINT(2)=.TRUE.
      LPRINT(3)=.TRUE.
      LPRINT(4)=.TRUE.
      LPRINT(5)=.TRUE.
      LPRINT(6)=.TRUE.
      LPRINT(7)=.TRUE.
      LPPRIN=.TRUE.
      LCPRIN=.TRUE.
C
      RELAX(1)=0.5DO
      RELAX(2)=0.5DO
      RELAX(3)=0.7DO
      RELAX(4)=1.DO
      RELAX(5)=1.DO
      RELAX(6)=1.DO
      RELAX(7)=1.DO
      PRELAX=0.8D0
      IMONIT=1
      CALL MONCON
C
      CHGTOL=1.D-4
      DWDES=(WFD-1.DO)/DFLOAT(IDEAL)
C
      NITMAX(4)=30
      NITMAX(5)=30
      NITMAX(6)=30
      NITMAX(7)=30
      NSWP(1)=1
      NSWP(2)=1
      NSWP(3)=1
      NSWP(4)=5
      NSWP(5)=5
      NSWP(6)=5
      NSWP(7)=5
      NPSWP(1)=1
```

```
      NPSWP(2)=5
      NPITMX(1)=10
      NPITMX(2)=20
      TOL(4)=1.D-12
      TOL(5)=1.D-12
      TOL(6)=1.D-12
      TOL(7)=1.D-12
      PTOL(1)=1.D-6
      PTOL(2)=1.D-6
C
C---  INITIAL CONDITIONS AND INITIALIZATION OF DEPENDENT VARIABLES
C
      DO 100 I=1,L1
      DO 100 J=1,M1
      U(I,J)=0.D0
      FU(I,J,1)=0.D0
      V(I,J)=0.D0
      FU(I,J,2)=0.D0
100   CONTINUE
C
C---  ASSIGN INITIAL W-VALUES
C
      DO 50 J=1,M1
      DO 50 I=2,L1
50    WU(I,J)=1.D0
      DO 70 J=1,M1
70    WU(1,J)=0.D0
C
C---  INITIAL CONDITION FOR THE RECTANGULAR DUCT
C
      IF (IPROB.NE.1) GOTO 80
      DO 85 I=1,L1
85    WU(I,1)=0.D0
C
C---  CORRECTION OF THE W-VELOCITIES TO YIELD THE CORRECT MASS FLUX
C
80    CALMF=0.D0
      DO 110 J=1,M2
      JP1=J+1
      DO 110 I=1,L2
      IP1=I+1
      DET=X(I,J)*Y(IP1,J)+X(IP1,J)*Y(IP1,JP1)+X(IP1,JP1)*Y(I,J)
     1   -Y(I,J)*X(IP1,J)-Y(IP1,J)*X(IP1,JP1)-Y(IP1,JP1)*X(I,J)
      EVOL=DABS(DET)/6.D0
      CALMF=CALMF+(WU(I,J)+WU(IP1,J)+WU(IP1,JP1))*EVOL
      DET=X(I,J)*Y(IP1,JP1)+X(IP1,JP1)*Y(I,JP1)+X(I,JP1)*Y(I,J)
     1   -Y(I,J)*X(IP1,JP1)-Y(IP1,JP1)*X(I,JP1)-Y(I,JP1)*X(I,J)
      EVOL=DABS(DET)/6.D0
110   CALMF=CALMF+(WU(I,J)+WU(IP1,JP1)+WU(I,JP1))*EVOL
      CALMF=CALMF*RHOA
      FAC=SPMF/CALMF
      WRITE(6,112) CALMF,SPMF,FAC
112   FORMAT(//3X,'CALMF = ',1PD15.7,//3X,'SPMF = ',1PD15.7,
     1 //3X,'FAC = ',1PD15.7)
      DO 120 J=1,M1
      DO 120 I=1,L1
120   WU(I,J)=WU(I,J)*FAC
      DO 130 J=1,M1
```

```
      DO 130 I=1,L1
130   W(I,J)=WU(I,J)
C
C---  HEAT TRANSFER PROBLEM
C
C
      DO 150 J=1,M1
      DO 150 I=2,L1
      FU(I,J,4)=TI
150   FU(I,J,6)=TI
      DO 154 J=1,M1
      FU(1,J,4)=TW
154   FU(1,J,6)=TW
      IF (IPROB.NE.1) GOTO 158
      DO 156 I=1,L1
      FU(I,1,4)=TW
156   FU(I,1,6)=TW
158   DO 160 J=1,M1
      DO 160 I=1,L1
      F(I,J,4)=FU(I,J,4)
      F(I,J,6)=FU(I,J,6)
      FU(I,J,5)=TI
      FU(I,J,7)=TI
      F(I,J,5)=TI
160   F(I,J,7)=TI
C
C---  BULK TEMPERATURE CALCULATION
C
      DO 175 NFS=4,6,2
      CALL BULK
      IF (NFS.EQ.4) FBU4=FB
      IF (NFS.EQ.6) FBU6=FB
175   CONTINUE
      DO 105 JP=1,MP1
      DO 105 IP=1,LP1
      P(IP,JP)=0.D0
105   PC(IP,JP)=0.D0
      PBAR=0.D0
      RETURN
C-------------------------------------------------------------------------
C     ************
      ENTRY OUTPUT
C     ************
      CALL PRINT
      ZSTAR=Z/DH/REY
      PBSTAR=PBAR/(0.5D0*RHOA)
      WRITE(6,205) ZSTAR,PBSTAR
205   FORMAT(/3X,'ZSTAR = ',1PD15.7,/3X,'PBSTAR = ',1PD15.7)
      WRITE(6,210)
210   FORMAT(///'1',13X,'SUMMARY OF RESULTS' /,
     1 2X,'ISTEP',7X,'Z/DH/REY   ',
     1 6X,' PBARSTAR  ',6X,'  W(L1,M1) ',6X,'NUSSELT(4)',6X,
     1 'NUSSELT(5) ',6X,'NUSSELT(6) ',6X,'NUSSELT(7)'/,2X,125('-'))
      DO 220 IS=1,ISTEP
      ZSTAR=TABLE(IS,1)/DH/REY
      PBSTAR=TABLE(IS,2)/0.5D0/RHOA
220   WRITE(6,230) IS,ZSTAR,PBSTAR,(TABLE(IS,JT),JT=3,7)
230   FORMAT(2X,I5,3X,7(1PD15.7,2X))
```

```
      RETURN
C-----------------------------------------------------------------------
C     ***********
      ENTRY DENSE
C     ***********
      DO 300 I=1,L2
      DO 300 J=1,M2
      RHO(I,J)=RHOA
300   CONTINUE
      RETURN
C-----------------------------------------------------------------------
C     ************
      ENTRY GAMSOR
C     ************
      DO 400 J=1,M2
      DO 400 I=1,L2
      SC(I,J)=0.D0
400   SP(I,J)=0.D0
      IF (NFS.GE.4) GOTO 410
      DO 420 J=1,M2
      DO 420 I=1,L2
420   GAM(I,J)=DMUA
      RETURN
410   DKDCP=DKDCP1
      IF (NFS.GE.6) DKDCP=DKDCP2
      DO 430 J=1,M2
      DO 430 I=1,L2
430   GAM(I,J)=DKDCP
      RETURN
C-----------------------------------------------------------------------
C     ***********
      ENTRY BOUND
C     ***********
      IF (IPROB.EQ.1) GOTO 570
      GOTO (505,505,503,503,552,503,554),NFS
503   DO 502 J=1,M1
      ACB(J)=AC(1,J)
      AEB(J)=AE(1,J)
      ANEB(J)=ANE(1,J)
      ANB(J)=AN(1,J)
C     *** NOTE THAT AWB(J) AND ASWB(J) ARE NOT INCLUDED HERE ***
      ASB(J)=AS(1,J)
502   ACONB(J)=ACON(1,J)
505   I=1
      DO 500 J=1,M1
      AC(I,J)=1.D0
      AE(I,J)=0.D0
      ANE(I,J)=0.D0
      AN(I,J)=0.D0
      AW(I,J)=0.D0
      ASW(I,J)=0.D0
      AS(I,J)=0.D0
500   ACON(I,J)=F(I,J,NFS)
      IF (NFS-2) 520,530,540
520   I=L1
      DO 525 J=1,M1
      AC(I,J)=1.D0
      AE(I,J)=0.D0
```

```
      ANE(I,J)=0.D0
      AN(I,J)=0.D0
      AW(I,J)=0.D0
      ASW(I,J)=0.D0
      AS(I,J)=0.D0
525   ACON(I,J)=F(I,J,NFS)
      RETURN
530   J=1
      DO 535 I=2,L1
      AC(I,J)=1.D0
      AE(I,J)=0.D0
      ANE(I,J)=0.D0
      AN(I,J)=0.D0
      AW(I,J)=0.D0
      ASW(I,J)=0.D0
      AS(I,J)=0.D0
535   ACON(I,J)=F(I,J,NFS)
C
C  SPECIAL PROCEDURE TO IMPLEMENT THE ZERO NORMAL VELOCITY CONDITION
C  AT THE TOP SYMMETRY LINE
C
      DO 537 I=2,L1
      AC(I,M1)=1.D0
      AE(I,M1)=0.D0
      ANE(I,M1)=0.D0
      AN(I,M1)=0.D0
      AW(I,M1)=0.D0
      ASW(I,M1)=0.D0
      AS(I,M1)=0.D0
537   ACON(I,M1)=TANPSI*F(I,M1,1)
      RETURN
540   RETURN
552   CPC=CP1
      GOTO 550
554   CPC=CP2
550   DO 560 J=1,M2
      JP1=J+1
      BFLUX=QW/CPC*0.5D0*DSQRT((X(1,JP1)-X(1,J))**2+(Y(1,JP1)-Y(1,J))
     1 **2)
      ACON(1,J)=ACON(1,J)+BFLUX
560   ACON(1,JP1)=ACON(1,JP1)+BFLUX
      RETURN
C
C---  RECTANGULAR DUCT BOUNDARY CONDITIONS
C
570   GOTO (710,710,730,730,750,730,770),NFS
730   DO 732 J=1,M1
      ACB(J)=AC(1,J)
      AEB(J)=AE(1,J)
      ANEB(J)=ANE(1,J)
      ANB(J)=AN(1,J)
      ASB(J)=AS(1,J)
732   ACONB(J)=ACON(1,J)
710   I=1
      DO 712 J=1,M1
      AC(I,J)=1.D0
      AE(I,J)=0.D0
      ANE(I,J)=0.D0
```

```
      AN(I,J)=0.D0
      AW(I,J)=0.D0
      ASW(I,J)=0.D0
      AS(I,J)=0.D0
712   ACON(I,J)=F(I,J,NFS)
      J=1
      DO 714 I=2,L1
      AC(I,J)=1.D0
      AE(I,J)=0.D0
      ANE(I,J)=0.D0
      AN(I,J)=0.D0
      AW(I,J)=0.D0
      ASW(I,J)=0.D0
      AS(I,J)=0.D0
714   ACON(I,J)=F(I,J,NFS)
      IF (NFS-2) 720,740,760
720   I=L1
      DO 722 J=1,M1
      AC(I,J)=1.D0
      AE(I,J)=0.D0
      ANE(I,J)=0.D0
      AN(I,J)=0.D0
      AW(I,J)=0.D0
      ASW(I,J)=0.D0
      AS(I,J)=0.D0
722   ACON(I,J)=F(I,J,NFS)
      RETURN
740   J=M1
      DO 745 I=2,L1
      AC(I,J)=1.D0
      AE(I,J)=0.D0
      ANE(I,J)=0.D0
      AN(I,J)=0.D0
      AW(I,J)=0.D0
      ASW(I,J)=0.D0
      AS(I,J)=0.D0
745   ACON(I,J)=F(I,J,NFS)
760   RETURN
750   CPC=CP1
      GOTO 752
770   CPC=CP2
752   DO 754 J=1,M2
      JP1=J+1
      BFLUX=QW/CPC*0.5D0*(Y(1,JP1)-Y(1,J))
      ACON(1,J)=ACON(1,J)+BFLUX
754   ACON(1,JP1)=ACON(1,JP1)+BFLUX
      DO 756 I=1,L2
      IP1=I+1
      BFLUX=QW/CPC*0.5D0*(X(IP1,1)-X(I,1))
      ACON(I,1)=ACON(I,1)+BFLUX
756   ACON(IP1,1)=ACON(IP1,1)+BFLUX
      RETURN
C-----------------------------------------------------------------------
C     ************
      ENTRY BTSVEL
C     ************
C
C---  BOUNDARY TREATMENT OF PSUEDO VELOCITIES
```

```
C
      IF (IPROB.EQ.1) GOTO 650
      IF (NFS-2) 600,610,620
600   DO 602 I=1,L1,L2
      DO 602 J=1,M1
      ACU(I,J)=1.D30
602   UHAT(I,J)=U(I,J)
      RETURN
610   J=1
      DO 612 I=1,L1
      ACV(I,J)=1.D30
612   VHAT(I,J)=V(I,J)
      I=1
      DO 614 J=2,M1
      ACV(I,J)=1.D30
614   VHAT(I,J)=V(I,J)
      J=M1
      DO 616 I=2,L1
      ACV(I,J)=-100.D0
616   VHAT(I,J)=UHAT(I,J)*TANPSI
      RETURN
620   DO 622 J=1,M1
      WHAT(1,J)=0.D0
622   CVAREA(1,J)=0.D0
      RETURN
C
C---  RECTANGULAR DUCT GEOMETRY
C
650   IF (NFS-2) 660,670,680
660   DO 662 I=1,L1,L2
      DO 662 J=1,M1
      ACU(I,J)=1.D30
662   UHAT(I,J)=U(I,J)
      J=1
      DO 664 I=1,L1
      ACU(I,J)=1.D30
664   UHAT(I,J)=U(I,J)
      RETURN
670   DO 672 J=1,M1,M2
      DO 672 I=1,L1
      ACV(I,J)=1.D30
672   VHAT(I,J)=V(I,J)
      I=1
      DO 674 J=2,M1
      ACV(I,J)=1.D30
674   VHAT(I,J)=V(I,J)
      RETURN
680   DO 682 J=1,M1
      WHAT(1,J)=0.D0
682   CVAREA(1,J)=0.D0
      DO 684 I=2,L1
      WHAT(I,1)=0.D0
684   CVAREA(I,1)=0.D0
      RETURN
C-----------------------------------------------------------------------
C     ************
      ENTRY PBOUND
C     ************
```

```
      RETURN
C-----------------------------------------------------------------------
C     ************
      ENTRY NUCALC
C     ************
C
C---  CALCULATION OF NUSSELT NUMBER
C
      DO 910 NFS=4,7
      CALL BULK
      GOTO (27,27,27,914,915,916,917),NFS
914   FBU=FBU4
      FBU4=FB
      DKDCP=DKDCP1
      GOTO 918
916   FBU=FBU6
      FBU6=FB
      DKDCP=DKDCP2
918   CNU=RHOA*FAREA/DKDCP*DH/PERIM*(FB-FBU)/DZ/(TW-FB)
      WRITE(6,940) NFS,FB,CNU,ISTEP
940   FORMAT(/3X,'NFS = ',I2,'     BULK TEMPERATURE = ',1PD15.7,
     1 '     NU = ',1PD15.7,'  FOR ISTEP = ',I3)
      TABLE(ISTEP,NFS)=CNU
      GOTO 910
C
915   DK=DK1
      GOTO 920
917   DK=DK2
920   FWAV=0.D0
C
C---  AVERAGE WALL TEMPERATURE
C
      DO 950 J=1,M2
      JP1=J+1
950   FWAV=FWAV+0.5D0*(F(1,J,NFS)+F(1,JP1,NFS))
     1 *DSQRT((X(1,JP1)-X(1,J))**2+(Y(1,JP1)-Y(1,J))**2)
      IF (IPROB.NE.1) GOTO 954
      DO 952 I=1,L2
      IP1=I+1
952   FWAV=FWAV+0.5D0*(F(I,1,NFS)+F(IP1,1,NFS))* (X(IP1,1)-X(I,1))
954   FWAV=FWAV/PERIM
      CNU=QW*DH/(FWAV-FB)/DK
      TABLE(ISTEP,NFS)=CNU
      WRITE(6,940) NFS,FB,CNU,ISTEP
910   CONTINUE
      RETURN
27    STOP
C-----------------------------------------------------------------------
C     ************
      ENTRY RESET
C     ************
C
C---  RESET THE CONTROL PARAMETERS SET IN PREVIOUS ANALYSES
C
      ITMAX=20
      LSTEP=3
      RELAX(1)=0.7D0
      RELAX(2)=0.7D0
```

```
      RELAX(3)=0.7D0
      PRELAX=1.0D0
      LCPRIN=.FALSE.
      LPPRIN=.FALSE.
      IMONIT=0
      RETURN
C-----------------------------------------------------------------------
C
C---  FORMAT STATEMENTS
C
1010  FORMAT(9A8)
1020  FORMAT(3I10)
1030  FORMAT(4D10.0)
1040  FORMAT(7(A8,2X))
C
      END
C***********************************************************************
      SUBROUTINE SUPPLY
C***********************************************************************
      IMPLICIT REAL*8(A-H,O-Z)
      LOGICAL LSOLVE,LCPRIN,LPRINT,LPPRIN
      COMMON ASTORE(3528),X(21,21),Y(21,21),F(21,21,7),FU(21,21,7),
     1 FP(11,11,2),RHO(21,21),GAM(21,21),
     2 SC(21,21),SP(21,21),ACU(21,21),UHAT(21,21),
     3 D1T1(10,10,2),D2T1(10,10,2),D3T1(10,10,2),
     4 D1T2(10,10,2),D2T2(10,10,2),D3T2(10,10,2)
      COMMON /THRD/Z,DZ,DPDZ,DPDZC,PBAR,SPMF,WFD,CNUFD(4),LSTEP,ISTEP,
     1 ITMAX,ISTART,IPROB
      COMMON /PARM/RELAX(7),PRELAX
      COMMON /MONIT/LSOLVE(7),LCPRIN,LPRINT(7),LPPRIN
      COMMON /LABEL/TITLE(7),HDG(9)
      COMMON /INDX/NSWP(7),NPSWP(2),L1,L2,L3,M1,M2,M3,
     1 LP1,LP2,LP3,MP1,MP2,MP3,NFS,NFSMAX,NPS,NUME,IMONIT,LAST,
     2 LMID,MMID,LPMID,MPMID,IPREF,JPREF,ITER,IC(3),JC(3),IDEAL,
     3 IR,IRP1,IRM1,JR,JRP1,JRM1,IPR,IPRP1,IPRP2,IPRM1,IPRM2,JPR,JPRP1,
     4 JPRP2,JPRM1,JPRM2,NITMAX(7),NPITMX(2)
      COMMON /CONV/TOL(7),PTOL(2),DWDES,FCK(3,2),DPDZCK,CHGTOL,CHGCK
      COMMON /RODBUN/S,RAD,SDR,WBAR,FAREA,PERIM,PHY,DH,DHDR,XL,YL,TANPSI
     1 ,PSI,FBU4,FBU6,FB,FWAV,RHOA,CP1,DK1,DKDCP1,CP2,DK2,DKDCP2,
     2 RPOW,XPOW,YPOW,DMUA,REY,QW,  TAUW(21),TW,TI
C-----------------------------------------------------------------------
      LOGICAL LPR(9)
      DIMENSION W(21,21)
      DIMENSION FPR(21,21,9),FPPR(11,11,3),TITFPR(9),TITPPR(3)
      EQUIVALENCE (W(1),F(1,1,3))
      DATA TITFPR(1)/'X-COORD '/,TITFPR(2)/'Y-COORD '/
      DATA TITPPR/'XP-COORD','YP-COORD','PRESSURE'/
      EQUIVALENCE (FPR(1),X(1)),(FPPR(1),FP(1))
C     ***********
      ENTRY PRINT
C     ***********
10    FORMAT(25X,26('*'),4X,A8,4X,26('*'))
20    FORMAT(8X, 3HI =,I6,10I11)
21    FORMAT(7X,4HIP =,I6,10I11)
30    FORMAT(1X, 3HJ =)
31    FORMAT(1X,4HJP =)
40    FORMAT(6X,I2,3X,1P11D11.3)
50    FORMAT(1H )
```

```
C-----------------------------------------------------------------------
      LPR(1)=LCPRIN
      LPR(2)=LCPRIN
      DO 5 I=1,NFSMAX
      LPR(I+2)=LPRINT(I)
5     TITFPR(I+2)=TITLE(I)
      NPRMAX=NFSMAX+2
      DO 100 NPR=1,NPRMAX
      IF (.NOT.LPR(NPR)) GOTO 100
      WRITE(6,50)
      WRITE(6,10) TITFPR(NPR)
      IBEG=-10
110   CONTINUE
      IBEG=IBEG+11
      IEND=IBEG+10
      IF (IEND.GT.L1) IEND=L1
      WRITE(6,50)
      WRITE(6,20) (I,I=IBEG,IEND)
      WRITE(6,30)
      DO 120 JJ=1,M1
      J=M1+1-JJ
      WRITE(6,40) J,(FPR(I,J,NPR),I=IBEG,IEND)
120   CONTINUE
      IF (IEND.LT.L1) GOTO 110
100   CONTINUE
      IF (.NOT.LPPRIN) RETURN
      IF (.NOT.LCPRIN) GOTO 200
      DO 210 JP=1,MP1
      J=2*JP-1
      DO 210 IP=1,LP1
      I=2*IP-1
      FPPR(IP,JP,3)=X(I,J)
210   FPPR(IP,JP,2)=Y(I,J)
200   CONTINUE
      LPR(3)=LPPRIN
      DO 300 NPR=1,3
      NPPR=4-NPR
      IF (.NOT.LPR(NPR)) GOTO 300
      WRITE(6,50)
      WRITE(6,10) TITPPR(NPR)
      IBEG=-10
310   CONTINUE
      IBEG=IBEG+11
      IEND=IBEG+10
      IF (IEND.GT.LP1) IEND=LP1
      WRITE(6,50)
      WRITE(6,21) (IP,IP=IBEG,IEND)
      WRITE(6,31)
      DO 320 JJ=1,MP1
      JP=MP1+1-JJ
      WRITE(6,40) JP,(FPPR(IP,JP,NPPR),IP=IBEG,IEND)
320   CONTINUE
      IF (IEND.LT.LP1) GOTO 310
300   CONTINUE
      WRITE(6,330) PBAR,DPDZ
330   FORMAT(//3X,'PBAR = ',1PD15.7,//3X,'DP/DZ = ',1PD15.7,/)
      RETURN
C-----------------------------------------------------------------------
```

```
C     ************
      ENTRY DEFGRD
C     ************
C
C---  DEFAULT GRID
C
      IF (IPROB.EQ.2) GOTO 850
C
C---  IPROB=1 -----> RECTANGULAR DUCT
C
C
      DO 810 JP=1,MP1
      J=2*JP-1
      DO 810 IP=1,LP1
      I=2*IP-1
      X(I,J)=(DFLOAT(IP-1)/DFLOAT(LP2))**XPOW*XL
810   Y(I,J)=(DFLOAT(JP-1)/DFLOAT(MP2))**YPOW*YL
      RETURN
C
C---  IPROB=2 -----> ROD-BUNDLE ARRAY
C
850   S=RAD*SDR
      PHY=DATAN(1.DO)*4.DO
      DPSI=PSI/DFLOAT(MP2)
      TANPSI=DTAN(PSI)
      DO 860 JP=1,MP1
      J=2*JP-1
      PSIP=DFLOAT(JP-1)*DPSI
      RFINAL=S/DCOS(PSIP)
      RDIFF=RFINAL-RAD
      DO 860 IP=1,LP1
      I=2*IP-1
      X(I,J)=(RAD+RDIFF*(DFLOAT(IP-1)/DFLOAT(LP2))**RPOW)*DCOS(PSIP)
860   Y(I,J)=(RAD+RDIFF*(DFLOAT(IP-1)/DFLOAT(LP2))**RPOW)*DSIN(PSIP)
      RETURN
C-----------------------------------------------------------------------
C     ************
      ENTRY DCALC
C     ************
C
C     VELOCITY NODES
C
      DO 410 IP=1,LP2
      I=2*IP-1
      IP1=I+1
      IP2=I+2
      DO 410 JP=1,MP2
      J=2*JP-1
      JP1=J+1
      JP2=J+2
      X(IP1,J)=(X(I,J)+X(IP2,J))*0.5DO
      Y(IP1,J)=(Y(I,J)+Y(IP2,J))*0.5DO
      X(IP1,JP1)=(X(I,J)+X(IP2,JP2))*0.5DO
      Y(IP1,JP1)=(Y(I,J)+Y(IP2,JP2))*0.5DO
      X(I,JP1)=(X(I,J)+X(I,JP2))*0.5DO
410   Y(I,JP1)=(Y(I,J)+Y(I,JP2))*0.5DO
      DO 430 I=2,L2,2
      IP1=I+1
```

```
      IM1=I-1
      X(I,M1)=(X(IM1,M1)+X(IP1,M1))*0.5D0
430   Y(I,M1)=(Y(IM1,M1)+Y(IP1,M1))*0.5D0
      DO 440 J=2,M2,2
      JP1=J+1
      JM1=J-1
      X(L1,J)=(X(L1,JP1)+X(L1,JM1))*0.5D0
440   Y(L1,J)=(Y(L1,JP1)+Y(L1,JM1))*0.5D0
C
C  CALCULATION OF THE COEFFICIENTS D FOR EACH TRIANGULAR ELEMENT
C
      DO 420 JP=1,MP2
      J=2*JP-1
      JP2=J+2
      DO 420 IP=1,LP2
      I=2*IP-1
      IP2=I+2
C  ******
C  TYPE 1
C  ******
      DET=X(I,J)*Y(IP2,J)+X(IP2,J)*Y(IP2,JP2)+X(IP2,JP2)*Y(I,J)
     1   -Y(I,J)*X(IP2,J)-Y(IP2,J)*X(IP2,JP2)-Y(IP2,JP2)*X(I,J)
      FAC=DABS(DET)/DET/24.D0
      D1T1(IP,JP,1)=(Y(IP2,JP2)-Y(IP2,J))*FAC
      D1T1(IP,JP,2)=(X(IP2,J)-X(IP2,JP2))*FAC
      D2T1(IP,JP,1)=(Y(I,J)-Y(IP2,JP2))*FAC
      D2T1(IP,JP,2)=(X(IP2,JP2)-X(I,J))*FAC
      D3T1(IP,JP,1)=(Y(IP2,J)-Y(I,J))*FAC
      D3T1(IP,JP,2)=(X(I,J)-X(IP2,J))*FAC
C  ******
C  TYPE 2
C  ******
      DET=X(I,J)*Y(IP2,JP2)+X(IP2,JP2)*Y(I,JP2)+X(I,JP2)*Y(I,J)
     1   -Y(I,J)*X(IP2,JP2)-Y(IP2,JP2)*X(I,JP2)-Y(I,JP2)*X(I,J)
      FAC=DABS(DET)/DET/24.D0
      D1T2(IP,JP,1)=(Y(I,JP2)-Y(IP2,JP2))*FAC
      D1T2(IP,JP,2)=(X(IP2,JP2)-X(I,JP2))*FAC
      D2T2(IP,JP,1)=(Y(I,J)-Y(I,JP2))*FAC
      D2T2(IP,JP,2)=(X(I,JP2)-X(I,J))*FAC
      D3T2(IP,JP,1)=(Y(IP2,JP2)-Y(I,J))*FAC
      D3T2(IP,JP,2)=(X(I,J)-X(IP2,JP2))*FAC
420   CONTINUE
C
C
C---  CALCULATION OF FLOW AREA, PERIMETERS AND HYDRAULIC DIAMETERS
C
      FAREA=0.D0
      DO 450 J=1,M2
      JP1=J+1
      DO 450 I=1,L2
      IP1=I+1
      FAREA=FAREA
     1 +DABS(X(I,J)*Y(IP1,J)+X(IP1,J)*Y(IP1,JP1)+X(IP1,JP1)*Y(I,J)
     2      -Y(I,J)*X(IP1,J)-Y(IP1,J)*X(IP1,JP1)-Y(IP1,JP1)*X(I,J))/2.D0
     3 +DABS(X(I,J)*Y(IP1,JP1)+X(IP1,JP1)*Y(I,JP1)+X(I,JP1)*Y(I,J)
     4      -Y(I,J)*X(IP1,JP1)-Y(IP1,JP1)*X(I,JP1)-Y(I,JP1)*X(I,J))/2.D0
450   CONTINUE
C
```

```
C---   WETTED PERIMETER
C
       PERIM=0.DO
C
       DO 470 J=1,M2
       JP1=J+1
470    PERIM=PERIM+DSQRT((X(1,JP1)-X(1,J))**2+(Y(1,JP1)-Y(1,J))**2)
       IF (IPROB.EQ.1) PERIM=XL+YL
       DH=4.DO*FAREA/PERIM
       RETURN
C-------------------------------------------------------------------------
C      ************
       ENTRY DEFVAL
C      ************
C
C  SPECIFICATION OF DEFAULT VALUES
C
       DO 500 NF=1,7
       LSOLVE(NF)=.FALSE.
       LPRINT(NF)=.FALSE.
500    RELAX(NF)=1.DO
       PRELAX=1.DO
       Z=0.DO
       DZ=1.D-5
       PBAR=0.DO
       DPDZ=0.DO
       IMONIT=0
       ISTEP=0
       ITER=1
       ITMAX=10
       LAST=1
       LSTEP=1
       LCPRIN=.FALSE.
       LPPRIN=.FALSE.
       IPREF=1
       JPREF=1
       DO 510 NF=1,7
       NSWP(NF)=1
       NITMAX(NF)=5
510    TOL(NF)=1.D-6
       NPSWP(1)=1
       NPSWP(2)=5
       NPITMX(1)=10
       NPITMX(2)=20
C
C---   DEFAULT MONITORING POINTS
C
       IC(1)=10
       IC(2)=6
       IC(3)=11
       JC(1)=10
       JC(2)=6
       JC(3)=11
       IR=6
       JR=6
C
       DO 520 NP=1,2
520    PTOL(NP)=1.D-6
```

```
      IDEAL=25
      CHGTOL=1.D-4
      RETURN
C-----------------------------------------------------------------------
C     ************
      ENTRY GRIDCT
C     ************
      LP2=LP1-1
      LP3=LP1-2
      MP2=MP1-1
      MP3=MP1-2
      L1=2*LP1-1
      L2=L1-1
      L3=L1-2
      M1=2*MP1-1
      M2=M1-1
      M3=M1-2
      LMID=L1/2+1
      MMID=M1/2+1
      LPMID=LP1/2+1
      MPMID=MP1/2+1
      RETURN
C-----------------------------------------------------------------------
C
      ENTRY MONCON
C
C---  MONITORING CONSTANTS
      IRP1=IR+1
      IRM1=IR-1
      JRP1=JR+1
      JRM1=JR-1
      IPR=LPMID
      IPRP1=IPR+1
      IPRP2=IPR+2
      IPRM1=IPR-1
      IPRM2=IPR-2
      JPR=MPMID
      JPRP1=JPR+1
      JPRP2=JPR+2
      JPRM1=JPR-1
      JPRM2=JPR-2
      RETURN
C
C-----------------------------------------------------------------------
C     **********
      ENTRY BULK
C     **********
C     BULK TEMPERATURE CALCULATION
C
      FB=0.D0
      DO 900 J=1,M2
      JP1=J+1
      DO 900 I=1,L2
      IP1=I+1
C
C  TYPE 1
C
      EVOL=DABS(X(I,J)*Y(IP1,J)+X(IP1,J)*Y(IP1,JP1)+X(IP1,JP1)*Y(I,J)
```

```
     1 -Y(I,J)*X(IP1,J)-Y(IP1,J)*X(IP1,JP1)-Y(IP1,JP1)*X(I,J))/6.D0
       FB=FB+(F(I,J,NFS)*W(I,J)+F(IP1,J,NFS)*W(IP1,J)
     1 +F(IP1,JP1,NFS)*W(IP1,JP1))*EVOL
C
C  TYPE 2
C
       EVOL=DABS(X(I,J)*Y(IP1,JP1)+X(IP1,JP1)*Y(I,JP1)+X(I,JP1)*Y(I,J)
     1 -Y(I,J)*X(IP1,JP1)-Y(IP1,JP1)*X(I,JP1)-Y(I,JP1)*X(I,J))/6.D0
       FB=FB+(F(I,J,NFS)*W(I,J)+F(IP1,JP1,NFS)*W(IP1,JP1)
     1 +F(I,JP1,NFS)*W(I,JP1))*EVOL
900    CONTINUE
       FB=FB/FAREA
       RETURN
C-------------------------------------------------------------------------
C      ************
       ENTRY PRTINP
C      ************
C
C---   PRINT INPUT PARAMETERS
C
       WRITE(6,1010)
       WRITE(6,1020) HDG,IPROB
       WRITE(6,1030) ISTEP,ITER
       WRITE(6,1040) LP1,MP1,NFSMAX,IPROB,LSTEP,ITMAX,IDEAL
       WRITE(6,1050)
       NP=1
       WRITE(6,1060) NP,NPSWP(1),NPITMX(1),PTOL(1),PRELAX
       NP=2
       PRELA2=1.D0
       WRITE(6,1060) NP,NPSWP(2),NPITMX(2),PTOL(2),PRELA2
       WRITE(6,1070)
       DO 1500 NF=1,NFSMAX
       WRITE(6,1060) NF,NSWP(NF),NITMAX(NF),TOL(NF),RELAX(NF)
1500   CONTINUE
       WRITE(6,1080)
       RETURN
C-------------------------------------------------------------------------
C
C---   FORMAT STATEMENTS
C
1010   FORMAT('1',//,13X,88('*'),/,13X,'*',86X,'*',/,
     1   13X,'*',2X,'C O N T R O L - V O L U M E   F I N I T E - E L E'
     2   ,' M E N T   M E T H O D              *',/,13X,'*',86X,'*',/,
     3   13X,'*  F O R   T H R E E - D I M E N S I O N A L   P A R A B'
     4   ,' O L I C   F L O W S              *',/13X,'*',86X,'*',/,13X,
     5   '*  A N D   H E A T   T R A N S F E R',51X,'*',/13X,'*',86X,
     6   '*',/,13X,88('*')///)
1020   FORMAT(7X,'TEST CASE',T31,':',T37,9A8,/7X,'---------',//
     1 7X,' IPROB = ',I1)
1030   FORMAT(//7X,'STARTING FROM ISTEP = ',I3,//20X,'ITER = ',I3//)
1040   FORMAT(//7X,'INPUT PARAMETERS :',//,7X,'----------------',
     1   //,T12,'LP1',T27,'MP1',T42,'NFSMAX',T57,'IPROB',
     2   /T12,I3,T27,I3,T43,I1,T59,I1,
     3   //,T12,'LSTEP',T27,'ITMAX',T42,'IDEAL',/,T13,I3,T28,I3,T43,I3)
1050   FORMAT(//T12,'NP',T27,'NPSWP',T42,'NPITMX',
     1   T57,'PTOL',T72,'PRELAX')
1060   FORMAT(T12,I2,T28,I3,T43,I3,T56,1PD9.2,T71,1PD9.2)
1070   FORMAT(//T12,'NF',T27,'NSWP',T42,'NITMAX',T57,'TOL',T72,'RELAX')
```

```
1080  FORMAT(1H1)
      END
C*****************************************************************
      SUBROUTINE COEFF
C*****************************************************************
      IMPLICIT REAL*8(A-H,O-Z)
      LOGICAL LSOLVE,LCPRIN,LPRINT,LPPRIN
      COMMON ASTORE(3528),X(21,21),Y(21,21),F(21,21,7),FU(21,21,7),
     1 FP(11,11,2),RHO(21,21),GAM(21,21),
     2 SC(21,21),SP(21,21),ACU(21,21),UHAT(21,21),
     3 D1T1(10,10,2),D2T1(10,10,2),D3T1(10,10,2),
     4 D1T2(10,10,2),D2T2(10,10,2),D3T2(10,10,2)
      COMMON /THRD/Z,DZ,DPDZ,DPDZC,PBAR,SPMF,WFD,CNUFD(4),LSTEP,ISTEP,
     1 ITMAX,ISTART,IPROB
      COMMON /PARM/RELAX(7),PRELAX
      COMMON /MONIT/LSOLVE(7),LCPRIN,LPRINT(7),LPPRIN
      COMMON /LABEL/TITLE(7),HDG(9)
      COMMON /INDX/NSWP(7),NPSWP(2),L1,L2,L3,M1,M2,M3,
     1 LP1,LP2,LP3,MP1,MP2,MP3,NFS,NFSMAX,NPS,NUME,IMONIT,LAST,
     2 LMID,MMID,LPMID,MPMID,IPREF,JPREF,ITER,IC(3),JC(3),IDEAL,
     3 IR,IRP1,IRM1,JR,JRP1,JRM1,IPR,IPRP1,IPRP2,IPRM1,IPRM2,JPR,JPRP1,
     4 JPRP2,JPRM1,JPRM2,NITMAX(7),NPITMX(2)
      COMMON /CONV/TOL(7),PTOL(2),DWDES,FCK(3,2),DPDZCK,CHGTOL,CHGCK
      COMMON /RODBUN/S,RAD,SDR,WBAR,FAREA,PERIM,PHY,DH,DHDR,XL,YL,TANPSI
     1 ,PSI,FBU4,FBU6,FB,FWAV,RHOA,CP1,DK1,DKDCP1,CP2,DK2,DKDCP2,
     2 RPOW,XPOW,YPOW,DMUA,REY,QW, TAUW(21),TW,TI
C-----------------------------------------------------------------
      DIMENSION AC(21,21),AE(21,21),ANE(21,21),AN(21,21),
     1 AW(21,21),ASW(21,21),AS(21,21),ACON(21,21)
      DIMENSION U(21,21),V(21,21),W(21,21),WU(21,21),P(11,11),PC(11,11),
     1 VHAT(21,21),ACV(21,21),WHAT(21,21)
      EQUIVALENCE (ASTORE(1),AC(1)),(ASTORE(442),AE(1)),(ASTORE( 883),
     1 ANE(1)),(ASTORE(1324),AN(1)),(ASTORE(1765),AW(1)),
     2 (ASTORE(2206),ASW(1)),(ASTORE(2647),AS(1)),(ASTORE(3088),
     3 ACON(1))
      EQUIVALENCE (F(1),U(1)),(F(1,1,2),V(1)),(F(1,1,3),W(1))
      EQUIVALENCE (FU(1,1,3),WU(1))
      EQUIVALENCE (FP(1),P(1)),(FP(1,1,2),PC(1))
      EQUIVALENCE (SC(1),VHAT(1)),(SP(1),ACV(1)),(SC(1),WHAT(1))
C-----------------------------------------------------------------
      DIMENSION XE(3),YE(3),XXP(3),XPM(3),XM(3),YM(3),XIM(3),XIH(3),
     1 XI(3),FO(3),FM(3),FH(3),YMUL(3),XIMUL(3),UE(3),VE(3),UM(3),VM(3),
     2 CC(3,3),BCC(3),IE(3),JE(3)
      DIMENSION CVMASS(21,21),CVAREA(21,21)
      EQUIVALENCE (UHAT(1),CVMASS(1)),(ACU(1),CVAREA(1))
      DIMENSION NFSORD(7)
      DATA NFSORD/3,1,2,4,5,6,7/
C-----------------------------------------------------------------
C
C  ******************************************************
C  * C O N V E C T I O N - D I F F U S I O N   P A R T *
C  ******************************************************
C
      REWIND 8
      DO 100 NFT=1,NFSMAX
      NF=NFSORD(NFT)
      IF(LSOLVE(NF)) GOTO 110
      GOTO 100
```

```
110   CONTINUE
C  ****************************************************************
C  CALCULATION OF ALL COEFFICIENTS (CONVECTION-DIFFUSION PROBLEM)
C  ****************************************************************
      DO 105 J=1,M1
      DO 105 I=1,L1
      AC(I,J)=0.D0
      AE(I,J)=0.D0
      ANE(I,J)=0.D0
      AN(I,J)=0.D0
      AW(I,J)=0.D0
      ASW(I,J)=0.D0
      AS(I,J)=0.D0
105   ACON(I,J)=0.D0
      IF (NF.NE.3) GOTO 107
      DO 108 J=1,M1
      DO 108 I=1,L1
      CVMASS(I,J)=0.D0
108   CVAREA(I,J)=0.D0
107   DO 120 NUME=1,2
C
C  SPECIFICATION OF THE DENSITY, GAMMA AND SOURCE TERMS
C
      NFS=NF
      CALL DENSE
      CALL GAMSOR
      DO 130 I=1,L2
      DO 130 J=1,M2
      RHOE=RHO(I,J)
      GAME=GAM(I,J)
C
C  ASSIGN INDICES FOR EACH KIND OF TRIANGLE
C
      IP1=I+1
      JP1=J+1
      IE(1)=I
      JE(1)=J
      IF (NUME.NE.1) GOTO 140
C  ******
C  TYPE 1
C  ******
      IE(2)=IP1
      JE(2)=J
      IE(3)=IP1
      JE(3)=JP1
      GOTO 150
C  ******
C  TYPE 2
C  ******
140   IE(2)=IP1
      JE(2)=JP1
      IE(3)=I
      JE(3)=JP1
C
C  COMPUTE THE COORDINATES OF ORIGIN O
C
150   XO=(X(IE(1),JE(1))+X(IE(2),JE(2))+X(IE(3),JE(3)))/3.D0
      YO=(Y(IE(1),JE(1))+Y(IE(2),JE(2))+Y(IE(3),JE(3)))/3.D0
```

```
C
C  SHIFT (ELEMENT) COORDS TO 0
C
      DO 160 N=1,3
      XE(N)=X(IE(N),JE(N))-XO
      YE(N)=Y(IE(N),JE(N))-YO
C
C  ASSIGN VALUES FOR Z FOR THE CASE OF PURE DIFFUSION
C
160   XI(N)=XE(N)
C
C  AVERAGE VELOCITY COMPONENTS IN ELEMENT
C
      UAV=(F(IE(1),JE(1),1)+F(IE(2),JE(2),1)+F(IE(3),JE(3),1))/3.D0
      VAV=(F(IE(1),JE(1),2)+F(IE(2),JE(2),2)+F(IE(3),JE(3),2))/3.D0
C
C  AREA OF ELEMENT (VOLUME WITH UNIT DEPTH)/3.D0
C
      EVOL=DABS(XE(1)*YE(2)+XE(2)*YE(3)+XE(3)*YE(1)
     1-XE(1)*YE(3)-XE(2)*YE(1)-XE(3)*YE(2))/6.D0
      RHODDZ=RHOE/DZ*EVOL
      RS=-EVOL*SP(I,J)
      ASC=EVOL*SC(I,J)
      IF (NF.NE.3) GOTO 161
      DO 162 N=1,3
      CVAREA(IE(N),JE(N))=CVAREA(IE(N),JE(N))+EVOL
162   CVMASS(IE(N),JE(N))=CVMASS(IE(N),JE(N))+EVOL*RHOE
C
C  AVERAGE VELOCITY IN ELEMENT
C
161   AVEL=DSQRT(UAV**2+VAV**2)
C
C  ELEMENT "PECLET NUMBER"
C
      FAC=RHOE*AVEL/GAME
      IF (FAC .LE. 1.D-15) GOTO 170
C
C  SPIN COORDS
C
      COSA=UAV/AVEL
      SINA=VAV/AVEL
      DO 180 N=1,3
      XT=XE(N)
      YT=YE(N)
      XE(N)=XT*COSA+YT*SINA
      YE(N)=YT*COSA-XT*SINA
      UE(N)=F(IE(N),JE(N),1)*COSA+F(IE(N),JE(N),2)*SINA
180   VE(N)=F(IE(N),JE(N),2)*COSA-F(IE(N),JE(N),1)*SINA
      XMAX=DMAX1(XE(1),XE(2),XE(3))
      DO 190 N=1,3
190   XXP(N)=DEXP(FAC*(XE(N)-XMAX))
      XPO=DEXP(-FAC*XMAX)
C
C  EXPONENTIAL FOR MIDDLE POINTS
C
      XPM(1)=DSQRT(XXP(2)*XXP(3))
      XPM(2)=DSQRT(XXP(1)*XXP(3))
      XPM(3)=DSQRT(XXP(1)*XXP(2))
```

```
C
C  CALCULATE Z (XI) AT NODES,MIDDLE AND HALF POINTS
C
      DO 200 N=1,3
      XI(N)=(XXP(N)-1.D0)/FAC
      XIM(N)=(XPM(N)-1.D0)/FAC
200   XIH(N)=(DSQRT(XPM(N)*XPO)-1.D0)/FAC
170   CONTINUE
C
C  DETERMINANT
C
      DET=XI(1)*YE(2)+XI(2)*YE(3)+XI(3)*YE(1)
     1   -XI(1)*YE(3)-XI(2)*YE(1)-XI(3)*YE(2)
      FAC=-GAME/DET
C
C  X-Y COORDS FOR MIDDLE POINTS
C
      XM(1)=(XE(2)+XE(3))/2.D0
      YM(1)=(YE(2)+YE(3))/2.D0
      XM(2)=(XE(1)+XE(3))/2.D0
      YM(2)=(YE(1)+YE(3))/2.D0
      XM(3)=(XE(1)+XE(2))/2.D0
      YM(3)=(YE(1)+YE(2))/2.D0
      YMUL(1)=YE(2)-YE(3)
      YMUL(2)=YE(3)-YE(1)
      YMUL(3)=YE(1)-YE(2)
      XIMUL(1)=XI(2)-XI(3)
      XIMUL(2)=XI(3)-XI(1)
      XIMUL(3)=XI(1)-XI(2)
C
C  CONDUCTION PART OF THE COEFFICIENTS (A)
C
      DO 210 NN=1,3
      DO 210 N=1,3
210   CC(NN,N)=FAC*(YM(N)*YMUL(NN)+XM(N)*XIMUL(NN))
C
C  TEST ELEMENT "PECLET NUMBER"
C
      FAC=RHOE*AVEL/GAME
      IF (FAC .LE. 1.D-15) GOTO 220
C
C  CALCULATE THE CONVECTION PART
C
C
C  VELOCITIES COMPONENT (SPUN) AT MIDDLE POINTS
C
      UM(1)=(UE(2)+UE(3))/2.D0
      VM(1)=(VE(2)+VE(3))/2.D0
      UM(2)=(UE(1)+UE(3))/2.D0
      VM(2)=(VE(1)+VE(3))/2.D0
      UM(3)=(UE(1)+UE(2))/2.D0
      VM(3)=(VE(1)+VE(2))/2.D0
C
C  CALCULATE FO/U (ALSO = GO/V)
C
      FO(1)=XI(2)*YE(3)-XI(3)*YE(2)
      FO(2)=XI(3)*YE(1)-XI(1)*YE(3)
      FO(3)=XI(1)*YE(2)-XI(2)*YE(1)
```

```
      RDDET=RHOE/DET
      DO 230 N=1,3
      UH=(UM(N)+AVEL)/2.D0
      VH=VM(N)/2.D0
      YH=YM(N)/2.D0
      UXIAV=((UM(N)-AVEL)*XIM(N)+4.D0*(UH-AVEL)*XIH(N))/6.D0
      VXIAV= (VM(N)*XIM(N)+4.D0*VH*XIH(N))/6.D0
      UYAV=(UM(N)*YM(N)+4.D0*UH*YH)/6.D0
      VYAV=(VM(N)*YM(N)+4.D0*VH*YH)/6.D0
      DO 230 NN=1,3
      FAV=UH*FO(NN)-UYAV*XIMUL(NN)+UXIAV*YMUL(NN)
      GAV=VH*FO(NN)-VYAV*XIMUL(NN)+VXIAV*YMUL(NN)
230   CC(NN,N)=RDDET*(YM(N)*FAV-XM(N)*GAV)+CC(NN,N)
C
C  **********************
C  BOUNDARY CONTRIBUTIONS
C  **********************
C  THESE ARE REMOVED SINCE THEY ARE ZERO IN THE CASE OF DUCT FLOWS
C  WITHOUT LEAKAGE
220   IF (NUME.NE.1) GOTO 240
C  ************************************
C  GENERAL ASSEMBLY FOR TRIANGLE OF TYPE 1
C  ************************************
C  WRT (I,J)
      AC(I,J)=AC(I,J)+RS+CC(2,3)+CC(3,3)-CC(2,2)-CC(3,2)
     1 +RHODDZ*WU(I,J)
      AE(I,J)=AE(I,J)+CC(2,3)-CC(2,2)
      ANE(I,J)=ANE(I,J)+CC(3,3)-CC(3,2)
      ACON(I,J)=ACON(I,J)+ASC+RHODDZ*WU(I,J)*FU(I,J,NF)
C  WRT (I+1,J)
      AC(IP1,J)=AC(IP1,J)+RS+CC(1,1)+CC(3,1)-CC(1,3)-CC(3,3)
     1 +RHODDZ*WU(IP1,J)
      AN(IP1,J)=AN(IP1,J)+CC(3,1)-CC(3,3)
      AW(IP1,J)=AW(IP1,J)+CC(1,1)-CC(1,3)
      ACON(IP1,J)=ACON(IP1,J)+ASC+RHODDZ*WU(IP1,J)*FU(IP1,J,NF)
C  WRT (I+1,J+1)
      AC(IP1,JP1)=AC(IP1,JP1)+RS+CC(1,2)+CC(2,2)-CC(1,1)-CC(2,1)
     1 +RHODDZ*WU(IP1,JP1)
      ASW(IP1,JP1)=ASW(IP1,JP1)+CC(1,2)-CC(1,1)
      AS(IP1,JP1)=AS(IP1,JP1)+CC(2,2)-CC(2,1)
      ACON(IP1,JP1)=ACON(IP1,JP1)+ASC+RHODDZ*WU(IP1,JP1)*FU(IP1,JP1,NF)
      GOTO 130
C  ************************************
C  GENERAL ASSEMBLY FOR TRIANGLE OF TYPE 2
C  ************************************
C  WRT (I,J)
240   AC(I,J)=AC(I,J)+RS+CC(2,3)+CC(3,3)-CC(2,2)-CC(3,2)
     1 +RHODDZ*WU(I,J)
      ANE(I,J)=ANE(I,J)+CC(2,3)-CC(2,2)
      AN(I,J)=AN(I,J)+CC(3,3)-CC(3,2)
      ACON(I,J)=ACON(I,J)+ASC+RHODDZ*WU(I,J)*FU(I,J,NF)
C  WRT (I+1,J+1)
      AC(IP1,JP1)=AC(IP1,JP1)+RS+CC(1,1)+CC(3,1)-CC(1,3)-CC(3,3)
     1 +RHODDZ*WU(IP1,JP1)
      AW(IP1,JP1)=AW(IP1,JP1)+CC(3,1)-CC(3,3)
      ASW(IP1,JP1)=ASW(IP1,JP1)+CC(1,1)-CC(1,3)
      ACON(IP1,JP1)=ACON(IP1,JP1)+ASC+RHODDZ*WU(IP1,JP1)*FU(IP1,JP1,NF)
C  WRT (I,J+1)
```

```
      AC(I,JP1)=AC(I,JP1)+RS+CC(1,2)+CC(2,2)-CC(1,1)-CC(2,1)
     1 +RHODDZ*WU(I,JP1)
      AS(I,JP1)=AS(I,JP1)+CC(1,2)-CC(1,1)
      AE(I,JP1)=AE(I,JP1)+CC(2,2)-CC(2,1)
      ACON(I,JP1)=ACON(I,JP1)+ASC+RHODDZ*WU(I,JP1)*FU(I,JP1,NF)
130   CONTINUE
120   CONTINUE
C  ****************
C  UNDER RELAXATION
C  ****************
      DO 260 J=1,M1
      DO 260 I=1,L1
      AC(I,J)=AC(I,J)/RELAX(NF)
260   ACON(I,J)=ACON(I,J)+AC(I,J)*(1.DO-RELAX(NF))*F(I,J,NF)
C
      IF (NF-2) 300,400,500
C-----------------------------------------------------------------------
C  UHAT COMPUTATION
C-----------------------------------------------------------------------
C
C  BOUNDARY POINTS
C
300   UHAT(1,1)=(AE(1,1)*U(2,1)+ANE(1,1)*U(2,2)+AN(1,1)*U(1,2)
     1 +ACON(1,1))/AC(1,1)
      UHAT(L1,1)=(AN(L1,1)*U(L1,2)+AW(L1,1)*U(L2,1)
     1 +ACON(L1,1))/AC(L1,1)
      UHAT(L1,M1)=(AW(L1,M1)*U(L2,M1)+ASW(L1,M1)*U(L2,M2)
     1 +AS(L1,M1)*U(L1,M2)+ACON(L1,M1))/AC(L1,M1)
      UHAT(1,M1)=(AS(1,M1)*U(1,M2)+AE(1,M1)*U(2,M1)
     1 +ACON(1,M1))/AC(1,M1)
      DO 310 I=2,L2
      IP1=I+1
      IM1=I-1
      UHAT(I,1)=(AE(I,1)*U(IP1,1)+ANE(I,1)*U(IP1,2)
     1 +AN(I,1)*U(I,2)+AW(I,1)*U(IM1,1)+ACON(I,1))/AC(I,1)
310   UHAT(I,M1)=(AW(I,M1)*U(IM1,M1)+ASW(I,M1)*U(IM1,M2)
     1 +AS(I,M1)*U(I,M2)+AE(I,M1)*U(IP1,M1)+ACON(I,M1))/AC(I,M1)
      DO 320 J=2,M2
      JP1=J+1
      JM1=J-1
      UHAT(1,J)=(AS(1,J)*U(1,JM1)+AE(1,J)*U(2,J)+ANE(1,J)*U(2,JP1)
     1 +AN(1,J)*U(1,JP1)+ACON(1,J))/AC(1,J)
320   UHAT(L1,J)=(AN(L1,J)*U(L1,JP1)+AW(L1,J)*U(L2,J)
     1 +ASW(L1,J)*U(L2,JM1)+AS(L1,J)*U(L1,JM1)+ACON(L1,J))/AC(L1,J)
C
C  INTERNAL POINTS
C
      DO 330 J=2,M2,2
      JP1=J+1
      JM1=J-1
      DO 330 I=2,L2
      IP1=I+1
      IM1=I-1
      UHAT(I,J)=(AE(I,J)*U(IP1,J)+ANE(I,J)*U(IP1,JP1)
     1 +AN(I,J)*U(I,JP1)+AW(I,J)*U(IM1,J)
     2 +ASW(I,J)*U(IM1,JM1)+AS(I,J)*U(I,JM1)
     3 +ACON(I,J))/AC(I,J)
330   CONTINUE
```

```
      DO 340 J=3,M3,2
      JP1=J+1
      JM1=J-1
      DO 340 I=2,L2,2
      IP1=I+1
      IM1=I-1
      UHAT(I,J)=(AE(I,J)*U(IP1,J)+ANE(I,J)*U(IP1,JP1)
     1 +AN(I,J)*U(I,JP1)+AW(I,J)*U(IM1,J)
     2 +ASW(I,J)*U(IM1,JM1)+AS(I,J)*U(I,JM1)
     3 +ACON(I,J))/AC(I,J)
340   CONTINUE
      DO 350 J=1,M1
      DO 350 I=1,L1
350   ACU(I,J)=AC(I,J)
      NFS=1
      CALL BTSVEL
      WRITE(8) ASTORE
      GOTO 100
C-----------------------------------------------------------------------
C  VHAT COMPUTATION
C-----------------------------------------------------------------------
C
C  BOUNDARY POINTS
C
400   VHAT(1,1)=(AE(1,1)*V(2,1)+ANE(1,1)*V(2,2)+AN(1,1)*V(1,2)
     1 +ACON(1,1))/AC(1,1)
      VHAT(L1,1)=(AN(L1,1)*V(L1,2)+AW(L1,1)*V(L2,1)
     1 +ACON(L1,1))/AC(L1,1)
      VHAT(L1,M1)=(AW(L1,M1)*V(L2,M1)+ASW(L1,M1)*V(L2,M2)
     1 +AS(L1,M1)*V(L1,M2)+ACON(L1,M1))/AC(L1,M1)
      VHAT(1,M1)=(AS(1,M1)*V(1,M2)+AE(1,M1)*V(2,M1)
     1 +ACON(1,M1))/AC(1,M1)
      DO 410 I=2,L2
      IP1=I+1
      IM1=I-1
      VHAT(I,1)=(AE(I,1)*V(IP1,1)+ANE(I,1)*V(IP1,2)
     1 +AN(I,1)*V(I,2)+AW(I,1)*V(IM1,1)+ACON(I,1))/AC(I,1)
410   VHAT(I,M1)=(AW(I,M1)*V(IM1,M1)+ASW(I,M1)*V(IM1,M2)
     1 +AS(I,M1)*V(I,M2)+AE(I,M1)*V(IP1,M1)+ACON(I,M1))/AC(I,M1)
      DO 420 J=2,M2
      JP1=J+1
      JM1=J-1
      VHAT(1,J)=(AS(1,J)*V(1,JM1)+AE(1,J)*V(2,J)+ANE(1,J)*V(2,JP1)
     1 +AN(1,J)*V(1,JP1)+ACON(1,J))/AC(1,J)
420   VHAT(L1,J)=(AN(L1,J)*V(L1,JP1)+AW(L1,J)*V(L2,J)
     1 +ASW(L1,J)*V(L2,JM1)+AS(L1,J)*V(L1,JM1)+ACON(L1,J))/AC(L1,J)
C
C  INTERNAL POINTS
C
      DO 430 J=2,M2,2
      JP1=J+1
      JM1=J-1
      DO 430 I=2,L2
      IP1=I+1
      IM1=I-1
      VHAT(I,J)=(AE(I,J)*V(IP1,J)+ANE(I,J)*V(IP1,JP1)
     1 +AN(I,J)*V(I,JP1)+AW(I,J)*V(IM1,J)
     2 +ASW(I,J)*V(IM1,JM1)+AS(I,J)*V(I,JM1)
```

```
     3  +ACON(I,J))/AC(I,J)
430    CONTINUE
       DO 440 J=3,M3,2
       JP1=J+1
       JM1=J-1
       DO 440 I=2,L2,2
       IP1=I+1
       IM1=I-1
       VHAT(I,J)=(AE(I,J)*V(IP1,J)+ANE(I,J)*V(IP1,JP1)
     1  +AN(I,J)*V(I,JP1)+AW(I,J)*V(IM1,J)
     2  +ASW(I,J)*V(IM1,JM1)+AS(I,J)*V(I,JM1)
     3  +ACON(I,J))/AC(I,J)
440    CONTINUE
       DO 450 J=1,M1
       DO 450 I=1,L1
450    ACV(I,J)=AC(I,J)
       NFS=2
       CALL BTSVEL
       WRITE(8) ASTORE
C  *************************
C  COMPUTE THE PRESSURE FIELD
C  *************************
       CALL PRES
C  ********************************
C  CALCULATE THE VELOCITIES U AND V
C  ********************************
       REWIND 8
       DO 1000 NFV=1,2
       IF (.NOT.LSOLVE(NFV))GOTO 1000
       READ(8) ASTORE
       DO 1010 JP=1,MP2
       JPP1=JP+1
       J=2*JP-1
       JP1=J+1
       JP2=J+2
       DO 1010 IP=1,LP2
       IPP1=IP+1
       I=2*IP-1
       IP1=I+1
       IP2=I+2
       PGRAD1=D1T1(IP,JP,NFV)*P(IP,JP)+D2T1(IP,JP,NFV)*P(IPP1,JP)
     1  +D3T1(IP,JP,NFV)*P(IPP1,JPP1)
       PGRAD2=D1T2(IP,JP,NFV)*P(IP,JP)+D2T2(IP,JP,NFV)*P(IPP1,JPP1)
     1  +D3T2(IP,JP,NFV)*P(IP,JPP1)
       ACON(I,J)=ACON(I,J)+PGRAD1+PGRAD2
       ACON(IP1,J)=ACON(IP1,J)+3.D0*PGRAD1
       ACON(IP2,J)=ACON(IP2,J)+PGRAD1
       ACON(I,JP1)=ACON(I,JP1)+3.D0*PGRAD2
       ACON(IP1,JP1)=ACON(IP1,JP1)+3.D0*(PGRAD1+PGRAD2)
       ACON(IP2,JP1)=ACON(IP2,JP1)+3.D0*PGRAD1
       ACON(I,JP2)=ACON(I,JP2)+PGRAD2
       ACON(IP1,JP2)=ACON(IP1,JP2)+3.D0*PGRAD2
1010   ACON(IP2,JP2)=ACON(IP2,JP2)+PGRAD1+PGRAD2
       NFS=NFV
       CALL BOUND
       CALL SOLVE
1000   CONTINUE
C
```

```
C  PRESSURE CORRECTION COMPUTATION
C
      CALL PCORR
C
C  CORRECTION OF VELOCITIES
C
C  CORRECTION OF U
C
      IF (.NOT.LSOLVE(1)) GOTO 2100
      DO 2010 JP=1,MP2
      JPP1=JP+1
      J=2*JP-1
      JP1=J+1
      JP2=J+2
      DO 2010 IP=1,LP2
      IPP1=IP+1
      I=2*IP-1
      IP1=I+1
      IP2=I+2
      PGRAD1=D1T1(IP,JP,1)*PC(IP,JP)+D2T1(IP,JP,1)*PC(IPP1,JP)
     1 +D3T1(IP,JP,1)*PC(IPP1,JPP1)
      PGRAD2=D1T2(IP,JP,1)*PC(IP,JP)+D2T2(IP,JP,1)*PC(IPP1,JPP1)
     1 +D3T2(IP,JP,1)*PC(IP,JPP1)
      U(I,J)=U(I,J)+(PGRAD1+PGRAD2)/ACU(I,J)
      U(IP1,J)=U(IP1,J)+3.D0*PGRAD1/ACU(IP1,J)
      U(IP2,J)=U(IP2,J)+PGRAD1/ACU(IP2,J)
      U(I,JP1)=U(I,JP1)+3.D0*PGRAD2/ACU(I,JP1)
      U(IP1,JP1)=U(IP1,JP1)+3.D0*(PGRAD1+PGRAD2)/ACU(IP1,JP1)
      U(IP2,JP1)=U(IP2,JP1)+3.D0*PGRAD1/ACU(IP2,JP1)
      U(I,JP2)=U(I,JP2)+PGRAD2/ACU(I,JP2)
      U(IP1,JP2)=U(IP1,JP2)+3.D0*PGRAD2/ACU(IP1,JP2)
2010  U(IP2,JP2)=U(IP2,JP2)+(PGRAD1+PGRAD2)/ACU(IP2,JP2)
C
C  CORRECTION OF V
C
2100  DO 2110 JP=1,MP2
      JPP1=JP+1
      J=2*JP-1
      JP1=J+1
      JP2=J+2
      DO 2110 IP=1,LP2
      IPP1=IP+1
      I=2*IP-1
      IP1=I+1
      IP2=I+2
      PGRAD1=D1T1(IP,JP,2)*PC(IP,JP)+D2T1(IP,JP,2)*PC(IPP1,JP)
     1 +D3T1(IP,JP,2)*PC(IPP1,JPP1)
      PGRAD2=D1T2(IP,JP,2)*PC(IP,JP)+D2T2(IP,JP,2)*PC(IPP1,JPP1)
     1 +D3T2(IP,JP,2)*PC(IP,JPP1)
      V(I,J)=V(I,J)+(PGRAD1+PGRAD2)/ACV(I,J)
      V(IP1,J)=V(IP1,J)+3.D0*PGRAD1/ACV(IP1,J)
      V(IP2,J)=V(IP2,J)+PGRAD1/ACV(IP2,J)
      V(I,JP1)=V(I,JP1)+3.D0*PGRAD2/ACV(I,JP1)
      V(IP1,JP1)=V(IP1,JP1)+3.D0*(PGRAD1+PGRAD2)/ACV(IP1,JP1)
      V(IP2,JP1)=V(IP2,JP1)+3.D0*PGRAD1/ACV(IP2,JP1)
      V(I,JP2)=V(I,JP2)+PGRAD2/ACV(I,JP2)
      V(IP1,JP2)=V(IP1,JP2)+3.D0*PGRAD2/ACV(IP1,JP2)
2110  V(IP2,JP2)=V(IP2,JP2)+(PGRAD1+PGRAD2)/ACV(IP2,JP2)
```

```
C
C   ** SPECIAL PROCEDURE FOR SYMMETRY LINE
C
      IF (IPROB.EQ.1) GOTO 2114
      DO 2112 I=2,L1
2112  V(I,M1)=U(I,M1)*TANPSI
C ** TESTING **
2114  CONTINUE
      NFS=1
      CALL PTVEL
      NFS=2
      CALL PTVEL
      GOTO 100
C
500   IF (NF.NE.3) GOTO 650
C
C   WHAT COMPUTATION
C
C   BOUNDARY POINTS
C
      WHAT(1,1)=(AE(1,1)*W(2,1)+ANE(1,1)*W(2,2)+AN(1,1)*W(1,2)
     1 +ACON(1,1))/AC(1,1)
      WHAT(L1,1)=(AN(L1,1)*W(L1,2)+AW(L1,1)*W(L2,1)
     1 +ACON(L1,1))/AC(L1,1)
      WHAT(L1,M1)=(AW(L1,M1)*W(L2,M1)+ASW(L1,M1)*W(L2,M2)
     1 +AS(L1,M1)*W(L1,M2)+ACON(L1,M1))/AC(L1,M1)
      WHAT(1,M1)=(AS(1,M1)*W(1,M2)+AE(1,M1)*W(2,M1)
     1 +ACON(1,M1))/AC(1,M1)
      DO 510 I=2,L2
      IP1=I+1
      IM1=I-1
      WHAT(I,1)=(AE(I,1)*W(IP1,1)+ANE(I,1)*W(IP1,2)
     1 +AN(I,1)*W(I,2)+AW(I,1)*W(IM1,1)+ACON(I,1))/AC(I,1)
510   WHAT(I,M1)=(AW(I,M1)*W(IM1,M1)+ASW(I,M1)*W(IM1,M2)
     1 +AS(I,M1)*W(I,M2)+AE(I,M1)*W(IP1,M1)+ACON(I,M1))/AC(I,M1)
      DO 520 J=2,M2
      JP1=J+1
      JM1=J-1
      WHAT(1,J)=(AS(1,J)*W(1,JM1)+AE(1,J)*W(2,J)+ANE(1,J)*W(2,JP1)
     1 +AN(1,J)*W(1,JP1)+ACON(1,J))/AC(1,J)
520   WHAT(L1,J)=(AN(L1,J)*W(L1,JP1)+AW(L1,J)*W(L2,J)
     1 +ASW(L1,J)*W(L2,JM1)+AS(L1,J)*W(L1,JM1)+ACON(L1,J))/AC(L1,J)
C
C   INTERNAL POINTS
C
      DO 530 J=2,M2
      JP1=J+1
      JM1=J-1
      DO 530 I=2,L2
      IP1=I+1
      IM1=I-1
      WHAT(I,J)=(AE(I,J)*W(IP1,J)+ANE(I,J)*W(IP1,JP1)
     1 +AN(I,J)*W(I,JP1)+AW(I,J)*W(IM1,J)
     2 +ASW(I,J)*W(IM1,JM1)+AS(I,J)*W(I,JM1)
     3 +ACON(I,J))/AC(I,J)
530   CONTINUE
      NFS=NF
      CALL BTSVEL
```

```
C
C  COMPUTATION OF DP/DZ
C
      CALMF=0.DO
      CALM=0.DO
      DO 580 J=1,M1
      DO 580 I=1,L1
      CALMF=CALMF+CVMASS(I,J)*WHAT(I,J)
580   CALM=CALM+CVMASS(I,J)*CVAREA(I,J)/AC(I,J)
      DPDZ=-(SPMF-CALMF)/CALM
      WRITE(6,585) DPDZ
585   FORMAT(/3X,'DP/DZ CALCULATED = ',1PD15.7)
      DO 590 J=1,M1
      DO 590 I=1,L1
590   ACON(I,J)=ACON(I,J)-DPDZ*CVAREA(I,J)
C  (NOTE THAT THE INCONSISTENCY IN TREATING ACON BY HAVING CVAREA=0
C   FOR SPECIFIED W B.C. IS OVERCOMED IN THE CALLING TO BOUND)
C
      CALL BOUND
      CALL SOLVE
C
      CALMF=0.DO
      DO 600 J=1,M1
      DO 600 I=1,L1
600   CALMF=CALMF+CVMASS(I,J)*W(I,J)
      DPDZC=-(SPMF-CALMF)/CALM
C
C
C  CORRECTION OF W
C
      DO 610 J=1,M1
      DO 610 I=1,L1
610   W(I,J)=W(I,J)-CVAREA(I,J)*DPDZC/AC(I,J)
      GOTO 100
650   NFS=NF
      CALL BOUND
      CALL SOLVE
100   CONTINUE
      RETURN
      END
C*********************************************************************
      SUBROUTINE PAPC
C*********************************************************************
      IMPLICIT REAL*8(A-H,O-Z)
      LOGICAL LSOLVE,LCPRIN,LPRINT,LPPRIN
      COMMON ASTORE(3528),X(21,21),Y(21,21),F(21,21,7),FU(21,21,7),
     1 FP(11,11,2),RHO(21,21),GAM(21,21),
     2 SC(21,21),SP(21,21),ACU(21,21),UHAT(21,21),
     3 D1T1(10,10,2),D2T1(10,10,2),D3T1(10,10,2),
     4 D1T2(10,10,2),D2T2(10,10,2),D3T2(10,10,2)
      COMMON /THRD/Z,DZ,DPDZ,DPDZC,PBAR,SPMF,WFD,CNUFD(4),LSTEP,ISTEP,
     1 ITMAX,ISTART,IPROB
      COMMON /PARM/RELAX(7),PRELAX
      COMMON /MONIT/LSOLVE(7),LCPRIN,LPRINT(7),LPPRIN
      COMMON /LABEL/TITLE(7),HDG(9)
      COMMON /INDX/NSWP(7),NPSWP(2),L1,L2,L3,M1,M2,M3,
     1 LP1,LP2,LP3,MP1,MP2,MP3,NFS,NFSMAX,NPS,NUME,IMONIT,LAST,
     2 LMID,MMID,LPMID,MPMID,IPREF,JPREF,ITER,IC(3),JC(3),IDEAL,
```

```
     3 IR,IRP1,IRM1,JR,JRP1,JRM1,IPR,IPRP1,IPRP2,IPRM1,IPRM2,JPR,JPRP1,
     4 JPRP2,JPRM1,JPRM2,NITMAX(7),NPITMX(2)
      COMMON /CONV/TOL(7),PTOL(2),DWDES,FCK(3,2),DPDZCK,CHGTOL,CHGCK
      COMMON /RODBUN/S,RAD,SDR,WBAR,FAREA,PERIM,PHY,DH,DHDR,XL,YL,TANPSI
     1 ,PSI,FBU4,FBU6,FB,FWAV,RHOA,CP1,DK1,DKDCP1,CP2,DK2,DKDCP2,
     2 RPOW,XPOW,YPOW,DMUA,REY,QW,  TAUW(21),TW,TI
C-----------------------------------------------------------------------
      DIMENSION APC(11,11),APE(11,11),APNE(11,11),APN(11,11),
     1 APNW(11,11),APW(11,11),APSW(11,11),APS(11,11),APSE(11,11),
     2 APENE(11,11),APNNE(11,11),APWSW(11,11),APSSW(11,11),APCON(11,11)
      DIMENSION U(21,21),V(21,21),W(21,21),WU(21,21),P(11,11),PC(11,11),
     1 VHAT(21,21),ACV(21,21)
      EQUIVALENCE (ASTORE(1),APC(1)),(ASTORE(122),APE(1)),(ASTORE(243),
     1 APNE(1)),(ASTORE(364),APN(1)),(ASTORE(485),APNW(1)),
     2 (ASTORE(606),APW(1)),(ASTORE( 727),APSW(1)),(ASTORE( 848),
     3 APS(1)),(ASTORE( 969),APSE(1)),(ASTORE(1090),APENE(1)),
     4 (ASTORE(1211),APNNE(1)),(ASTORE(1332),APWSW(1)),
     5 (ASTORE(1453),APSSW(1)),(ASTORE(1574),APCON(1))
      EQUIVALENCE (F(1),U(1)),(F(1,1,2),V(1)),(F(1,1,3),W(1))
      EQUIVALENCE (FU(1,1,3),WU(1))
      EQUIVALENCE (FP(1),P(1)),(FP(1,1,2),PC(1))
      EQUIVALENCE (SC(1),VHAT(1)),(SP(1),ACV(1))
C-----------------------------------------------------------------------
      DIMENSION AC1(2),AC2(2),AC3(2),FAC(3,2),G(3),CP(3,3),
     1 CPO(3,3),B(3,3),BO(3,3)
      DIMENSION DRWDZ(11,11)
      EQUIVALENCE (GAM(1),DRWDZ(1))
      DIMENSION C1(3),C2(3),C3(3)
C-----------------------------------------------------------------------
C     **********
      ENTRY PRES
C     **********
C
C  INITIALIZE ALL COEFFICIENTS
C
      DO 10 JP=1,MP1
      DO 10 IP=1,LP1
      APC(IP,JP)=0.D0
      APE(IP,JP)=0.D0
      APNE(IP,JP)=0.D0
      APN(IP,JP)=0.D0
      APNW(IP,JP)=0.D0
      APW(IP,JP)=0.D0
      APSW(IP,JP)=0.D0
      APS(IP,JP)=0.D0
      APSE(IP,JP)=0.D0
      APENE(IP,JP)=0.D0
      APNNE(IP,JP)=0.D0
      APWSW(IP,JP)=0.D0
      APSSW(IP,JP)=0.D0
      APCON(IP,JP)=0.D0
      DRWDZ(IP,JP)=0.D0
10    CONTINUE
      NUME=1
      DO 110 NUMPE=1,2
      IF (NUMPE.EQ.2) CALL DENSE
C
C  BOUNDARY CONTRIBUTIONS
```

```
C  (REMOVED FOR THIS VERSION-NO LEAKAGE AND NO OUTFLOW)
C
C  INTERNAL CONTRIBUTIONS
C
50    DO 120 JP=1,MP2
      JPP1=JP+1
      JPM1=JP-1
      J=2*JP-1
      JP1=J+1
      JP2=J+2
      DO 120 IP=1,LP2
      IPP1=IP+1
      IPM1=IP-1
      I=2*IP-1
      IP1=I+1
      IP2=I+2
      IF (NUMPE.EQ.2) GOTO 130
C
C  TYPE 1 PRELIMINARIES
      I1=IP2
      I2=IP1
      I3=IP1
      J1=JP1
      J2=JP1
      J3=J
      DET=X(I1,J1)*Y(I2,J2)+X(I2,J2)*Y(I3,J3)+X(I3,J3)*Y(I1,J1)
     1    -Y(I1,J1)*X(I2,J2)-Y(I2,J2)*X(I3,J3)-Y(I3,J3)*X(I1,J1)
      AREA=DABS(DET)/6.DO
      RHOE=RHO(IP1,J)
      RHOD2=RHOE*0.5D0
      DRWDZ(IP,JP)=DRWDZ(IP,JP)+(WU(I,J)-W(I,J)+(WU(IP1,J)-W(IP1,J)
     1 +WU(IP1,JP1)-W(IP1,JP1))*1.5DO)*RHOE*AREA/DZ
      DRWDZ(IPP1,JP)=DRWDZ(IPP1,JP)+(WU(IP2,J)-W(IP2,J)
     1 +(WU(IP2,JP1)-W(IP2,JP1)+WU(IP1,J)-W(IP1,J))*1.5D0)
     2 *RHOE*AREA/DZ
      DRWDZ(IPP1,JPP1)=DRWDZ(IPP1,JPP1)+(WU(IP2,JP2)-W(IP2,JP2)
     1 +(WU(IP1,JP1)-W(IP1,JP1)+WU(IP2,JP1)-W(IP2,JP1))*1.5DO)
     2 *RHOE*AREA/DZ
      GOTO 140
C
C  TYPE 2 PRELIMINARIES
C
130   I1=IP1
      I2=I
      I3=IP1
      J1=JP2
      J2=JP1
      J3=JP1
      DET=X(I1,J1)*Y(I2,J2)+X(I2,J2)*Y(I3,J3)+X(I3,J3)*Y(I1,J1)
     1    -Y(I1,J1)*X(I2,J2)-Y(I2,J2)*X(I3,J3)-Y(I3,J3)*X(I1,J1)
      AREA=DABS(DET)/6.DO
      RHOE=RHO(I,JP1)
      RHOD2=RHOE*0.5D0
      DRWDZ(IP,JP)=DRWDZ(IP,JP)+(WU(I,J)-W(I,J)+(WU(IP1,JP1)-W(IP1,JP1)
     1 +WU(I,JP1)-W(I,JP1))*1.5D0)*RHOE*AREA/DZ
      DRWDZ(IPP1,JPP1)=DRWDZ(IPP1,JPP1)+(WU(IP2,JP2)-W(IP2,JP2)
     1 +(WU(IP1,JP2)-W(IP1,JP2)+WU(IP1,JP1)-W(IP1,JP1))*1.5DO)
     2 *RHOE*AREA/DZ
```

```
      DRWDZ(IP,JPP1)=DRWDZ(IP,JPP1)+(WU(I,JP2)-W(I,JP2)
     1 +(WU(I,JP1)-W(I,JP1)+WU(IP1,JP2)-W(IP1,JP2))*1.5D0)
     2 *RHOE*AREA/DZ
C
140   AC1(1)=ACU(I1,J1)
      AC2(1)=ACU(I2,J2)
      AC3(1)=ACU(I3,J3)
      AC1(2)=ACV(I1,J1)
      AC2(2)=ACV(I2,J2)
      AC3(2)=ACV(I3,J3)
      YO=(Y(I1,J1)+Y(I2,J2)+Y(I3,J3))/3.D0
      FAC(1,1)=(Y(I1,J1)-YO)*RHOD2
      FAC(2,1)=(Y(I2,J2)-YO)*RHOD2
      FAC(3,1)=(Y(I3,J3)-YO)*RHOD2
      XO=(X(I1,J1)+X(I2,J2)+X(I3,J3))/3.D0
      FAC(1,2)=(XO-X(I1,J1))*RHOD2
      FAC(2,2)=(XO-X(I2,J2))*RHOD2
      FAC(3,2)=(XO-X(I3,J3))*RHOD2
C
C  CALCULATION OF G
C
      G(1)=(FAC(1,1)*(4.D0*UHAT(I1,J1)+UHAT(I2,J2)+UHAT(I3,J3))
     1-+FAC(1,2)*(4.D0*VHAT(I1,J1)+VHAT(I2,J2)+VHAT(I3,J3)))/3.D0
      G(2)=(FAC(2,1)*(UHAT(I1,J1)+4.D0*UHAT(I2,J2)+UHAT(I3,J3))
     1 +FAC(2,2)*(VHAT(I1,J1)+4.D0*VHAT(I2,J2)+VHAT(I3,J3)))/3.D0
      G(3)=(FAC(3,1)*(UHAT(I1,J1)+UHAT(I2,J2)+4.D0*UHAT(I3,J3))
     1 +FAC(3,2)*(VHAT(I1,J1)+VHAT(I2,J2)+4.D0*VHAT(I3,J3)))/3.D0
C
C  INITIALIZE THE MATRICES B AND BO
C
      DO 150 JJ=1,3
      DO 150 II=1,3
      B(II,JJ)=0.D0
150   BO(II,JJ)=0.D0
C
C  CALCULATION OF THE COEFFICIENTS D (FOR U AND FOR V)
C
      DO 160 NFV=1,2
      IF (NUMPE.EQ.2) GOTO 170
C
C  TRIANGLE OF TYPE 1
C
      D1=D1T1(IP,JP,NFV)
      D2=D2T1(IP,JP,NFV)
      D3=D3T1(IP,JP,NFV)
      IF (IPP1.EQ.LP1) GOTO 162
      D11=D2T2(IPP1,JP,NFV)
      D12=D1T2(IPP1,JP,NFV)
      D13=D3T2(IPP1,JP,NFV)
      GOTO 164
C
C  RIGHT-HAND SIDE BOUNDARY
C
162   D11=0.D0
      D12=0.D0
      D13=0.D0
C
164   D21=D1T2(IP,JP,NFV)
```

```
      D22=D3T2(IP,JP,NFV)
      D23=D2T2(IP,JP,NFV)
      IF (JP.EQ.1) GOTO 166
      D31=D3T2(IP,JPM1,NFV)
      D32=D2T2(IP,JPM1,NFV)
      D33=D1T2(IP,JPM1,NFV)
      GOTO 180
C
C   BOTTOM SIDE BOUNDARY
C
166   D31=0.DO
      D32=0.DO
      D33=0.DO
      GOTO 180
C
C   TRIANGLE OF TYPE 2
C
170   D1=D1T2(IP,JP,NFV)
      D2=D2T2(IP,JP,NFV)
      D3=D3T2(IP,JP,NFV)
      IF (JPP1.EQ.MP1) GOTO 172
      D11=D3T1(IP,JPP1,NFV)
      D12=D2T1(IP,JPP1,NFV)
      D13=D1T1(IP,JPP1,NFV)
      GOTO 174
C
C   TOP-SIDE BOUNDARY
C
172   D11=0.DO
      D12=0.DO
      D13=0.DO
C
174   IF (IP.EQ.1) GOTO 176
      D21=D2T1(IPM1,JP,NFV)
      D22=D1T1(IPM1,JP,NFV)
      D23=D3T1(IPM1,JP,NFV)
      GOTO 178
C
C   LEFT-HAND SIDE BOUNDARY
C
176   D21=0.DO
      D22=0.DO
      D23=0.DO
C
178   D31=D1T1(IP,JP,NFV)
      D32=D3T1(IP,JP,NFV)
      D33=D2T1(IP,JP,NFV)
C
C   CALCULATION OF CPU AND CPV (BOTH HERE DENOTED BY CP)
C
180   C1(1)=D1/AC1(NFV)
      C2(1)=(D1+D21)/AC2(NFV)
      C3(1)=(D1+D31)/AC3(NFV)
      C1(2)=(D2+D12)/AC1(NFV)
      C2(2)=D2/AC2(NFV)
      C3(2)=(D2+D32)/AC3(NFV)
      C1(3)=(D3+D13)/AC1(NFV)
      C2(3)=(D3+D23)/AC2(NFV)
```

```
      C3(3)=D3/AC3(NFV)
C
C  ** SPECIAL PROCEDURE FOR TOP SKEWED SYMMETRY LINE
C
      IF (NFV.NE.2 .OR. NUMPE.NE.2 .OR. JP.NE.MP2.OR.IPROB.EQ.1)
     1      GOTO 182
      C1(1)=D1T2(IP,MP2,1)*TANPSI/AC1(1)
      C1(2)=D2T2(IP,MP2,1)*TANPSI/AC1(1)
      C1(3)=D3T2(IP,MP2,1)*TANPSI/AC1(1)
182   DO 184 II=1,3
      CP(1,II)=4.DO*C1(II)+C2(II)+C3(II)
      CP(2,II)=C1(II)+4.DO*C2(II)+C3(II)
184   CP(3,II)=C1(II)+C2(II)+4.DO*C3(II)
      C1(1)=D11/AC1(NFV)
      C2(2)=D22/AC2(NFV)
      C3(3)=D33/AC3(NFV)
      CPO(1,1)=4.DO*C1(1)
      CPO(2,1)=C1(1)
      CPO(3,1)=C1(1)
      CPO(1,2)=C2(2)
      CPO(2,2)=4.DO*C2(2)
      CPO(3,2)=C2(2)
      CPO(1,3)=C3(3)
      CPO(2,3)=C3(3)
      CPO(3,3)=4.DO*C3(3)
C
C  CALCULATION OF THE COEFFICIENTS B AND BO
C
      DO 190 II=1,3
      DO 190 JJ=1,3
      B(II,JJ)=B(II,JJ)+FAC(II,NFV)*CP(II,JJ)
190   BO(II,JJ)=BO(II,JJ)+FAC(II,NFV)*CPO(II,JJ)
160   CONTINUE
C-----------------------------------------------------------------------
C  ASSEMBLY
C-----------------------------------------------------------------------
      IF (NUMPE.NE.1) GOTO 200
C  ******
C  TYPE 1
C  ******
C  WRT (IP,JP)
      APC(IP,JP)=APC(IP,JP)+B(2,1)-B(3,1)
      APE(IP,JP)=APE(IP,JP)+B(3,2)-B(2,2)
      APNE(IP,JP)=APNE(IP,JP)+B(3,3)-B(2,3)
      APENE(IP,JP)=APENE(IP,JP)+BO(3,1)-BO(2,1)
      APN(IP,JP)=APN(IP,JP)+BO(3,2)-BO(2,2)
      APS(IP,JP)=APS(IP,JP)+BO(3,3)-BO(2,3)
      APCON(IP,JP)=APCON(IP,JP)+G(3)-G(2)
C  WRT (IP+1,JP)
      APC(IPP1,JP)=APC(IPP1,JP)+B(3,2)-B(1,2)
      APW(IPP1,JP)=APW(IPP1,JP)+B(1,1)-B(3,1)
      APN(IPP1,JP)=APN(IPP1,JP)+B(1,3)-B(3,3)
      APNE(IPP1,JP)=APNE(IPP1,JP)+BO(1,1)-BO(3,1)
      APNW(IPP1,JP)=APNW(IPP1,JP)+BO(1,2)-BO(3,2)
      APSW(IPP1,JP)=APSW(IPP1,JP)+BO(1,3)-BO(3,3)
      APCON(IPP1,JP)=APCON(IPP1,JP)+G(1)-G(3)
C  WRT (IP+1,JP+1)
      APC(IPP1,JPP1)=APC(IPP1,JPP1)+B(1,3)-B(2,3)
```

```
      APSW(IPP1,JPP1)=APSW(IPP1,JPP1)+B(2,1)-B(1,1)
      APS(IPP1,JPP1)=APS(IPP1,JPP1)+B(2,2)-B(1,2)
      APE(IPP1,JPP1)=APE(IPP1,JPP1)+BO(2,1)-BO(1,1)
      APW(IPP1,JPP1)=APW(IPP1,JPP1)+BO(2,2)-BO(1,2)
      APSSW(IPP1,JPP1)=APSSW(IPP1,JPP1)+BO(2,3)-BO(1,3)
      APCON(IPP1,JPP1)=APCON(IPP1,JPP1)+G(2)-G(1)
      GOTO 120
C
C  ASSEMBLY FOR TRIANGLE OF TYPE 2
C
C  WRT (IP,JP)
200   APC(IP,JP)=APC(IP,JP)+B(2,1)-B(3,1)
      APNE(IP,JP)=APNE(IP,JP)+B(3,2)-B(2,2)
      APN(IP,JP)=APN(IP,JP)+B(3,3)-B(2,3)
      APNNE(IP,JP)=APNNE(IP,JP)+BO(3,1)-BO(2,1)
      APW(IP,JP)=APW(IP,JP)+BO(3,2)-BO(2,2)
      APE(IP,JP)=APE(IP,JP)+BO(3,3)-BO(2,3)
      APCON(IP,JP)=APCON(IP,JP)+G(3)-G(2)
C  WRT (IP+1,JP+1)
      APC(IPP1,JPP1)=APC(IPP1,JPP1)+B(3,2)-B(1,2)
      APSW(IPP1,JPP1)=APSW(IPP1,JPP1)+B(1,1)-B(3,1)
      APW(IPP1,JPP1)=APW(IPP1,JPP1)+B(1,3)-B(3,3)
      APN(IPP1,JPP1)=APN(IPP1,JPP1)+BO(1,1)-BO(3,1)
      APWSW(IPP1,JPP1)=APWSW(IPP1,JPP1)+BO(1,2)-BO(3,2)
      APS(IPP1,JPP1)=APS(IPP1,JPP1)+BO(1,3)-BO(3,3)
      APCON(IPP1,JPP1)=APCON(IPP1,JPP1)+G(1)-G(3)
C  WRT (IP,JP+1)
      APC(IP,JPP1)=APC(IP,JPP1)+B(1,3)-B(2,3)
      APS(IP,JPP1)=APS(IP,JPP1)+B(2,1)-B(1,1)
      APE(IP,JPP1)=APE(IP,JPP1)+B(2,2)-B(1,2)
      APNE(IP,JPP1)=APNE(IP,JPP1)+BO(2,1)-BO(1,1)
      APSW(IP,JPP1)=APSW(IP,JPP1)+BO(2,2)-BO(1,2)
      APSE(IP,JPP1)=APSE(IP,JPP1)+BO(2,3)-BO(1,3)
      APCON(IP,JPP1)=APCON(IP,JPP1)+G(2)-G(1)
120   CONTINUE
110   CONTINUE
      WRITE(8) ASTORE,DRWDZ
C
C  UNDERRELAXATION OF PRESSURE
C  (ALSO THE TERM DRWDZ IN THE CONTINUITY EQUATION IS ADDED TO APCON)
C
      DO 115 JP=1,MP1
      DO 115 IP=1,LP1
      APC(IP,JP)=APC(IP,JP)/PRELAX
115   APCON(IP,JP)=APCON(IP,JP)+APC(IP,JP)*(1.D0-PRELAX)*P(IP,JP)
     1 +DRWDZ(IP,JP)
      NPS=1
      CALL PBOUND
      CALL PSOLVE
      RETURN
C-----------------------------------------------------------------------
      ENTRY PCORR
C-----------------------------------------------------------------------
      READ (8) ASTORE,APCON
      NUME=2
      DO 410 NUMPER=1,2
      NUMPE=3-NUMPER
      IF (NUMPE.EQ.1) CALL DENSE
```

```
C
C  BOUNDARY CONTRIBUTIONS
C  (REMOVED)
C
C  INTERNAL CONTRIBUTIONS
C
350   DO 415 JP=1,MP2
      JPP1=JP+1
      J=2*JP-1
      JP1=J+1
      JP2=J+2
      DO 415 IP=1,LP2
      IPP1=IP+1
      I=2*IP-1
      IP1=I+1
      IP2=I+2
      IF (NUMPE.EQ.2) GOTO 420
C
C  TYPE 1 PRELIMINARIES
C
      I1=IP2
      I2=IP1
      I3=IP1
      J1=JP1
      J2=JP1
      J3=J
      RHOD2=RHO(IP1,J)*0.5D0
      GOTO 430
C
C  TYPE 2 PRELIMINARIES
C
420   I1=IP1
      I2=I
      I3=IP1
      J1=JP2
      J2=JP1
      J3=JP1
      RHOD2=RHO(I,JP1)*0.5D0
C
430   YO=(Y(I1,J1)+Y(I2,J2)+Y(I3,J3))/3.D0
      FAC(1,1)=(Y(I1,J1)-YO)*RHOD2
      FAC(2,1)=(Y(I2,J2)-YO)*RHOD2
      FAC(3,1)=(Y(I3,J3)-YO)*RHOD2
      XO=(X(I1,J1)+X(I2,J2)+X(I3,J3))/3.D0
      FAC(1,2)=(XO-X(I1,J1))*RHOD2
      FAC(2,2)=(XO-X(I2,J2))*RHOD2
      FAC(3,2)=(XO-X(I3,J3))*RHOD2
C
C  CALCULATION OF G
C
      G(1)=(FAC(1,1)*(4.D0*U(I1,J1)+U(I2,J2)+U(I3,J3))
     1  +FAC(1,2)*(4.D0*V(I1,J1)+V(I2,J2)+V(I3,J3)))/3.D0
      G(2)=(FAC(2,1)*(U(I1,J1)+4.D0*U(I2,J2)+U(I3,J3))
     1  +FAC(2,2)*(V(I1,J1)+4.D0*V(I2,J2)+V(I3,J3)))/3.D0
      G(3)=(FAC(3,1)*(U(I1,J1)+U(I2,J2)+4.D0*U(I3,J3))
     1  +FAC(3,2)*(V(I1,J1)+V(I2,J2)+4.D0*V(I3,J3)))/3.D0
C-----------------------------------------------------------------
      IF (NUMPE.EQ.2) GOTO 440
```

```
C
C  ASSEMBLY FOR TRIANGLE OF TYPE 1
C
      APCON(IP,JP)=APCON(IP,JP)+G(3)-G(2)
      APCON(IPP1,JP)=APCON(IPP1,JP)+G(1)-G(3)
      APCON(IPP1,JPP1)=APCON(IPP1,JPP1)+G(2)-G(1)
      GOTO 415
C
C  ASSEMBLY FOR TRIANGLE OF TYPE 2
C
440   APCON(IP,JP)=APCON(IP,JP)+G(3)-G(2)
      APCON(IPP1,JPP1)=APCON(IPP1,JPP1)+G(1)-G(3)
      APCON(IP,JPP1)=APCON(IP,JPP1)+G(2)-G(1)
415   CONTINUE
410   CONTINUE
C-----------------------------------------------------------------------
      NPS=2
      CALL PBOUND
      CALL PSOLVE
      SSUM=0.D0
      SMAX=0.D0
      DO 510 JP=1,MP1
      DO 510 IP=1,LP1
      SOURCE=DABS(APCON(IP,JP))
      SSUM=SSUM+SOURCE
      SMAX=DMAX1(SMAX,SOURCE)
510   CONTINUE
      SAV=SSUM/DFLOAT(LP1*MP1)
      WRITE(6,520) SAV,SMAX
520   FORMAT(//3X,'SAV = ',1PD15.5,//,3X,'SMAX = ',1PD15.7)
      RETURN
      END
C***********************************************************************
      SUBROUTINE PSOLVE
C***********************************************************************
      IMPLICIT REAL*8(A-H,O-Z)
      LOGICAL LSOLVE,LCPRIN,LPRINT,LPPRIN
      COMMON ASTORE(3528),X(21,21),Y(21,21),F(21,21,7),FU(21,21,7),
     1 FP(11,11,2),RHO(21,21),GAM(21,21),
     2 SC(21,21),SP(21,21),ACU(21,21),UHAT(21,21),
     3 D1T1(10,10,2),D2T1(10,10,2),D3T1(10,10,2),
     4 D1T2(10,10,2),D2T2(10,10,2),D3T2(10,10,2)
      COMMON /THRD/Z,DZ,DPDZ,DPDZC,PBAR,SPMF,WFD,CNUFD(4),LSTEP,ISTEP,
     1 ITMAX,ISTART,IPROB
      COMMON /PARM/RELAX(7),PRELAX
      COMMON /MONIT/LSOLVE(7),LCPRIN,LPRINT(7),LPPRIN
      COMMON /LABEL/TITLE(7),HDG(9)
      COMMON /INDX/NSWP(7),NPSWP(2),L1,L2,L3,M1,M2,M3,
     1 LP1,LP2,LP3,MP1,MP2,MP3,NFS,NFSMAX,NPS,NUME,IMONIT,LAST,
     2 LMID,MMID,LPMID,MPMID,IPREF,JPREF,ITER,IC(3),JC(3),IDEAL,
     3 IR,IRP1,IRM1,JR,JRP1,JRM1,IPR,IPRP1,IPRP2,IPRM1,IPRM2,JPR,JPRP1,
     4 JPRP2,JPRM1,JPRM2,NITMAX(7),NPITMX(2)
      COMMON /CONV/TOL(7),PTOL(2),DWDES,FCK(3,2),DPDZCK,CHGTOL,CHGCK
      COMMON /RODBUN/S,RAD,SDR,WBAR,FAREA,PERIM,PHY,DH,DHDR,XL,YL,TANPSI
     1 ,PSI,FBU4,FBU6,FB,FWAV,RHOA,CP1,DK1,DKDCP1,CP2,DK2,DKDCP2,
     2 RPOW,XPOW,YPOW,DMUA,REY,QW, TAUW(21),TW,TI
C-----------------------------------------------------------------------
      DIMENSION APC(11,11),APE(11,11),APNE(11,11),APN(11,11),
```

```
     1 APNW(11,11),APW(11,11),APSW(11,11),APS(11,11),APSE(11,11),
     2 APENE(11,11),APNNE(11,11),APWSW(11,11),APSSW(11,11),APCON(11,11)
      EQUIVALENCE (ASTORE(1),APC(1)),(ASTORE(122),APE(1)),(ASTORE(243),
     1 APNE(1)),(ASTORE(364),APN(1)),(ASTORE(485),APNW(1)),
     2 (ASTORE(606),APW(1)),(ASTORE( 727),APSW(1)),(ASTORE( 848),
     3 APS(1)),(ASTORE( 969),APSE(1)),(ASTORE(1090),APENE(1)),
     4 (ASTORE(1211),APNNE(1)),(ASTORE(1332),APWSW(1)),
     5 (ASTORE(1453),APSSW(1)),(ASTORE(1574),APCON(1))
C-----------------------------------------------------------------------
      DIMENSION PT(11),QT(11)
C     ****
C---  TDMA
C     ****
      IF (IMONIT.EQ.1) WRITE(6,10) NPS
10    FORMAT(//3X,'CONVERGENCE MONITOR FOR NPS = ',I1//,
     1 3X,'SWEEP',4X,'CENTRE',12X,'SW',16X,'SE',16X,'NW',16X,'NE',
     2 16X,'RESIDUAL'/)
      NITER=1
316   DO 110 INDEX=1,2
C
C---  I-SWEEP
C
      DO 120 II=1,LP1
      I=II
      IF (INDEX.EQ.2) I=LP1+1-II
      IP1=I+1
      IM1=I-1
      D=APCON(I,1)
      IF (I.EQ.1) GOTO 130
      D=D+APW(I,1)*FP(IM1,1,NPS)+APNW(I,1)*FP(IM1,2,NPS)
      IF (I.EQ.LP1) GOTO 140
130   D=D+APE(I,1)*FP(IP1,1,NPS)+APNE(I,1)*FP(IP1,2,NPS)
     1 +APNNE(I,1)*FP(IP1,3,NPS)
      IF (I.EQ.LP2) GOTO 140
      D=D+APENE(I,1)*FP(I+2,2,NPS)
140   PT(1)=APN(I,1)/APC(I,1)
      QT(1)=D/APC(I,1)
      D=APCON(I,2)
      IF (I.EQ.1) GOTO 142
      D=D+APNW(I,2)*FP(IM1,3,NPS)
     1 +APW(I,2)*FP(IM1,2,NPS)+APSW(I,2)*FP(IM1,1,NPS)
      IF (I.EQ.2) GOTO 142
      D=D+APWSW(I,2)*FP(I-2,1,NPS)
      IF (I.EQ.LP1) GOTO 145
142   D=D+APSE(I,2)*FP(IP1,1,NPS)+APE(I,2)*FP(IP1,2,NPS)
     1 +APNE(I,2)*FP(IP1,3,NPS)+APNNE(I,2)*FP(IP1,4,NPS)
      IF (I.EQ.LP2) GOTO 145
      D=D+APENE(I,2)*FP(I+2,3,NPS)
145   DENOM=APC(I,2)-APS(I,2)*PT(1)
      PT(2)=APN(I,2)/DENOM
      QT(2)=(APS(I,2)*QT(1)+D)/DENOM
      DO 150 J=3,MP3
      D=APCON(I,J)
      IF (I.EQ.1) GOTO 160
      D=D+APW(I,J)*FP(IM1,J,NPS)+APNW(I,J)*FP(IM1,J+1,NPS)
     1 +APSW(I,J)*FP(IM1,J-1,NPS)
     2 +APSSW(I,J)*FP(IM1,J-2,NPS)
      IF (I.EQ.2) GOTO 160
```

```
      D=D+APWSW(I,J)*FP(I-2,J-1,NPS)
      IF (I.EQ.LP1) GOTO 170
160   D=D+APE(I,J)*FP(IP1,J,NPS)+APNE(I,J)*FP(IP1,J+1,NPS)
     1 +APSE(I,J)*FP(IP1,J-1,NPS)
     2 +APNNE(I,J)*FP(IP1,J+2,NPS)
      IF (I.EQ.LP2) GOTO 170
      D=D+APENE(I,J)*FP(I+2,J+1,NPS)
170   DENOM=APC(I,J)-APS(I,J)*PT(J-1)
      PT(J)=APN(I,J)/DENOM
150   QT(J)=(APS(I,J)*QT(J-1)+D)/DENOM
      D=APCON(I,MP2)
      IF (I.EQ.1) GOTO 152
      D=D+APNW(I,MP2)*FP(IM1,MP1,NPS)+APW(I,MP2)*FP(IM1,MP2,NPS)
     1 +APSW(I,MP2)*FP(IM1,MP3,NPS)+APSSW(I,MP2)*FP(IM1,MP2-2,NPS)
      IF (I.EQ.2) GOTO 152
      D=D+APWSW(I,MP2)*FP(I-2,MP3,NPS)
      IF (I.EQ.LP1) GOTO 155
152   D=D+APSE(I,MP2)*FP(IP1,MP3,NPS)+APE(I,MP2)*FP(IP1,MP2,NPS)
     1 +APNE(I,MP2)*FP(IP1,MP1,NPS)
      IF (I.EQ.LP2) GOTO 155
      D=D+APENE(I,MP2)*FP(I+2,MP1,NPS)
155   DENOM=APC(I,MP2)-APS(I,MP2)*PT(MP3)
      PT(MP2)=APN(I,MP2)/DENOM
      QT(MP2)=(APS(I,MP2)*QT(MP3)+D)/DENOM
      D=APCON(I,MP1)
      IF (I.EQ.1) GOTO 180
      D=D+APW(I,MP1)*FP(IM1,MP1,NPS)+APSW(I,MP1)*FP(IM1,MP2,NPS)
     1 +APSSW(I,MP1)*FP(IM1,MP3,NPS)
      IF (I.EQ.2) GOTO 180
      D=D+APWSW(I,MP1)*FP(I-2,MP2,NPS)
      IF (I.EQ.LP1) GOTO 190
180   D=D+APE(I,MP1)*FP(IP1,MP1,NPS)+APSE(I,MP1)*FP(IP1,MP2,NPS)
190   PT(MP1)=0.D0
      QT(MP1)=(APS(I,MP1)*QT(MP2)+D)/(APC(I,MP1)-APS(I,MP1)*PT(MP2))
C---  BACK SUBSTITUTION
      FP(I,MP1,NPS)=QT(MP1)
      DO 200 JJ=1,MP2
      J=MP1-JJ
200   FP(I,J,NPS)=PT(J)*FP(I,J+1,NPS)+QT(J)
120   CONTINUE
C
C---  J-SWEEP
C
      DO 220 JJ=1,MP1
      J=JJ
      IF (INDEX.EQ.2) J=MP1+1-JJ
      JP1=J+1
      JM1=J-1
      D=APCON(1,J)
      IF (J.EQ.1) GOTO 230
      D=D+APS(1,J)*FP(1,JM1,NPS)+APSE(1,J)*FP(2,JM1,NPS)
      IF (J.EQ.MP1) GOTO 240
230   D=D+APN(1,J)*FP(1,JP1,NPS)+APNE(1,J)*FP(2,JP1,NPS)
     1 +APENE(1,J)*FP(3,JP1,NPS)
      IF (J.EQ.MP2) GOTO 240
      D=D+APNNE(1,J)*FP(2,J+2,NPS)
240   PT(1)=APE(1,J)/APC(1,J)
      QT(1)=D/APC(1,J)
```

```
      D=APCON(2,J)
      IF (J.EQ.1) GOTO 242
      D=D+APSW(2,J)*FP(1,JM1,NPS)+APS(2,J)*FP(2,JM1,NPS)
     1 +APSE(2,J)*FP(3,JM1,NPS)
      IF (J.EQ.2) GOTO 242
      D=D+APSSW(2,J)*FP(1,J-2,NPS)
      IF (J.EQ.MP1) GOTO 245
242   D=D+APNE(2,J)*FP(3,JP1,NPS)+APN(2,J)*FP(2,JP1,NPS)
     1 +APNW(2,J)*FP(1,JP1,NPS)+APENE(2,J)*FP(4,JP1,NPS)
      IF (J.EQ.MP2) GOTO 245
      D=D+APNNE(2,J)*FP(3,J+2,NPS)
245   DENOM=APC(2,J)-APW(2,J)*PT(1)
      PT(2)=APE(2,J)/DENOM
      QT(2)=(APW(2,J)*QT(1)+D)/DENOM
      DO 250 I=3,LP3
      D=APCON(I,J)
      IF (J.EQ.1) GOTO 260
      D=D+APS(I,J)*FP(I,JM1,NPS)+APSW(I,J)*FP(I-1,JM1,NPS)
     1 +APSE(I,J)*FP(I+1,JM1,NPS)+APWSW(I,J)*FP(I-2,JM1,NPS)
      IF (J.EQ.2) GOTO 260
      D=D+APSSW(I,J)*FP(I-1,J-2,NPS)
      IF (J.EQ.MP1) GOTO 270
260   D=D+APN(I,J)*FP(I,JP1,NPS)+APNW(I,J)*FP(I-1,JP1,NPS)
     1 +APNE(I,J)*FP(I+1,JP1,NPS)
     2 +APENE(I,J)*FP(I+2,JP1,NPS)
      IF (J.EQ.MP2) GOTO 270
      D=D+APNNE(I,J)*FP(I+1,J+2,NPS)
270   DENOM=APC(I,J)-APW(I,J)*PT(I-1)
      PT(I)=APE(I,J)/DENOM
250   QT(I)=(APW(I,J)*QT(I-1)+D)/DENOM
      D=APCON(LP2,J)
      IF (J.EQ.1) GOTO 252
      D=D+APSW(LP2,J)*FP(LP3,JM1,NPS)+APS(LP2,J)*FP(LP2,JM1,NPS)
     1 +APSE(LP2,J)*FP(LP1,JM1,NPS)+APWSW(LP2,J)*FP(LP2-2,JM1,NPS)
      IF (J.EQ.2) GOTO 252
      D=D+APSSW(LP2,J)*FP(LP3,J-2,NPS)
      IF (J.EQ.MP1) GOTO 255
252   D=D+APNW(LP2,J)*FP(LP3,JP1,NPS)
     1 +APN(LP2,J)*FP(LP2,JP1,NPS)+APNE(LP2,J)*FP(LP1,JP1,NPS)
      IF (J.EQ.MP2) GOTO 255
      D=D+APNNE(LP2,J)*FP(LP1,J+2,NPS)
255   DENOM=APC(LP2,J)-APW(LP2,J)*PT(LP3)
      PT(LP2)=APE(LP2,J)/DENOM
      QT(LP2)=(APW(LP2,J)*QT(LP3)+D)/DENOM
      D=APCON(LP1,J)
      IF (J.EQ.1) GOTO 280
      D=D+APS(LP1,J)*FP(LP1,JM1,NPS)+APSW(LP1,J)*FP(LP2,JM1,NPS)
     1 +APWSW(LP1,J)*FP(LP3,JM1,NPS)
      IF (J.EQ.2) GOTO 280
      D=D+APSSW(LP1,J)*FP(LP2,J-2,NPS)
      IF (J.EQ.MP1) GOTO 290
280   D=D+APN(LP1,J)*FP(LP1,JP1,NPS)+APNW(LP1,J)*FP(LP2,JP1,NPS)
290   PT(LP1)=0.D0
      QT(LP1)=(APW(LP1,J)*QT(LP2)+D)/(APC(LP1,J)-APW(LP1,J)*PT(LP2))
C
C---  BACK SUBSTITUTION
C
      FP(LP1,J,NPS)=QT(LP1)
```

```
      DO 300 II=1,LP2
      I=LP1-II
300   FP(I,J,NPS)=PT(I)*FP(I+1,J,NPS)+QT(I)
220   CONTINUE
110   CONTINUE
      R=APC(IPR,JPR)*FP(IPR,JPR,NPS)-APE(IPR,JPR)*FP(IPRP1,JPR,NPS)
     1 -APNE(IPR,JPR)*FP(IPRP1,JPRP1,NPS)-APN(IPR,JPR)*FP(IPR,JPRP1,NPS)
     2 -APNW(IPR,JPR)*FP(IPRM1,JPRP1,NPS)
     3 -APW(IPR,JPR)*FP(IPRM1,JPR,NPS)-APSW(IPR,JPR)*FP(IPRM1,JPRM1,NPS)
     4 -APS(IPR,JPR)*FP(IPR,JPRM1,NPS)-APSE(IPR,JPR)*FP(IPRP1,JPRM1,NPS)
     5 -APENE(IPR,JPR)*FP(IPRP2,JPRP1,NPS)-APNNE(IPR,JPR)*
     6  FP(IPRP1,JPRP2,NPS)-APWSW(IPR,JPR)*FP(IPRM2,JPRM1,NPS)
     7 -APSSW(IPR,JPR)*FP(IPRM1,JPRM2,NPS)-APCON(IPR,JPR)
      IF(IMONIT.EQ.0) GOTO 100
      WRITE(6,310) NITER,FP(LPMID,MPMID,NPS),FP(2,2,NPS),FP(LP2,2,NPS),
     1 FP(2,MP2,NPS),FP(LP2,MP2,NPS),R
310   FORMAT(3X,I4,5X,6(1PD15.8,3X))
C
C  CONVERGENCE TEST
C
100   NITER=NITER+1
      IF (NITER.LE.NPSWP(NPS)) GOTO 316
      IF (DABS(R).LT.PTOL(NPS)) RETURN
      IF (NITER.LE.NPITMX(NPS)) GOTO 316
      WRITE (6,314)
314   FORMAT(//3X,'MAXIMUM NUMBER OF ITERATIONS EXCEEDED')
      RETURN
      END
C*********************************************************************
      SUBROUTINE SOLVE
C*********************************************************************
      IMPLICIT REAL*8(A-H,O-Z)
      LOGICAL LSOLVE,LCPRIN,LPRINT,LPPRIN
      COMMON ASTORE(3528),X(21,21),Y(21,21),F(21,21,7),FU(21,21,7),
     1 FP(11,11,2),RHO(21,21),GAM(21,21),
     2 SC(21,21),SP(21,21),ACU(21,21),UHAT(21,21),
     3 D1T1(10,10,2),D2T1(10,10,2),D3T1(10,10,2),
     4 D1T2(10,10,2),D2T2(10,10,2),D3T2(10,10,2)
      COMMON /THRD/Z,DZ,DPDZ,DPDZC,PBAR,SPMF,WFD,CNUFD(4),LSTEP,ISTEP,
     1 ITMAX,ISTART,IPROB
      COMMON /PARM/RELAX(7),PRELAX
      COMMON /MONIT/LSOLVE(7),LCPRIN,LPRINT(7),LPPRIN
      COMMON /LABEL/TITLE(7),HDG(9)
      COMMON /INDX/NSWP(7),NPSWP(2),L1,L2,L3,M1,M2,M3,
     1 LP1,LP2,LP3,MP1,MP2,MP3,NFS,NFSMAX,NPS,NUME,IMONIT,LAST,
     2 LMID,MMID,LPMID,MPMID,IPREF,JPREF,ITER,IC(3),JC(3),IDEAL,
     3 IR,IRP1,IRM1,JR,JRP1,JRM1,IPR,IPRP1,IPRP2,IPRM1,IPRM2,JPR,JPRP1,
     4 JPRP2,JPRM1,JPRM2,NITMAX(7),NPITMX(2)
      COMMON /CONV/TOL(7),PTOL(2),DWDES,FCK(3,2),DPDZCK,CHGTOL,CHGCK
      COMMON /RODBUN/S,RAD,SDR,WBAR,FAREA,PERIM,PHY,DH,DHDR,XL,YL,TANPSI
     1 ,PSI,FBU4,FBU6,FB,FWAV,RHOA,CP1,DK1,DKDCP1,CP2,DK2,DKDCP2,
     2 RPOW,XPOW,YPOW,DMUA,REY,QW, TAUW(21),TW,TI
C-----------------------------------------------------------------------
      DIMENSION AC(21,21),AE(21,21),ANE(21,21),AN(21,21),
     1 AW(21,21),ASW(21,21),AS(21,21),ACON(21,21)
      EQUIVALENCE (ASTORE(1),AC(1)),(ASTORE(442),AE(1)),(ASTORE( 883),
     1 ANE(1)),(ASTORE(1324),AN(1)),(ASTORE(1765),AW(1)),
     2 (ASTORE(2206),ASW(1)),(ASTORE(2647),AS(1)),(ASTORE(3088),
```

```
     3 ACON(1))
C-----------------------------------------------------------------------
      DIMENSION PT(21),QT(21)
C  ****
C  TDMA
C  ****
      IF (IMONIT.EQ.1) WRITE(6,10) NFS
10    FORMAT(//3X,'CONVERGENCE MONITOR FOR NFS = ',I1//,
     1 3X,'SWEEP',4X,'CENTRE',12X,'SW',16X,'SE',16X,'NW',16X,'NE',
     2 16X,'RESIDUAL'/)
      NITER=1
316   DO 110 INDEX=1,2
C
C  I-SWEEP
C
      DO 120 II=1,L1
      I=II
      IF (INDEX.EQ.2) I=L1+1-II
      IP1=I+1
      IM1=I-1
      D=ACON(I,1)
      IF (I.EQ.1) GOTO 130
      D=D+AW(I,1)*F(IM1,1,NFS)
130   IF (I.EQ.L1) GOTO 140
      D=D+AE(I,1)*F(IP1,1,NFS)+ANE(I,1)*F(IP1,2,NFS)
140   PT(1)=AN(I,1)/AC(I,1)
      QT(1)=D/AC(I,1)
      DO 150 J=2,M2
      D=AGON(I,J)
      IF (I.EQ.1) GOTO 160
      D=D+AW(I,J)*F(IM1,J,NFS)
     1 +ASW(I,J)*F(IM1,J-1,NFS)
160   IF (I.EQ.L1) GOTO 170
      D=D+AE(I,J)*F(IP1,J,NFS)+ANE(I,J)*F(IP1,J+1,NFS)
170   DENOM=AC(I,J)-AS(I,J)*PT(J-1)
      PT(J)=AN(I,J)/DENOM
150   QT(J)=(AS(I,J)*QT(J-1)+D)/DENOM
      D=ACON(I,M1)
      IF (I.EQ.1) GOTO 180
      D=D+AW(I,M1)*F(IM1,M1,NFS)+ASW(I,M1)*F(IM1,M2,NFS)
180   IF (I.EQ.L1) GOTO 190
      D=D+AE(I,M1)*F(IP1,M1,NFS)
190   PT(M1)=0.D0
      QT(M1)=(AS(I,M1)*QT(M2)+D)/(AC(I,M1)-AS(I,M1)*PT(M2))
C  BACK SUBSTITUTION
      F(I,M1,NFS)=QT(M1)
      DO 200 JJ=1,M2
      J=M1-JJ
200   F(I,J,NFS)=PT(J)*F(I,J+1,NFS)+QT(J)
120   CONTINUE
C
C  J-SWEEP
C
      DO 220 JJ=1,M1
      J=JJ
      IF (INDEX.EQ.2) J=M1+1-JJ
      JP1=J+1
      JM1=J-1
```

```
      D=ACON(1,J)
      IF(J.EQ.1) GOTO 230
      D=D+AS(1,J)*F(1,JM1,NFS)
230   IF (J.EQ.M1) GOTO 240
      D=D+AN(1,J)*F(1,JP1,NFS)+ANE(1,J)*F(2,JP1,NFS)
240   PT(1)=AE(1,J)/AC(1,J)
      QT(1)=D/AC(1,J)
      DO 250 I=2,L2
      D=ACON(I,J)
      IF (J.EQ.1) GOTO 260
      D=D+AS(I,J)*F(I,JM1,NFS)+ASW(I,J)*F(I-1,JM1,NFS)
260   IF (J.EQ.M1) GOTO 270
      D=D+AN(I,J)*F(I,JP1,NFS)
     1 +ANE(I,J)*F(I+1,JP1,NFS)
270   DENOM=AC(I,J)-AW(I,J)*PT(I-1)
      PT(I)=AE(I,J)/DENOM
250   QT(I)=(AW(I,J)*QT(I-1)+D)/DENOM
      D=ACON(L1,J)
      IF (J.EQ.1) GOTO 280
      D=D+AS(L1,J)*F(L1,JM1,NFS)+ASW(L1,J)*F(L2,JM1,NFS)
280   IF (J.EQ.M1) GOTO 290
      D=D+AN(L1,J)*F(L1,JP1,NFS)
290   PT(L1)=0.D0
      QT(L1)=(AW(L1,J)*QT(L2)+D)/(AC(L1,J)-AW(L1,J)*PT(L2))
C  BACK SUBSTITUTION
      F(L1,J,NFS)=QT(L1)
      DO 300 II=1,L2
      I=L1-II
300   F(I,J,NFS)=PT(I)*F(I+1,J,NFS)+QT(I)
220   CONTINUE
110   CONTINUE
      R=AC(IR,JR)*F(IR,JR,NFS)-AE(IR,JR)*F(IRP1,JR,NFS)
     1 -ANE(IR,JR)*F(IRP1,JRP1,NFS)-AN(IR,JR)*F(IR,JRP1,NFS)
     2 -AW(IR,JR)*F(IRM1,JR,NFS)-ASW(IR,JR)*F(IRM1,JRM1,NFS)
     3 -AS(IR,JR)*F(IR,JRM1,NFS)-ACON(IR,JR)
      IF(IMONIT.EQ.0) GOTO 100
      WRITE(6,310) NITER,F(LMID,MMID,NFS),F(2,2,NFS),F(L2,2,NFS),
     1 F(2,M2,NFS),F(L2,M2,NFS),R
310   FORMAT(3X,I4,5X,6(1PD15.8,3X))
C
C  CONVERGENCE TEST
C
100   NITER=NITER+1
      IF (NITER.LE.NSWP(NFS)) GOTO 316
      IF (DABS(R).LT.TOL(NFS)) RETURN
      IF (NITER.LE.NITMAX(NFS)) GOTO 316
      WRITE (6,314)
314   FORMAT(//3X,'MAXIMUM NUMBER OF ITERATIONS EXCEEDED')
      RETURN
      END
C
      SUBROUTINE TEST
C*****************************************************************
      IMPLICIT REAL*8(A-H,O-Z)
      LOGICAL LSOLVE,LCPRIN,LPRINT,LPPRIN
      COMMON ASTORE(3528),X(21,21),Y(21,21),F(21,21,7),FU(21,21,7),
     1 FP(11,11,2),RHO(21,21),GAM(21,21),
     2 SC(21,21),SP(21,21),ACU(21,21),UHAT(21,21),
```

```
     3 D1T1(10,10,2),D2T1(10,10,2),D3T1(10,10,2),
     4 D1T2(10,10,2),D2T2(10,10,2),D3T2(10,10,2)
      COMMON /THRD/Z,DZ,DPDZ,DPDZC,PBAR,SPMF,WFD,CNUFD(4),LSTEP,ISTEP,
     1 ITMAX,ISTART,IPROB
      COMMON /PARM/RELAX(7),PRELAX
      COMMON /MONIT/LSOLVE(7),LCPRIN,LPRINT(7),LPPRIN
      COMMON /LABEL/TITLE(7),HDG(9)
      COMMON /INDX/NSWP(7),NPSWP(2),L1,L2,L3,M1,M2,M3,
     1 LP1,LP2,LP3,MP1,MP2,MP3,NFS,NFSMAX,NPS,NUME,IMONIT,LAST,
     2 LMID,MMID,LPMID,MPMID,IPREF,JPREF,ITER,IC(3),JC(3),IDEAL,
     3 IR,IRP1,IRM1,JR,JRP1,JRM1,IPR,IPRP1,IPRP2,IPRM1,IPRM2,JPR,JPRP1,
     4 JPRP2,JPRM1,JPRM2,NITMAX(7),NPITMX(2)
      COMMON /CONV/TOL(7),PTOL(2),DWDES,FCK(3,2),DPDZCK,CHGTOL,CHGCK
      COMMON /RODBUN/S,RAD,SDR,WBAR,FAREA,PERIM,PHY,DH,DHDR,XL,YL,TANPSI
     1 ,PSI,FBU4,FBU6,FB,FWAV,RHOA,CP1,DK1,DKDCP1,CP2,DK2,DKDCP2,
     2 RPOW,XPOW,YPOW,DMUA,REY,QW, TAUW(21),TW,TI
C-----------------------------------------------------------------------
30    FORMAT(//3X,'CORRECTED VALUE FOR NFS = ',I1//,
     1 3X,'      ',4X,'CENTRE',12X,'SW',16X,'SE',16X,'NW',16X,'NE'/)
35    FORMAT(3X,4X,5X,5(1PD15.8,3X))
C-----------------------------------------------------------------------
      ENTRY PTVEL
      WRITE(6,30) NFS
      WRITE(6,35) F(LMID,MMID,NFS),F(2,2,NFS),F(L2,2,NFS),
     1 F(2,M2,NFS),F(L2,M2,NFS)
      RETURN
      END
//
```